FERRORESONANCE SIMULATION STUDIES OF TRANSMISSION SYSTEMS

A thesis submitted to

THE UNIVERSITY OF MANCHESTER

for the degree of

DOCTOR OF PHILOSOPHY

in the Faculty of Engineering and Physical Sciences

2010

Swee Peng Ang

School of Electrical and Electronic Engineering

LIST OF CONTENTS

LIST OF FIGURES

CHAPTER 1: INTRODUCTION

CHAPTER 2: LITERATURE REVIEW

CHAPTER 3: SINGLE-PHASE FERRORESONANCE - A CASE STUDY

CHAPTER 4: SYSTEM COMPONENT MODELS FOR FERRORESONANCE

CHAPTER 5: MODELING OF 400 KV THORPE-MARSH/BRINSWORTH SYSTEM

CHAPTER 6: MODELING OF 400 KV IRON-ACTON/MELKSHAM SYSTEM

LIST OF TABLES

CHAPTER 1: INTRODUCTION

CHAPTER 2: LITERATURE REVIEW

CHAPTER 3: SINGLE-PHASE FERRORESONANCE - A CASE STUDY

CHAPTER 4: SYSTEM COMPONENT MODELS FOR FERRORESONANCE

CHAPTER 5: MODELING OF 400 KV THORPE-MARSH/BRINSWORTH SYSTEM

CHAPTER 6: MODELING OF 400 KV IRON-ACTON/MELKSHAM SYSTEM

LIST OF PUBLICATIONS

Conferences:

(1) Swee Peng Ang, Jie Li, Zhongdong Wang and Paul Jarman, “FRA Low Frequency Characteristic Study Using Duality Transformer Core Modeling,” 2008 International Conference on Condition Monitoring and Diagnosis, Beijing, China, April 21-24, 2008.

(2) S. P. Ang, Z. D. Wang, P. Jarman, and M. Osborne, "Power Transformer Ferroresonance Suppression by Shunt Reactor Switching," in *The 44th International Universities' Power Engineering Conference 2009 (UPEC 2009).*

(3) Jinsheng Peng, Swee Peng Ang, Haiyu Li, and Zhongdong Wang, "Comparisons of Normal and Sympathetic Inrush and Their Implications toward System Voltage Depression," in *The 45th International Universities' Power Engineering Conference 2010 (UPEC 2010)* Cardiff University, Wales, UK, 31st August - 3rd September 2010.

(4) Swee Peng Ang, Jinsheng Peng, and Zhongdong Wang, "Identification of Key Circuit Parameters for the Initiation of Ferroresonance in a 400-kV Transmission Syetem," in *International Conference on High Voltage Engineering and Application (ICHVE 2010)* New Orleans, USA, 11-14 October 2010.

(5) Rui Zhang, Swee Peng Ang, Haiyu Li, and Zhongdong Wang, "Complexity of Ferroresonance Phenomena: Sensitivity studies from a single-phase system to three-phase reality" in *International Conference on High Voltage Engineering and Application (ICHVE 2010)* New Orleans, USA, 11-14 October 2010.

ABSTRACT

The onset of a ferroresonance phenomenon in power systems is commonly caused by the reconfiguration of a circuit into the one consisting of capacitances in series and interacting with transformers. The reconfiguration can be due to switching operations of de-energisation or the occurrence of a fault. Sustained ferroresonance without immediate mitigation measures can cause the transformers to stay in a state of saturation leading to excessive flux migrating to transformer tanks via internal accessories. The symptom of such an event can be unwanted humming noises being generated but the real threatening implication is the possible overheating which can result in premature ageing and failures.

The main objective of this thesis is to determine the accurate models for transformers, transmission lines, circuit breakers and cables under transient studies, particularly for ferroresonance. The modeling accuracy is validated on a particular 400/275 kV transmission system by comparing the field test recorded voltage and current waveforms with the simulation results obtained using the models. In addition, a second case study involving another 400/275 kV transmission system with two transformers is performed to investigate the likelihood of the occurrence of sustained fundamental frequency ferroresonance mode and a possible quenching mechanism using the 13 kV tertiary connected reactor. A sensitivity study on transmission line lengths was also carried out to determine the probability function of occurrence of various ferroresonance modes. To reproduce the sustained fundamental and the subharmonic ferroresonance modes, the simulation studies revealed that three main power system components which are involved in ferroresonance, i.e. the circuit breaker, the transmission line and the transformer, can be modeled using time-controlled switch, the PI, Bergeron or Marti line model, and the BCTRAN+ or HYBRID transformer model. Any combination of the above component models can be employed to accurately simulate the ferroresonance system circuit.

Simulation studies also revealed that the key circuit parameter to initiate transformer ferroresonance in a transmission system is the circuit-to-circuit capacitance of a double-circuit overhead line. The extensive simulation studies also suggested that the ferroresonance phenomena are far more complex and sensitive to the minor changes of system parameters and circuit breaker operations. Adding with the non-linearity of transformer core characteristics, repeatability is not always guaranteed for simulation and experimental studies. All simulation studies are carried out using an electromagnetic transient program, called ATPDraw.

DECLARATION

No portion of the work referred to in this thesis has been submitted in support of an application for another degree of qualification of this or any other university, or other institution of learning.

COPYRIGHT STATEMENT

i. The author of this thesis (including any appendices and/or schedules to this thesis) owns certain copyright or related right in it (the "Copyright") and s/he has given The University of Manchester certain rights to use such Copyright, including for administrative purposes.

ii. Copies of this thesis, either in full or in extracts and whether in hard or electronic copy, may be made **only** in accordance with the Copyright, Designs and Patents Act 1988 (as amended) and regulations issued under it or, where appropriate, in accordance with licensing agreements which the University has from time to time. This page must form part of any such copies made.

iii. The ownership of certain Copyright, patents, designs, trade marks and other intellectual property (the "Intellectual Property") and any reproductions of copyright works in the thesis, for example graphs and tables ("Reproductions"), which may be described in this thesis, may not be owned by the author and may be owned by third parties. Such Intellectual Property and Reproductions cannot and must not be made available for use without the prior written permission of the owner(s) of the relevant Intellectual Property and/or Reproductions.

iv. Further information on the conditions under which disclosure, publication and commercialisation of this thesis, the Copyright and any Intellectual Property and/or Reproductions described in it may take place is available in the University IP Policy (see http://www.campus.manchester.ac.uk/medialibrary/policies/intellectual-property.pdf), in any relevant Thesis restriction declarations deposited in the University Library, The University Library's regulations (see http://www.manchester.ac.uk/library/aboutus/regulations) and in The University's policy on presentation of Theses.

ACKNOWLEDGEMENT

Writing a thesis, as with any other large project, requires the coordinated efforts of many people. I would like to thank the following people. Without their efforts and guidance this thesis would never have been completed.

I would like to express my indebted gratitude to my supervisor Prof. Zhongdong Wang for her outstanding support, contribution and invaluable assistance in the achievement and development of my Ph.D thesis. Her wise experience in the field of electrical power engineering has enlightened me throughout the project.

Collaborations with Paul Jarman and Mark Osborne of National Grid, UK give my project the focus and direction, I would like to thank them for their assistance in providing technical support.

Jinsheng Peng's assistance with performing ATP-EMTP simulations on the Brinsworth system in investigating the initiation of ferroresonant modes is greatly appreciated. Useful discussions with Mr. Syed Mohammad Sadegh Mir Ghafourian, a fellow Ph.D student is appreciated regarding the circuit breaker re-ignition mechanism in developing an EMTP model.

I would like also to express my special thanks to the Ministry of Education, Government of Brunei Darussalam for providing a government scholarship to pursue my Ph.D research at the University of Manchester, UK.

Last but not least, my special thanks to my beloved parents, brothers, sisters, my wife and my three sons for their patience and encouragement. This thesis took a great deal of time away from them. All involved gave me confidence and unending support.

CHAPTER 1

1. INTRODUCTION

1.1 Introduction

Power system is considered to be the most sophisticated network which consists of electrical, mechanical, electronic and control hardware designed, built and operated by electrical engineers. The function of a power system is to deliver electrical energy as economically as possible with minimum environmental impact such as reduction in carbon dioxide (CO2) emission. In addition, the transfer of electrical energy to the load centers via transmission and distribution systems are achieved with maximum efficiency and optimum reliability at nominal voltage and frequency. In view of this, the establishment of the system is considered to be the most expensive in terms of capital investment, in comparison with other systems, such as, communication, gas, water, sewage etc.

Nowadays, because of technological advancement, industrial globalization and continuous increasing levels of network integrations, the grid system is increasingly vulnerable and sensitive to system disturbances. Such events may be due to switching activities (i.e. ON and OFF) of loads, or as a result of component switching such as reactor switching, the energisation and de-energisation of system components for commissioning and maintenance purposes. Other sources of switching events are the switching off of protection zones after the occurrence of short-circuit, or a lightning stroke [1] impinging to the nearest high-voltage transmission line. For these reasons, the systems are never operated in a continuous steady state condition, it is a system consisting of a mixture of normal operating and transient states. Yet, the duration of the transient state in a system is not significant as compared to the steady state operating time. There are some instances that this transient can subject system components to excessive stresses due to overvoltage and overcurrent. Thus, premature aging of component insulation structures can happen and sometimes they can finally develop into an extreme stage of breakdown. In some cases, this effect may become ecologically most intrusive in terms of thermal, chemical and potentially radiological pollution. Another adverse impact is the widespread of problems in a system, which may disable a component, trip off a plant, or cause power outage in hospitals or in a city hence halting some businesses.

Transient events are due to the attended power system parameters such as resistance, inductance and capacitance of transmission line, transformer, cable, capacitive shunt reactors, inductive shunt reactors etc. Owing to such parameters and the adding up of capacitive and inductive components into the integrated power system, the frequency range of transient phenomena can extend from DC to several MHz [2]. Depending on the frequency range the types of transient events are classified into high- and low-frequency transients.

The nature of high frequency transient mainly depends on the load and the status of circuit breaker when separating its contacts close to a current zero passage [1]. High frequency oscillation will occur if re-ignition takes place between the separated contacts of a circuit breaker, that is when the transient recovery voltage (TRV) exceeds the breakdown voltage of the contact gap.

Depending on the circuit configuration, the large number of various sources of capacitances in the network and certain sequence of switching events, a low frequency transient known as *ferroresonance* can exhibit in the system. The word *ferroresonance* means the resonanance between the network parameters with ferromagnetic material, particularly with the presence of transformers working at no-load condition.

1.2 Background of Ferroresonance

Linear resonance only occurs in the circuit of Figure 1.1 as an example, consisting of a series connected resistor, inductor and capacitor when the source is tuned to the natural frequency of the circuit. The capacitive and inductive reactances of the circuit are identical at the resonance frequency as given by:

$$f_R = \frac{1}{2\pi\sqrt{LC}} \quad \text{(Hz)}$$

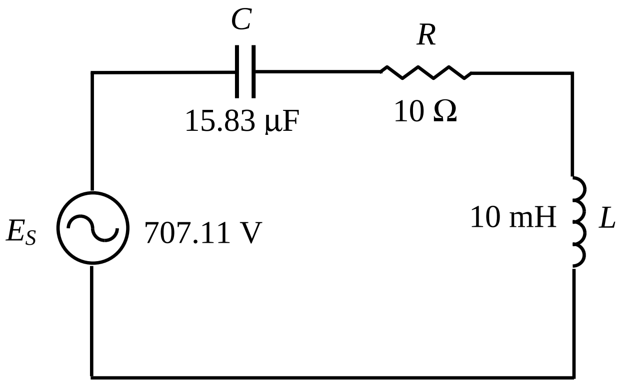

Figure 1.1: Linear resonance circuit

The voltages appearing across the inductor, *L* and capacitor, *C* in this condition can reach several times of the source voltage. Figure 1.2 shows the characteristics of the capacitor voltage, the inductor voltage and the supply current when the main supply frequency is varied from 20 Hz up to 600 Hz. At resonance, the graph shows that the voltage across the inductor and capacitor reaches their peak values when the natural frequency of the system is tuned to about 400 Hz. This condition also suggests that both the V_L and V_c exceed the main supply voltage. Furthermore, the current in the circuit is at its maximum because the impedance of the circuit is minimum, merely resistive.

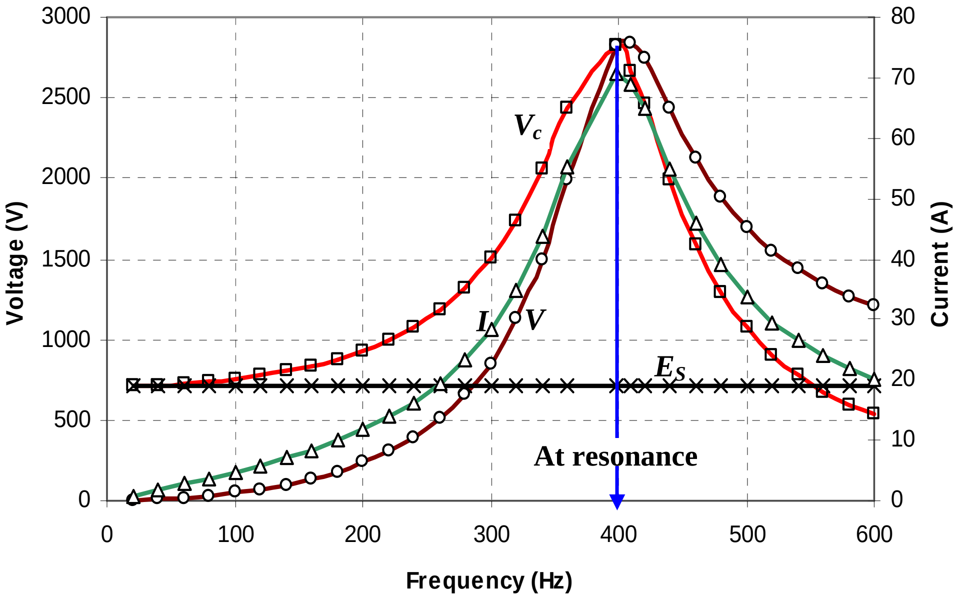

Figure 1.2: Characteristic of V_c, V_L, I and E_s at resonance

The linear circuit of Figure 1.1 when subjected to resonance condition produces an expected and repeatable response to the applied source voltage. Sinusoidal voltages appear across any points in the circuit without any distortion.

In contrast, things are not quite the same in a nonlinear series circuit as what happened in the linear series resonance. The linear inductor of Figure 1.1 is replaced by a nonlinear inductor (ferromagnetic material). An example of ferromagnetic material is a transformer core. The series connection consists of an alternating source (E_S), a resistor (R), a capacitor (C) and a nonlinear inductor (L_m) as shown in Figure 1.3, which is referred to as ferroresonance circuit.

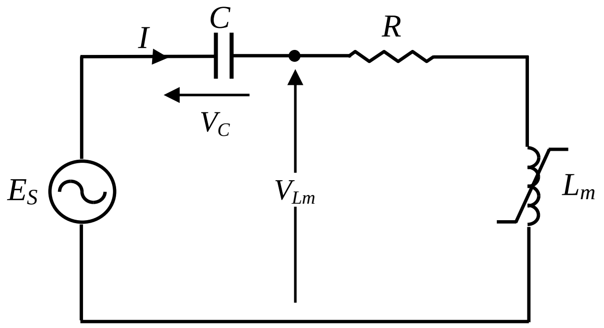

Figure 1.3: Ferroresonant circuit

In the linear circuit, resonance condition occurs at only one frequency with a fixed value of L and C. On the other hand, the nonlinear circuit can exhibit multiple values of inductances when the core is driven into saturation therefore this implies that there is a wide range of capacitances that can potentially leads to ferroresonance at a given frequency [3] which is shown in Figure 1.4.

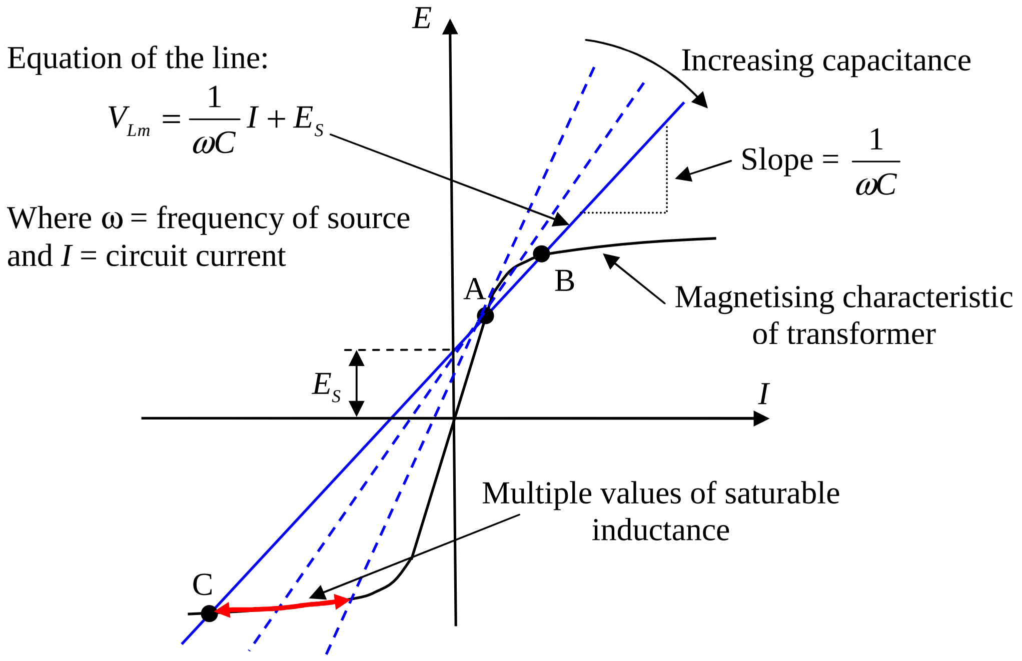

Figure 1.4: *E-I* characteristic of ferroresonance circuit

Ferroresonance can exhibit more than one steady state responses for a set of given system parameter values [4]. Damaging overvoltages and overcurrents can be induced into a system due to ferroresonance.

The comparison between the linear and ferroresonance is shown in Table 1.1.

Table 1.1: Comparison between linear resonance and ferroresonance

Network	System Parameters	Resonance	Response
Linear circuit	Resistance, capacitance, inductor	Resonance occurs at one frequency when the source frequency is varied.	Only one sinusoidal steady state overvoltage and overcurrent occurs.
Nonlinear circuit	Resistance, capacitance, nonlinear inductor (ferromagnetic material)	Ferroresonance occurs at a given frequency when one of the saturated core inductances matches with the capacitance of the network.	Several steady state overvoltages and overcurrents can occur.

1.3 Types of Ferroresonance Modes

In the previous section, the distinctive difference between the linear resonance and ferroresonance has been described. The fundamental elements involved in the ferroresonance circuit are a resistance, a capacitance and a nonlinear inductor. The development of the ferroresonance circuit taking place in the power system is mostly due to the reconfiguration of a particular circuit caused by switching events. Immediately after the switching event, initial transient overvoltage will firstly occur and this is followed by the next phase of the transient where the system may arrive at a more steady condition. Due to the non-linearity of the ferroresonance circuit, there can be several steady state ferroresonance responses randomly [5-14] induced into a system. Basically, there are four types of steady-state responses a ferroresonance circuit can possibly have: they are the fundamental mode, subharmonic mode, quasi-periodic mode and chaotic mode. Each of the classifications and its characteristics are depicted in Figure 1.5 to Figure 1.8 [4]. FFT and Poincarè map are normally employed to analyse the types of ferroresonance modes.

1.3.1 Fundamental Mode

The periodic response has the same period, T as the power system. The frequency spectrum of the signals consists of fundamental frequency component as the dominant one followed by decreasing contents of 3rd, 5th, 7th and nth odd harmonic. In addition, this type of response can also be identified by using the stroboscopic diagram of Figure 1.5 (c) which is also known as Poincarè plot, which can be obtained by simultaneously sampling of voltage, v and current, i at the fundamental frequency. Detailed explanation on this plot can be referred in the following section.

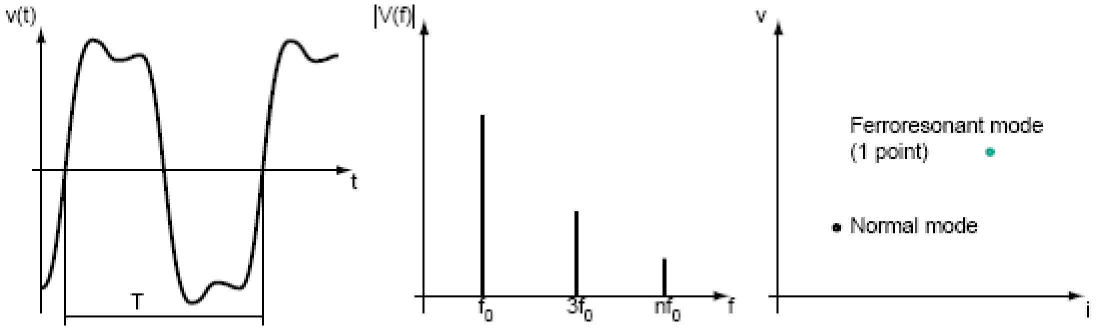

(a) Periodic signal (b) Frequency spectrum (c) Stroboscopic diagram

Figure 1.5: Fundamental mode

1.3.2 Subharmonic Mode

This type of ferroresonance signals has a period which is multiple of the source period, nT. The fundamental mode of ferroresonance is normally called a Period-1 (i.e. $f_0/1$ Hz) ferroresonance and a ferroresonance with a sub-multiple of the power system frequency is called a Period-n (i.e. f_0/n Hz) ferroresonance. Alternatively, the frequency contents are described having a spectrum of frequencies equal to f0/n with f0 denoting the fundamental frequency and n is an integer. With this signal, there are n points exist in the stroboscopic diagram which signifies predominant of fundamental frequency component with decreasing harmonic contents at other frequencies.

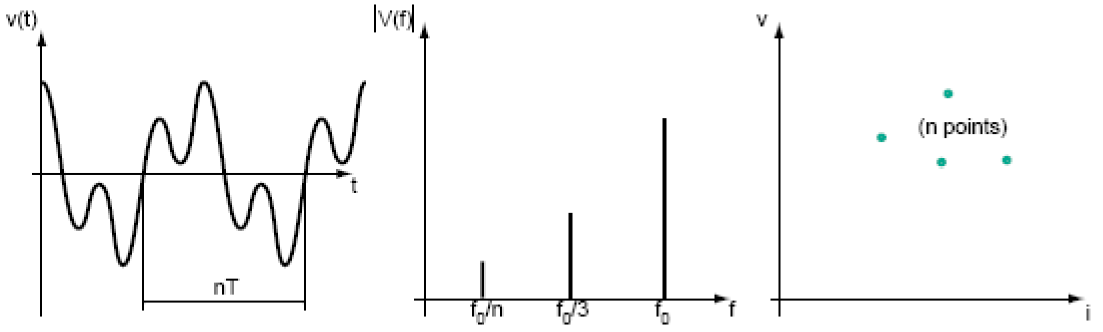

(a) Periodic signal (b) Frequency spectrum (c) Stroboscopic diagram

Figure 1.6: Subharmonic mode

1.3.3 Quasi-periodic Mode

This kind of signal is not periodic. The frequency contents in the signal are discontinuous in the frequency spectrum, whose frequencies are defined as: nf1+mf2 (where n and m are integers and f1/f2 an irrational real number). This type of response displays a feature employing a close cycle of dotted points on the stroboscopic plot. The set of points (closed curve) in the diagram is called an attractor to which all close by orbits will asympotate as $t \to \infty$, that is, in the steady state [73].

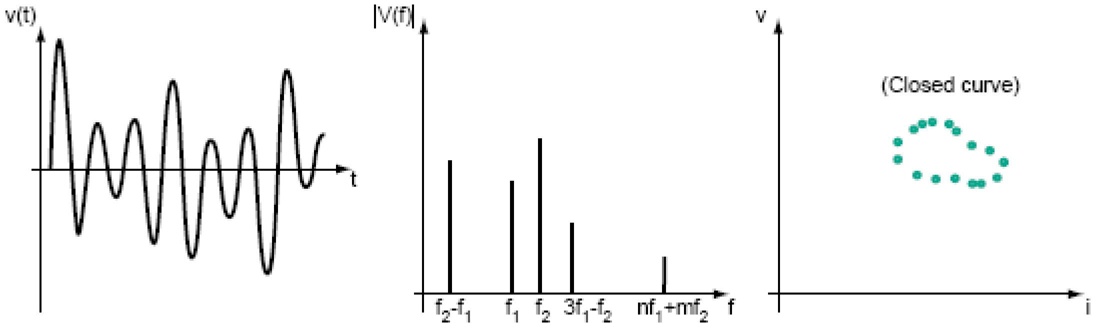

(a) Periodic signal (b) Frequency spectrum (c) Stroboscopic diagram

Figure 1.7: Quasi-periodic mode

1.3.4 Chaotic Mode

This mode has a signal exhibiting non-periodic with a continuous frequency spectrum i.e. it is not cancelled for any frequency. The stroboscopic plot consists of n points surrounding an area known as the strange attractor which appears to skip around randomly.

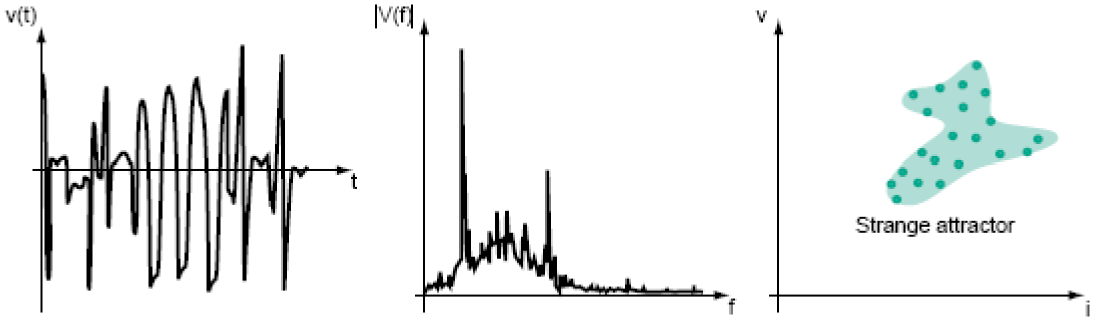

(a) Periodic signal (b) Frequency spectrum (c) Stroboscopic diagram

Figure 1.8: Chaotic mode

The simulation model in [11] reported 3 types of ferroresonance modes which have occurred in a circuit consisting of a voltage transformer (VT) located at a 275 kV substation.

❖ *Sustained Fundamental Frequency Ferroresonance Mode (Period-1)*

The periodic waveform induced was a sustained fundamental frequency ferroresonance which is shown in Figure 1.9. The magnitude of the response has reached 2 p.u. Since the sustained ferroresonant signal was initiated after the transient period therefore the starting point of the signal was obtained at t=90.00 s.

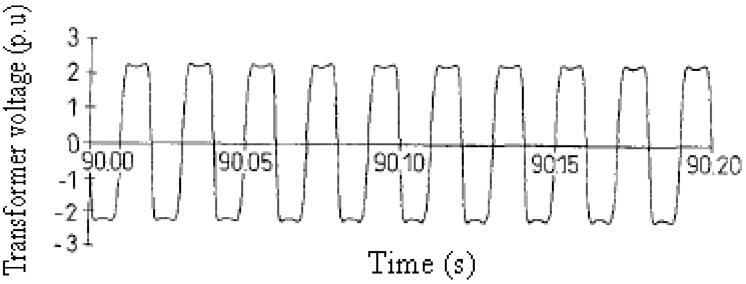

Figure 1.9: Time signal

In this study, tools such as power spectrum, Poincarè map and Phase-plane diagram have been employed to identify the type of ferroresonance response. The power spectrum of Figure 1.10 suggests that the response mainly consists of fundamental component (50 Hz) with the presence of high frequency components.

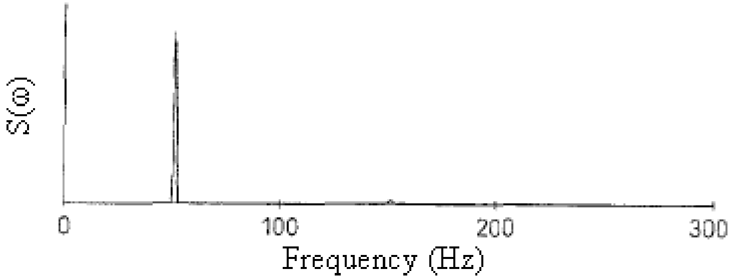

Figure 1.10: Power spectrum

The Poincarè plot of Figure 1.11 reveals that there is only one dot displayed on the diagram. The meaning of this is that it is a Period-1 response corresponds to the sampling frequency of 50 Hz.

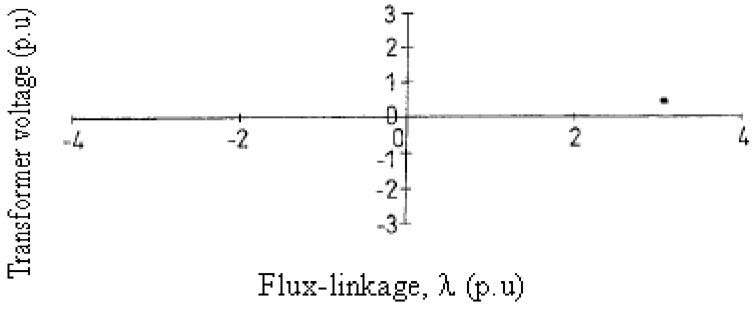

Figure 1.11: Poincarè plot

Alternative way of identifying the type of ferroresonance mode is to use a Phase-plane plot. Normally it is a plot of transformer voltage versus flux-linkage.

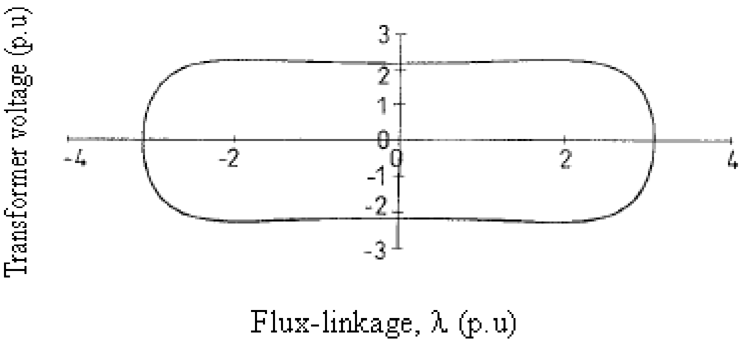

Figure 1.12: Phase-plane diagram

A phase-plane diagram provides an indication of the waveform periodicity since periodic signals follow a closed-loop trajectory. One closed-loop means that a fundamental frequency periodic signal; two closed-loops for a signal period twice the source period, and so on. The phase-plane diagram (i.e. voltage versus flux-linkage) of this response is shown in Figure 1.12. The orbit shown encompasses a time interval of only one period of excitation. The structure of the phase-plane diagram consists of only one major repeatedly loop for each phase which provides an indication of a fundamental frequency signal. Note that the phase-plot has been normalized.

❖ *Subharmonic Ferroresonance Mode*

Figure 1.13 shows the voltage waveform of the subharmonic mode induced across the transformer.

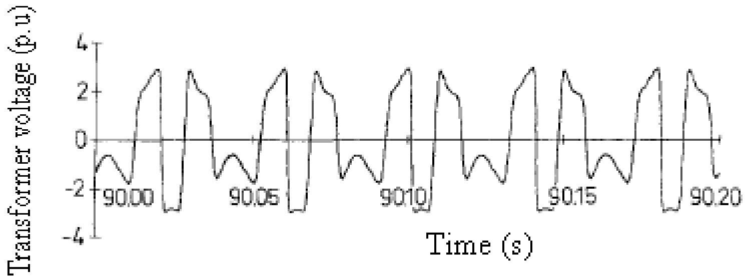

Figure 1.13: Time signal

The frequency spectrum of Figure 1.14 corresponds to the voltage waveform of Figure 1.13. The frequency that appears first is the 25 Hz followed by a sharp peak at 50 Hz.

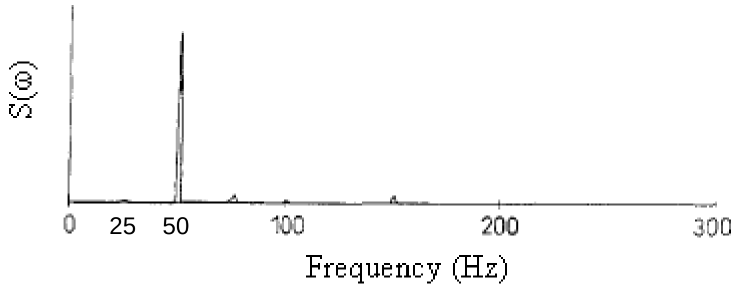

Figure 1.14: Power spectrum

The Poincarè plot of Figure 1.15 suggests that the voltage waveform is a Period-2 ferroresonance because there are two points on the diagram.

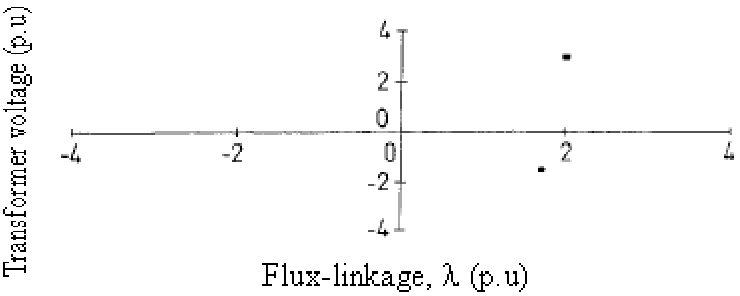

Figure 1.15: Poincarè plot

The Phase-plane diagram of Figure 1.16 shows that there are two closed-loops indicating for a signal period twice the source period.

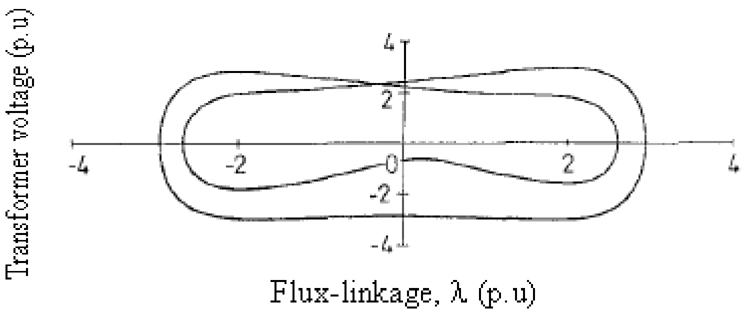

Figure 1.16: Phase-plane diagram

- ***Chaotic Ferroresonance Mode***

The voltage waveform of Figure 1.17 shows there is no indication of periodicity. The frequency spectrum of the signal reveals that there is a broad continuous frequency spectrum with a strong 50 Hz component (Figure 1.18).

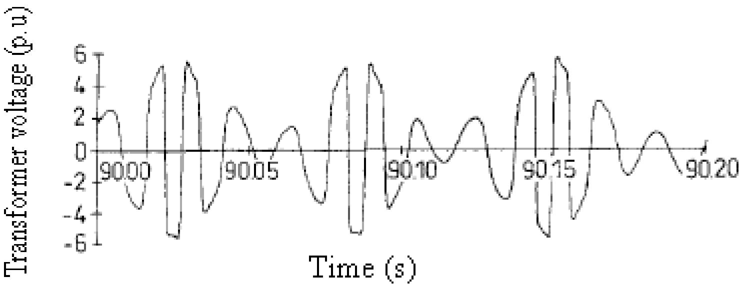

Figure 1.17: Time signal

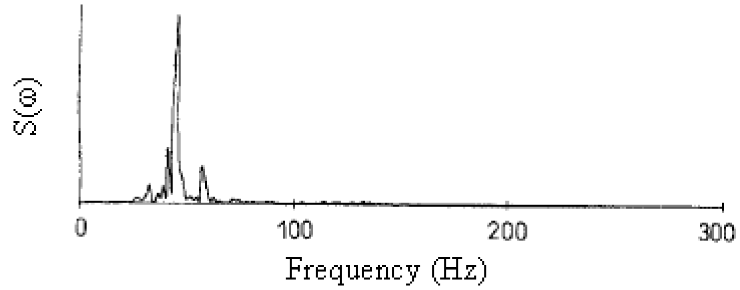

Figure 1.18: Power spectrum

A random of scattered set of dotted points can be seen of the Poincarè plot of Figure 1.19 and the trajectory of the phase-plane diagram of Figure 1.20 suggests that there is no indication of repeating.

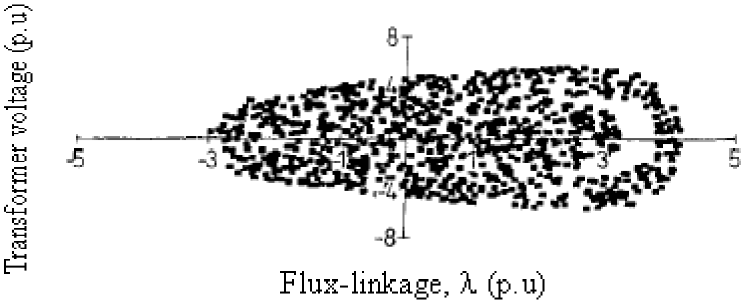

Figure 1.19: Poincarè plot

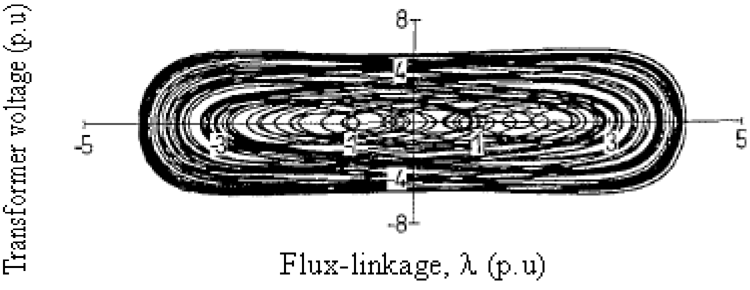

Figure 1.20: Phase-plane diagram

1.4 Effect of Ferroresonance on Power Systems

In the preceding section, the characteristics and features of each of the four distinctive ferroresonance modes have been highlighted. The impacts due to ferroresonance can cause undesirable effects on power system components. The implications of such phenomena experienced in [7, 14-16] have been reported. They are summarised as follows:

- [15] described that a 420-kV peak and distorted sustained fundamental mode ferroresonance waveform has been induced in C-phase 1000 MVA, 525/241.5-kV wye-connected bank of autotransformers. The consequences following the event were as follows: Nine minutes later, the gas accumulation alarm relay operated on the C-phase transformer. Arcing of C-phase switch was much more severe than that of the other two phases. No sign of damage although a smell of burnt insulation was reported. However, the gas analysis reported a significant amount of hydrogen, carbon dioxide and monoxide.

- Ferroresonance experienced in [14] was due to the switching events that have been carried out during the commissioning of a new 400-kV substation. It was reported that two voltage transformers (VT) terminating into the system had been driven into a sustained fundamental frequency ferroresonance of 2 p.u. The adverse impact upon the initiation of this phenomenon was that a very loud humming noise generated from the affected voltage transformer, heard by the local operator.

- In 1995, [16] reported that one of the buses in the station was disconnected from service for the purpose of commissioning the replaced circuit breaker and current transformers. At the same time, work on maintenance and trip testing were also carried out. After the switching operations, the potential transformers which were connected at the de-energised bus were energised by the adjacent live busbar, via the circuit breakers' grading capacitors. Following the switching events, a sustained fundamental frequency ferroresonance has been induced into the system. As a result, the response has caused an explosion to the potential transformer. The catastrophically failure was due to the excessive current in the primary winding of the affected potential transformer.

- [7] reported that the Station Service Transformer (SST) ferroresonance has been occurred at the 12-kV substation. The incident was due to the switching operations by firstly opening the circuit breaker and then the disconnector switch located at the riser pole surge arrester. The first ferroresonance test without arrestor installation has induced both the 3rd subharmonic and chaotic modes. As a result, the affected transformer creating loud noises like sound of crack and race engine. While for the second test, with the arrester, a sustained fundamental mode has been generated and thus has caused the explosion of riser pole arrester. The physical impact of the explosion has caused the ground lead of the disconnector explodes and the ruptures of the polymer housing.

It has been addressed from the above that the trigger mechanism of ferroresonance is switching events that reconfigure a circuit into ferroresonance circuit. In addition, the literatures presented in [3, 17, 18] documented that the existence of the phenomena can also result in any of the following symptom(s):

- Inappropriate time operation of protective devices and interference of control operation [3, 4, 18].
- Electrical equipment damage due to thermal effect or insulation breakdown and internal transformer heating triggering of the Bucholtz relay [3, 4, 18].
- Arcing across open phase switches or over surge arresters, particularly the use of the gapless ZnO [14].
- Premature ageing of equipment insulation structures [17].

Owing to the above consequences and symptoms, mitigation measures of ferroresonance are therefore necessary in order for the system to operate in a healthy environment.

1.5 Mitigation of Ferroresonance

The initiation of ferroresonance phenomena can cause distorted overvoltages and overcurrents to be induced into a system. The outcomes of this event have been highlighted in section 1.4 which are considered to be catastrophic when it occurs. There are generally two main ways of preventing the occurrence of ferroresonance [3, 4, 17].

- Avoid any switching operations that will reconfigure a circuit into a sudden inclusion of capacitance connected in series with transformer with no or light load condition [17].

- Provide damping of ferroresonance by introducing losses (i.e. load resistance) into the affected transformer. In other words, there is not sufficient energy supplied by the source to sustain the response [3, 4, 17].

1.6 Motivation

A survey paying attention onto the modeling of power system components for ferroresonance simulation study has been highlighted in the literature review in Chapter 2. It is shown that the main objective of developing the simulation models focused on validation of the models using the field test ferroresonance waveforms, then the use of the simulation tools to analyse the types of ferroresonant modes and finally performing the mitigation studies of ferroresonance. One of the main problems that ferroresonance studies employing digital simulation programs face is the lack of definitive criterion on how each of the power system components should be modeled. There is lacking of detailed guidelines on how the power system components such as the voltage source, transformer, transmission line, cable and circuit breaker should be modeled for ferroresonance studies. In addition, step-by-step systematic approaches of selecting an appropriate simulation model are still not explained in the literatures. Therefore, the motivation devoted in this thesis is directed towards achieving the following objectives:

- To provide a better understanding about the technical requirements on each of the power system components necessary for the development of simulation models for ferroresonance study.

- To provide a set of modeling guidelines required for choosing any of the available models.

- To identify the types of models suitable for the simulation studies required in this thesis.

To achieve the above objectives, a simulation model has been built on a 400/275 kV sub-transmission system undergone ferroresonance tests. Verification of the simulation results with the field test recordings have been performed, particularly the 50 Hz fundamental and 16.67 Hz subharmonic mode ferroresonance.

Based on the reasonable matching between the simulation and the field test recording waveforms, the modeling techniques which have been developed are then applied for the ferroresonance study of 400/275 kV sub-transmission system with the aim of assessing whether there is any likelihood of 50 Hz sustained fundamental frequency mode which can be initiated in the system, and also investigating an effective switch-in shunt reactor connected at the 13 kV tertiary winding for quenching purpose.

1.7 Methodology

The undesirable effects of ferroresonance phenomena subjected to power system components have been highlighted in section 1.4. Building a realistic model that would satisfactorily model such a transient event, employed either one of the following methods (1) analytical approach (2) analog simulation approach (3) real field test approach (4) laboratory measurement approach and (5) digital computer program approach.

Power system transient represented by analytical approach is difficult because of lengthy mathematical equations involved in arriving at the solutions required. Using analog simulators such as Transient Network Analyser (TNA) [19], the miniature approach of characterising power system model is rather expensive and requires floor areas to accommodate the equipment. Real network testing performed in the field is considered to be impractical at the design stage of a power system network. In view of those, a computer simulation program is therefore preferred as compared to the previous approaches. In this project, a graphical user interface (GUI) with a mouse-driven approach software called ATPDraw® is employed. In this program, the users can develop the simulation models of digital representation of the power circuit under study, by simply choosing the build-in predefined components.

To develop a complete simulation model in ATPDraw®, a block diagram as shown in Figure 1.21 is firstly drawn up outlining the approach which should be followed for simulation studies.

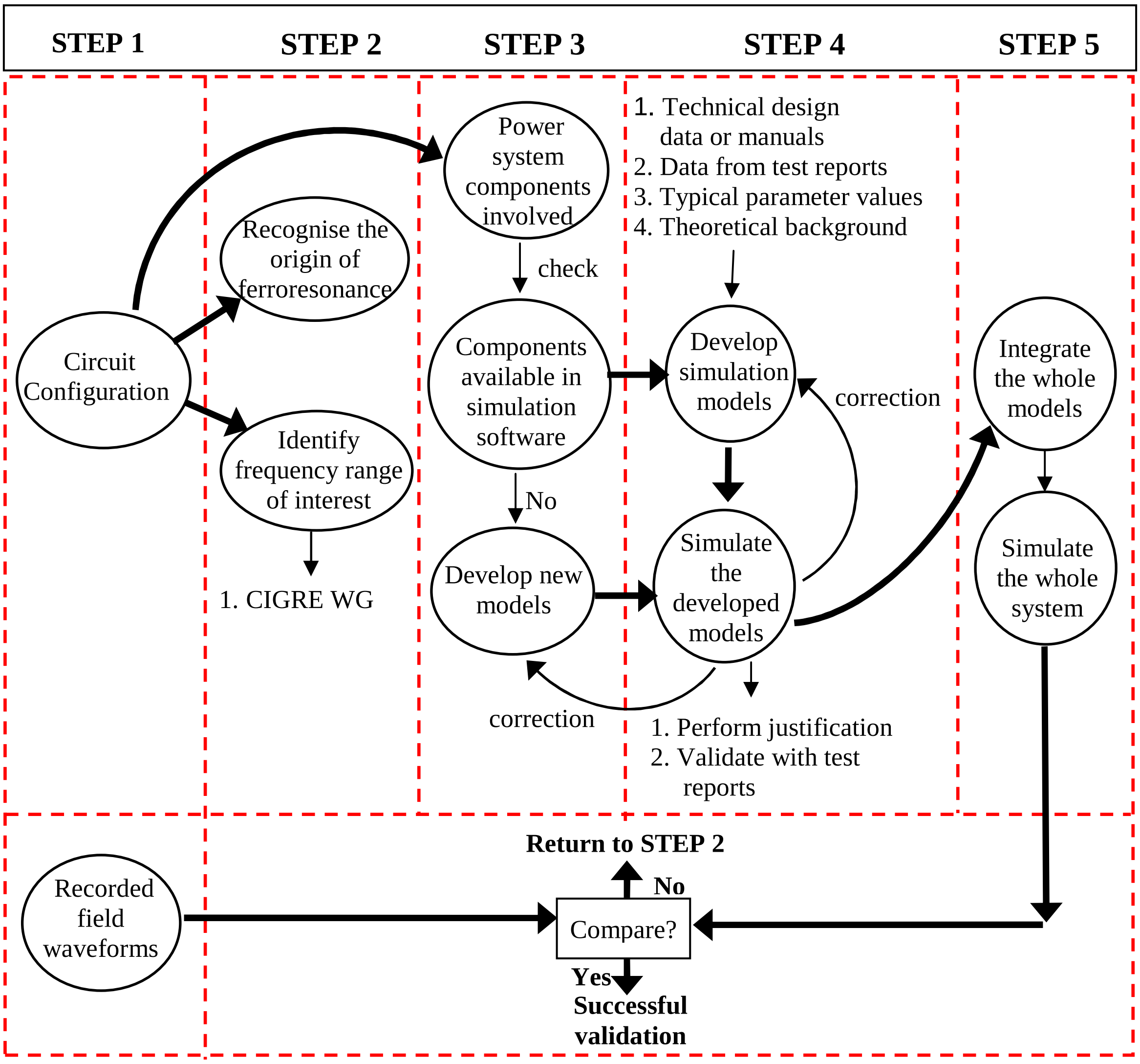

Figure 1.21: Outline of modeling methodology

As seen from the above figure, the initial step (STEP 1) before diving into the modeling of power system components is to obtain the detailed circuit configuration, description on how ferroresonance is initiated and finally the recorded field waveforms. From the phenomenon description the types of switching events and their relevant frequency range of interest are then identified (STEP 2), according to the document published by the CIGRE [20]. This is followed by STEP 3, check listing whether the types of power components in the circuit are available as the build-in predefined components in the simulation software. If it is found that the predefined components are readily available then the next stage is to study their theoretical background as well as its limitations for our purpose. In addition, the data required for the predefined components need to be carefully selected, which could be either the design parameters, typical values or test reports. More information in this matter can be obtained from utility/manufacturer involved in the project. A new model is sometimes necessary to build if it is found that the predefined component cannot serve the modeling requirements. Once the new or the predefined components have been developed, the next phase is to conduct validation and simulation studies. Once each of the developed simulation model has been tested or checked accordingly, then they are integrated into the actual circuit configuration. The simulation results are then compared with the actual field recorded waveform for validation. The process is then repeated if it is found out that the comparisons do not match what are expected.

Once the developed simulation model has been verified, the next stage of the simulation study can be scenario studies or sensitivity studies, aimed for in advance forecasting the consequences of switching operations of a power system network and planning for protection schemes. As an example, designing and evaluations of damping and quenching devices and to determine the thermal withstand capability of the devices can be parts of the study.

1.8 Thesis structure

There are seven chapters in this thesis. Overall they can be divided into four sections. Chapter 1 and 2 consist of the background; the objectives, the motivation, the methodology and literature review. Chapter 3 mainly concerns with exploring and understanding the behaviour of ferroresonance phenomenon and this leads into chapter 4 looking into modeling aspects of circuit breakers, transformers and transmission lines. The final stage of the project i.e. the development of two simulation models for two practical case scenarios, is covered in Chapter 5 and Chapter 6, followed by highlighting the contribution of the work and the work for future research.

Chapter 1: Introduction

In the first chapter, an overview of power system network and the introduction of the aspects of ferroresonance in terms of its occurrence, configuration, responses, impact and mitigation are introduced. In addition, the motivation together with the objective and the methodology of the projected are defined in this chapter.

Chapter 2: Literature Review

In this chapter, five different types of technology for time domain modeling ferroresonance, particularly the way that the components are taken into consideration are reviewed. Their advantages and disadvantages are emphased and compared with computer simulation program approach. The main issues encountered in modeling the real case system are highlighted here.

Chapter 3: Single-Phase Ferroresonance – A Case Study

The main aims of this chapter are twofold by considering an existing real case scenario including a single-phase equivalent transformer model connected to the circuit breaker including its grading capacitor and the influence of shunt capacitor of busbar. The first aim is to look into the influence of the core-loss and the degrees of core saturations. The second one is to investigate on how the initiation of fundamental and subharmonic mode ferroresonance can occur when being affected by both the grading capacitor and the shunt capacitor.

Chapter 4: System Component Models for Ferroresonance

This chapter concentrates on the modeling aspects of the power system component available in ATPDraw suitable for the study of ferroresonance, particularly looking into the circuit breaker, the transformers and the transmission lines. Each predefined model in ATPDraw is reviewed to determine the suitability for ferroresonance study.

Chapter 5: Modeling of 400 kV Thorpe-Marsh/Brinsworth System

There are two main objectives covered in this chapter; firstly the validation of the developed predefined models and secondly identifying the key parameter responsible for the occurrence of ferroresonance. For the first objective, finding out the suitability of the predefined models is carried out by modeling a real test case on the Thorpe-Marsh/Brinsworth system. The only way to find out the correctness of the modeled component is to compare the simulation results with the real field test recording results, in terms of 3-phase voltages and currents for both the Period-1 and Period-3 ferroresonance. An attempt in improving the deviation from the real measurement results is also conducted.

The second objective is to identify which parameter in the transmission system is the key parameter to cause ferroresonance to occur. Three components are believed to dominant the influence of ferroresonance; they are the transformer's coupling capacitor, the cable capacitors and the transmission line coupling capacitors. The transmission line is modeled as a lumped element in PI representation. The way to find out their influence is by simulating the system stage by stage without firstly including the transformer's coupling capacitors and then secondly simulating the system without the presence of cable capacitance, and finally looking into the individual capacitors of the line.

Chapter 6: Modeling of 400 kV Iron-Action/Melksham System

Following the modeling experiences which are gained from Chapter 5, modeling of another real case system "Iron-Acton/Melksham system" is carried out in this chapter. The system is believed to have potential risk of initiating Period-1 ferroresonance because of the complex arrangement of the mesh-corner substation. The inquiry from National Grid is to evaluate the system whether there is any likelihood of occurrence Period-1 ferroresonance. If it does, a mitigation measure by employing a shunt reactor connected to the 13 kV winding is suggested to switch-in. The power rating of shunt reactor is chosen according to a series of evaluations so that the ferroresonance is effectively suppressed without any failure. In addition, sensitivity study on transmission line lengths is also carried out to determine the probability function of occurrence of various ferroresonance modes.

Chapter 7: Conclusion and Future work

In this last chapter, the conclusion for each chapter is drawn along with the papers published as a result of this work. The contribution towards the users about this work and finally the room for future work is highlighted.

CHAPTER 2

2. LITERATURE REVIEW

2.1 Introduction

This chapter presents a survey of different approaches for power system ferroresonance study, particularly looking into the modeling aspects of each of the component in the integrated power system. The most appropriate "Fit for Purpose" way of modeling a power system network is firstly comparing the simulation results with the recorded field test results. If the simulation results are beyond expectation then there is work to be done to rectify the problems in terms of individual components modelling for justifications.

There are five different approaches for the study of ferroresonance in the literatures which have been identified and they are explained as follows.

2.2 Analytical Approach

A substantial amount of analytical work has been presented in the literature employing various mathematical methods to study ferroresonance in power systems. The following presents some of the work which has been found in [10-12, 21-24].

A series of paper published by ***Emin*** **and** ***Milicevic*** [10-12, 21, 22] investigated a circuit configuration as shown in Figure 2.1 where ferroresonance incidence was induced onto the 100 VA voltage transformer situated in London. The circuit was reconfigured into a ferroresonance circuit due to the opening of the circuit breaker and disconnector 2 leaving the transformer connected to the supply via the grading capacitor of the circuit breaker.

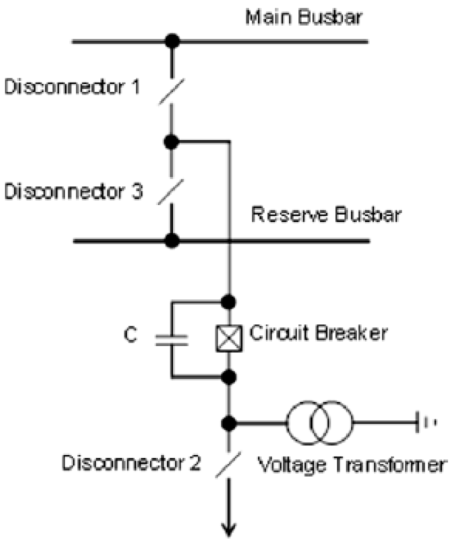

Figure 2.1: Section of a typical double-busbar 275 kV substation [12]

Following the switching events, the circuit of Figure 2.1 was then represented by its single-phase equivalent circuit of Figure 2.2 consisting of a voltage source connected to a voltage transformer with core losses (*R*), via grading capacitor (C_{series}) and phase-to-earth capacitance (C_{shunt}).

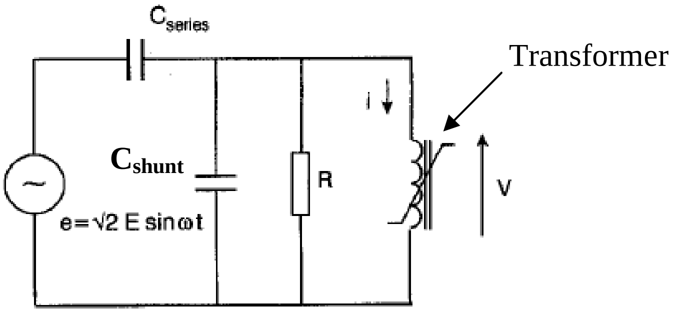

Figure 2.2: Section of a typical double-busbar 275 kV substation [11]

The transformer core characteristic was represented by a single-valued 7th order polynomial $i = a\lambda + b\lambda^7$ where $a = 3.24$ and $b = 0.41$. The mathematical representation of the circuit of Figure 2.2 is expressed by the following differential equation,

$$\frac{1}{\omega}\frac{dV}{dt} + \frac{V}{R\omega(C_{series} + C_{shunt})} + \frac{\left(a\lambda + b\lambda^7\right)}{\omega(C_{series} + C_{shunt})} = \frac{C_{series}}{(C_{series} + C_{shunt})}\sqrt{2}E\cos\theta \quad (2.1)$$

$$\frac{d\lambda}{dt} = V \text{ and } \frac{d\theta}{dt} = \omega \quad (2.2)$$

Where i= transformer current, λ = transformer flux-linkage, V= voltage across transformer, E = voltgae of the source and ω= frequency of the voltage source.

The solutions to the system equations were solved by using a Runge-Kutta-Fehlberg algorithm. The aim of developing the simulation model was to study how the losses would affect the initiation of ferroresonance. With the loss reduced to about mid way (*R* = 275 kV/120 W) of the rated one (*R* = 275 kV/250 W), a fundamental frequency ferroresonant mode has been induced into the system. When the loss reduced further to *R* = 275 kV/99 W, a subharmonic mode of 25 Hz was exhibited. However, when the loss was unrealistically varied to 8 W, the voltage signal with stochastic manner has been produced.

The paper written by ***Mozaffari, Henschel and Soudack*** [23, 25] studied a typical system of Figure 2.3 that can result in the occurrence of ferroresonance. The configuration of the system consisted of a 25 MVA, 110/44/4 kV three-phase autotransformer connecting to a 100 km length transmission line which included the line-to-line and the line-to-ground capacitances. The secondary side of the transformer is assumed to be connected at no-loaded or light-load condition. In addition the delta tertiary winding side is assumed to be open-circuited.

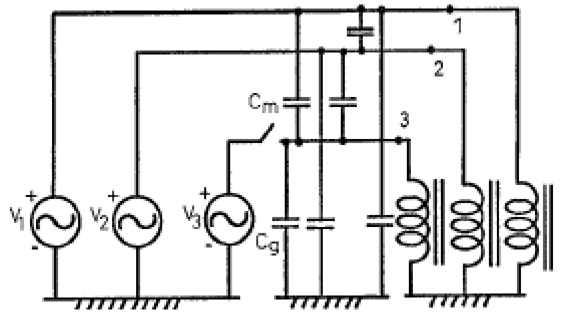

Figure 2.3: Model for ferroresonance circuit including line capacitance [25]

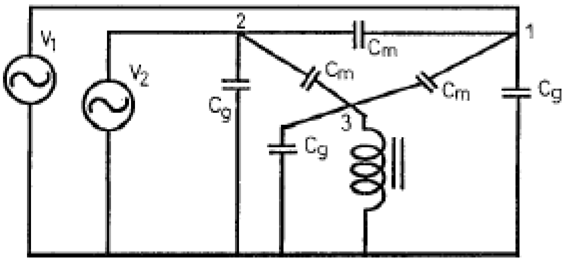

Figure 2.4: Circuit that feeds the disconnected coil [25]

The way the system has been reconfigured into ferroresonance condition is to open one of the phase conductors via a switch as can be seen from the diagram and its simplified circuit is shown in Figure 2.4. This circuit is then further simplified by applying a Thevenin's theorem by considering node 3 as the Thevenin's terminals with respect to ground, with the assumption that $V_1 = V_2$. Then the Thevenin's equivalent capacitance and voltage are

$$C = C_g + 2C_m \text{ and } E = V_1 \frac{C_m}{C_g + 2C_m} \tag{2.3}$$

Finally the single-phase Thevenin's equivalent circuit can be represented as shown in Figure 2.5 and it was modeled by using the second order flux-linkage differential equation.

$$\frac{d^2\phi}{dt^2} + \frac{1}{RC}\frac{d\phi}{dt} + \frac{1}{C}\left(a\phi + b\phi^n\right) = \omega_s E \cos\left(\omega_s t\right) \tag{2.4}$$

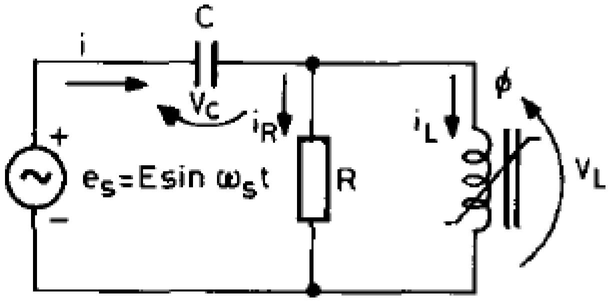

Figure 2.5: Basic ferroresonance circuit [25]

Where C_g = line-to-ground capacitor, C_m = line-to-line capacitor, C = Thevenin's capacitance, V_1 = supply voltage at line 1, ϕ = flux in the transformer core, ω_s = power frequency and E = supply voltage of the source.

The objective of the study was to investigate the influence of magnetisation core behavior with n^{th} order polynomial with n varying from 5 and 11 when the transformer is subjected to ferroresonance. Moreover, the effects of varying the magnitude of the supply voltage (E) and core losses were also studied. The solutions to the problems were carried out by using fourth-order Runge-Kutta method. The effects of varying the magnitude of the supply voltage, E while keeping the transformer losses and transmission line length unchanged for the degree of saturation n = 5 and 11 are presented as shown in the Bifurcation diagrams of Figure 2.6. Note that a Bifurcation diagram is a plot of the magnitudes taken from a family of Poincarè plot versus the parameters of the system being varied. In this case, the parameter being varied is the magnitude of the supply voltage, E with an aim to predict the different types of ferroresonance modes. Two degree of saturation with n=5 and 11 are investigated to see their differences in terms of inducing types of ferroresonance modes.

Table 2.1 shows the detailed parameters the system stands for when such study was carried out and the results from the calculations are shown in Figure 2.6 with the top one represents *n*=5 and the bottom is *n*=11.

Table 2.1: Effects of supply voltage, *E* on ferroresonance

Degree of saturation *(n)*	**Transformer losses**	**Transmission line length**	**Supply voltage (*E*)**	**Observations**
5	1% (R = 48.4 kΩ)	100 km	0.1875 p.u to 7.5 p.u	Figure 2.6 (Top diagram)
11				Figure 2.6 (Bottom diagram)

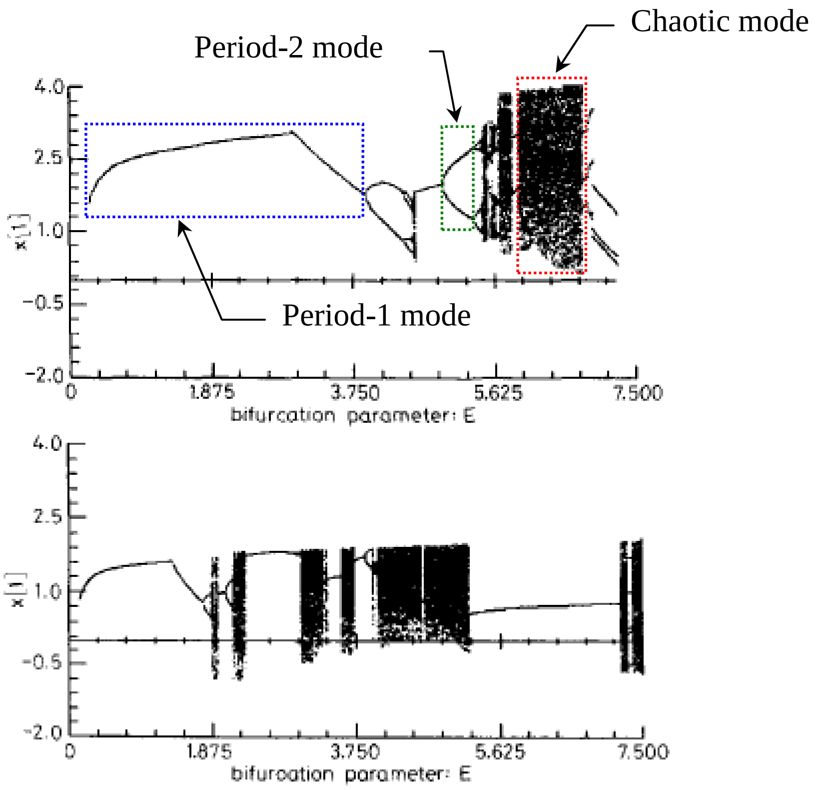
Chaotic mode

Period-2 mode

Period-1 mode

Figure 2.6: Bifurcation diagrams- Top: *n* = 5, Bottom: *n* = 11 [23]

The results of Figure 2.6 show that both saturations exhibited single-value area which indicates Period-1, dual value for Period-2 etc. One observation in the diagrams is that subharmonic plays an important role before the occurrence of chaotic mode. The study also suggested that different degrees of saturations of the transformer core characteristics have a significant impact of inducing different types of ferroresonance modes. In the study of varying the magnetising losses, it was found that Period-1 ferroresonance exists for *n* = 11 with the losses of 1%. The onset of Period-2 and Period-4 ferroresonance occurred when the losses was reduced further. However, the onset of chaotic mode occurred when the losses is further below 0.0004%. On the other hand when *n* = 5 with the losses of 0.0005%, Period-1 mode has been exhibited.

Tsao [24] published a paper in 2006 describing the power outage which occurred at the station was considered to be the most severe incident in the history of Taiwan. The cause of the catastrophic event is explained by referring to the single-line diagram of the Maanshan Nuclear Power Station (MNPS) depicted in Figure 2.7. Note that the shaded and the white boxes in the diagram represent the close and open states of the circuit breakers.

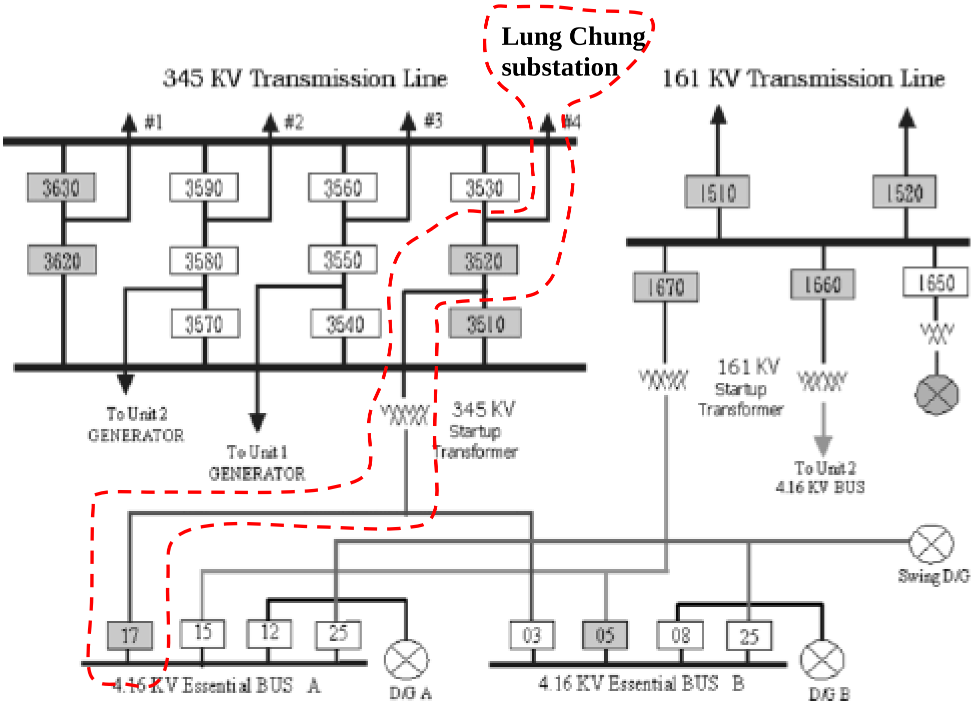

Figure 2.7: Distribution system of 4.16 kV essential bus at MNPS [24]

The initial cause of the outage was due to the accumulation of salt pollution over the insulator of the 345 kV transmission line. As a result of that, it was reported that more than 20 flashovers had occurred on the transmission line. This incident had eventually caused widespread problems of creating 23 switching surges and failure of two generators. One particular problem of interest was the flashover of the 345 kV transmission line #4 resulting in the gas circuit breaker at the Lung Chung substation tripped spontaneously, leaving the gas circuit breaker, 3520 and 3530 failed to trip because of the fault current cannot be detected. The outcome of this event has thus reconfigured part of the circuit (marked in red line of Figure 2.7) into an island system of Figure 2.8. Because of that, ferroresonance was then induced into the system and hence causing system outage.

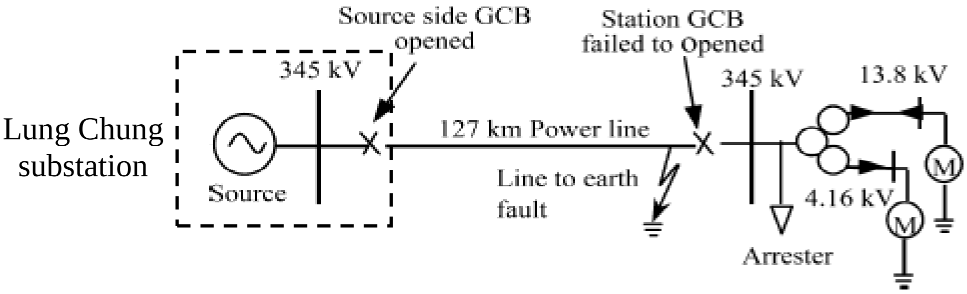

Figure 2.8: Island system at MNPS [24]

As can be seen in Figure 2.8, there were no voltage sources attached into the system and how could ferroresonance be possible to occur? The generating effect took place when the Reactor Coolanr Pump (RCP) motors have been interacted with the 127 km transmission line's coupling capacitances. Hence, the motor acts like an induction generator. Owing to that, the system thus reconfigured into a circuit consisting of voltage source, transformer and transmission line's capacitances, which are considered to be the main interaction components for ferroresonance condition. The ferroresonance condition circuit for the island system is shown in Figure 2.9.

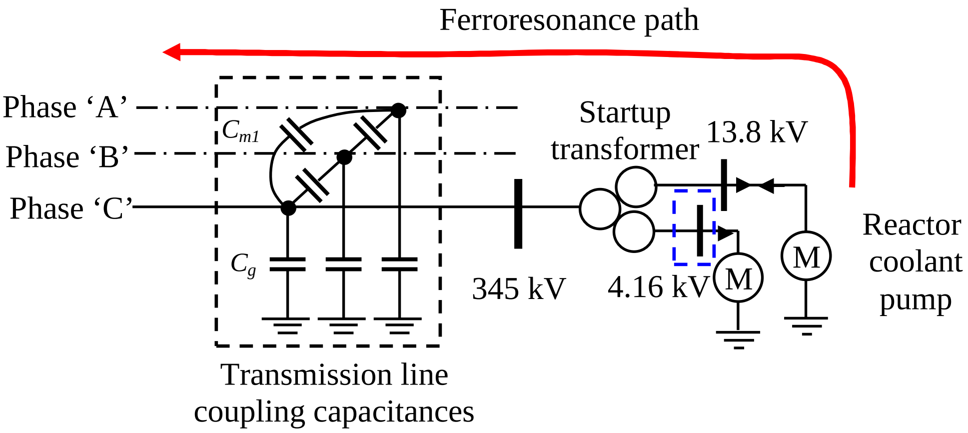

Figure 2.9: Ferroresonance condition - Island system at MNPS

The sequence of event in the system is shown in Figure 2.10. Initially at time t0 to t1, a flashover to ground had occurred at phase B and during that time the gas circuit breaker at Lung Chung substation had tripped but the ones from the supply side (i.e. 3520 and 3530) failed to trip thus reconfigured part of the network including the 127 km transmission line into islanding. In between t1 and t2, the overvoltage was produced from the generating effect due to the interaction between RCP motor and the transmission line coupling capacitances but the amplitude had been cut-off by the arrester to 1.4 per-units. Between t2 and t3, the phase A to phase B flashover and then to ground occurred due to the overvoltage thus all the four 4.16 kV bus tripped off because of under-voltage protection. This is followed by in between t3 and t4, two of the three 13.8 kV buses (consists of RCP and several motors) tripped, also due to under-voltage protection.

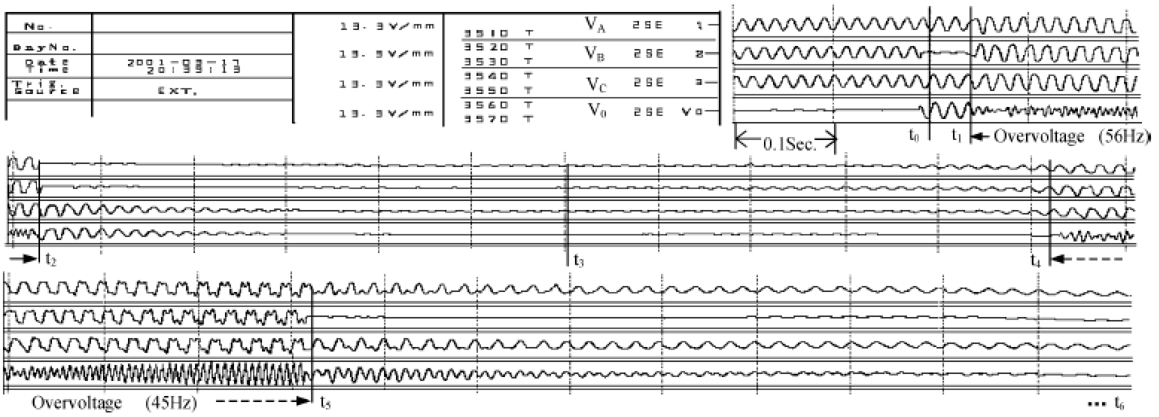

Figure 2.10: Oscillogram at the MNPS 345 kV switchyard [24]

In between t4 and t5, ferroresonance oscillation occurred due to the remaining 13.8 kV bus acting as generating effect interacting with the transformer and line coupling capacitance. The overvoltage was then clipped-off to 1.4 per-units by the arrester connected at the high voltage side of the transformer. During that instant, the overvoltage directly attacked the bushing of the air circuit breaker (#17) and it was found that the power-side connection end was badly destroyed. The cause of the damage was due to the cumulative effect of premature aging of the insulation as the breaker had been in service for 24 years. At the t5 and t6 interval, flashover occurred again at phase B due to the salt smog which is 4 km away from MNPS switchyard. Finally at t6, the remaining of the RCP on the 13.8 kV bus tripped and the incident ended.

Following the occurrence of islanding part of the network and the consequences as mentioned above, the root cause of the problem was investigated by modeling the network using mathematical equations. The mathematical expression to represent the power transformer is given as

$$\begin{bmatrix} V_{1t} \\ V_{2t} \end{bmatrix} = \begin{bmatrix} R_{1t} & 0 \\ 0 & R_{2t} \end{bmatrix} \begin{bmatrix} I_{1t} \\ I_{2t} \end{bmatrix} + \begin{bmatrix} L_{11t} & L_{12t} \\ L_{21t} & L_{22t} \end{bmatrix} \frac{d}{dt} \begin{bmatrix} I_{1t} \\ I_{2t} \end{bmatrix} \tag{2.5}$$

Where V_{1t}, V_{2t} = primary and secondary terminal voltages, I_{1t}, I_{2t} = primary and secondary currents, R_{1t}, R_{2t} = resistance at primary and secondary windings, L_{11t}, L_{22t} = self inductance at primary and secondary windings, L_{12t}, L_{21t} = mutual inductance between primar and secondary windings.

For the voltage equation to model an induction motor is expressed as

$$\begin{bmatrix} V_{sm} \\ V_{rm} \end{bmatrix} = \begin{bmatrix} R_{sm} & 0 \\ 0 & R_{rm} \end{bmatrix} \begin{bmatrix} I_{sm} \\ I_{rm} \end{bmatrix} + \begin{bmatrix} L_{ssm} & L_{srm} \\ L_{rsm} & L_{rrm} \end{bmatrix} \frac{d}{dt} \begin{bmatrix} I_{sm} \\ I_{rm} \end{bmatrix} + \omega_{rm} \begin{bmatrix} 0 & G_{srm} \\ G_{rsm} & 0 \end{bmatrix} \begin{bmatrix} I_{sm} \\ I_{rm} \end{bmatrix} \tag{2.6}$$

where V_{sm} = stator voltage, V_{rm} = rotor volatage, R_{sm} = resistance of stator, R_{rm} = resistance of rotor, L_{sm} = inductance of stator, L_{rm} = inductance of rotor, ω_{rm} = rotor speed, G = rotational performance of a rotational machine, called rotational inductance matrix.

The transmission line was modeled by connecting several equal PI sections in series to represent an approximate distributed line parameter. Then each of the models is combined to form a multi-machine interconnected system equation. Then, Runge-Kutta numerical and step-length integration method was employed to solve the set of first order differential equations.

The analytical method employed in the above literatures has the advantages of studying the parameters which influence the initiation of different ferroresonant modes. In addition, the boundaries between safe and ferroresonance regions can also be performed to determine the margins of parameters, which are required for system planning stage. However, the major drawbacks are that the circuit model is over simplified, and the mathematical equations involved are complex and require large computation time. In addition, its drawback is that the switching operations and the associated transient stage can not be considered.

2.3 Analog Simulation Approach

There are a number of analogue simulation approaches which have been employed to represent power systems for ferroresonance studies. The use of Electronic Differential Analyser (EDA), Analog Computer (ANACOM) and Transient Network Analyser (TNA) are among the miniature setups which have been considered in the past.

A paper published by ***Dolan*** [15] in 1972 documented a ferroresonance event of 1000 MVA 525/241.5 kV, 60 Hz Y-connected bank auto transformers, sited at the Big Eddy substation near Dallas, Oregon. The affected transformer in the substation connects to a transmission system as shown in Figure 2.11. The network consists of a 30.5 km un-transposed transmission line connected between John Day and Big Eddy substation. The phase ‘c’ of the John Day/Big Eddy line is run in parallel with phase ‘a’ of the line towards Oregon City. The distance between the two adjacent phases is 30.5 m apart. In 1969, the John Day/Big Eddy line had been isolated for maintenance purpose. The usual procedure to de-energise the John Day/Big Eddy line is to firstly open the high voltage side (525 kV) circuit breaker at John Day and then follow by opening the 230-kV breaker at Big Eddy substation. Ferroresonance path as marked in the dotted line is developed as shown in Figure 2.12.

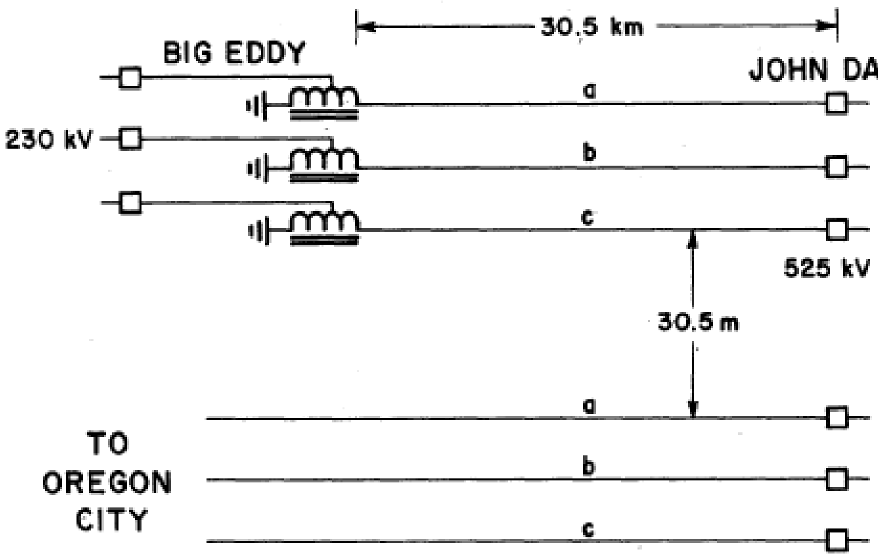

Figure 2.11: The Big Eddy and John Day transmission system [15]

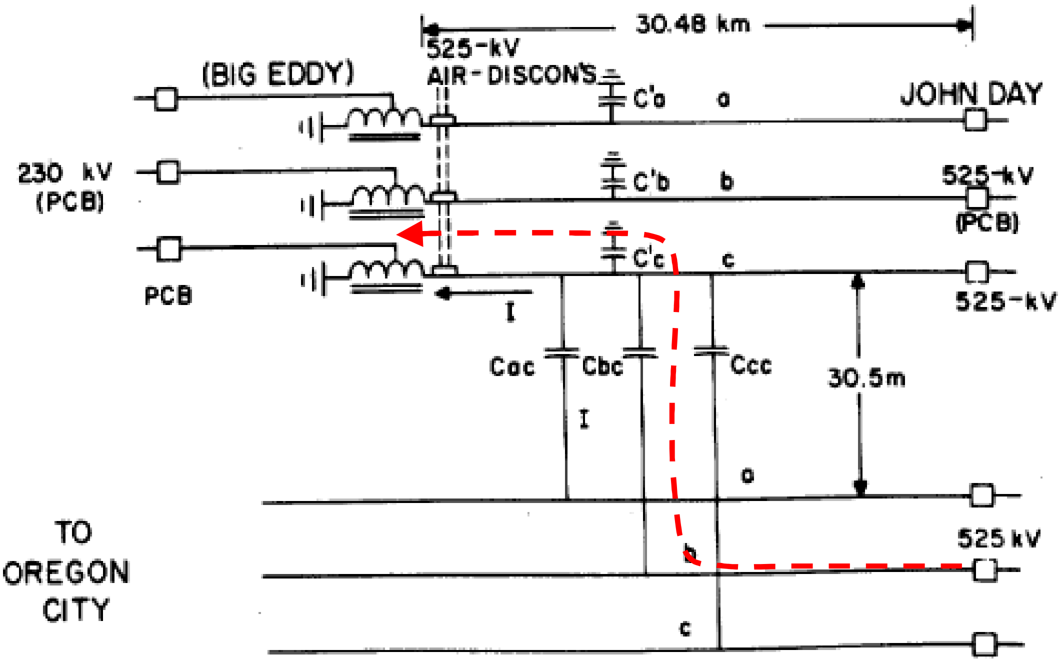

Figure 2.12: The Big Eddy/John Day system including coupling capacitances [15]

Following the occurrence of ferroresonance incidence, an analog simulator employed an Electronic Differential Analyser (EDA) was then used to investigate the cause of the phenomenon and the method to mitigate it. The equivalent representation of the affected system of Figure 2.11 was shown in Figure 2.13 in the EDA equipment.

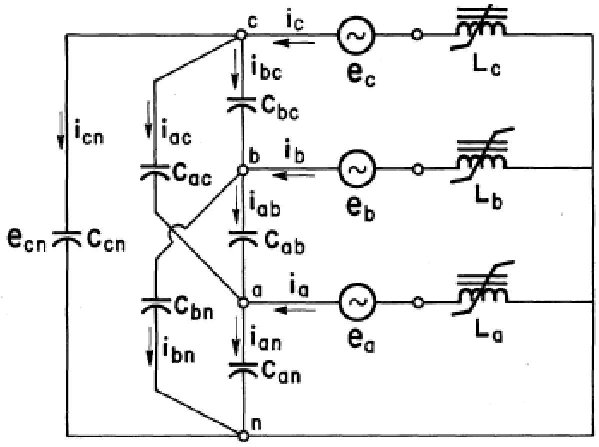

Figure 2.13: Equivalent circuit of Big Eddy and John Day 525/241.5 kV system [15]

The core characteristic of the transformer was represented by two slopes to account for the saturation curve. The iron loss was represented by a shunt resistor however the copper loss was not taken into consideration. As the exact core characteristic such as the knee point and the two slopes were unknown therefore the way it was determined was to carry out repeatedly variation of saturation curve until a sustained fundamental ferroresonance has been found. Once the miniature model has been setup then ferroresonance study is performed. The outcomes from the experiment are explained as follows:

(1) It was found that ferroresonance has been damped out when a closed delta connection was employed.

(2) Ferroresonance suppression has been found to speed up when a suitable value of resistor is connected in series with the delta-connected windings.

A paper presented in 1959 by ***Karlicek*** **and** ***Taylor*** [26] described a ferroresonance study by considering a typical connection of potential transformer for ground fault protection arrangement as shown in Figure 2.14.

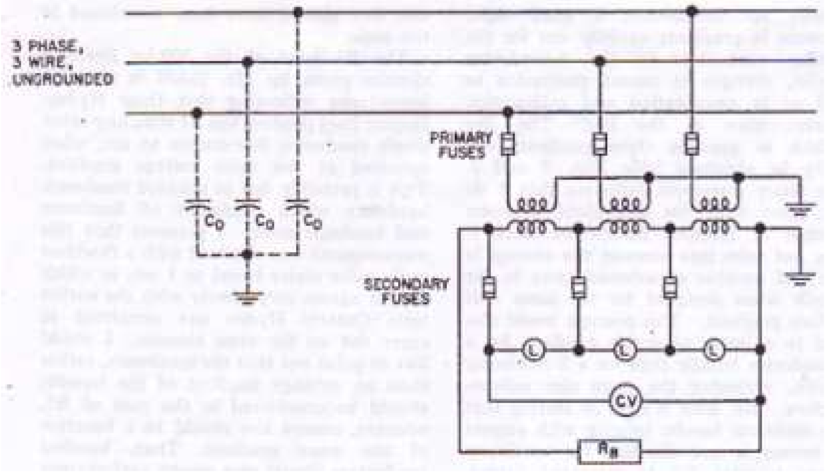

Figure 2.14: Typical connection of potential transformer used in a ground-fault detector scheme on 3-phase 3-wire ungrounded power system [26]

The circuit consists of three potential transformers configured into wye-ground broken-delta. The three lamps that are connected at the delta side are used as an indication for detecting the occurrence of any ground faults. In addition, the voltage relay (CV) connected at this winding is used for alarm triggering and breaker tripping. Under switching operations or arcing ground fault condition, unbalanced voltage occurred hence ferroresonance can be initiated between the nonlinear impedance of the transformer and the capacitance-to-ground of the circuit. In view of this, an analog computer called ANACOM was used to investigate the ferroresonance study and its mitigation measures. The analog simulation model was represented as shown in Figure 2.15.

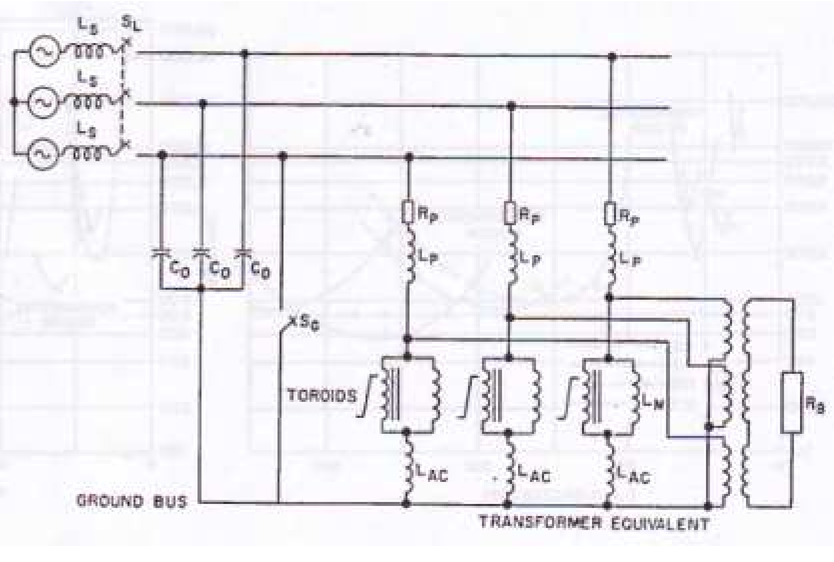

Figure 2.15: Anacom circuit to represent circuit of Figure 2.5 [26]

As can be seen from the figure, the adjustable lumped capacitance, C_o represents the distributed capacitance to ground of the power system and the source inductance by L_s. The saturable toroids connected in parallel with high magnetising reactance, and in series connection with linear inductor, L_{ac} are used to model the three potential transformers. The saturable toroids are used to represent flux switches. For a low voltage (i.e. flux) then the magnetising inductance is connected in parallel with L_m. For saturation region, the inductance of the toroids is small hence shorting L_m. L_{AC} are used to serve as adjusting the equivalent saturated or air-cored inductance. With this approach, the saturation curve for various transformers can be determined. The way to initiate ferroresonant oscillation was to firstly energise the circuit by closing the switch, S_L and then this is followed by momentary closing and opening the grounding switch, S_G. The resistance, R_B connected at the broken delta was used to damp out ferroresonance.

Papers published by ***Hopkison*** in [27, 28] presented his study on the initiation of ferroresonance under the event of single-phase switching of distribution transformer bank. Figure 2.16 shows the circuit which consists of a three-phase source, single-phase switching, an overhead line and a 3-phase transformer in wye-delta configuration.

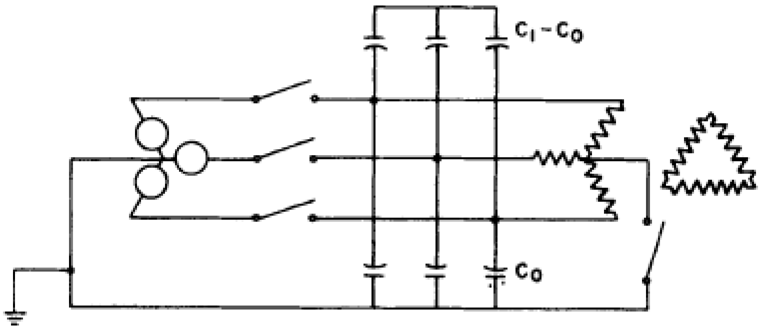

Figure 2.16: Possible ferroresonance circuit [27]

The transmission line of the system was represented by only its capacitances which include the ground capacitance, C_0 while the phase-to-phase capacitance was modeled as C_1-C_0, where C_1 and C_0 are the positive-sequence and zero-sequence capacitance respectively. It was assumed that the rest of the components such as the impedance (resistance and the inductance) of the line were negligible as compared to the capacitances.

The objectives of modeling the system were to determine the influence of various kVA ratings of transformers and voltage levels on ferroresonance. In addition, a number of practical ways of preventing ferroresonance were also investigated. In order to conduct these studies, the system of Figure 2.16 was modeled in Transient Network Analyser (TNA) as shown in Figure 2.17.

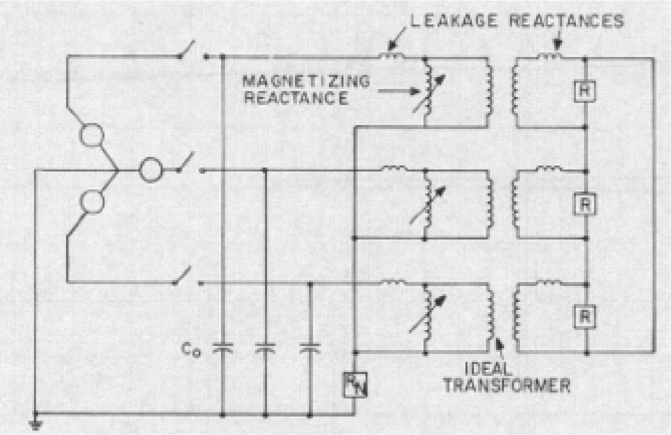

Figure 2.17: Three-phase equivalent system [28]

Modeling of transformer core was based on the voltage versus exciting current curve. The capacitances of winding terminals and ground (core and tank) were taken into consideration. These capacitances were determined based on geometrical relations using field theory. The conclusions are summarised as follows:

(1) Various kVA transformer ratings and voltage levels: results clearly showed that the lower kVA transformer ratings at the higher voltage levels are highly susceptible to encounter overvoltages.

(2) Several possible remedies:

- *Grounding the neutral*: resulted with normal steady-state with no overvoltages.
- *Opening one corner of delta*: resulted maximum overvoltages of twice the normal.
- *Grounding the neutral of delta*: resulted no overvoltages.
- *Using delta-delta connection*: resulted of 1.6 p.u of normal voltage from one phase energised.
- *Connecting the bank open-wye-open-delta*: resulted with no overvoltages.
- *Connecting shunt capacitors from each phase to ground*: resulted overvoltages as high as more than 4 p.u.

- *Using neutral resistor*: resulted no overvoltages if an appropriate value of the resistor is selected.
- *Using resistive load connected across each delta*: resulted no overvoltages if an appropriate value of the resistor is selected.

The employment of analog simulators such as the Electronic Differential Analyser (EDA), the Analog Computer (ANACOM) and the Transient Network Analyser (TNA) for ferroresonance study have their advantages and disadvantages. It offers great flexibility in representing the power system into a scaled down real circuit. This approach also provides better personal health and safe environment for testing, when we considered only low voltage and current magnitudes are used in the experiments. However, the major drawbacks are that the analog equipment required costly maintenance (calibration, replacement of ageing or faulty components) and also required large laboratory floor space to accommodate the equipment.

2.4 Real Field Test Approach

Real power system components such as transformers, transmission lines, circuit breakers, disconnectors, cables have been employed in existing circuit configurations for ferroresonance study. [29] reported the ways they carried out the ferroresonance tests.

Based on the technical report ***TR-3N*** documented in [29], a ferroresonant test was carried out in one of the National Grids' 400 kV transmission systems. The main aim of the test was to evaluate the breaking capability of two types of disconnector designs to break the ferroresonant current. The system consists of the circuit configuration as shown in Figure 5.1, in Chapter 5.

Prior to the test, the disconnector X303 at Thorpe Marsh 400 kV substation was kept open, the circuit breaker T10 at the Brinsworth 275 kV substation was kept open and all disconnectors and circuit breaker X420 are in service. The way the circuit subjected to the trigger of ferroresonance was to carry out point-on-wave (POW) switching using circuit breaker X420 at Brinsworth 400 kV substation. The opening of the X420 circuit breaker has thus energised the 1000 MVA power transformer via the transmission line's coupling capacitances. From the tests, a subharmonic mode ferroresonance of $16^{2/3}$ Hz has been triggered at +3 ms POW, showing the disconnector current and busbar voltage of 50 A_{peak} (Y-phase) and 100 kV_{peak} (Y-phase) respectively. In addition, a grumbling noise was reported from the affected transformer. In contrast to the onset of fundamental mode, the initiation was triggered at +11 ms POW, hence the induced current and voltage was 200 A_{peak} (Y-phase) and 300 kV_{peak} (Y-phase) respectively. Furthermore, a much louder grumbling noise has been generated from the transformer which can be heard at a distance of 50 m from the transformer. The voltage and current waveforms of both the modes are shown in Figure 5.2 and 5.3 in Chapter 5.

Both the phenomena have been successfully quenched by using the disconnectors however little arc has been observed for the subharmonic mode which can be seen in Figure 2.18. On the other hand, much more intense arc has been viewed for the fundamental mode which can be seen in Figure 2.19. One interesting point which has been noted here in this ferroresonant test is that when a second test was carried out by setting to +11 ms POW, the same switching angle at which fundamental mode was previously successfully triggered. However, ferroresonance failed to onset in the second test, not even the present of subharmonic mode ferroresonance. This clearly indicates that the onset of ferroresonance is difficult to predict.

Figure 2.18: Subharmonic mode ferroresonance quenching [29]

Figure 2.19: Fundamental mode ferroresonance quenching [29]

Real field ferroresonance tests employed in the existing power circuit configurations provide an advantage of including sophisticated and complex inherent elements of the full scale power components, without any circuit simplification. However, the major drawbacks are that the power components are put in a greater risk exposed to overvoltage which could cause a premature ageing and a possible catastrophic failure. In addition, the generation of harmonic signals from the tests can also cause problem to other neighboring systems.

2.5 Laboratory Measurement Approach

In this section, the study of ferroresonance used a simple low or medium voltage circuit to carry out experiments in laboratory. Ferroresonance study using this method has been found in the literatures [30, 31].

A laboratory work performed by ***Young*** [30] was to investigate the ferroresonance occurred in cable feed transformers. The laboratory setup for the circuit is shown in Figure 2.20 consisting of cable connected to a three-phase, 13 kV pad-mount distribution transformer. The transformer was energised via the three single-phase switches (denoted as load break cut-out) connected to the 13 kV grounded source. The cable was modeled by using capacitor modules connected at the terminal of the transformer.

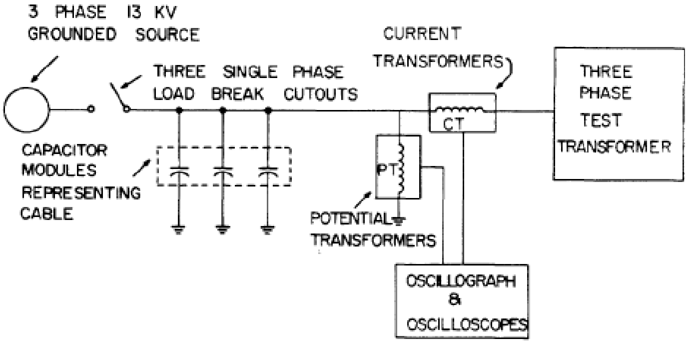

Figure 2.20: Laboratory setup [30]

The main aims of the laboratory set up were to investigate the influence of the following parameters on ferroresonance: (1) Transformer primary winding in delta, wye-ground, wye-ungrounded, and T connections, (2) The energisation and de-energisation of the transformer via switch (3) Cable lengths ranging from 100 to 5000 feet and (4) The damping resistance was varied from 0 to 4 % of the transformer rating. After the tests, the results were reported as follows:

- Ferroresonance overvoltages are more likely to occur when the test transformer was connected at no-load, for cable length of more than 100 feet.

- It has been recorded that the magnitudes of 2 to 4 p.u have been reached for the sustained voltage and up to 4 p.u for the transient voltage for delta and ungrounded wye-connected primary winding. On the other hand, the T-connected primary winding also produced the similar magnitudes for the sustained one but a magnitude as high as 9 p.u has been reached for the transient overvoltages.

- There has been no overvoltage produced following the single-phase switching of the test transformer employing the grounded-wye connection at the primary winding.

- The load of up to 4% of rated transformer power rating connected at the secondary side of the transformer was found to be effective in damping transient overvoltage. In addition, the probability for the sustained and transient voltages was found to be less likely to occur.

- The employment of the three-phase switching can eliminate the occurrence of ferroresonance.

- It has been observed that the T-connected winding transformer has provided a more likelihood for the occurrence of ferroresonance as compared to the delta and wye connections.

Another ferroresonance study based on laboratory was carried out by ***Roy*** in [31] . The way of the ferroresonance initiation in a 3-phase system of Figure 2.21 was to close one of the three switches, leaving the others open. The interaction between the circuit components which represents single-phase ferroresonance can be seen on the dotted line of Figure 2.21.

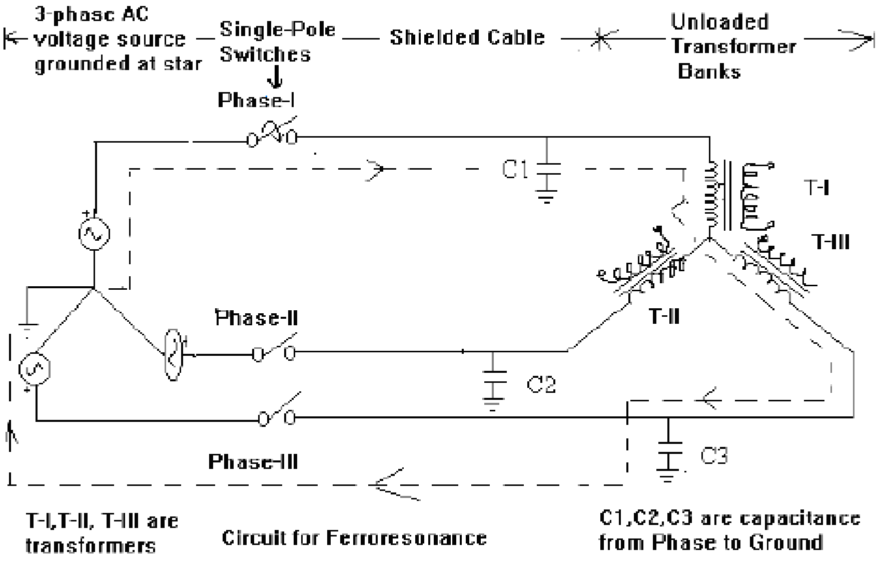

Figure 2.21: Transformer banks in series with capacitive impedance [31]

The single-phase circuit which has been set up for ferroresonance study is shown in Figure 2.22. The circuit consists of two single-phase transformer namely T-I and T-III connected in series with capacitor (C3) acting as the capacitance from phase-to-ground.

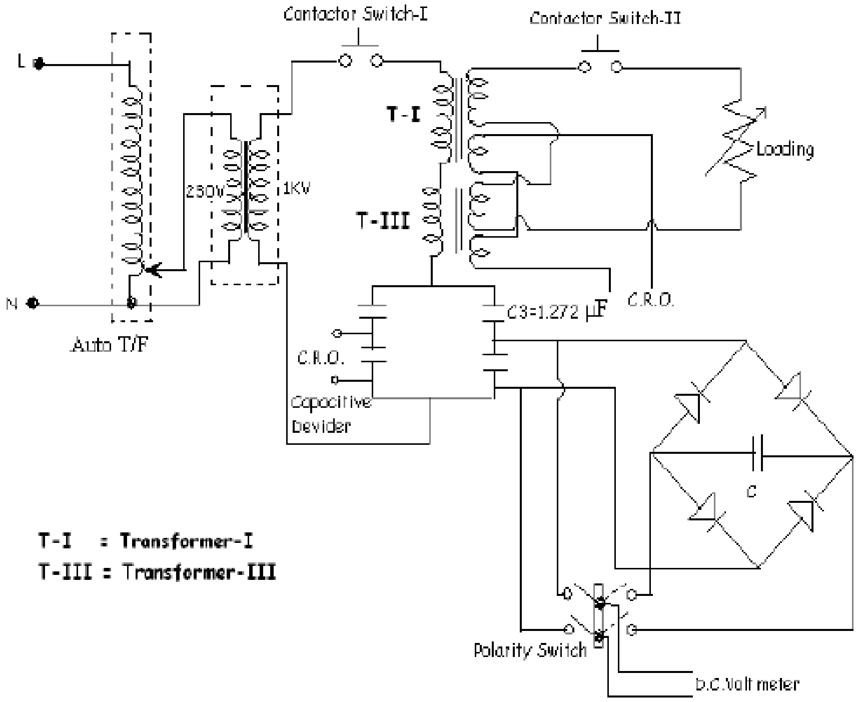

Figure 2.22: Transformers in series with capacitor (C3) for line model [31]

The type of ferroresonance studies which have been performed is described in the following. Firstly, to observe how the circuit response to ferroresonance when the supply voltage is allowed to vary, with or without stored charge in the capacitor. Secondly, the study with supply voltage fixed at 100% of the rated transformer with negative stored charges presents in the capacitor. Thirdly, the study of mitigation of ferroresonance by using damping resistor connected at the secondary side of the transformer. Finally, an interruption of short-circuit study was conducted by overloading the system with low resistance connected at the secondary side of the transformer. The results from the experiment are explained as follows:

(1) Supply voltage is varied:

- *Capacitor without stored charge*: Resulted no ferroresonance when the supply is 80% of the rated value of transformer. Sustained ferroresonance of 5.8 p.u occurred when the supply is 100% of the rated value of transformer.

- *Capacitor with negative stored charge*: It has resulted in a situation where capacitor voltage increased asymmetrically with positive value and approaching to a damaging voltage of 7.44 p.u.

- *Capacitor with positive stored charge*: This has resulted in the capacitor voltage being increased asymmetrically with negative amplitude of -7.31 p.u.

(2) Mitigation of ferroresonance by using damping resistor connected at the secondary side of the transformer

- *Initial stored charge = 0 V, applied voltage = 92% of rated transformer:* Initially, the ferroresonance has damped out when a load is applied at the secondary winding of the transformer but it reoccurs again when the load is removed from the transformer.

- *Initial stored charge = positive, applied voltage = 92% of rated transformer:* Even with the presence of the initial positive charge in the capacitor, the damping resistor will still be able to provide the damping effect. However, ferroresonance again re-built after removal of the resistor from the transformer.

(3) Interruption of short-circuit study by overloading the system with low resistance connected at the secondary side of the transformer

- A transient overvoltage of 4.11 p.u peak and then a sustained steady state voltage of 3.04 p.u have been noted before the fault has been interrupted. A sustained ferroresonance with voltage amplitude reached up to 6.02 p.u. has been induced when the low resistance load has been removed form the transformer.

Ferroresonance tests based on small scale laboratory setup have an advantage of studying the characteristics of ferroresonance of low-voltage equipment in a realistic manner.

2.6 Digital Computer Program Approach

An abundance of digital computer programs had employed for ferroresonance study. Some of which quoted from the literature in [13, 14, 16] can be referred in the following section.

Papers published by ***Escudero*** [13, 14] reported that a ferroresonance incident had occurred in the 400 kV substation consisting of the circuit arrangement as shown in Figure 2.23. The cause of the phenomenon was due to the switching events that have been carried out for commissioning of the new 400 kV substation.

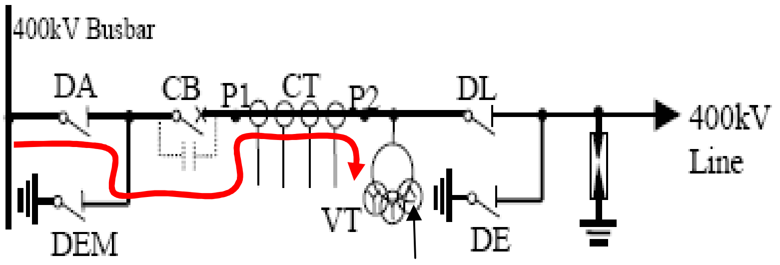

Damping resistor of 0.5 Ω connected in closed delta

Figure 2.23: 400 kV line bay [13, 14]

The commissioning of the system of Figure 2.23 was conducted as follows: the energisation of the VT's from the 400 kV busbar by disconnecting the line disconnector (DL) and then de-energised the VT's by opening the circuit breaker (CB). The effect after the switching events has thus reconfigured the circuit into ferroresonance condition involving the interaction between the circuit breaker's grading capacitor and the two voltage transformers.

Following the occurrence of ferroresonance as mentioned above and the failure of the damping resistor to suppress ferroresonance, an ATP/EMTP simulation package was employed to investigate the phenomena and to assess the mitigation alternative. The complete simulation model is shown in Figure 2.24.

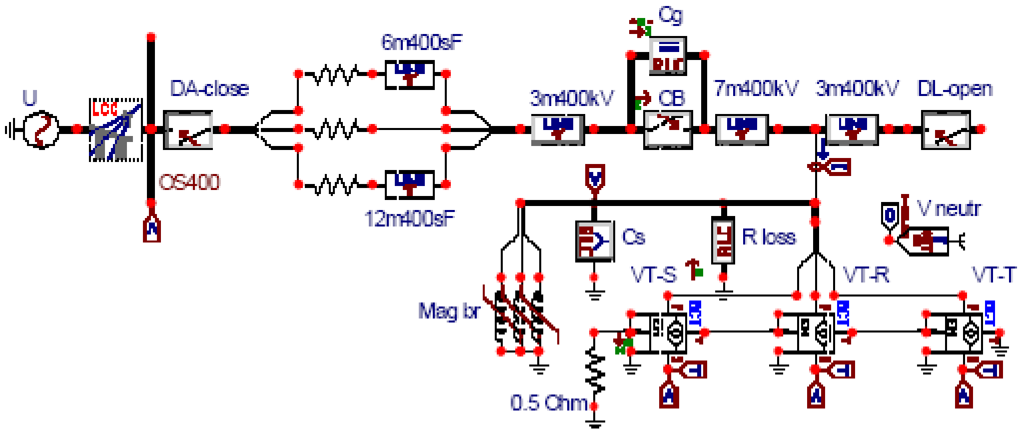

Figure 2.24: ATPDraw representation of 400 kV substation [14]

The voltage transformer was modeled with three single-phase transformer models using the BCTRAN+. The core characteristic of the transformer was externally modeled by using non-linear inductors with its saturation λ-i characteristic derived from SATURA supporting routine. The required data to convert into λ-i characteristic is obtained from the open-circuit test data given by the manufacturer. The hysteretic characteristic of the core was not taken into consideration because its measurement was not available for the type of transformer under study. The iron-losses were simply modeled by resistors.

An agreement between the recorded test measurement and simulation results was firstly obtained to justify the model before the key factors that influence the ferroresonance were analysed. The study was to investigate the types of ferroresonance modes when the length of busbar substation was varied, which corresponds to the capacitance value of busbar, with the grading capacitance kept unchanged. In addition, the safe operating area of busbar length was also identified. The results from the simulation studies are presented as follows:

For busbar substation capacitances:

(1) *10 pF - 100 pF and 950 pF - 2320 pF*: No ferroresonance has been identified for these ranges of capacitances. Normal steady-state responses have not been observed from the simulations.

(2) *110 pF - 950 pF*: Sustained fundamental mode ferroresonance have been induced with its amplitude reached up to 2.p.u.

(3) *2320 pF*: Subharmonic mode with Period-7 has been induced into the system. The frequency of the phenomenon is 7.1 Hz.

(4) *2590 pF*: In this case, the system responded to chaotic mode for about 4 seconds until it jumps into the normal steady-state 50 Hz response.

A paper published by ***Jacobson*** [16] investigated a severely damaged wound potential transformer caused by a sustained fundamental ferroresonance. The affected transformer is connected to the Dorsey bus which has the bus configuration as shown in Figure 2.25.

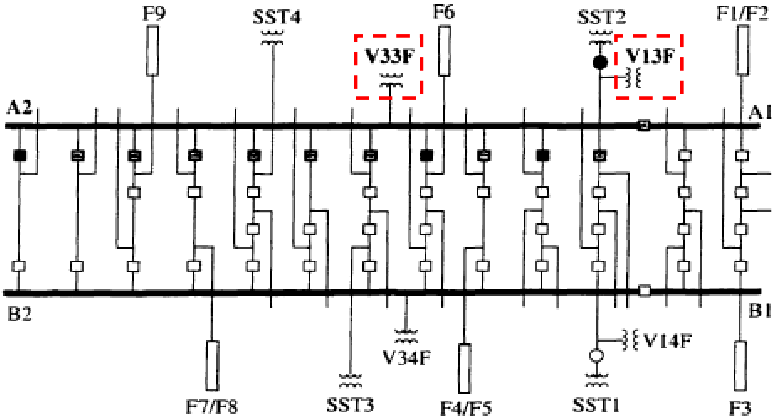

Figure 2.25: Dorsey bus configuration prior to explosion of potential transformer [16]

For the commission work and maintenance, Bus A2 was removed by opening the corresponding circuit breakers (shaded box of Figure 2.25) connected along side of Bus A2. After the switching events, one of the potential transformers (i.e. V13F) had undergone a disastrous failure and eventually exploded. The cause of the incidence can be clearly explained by referring to the diagram of Figure 2.26.

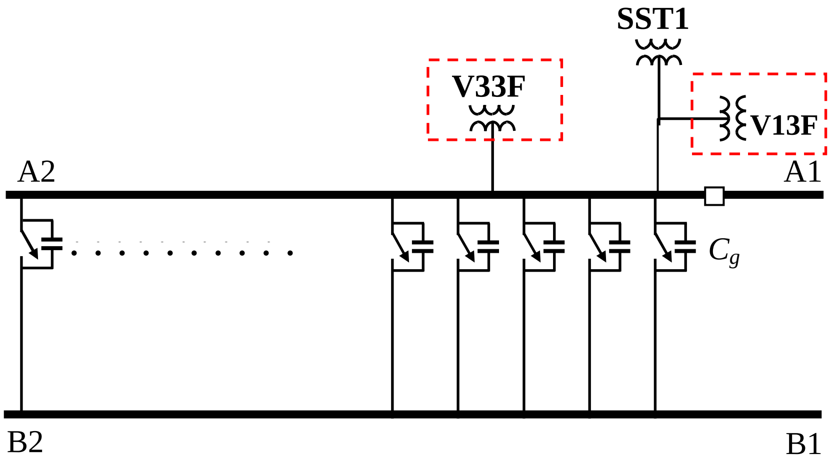

Figure 2.26: Dorsey bus configuration with grading capacitors (C_g)

The root cause of the problem was the existence of parallel connection of the grading capacitors of circuit breakers connected along bus A2 and B2 when the circuit breakers were open. The effect of this switching occasion has eventually reconfigured the Dorsey bus system into a ferroresonance condition consisting of the source, capacitance and transformers.

In view of the problem, a simulation model of Figure 2.27 using EMTP had been employed to duplicate the cause of the ferroresonance and also to investigate the best possible mitigation alternatives to rectify the problem. The system includes station service transformer (SST), two potential transformers (PT1 and PT2), equivalent grading capacitance of circuit breaker, bus capacitance between bus B2 and A2, and voltage source.

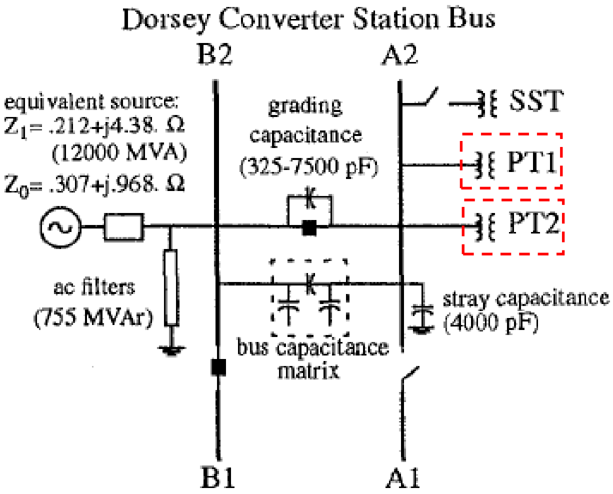

Figure 2.27: EMTP model – Main circuit components [16]

A strong equivalent source impedance has been employed to model the Dorsey bus terminal. The a.c filter is switched in at bus B2 and is used to assess its effectiveness of mitigating ferroresonance. The capacitances of the buses (i.e. bus B2 and A2) are also taken into consideration by referring to the geometry dimension of Figure 2.28.

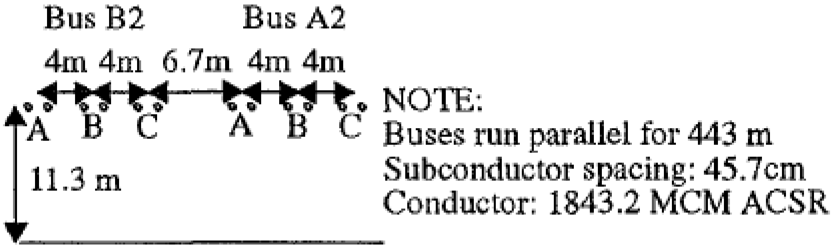

Figure 2.28: EMTP model – Bus model [16]

The 4-kVA potential transformers (PT1 and PT2) were modeled by considering core losses, winding resistance and excitation current with the circuit represented as shown in Figure 2.29. The iron losses have been represented by a constant resistance. The core characteristics of the transformers were modeled based on the manufacturer's data but the air-core (fully saturated) inductance of 62 H was assumed because it provides the ferroresonance response which is close to the field recording waveform.

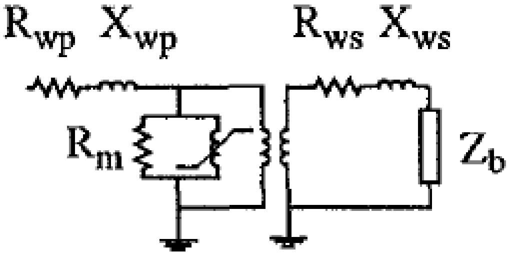

Figure 2.29: EMTP model – PT model [16]

On the other hand, the 10 MVA station service transformer (SST) was modeled based on the previous parameters taking into consideration of positive sequence impedance, core losses and the saturation characteristic. The air-core inductance has been provided by the manufacturer however the saturation curve is determined by applying extrapolation technique.

Once the ferroresonance response from the simulation is validated with the field recording one, ferroresonance study was then performed by considering the following recommendations:

(1) The study showed that the service station transformer (SST) has enough losses to damp out the occurrence of ferroresonance but this occurred at the grading capacitance of up to 4000 pF.

(2) A damping resistor of 200 Ω/phase was connected at the secondary side of SST to prevent this phenomenon if the grading capacitance has reach up to 7500 pF following circuit breakers upgrades.

Ferroresonance study employing digital simulation programs is considered to be inexpensive, maintenance free, does not required large floor space area, less time consuming and free from dangerous voltages and currents. However, one of the major disadvantages this approach encountered is that the true characteristic of the power components are difficult to fully and comprehensively represented in one of the predefined simulation models.

2.7 Summary

Five different approaches have been developed to study ferroresonance in the power system over many years. Each method has its own advantages and disadvantages and may be suitable at the time of its development. Table 2.2 summaries the advantages and disadvantages of each of the approaches.

Table 2.2: Advantages and disadvantages of each of the modeling approaches

Approach	**Advantages**	**Disadvantages**
Analytical method	- studying the parameters influence the initiation of different ferroresonant modes - the boundaries between safe and ferroresonant regions can be performed.	- circuit over simplified - involves complex mathematical equations - requires large computation time
Analog simulation	- offers great flexibility in representing the scaled down real circuit	- costly maintenance - requires large floor space to accommodate the equipment
Real field test	- including sophisticated and complex full scale power components without any circuit simplification.	- power components are put in a greater risk exposed to overvoltages and overcurrents - premature ageing and a possible catastrophic failure

Laboratory measurement	- studying the characteristics of ferroresonance of low-voltage equipment in a realistic manner	
Digital computer program	- inexpensive, maintenance free, does not required large floor area, less time consuming - free from dangerous overvoltages and overcurrents	- power system components are difficult to fully and comprehensively represented in a predefined simulation model alone.

.

In view of the computation power of modern computer and well-developed power system transient softwares, the current approach used in this thesis is to carry out simulation studies for understanding the network transients performance, to aid network design and to analyse the failure causes in the existing system.

CHAPTER 3

3. SINGLE-PHASE FERRORESONANCE – A CASE STUDY

3.1 Introduction

Ferroresonance has been identified as a nonlinear event which can cause damaging of power system equipment as a result of exhibiting overvoltages and overcurrents. In view of this, power network must function beyond the boundary of ferroresonant regions, and in addition minimise the likelihood of occurrence of such response when planning of expansion of network takes place. In order to achieve this, a comprehensive understanding of such phenomenon is essential for power system engineers, that is by looking into the variations of system parameters and transformer parameters which are known to directly influence ferroresonance response so as to gain a better understanding about its behaviour. As an initial stage of the current study, a single-phase ferroresonance equivalent circuit employing a potential transformer (PT) quoted in [16] is used as a case study. The studies aim to achieve the goals as follows:

(1) Identification of ferroresonant modes such as sustained fundamental, quasi-subharmonic, subharmonic and chaotic modes by varying both the grading and shunt capacitances for both high and low core nonlinearity characteristics.

(2) Suppression of sustained fundamental ferroresonant mode by having variation of core-losses introduced into the transformer core characteristic.

(3) Recognising the key parameters for providing initiation and sustainability of ferroresonance, particularly the sustained fundamental mode.

3.2 Single-Phase Circuit Configuration

Figure 3.1 shows the equivalent circuit of the studied potential transformer under load connected condition and the corresponding circuit arrangement.

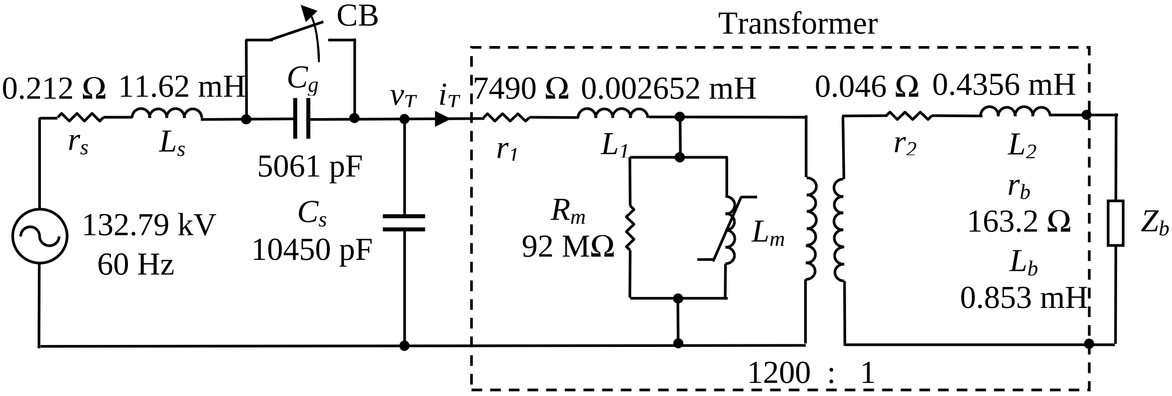

Figure 3.1: Single-phase ferroresonance circuit [16]

The primary side of the transformer is connected in series with a voltage source and a circuit breaker consisting of its grading capacitance (C_g). In addition, a ground capacitance (C_s) is also connected at the primary side of the transformer. The transformer includes primary and secondary winding resistance (r_1 and r_2) and leakage inductances (L_1 and L_2). The magnetising characteristic of this transformer is modeled by a nonlinear inductor (L_m), connected in parallel with a resistance (R_m) representing the core-losses. The secondary side of the transformer is connected with burden impedance, Z_b. This impedance is considered to be enormous if it is reflected to the primary side of the transformer and thus be much greater than the core impedance, which can be ignored. In view of this, the circuit under study has achieved the ferroresonance condition of interaction between capacitance and nonlinear inductor.

The magnetic behaviour of the transformer core is represented by a true non-linear inductor (L_m) to model the saturation effect which has the flux-linkage versus current characteristic as shown in Figure 3.2.

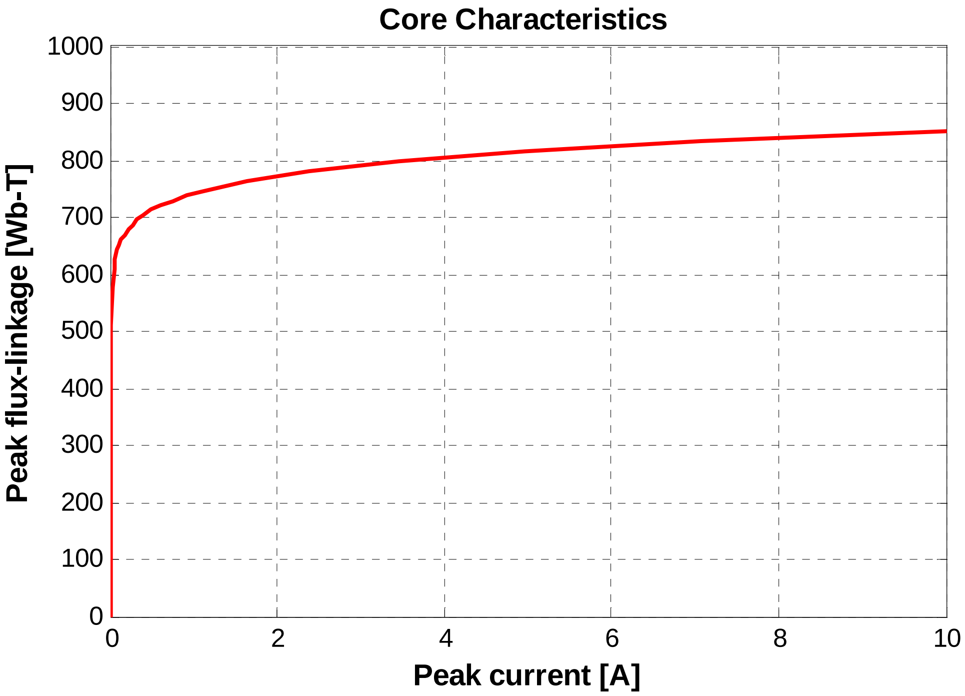

Figure 3.2: Magnetising characteristic [16]

With the parallel connection of both R_m and nonlinear inductance, L_m, the core characteristic of the transformer which now includes both the R_m and nonlinear L_m is depicted as shown in Figure 3.3.

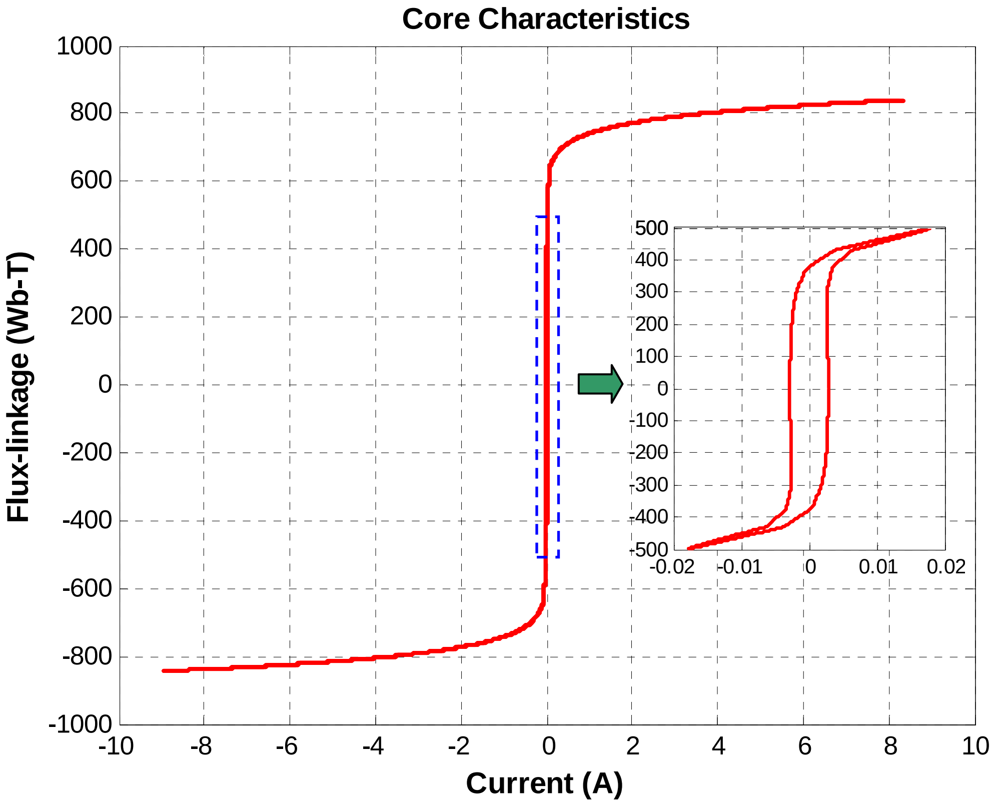

Figure 3.3: Core characteristic

3.3 ATPDraw Model

The circuit shown in Figure 3.3 is represented in detail using ATPDraw as shown in Figure 3.4. The value of the grading capacitance, C_g is 5061 pF and the ground capacitance, C_s is 10450 pF when the circuit is inducing a steady state ferroresonance response, following the opening of the circuit breaker, CB.

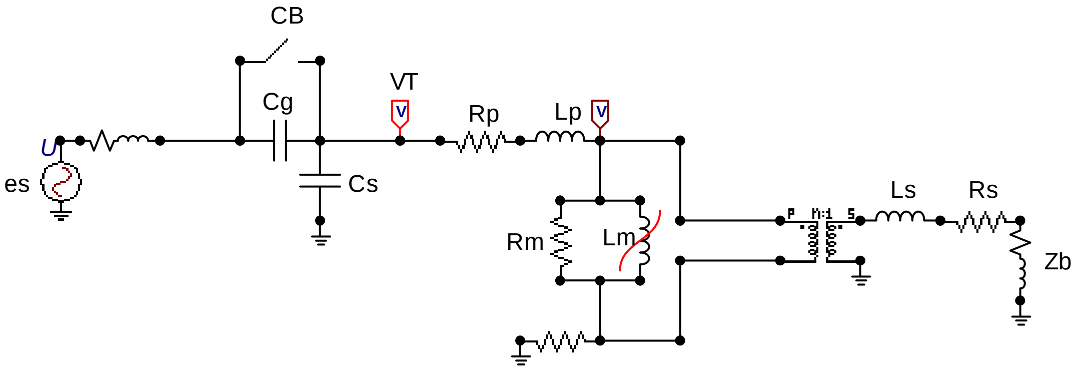

Figure 3.4: ATPDraw representation of Figure 3.1

Since the circuit of Figure 3.4 will be employed for ferroresonance study throughout this chapter, it is important to make sure that the developed simulation model in ATPDraw is correctly representative. In order to achieve this, the verification between the voltage waveform generated from ATPDraw and field recording waveforms have to agree with each other. The voltage waveform across the transformer produced from the simulation and the field recording are depicted in Figure 3.5.

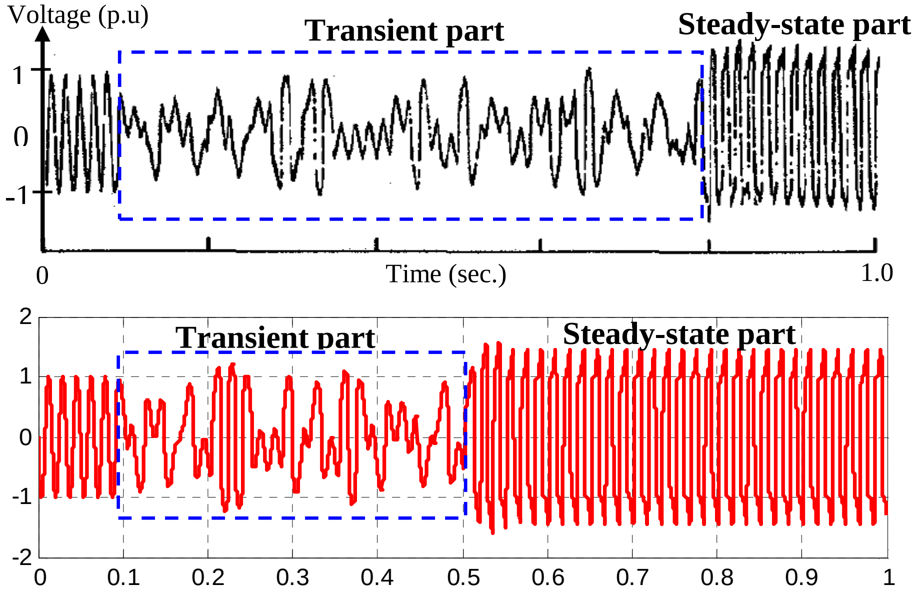

Figure 3.5: Top- Field recording waveform [16], bottom – simulation

Figure 3.5 shows both the field recording and simulation voltage waveforms, the shape and amplitude for the steady state voltage waveform were regenerated with reasonably good accuracy. However, the distinctive difference between them is the shape of the transient oscillatory voltage prior to steady state and the time for this voltage to settle down into the steady state. The figure shows that the field result takes longer time to reach steady state as compared with the simulation one. The transition from transient to steady-state response is random when the core operates around the knee area with the influence of system parameters. Exact matching between them is impossible to replicate, the main reasons are the ground capacitance that has been used in the simulation model is not exact, i.e. the influence by stray parameters cannot be accurately determined and validated, the magnetising characteristic (i.e. λ-i curve) cannot be modeled accurately and also the opening time of circuit breaker is not taken into consideration.

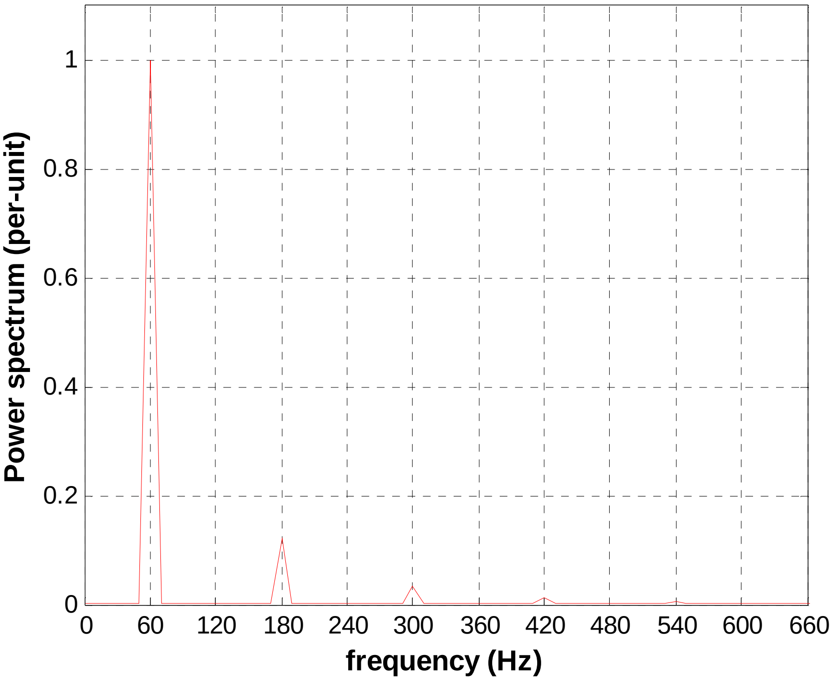

Figure 3.6: FFT plot

The frequency spectrum of the steady-state part voltage of Figure 3.5 is shown in Figure 3.6, which is known as the sustained fundamental ferroresonant mode or it is sometimes referred to as Period-1 response. It resonates at 60 Hz frequency with a sustainable amplitude of 1.41 per unit. The magnitude of this kind is the one which can cause major concern to power system components. In addition, the frequency content of the sustained resonant voltage as shown in the FFT plot of Figure 3.6 mainly consists of the fundamental frequency component as well as the existence of higher order frequency components such as the 3rd and the 5th, 7th and 9th harmonics.

3.4 Sensitivity Study on System Parameters

The main aim of this section is to provide the basis for interpreting various ferroresonant modes by carrying out the sensitivity studies of both the system and the transformer parameters. The following assumptions are made to facilitate the analysis: (1) There is no residual flux in the core at the time the circuit is energised (2) There is no initial charge on the capacitor (3) The circuit breaker (CB) is commanded to open at the current zero with current interruption as shown in Figure 3.7, where two operating events are simulated when the circuit breaker is open at t = 0.0137 seconds and 0.145 seconds, respectively. Once the breaker current is interrupted, the circuit can be either energised via the grading capacitance at the point of a positive or negative peak voltage. Note that the influence of residual flux and initial stored charge play an important role on the onset of ferroresonance as these parameters provide the initial condition which is sensitive to ferroresonant circuit. In addition, the current breaking time of circuit breaker in the simulation will also affect the onset of ferroresonance as it provides a different initial condition everytime the breaker operates.

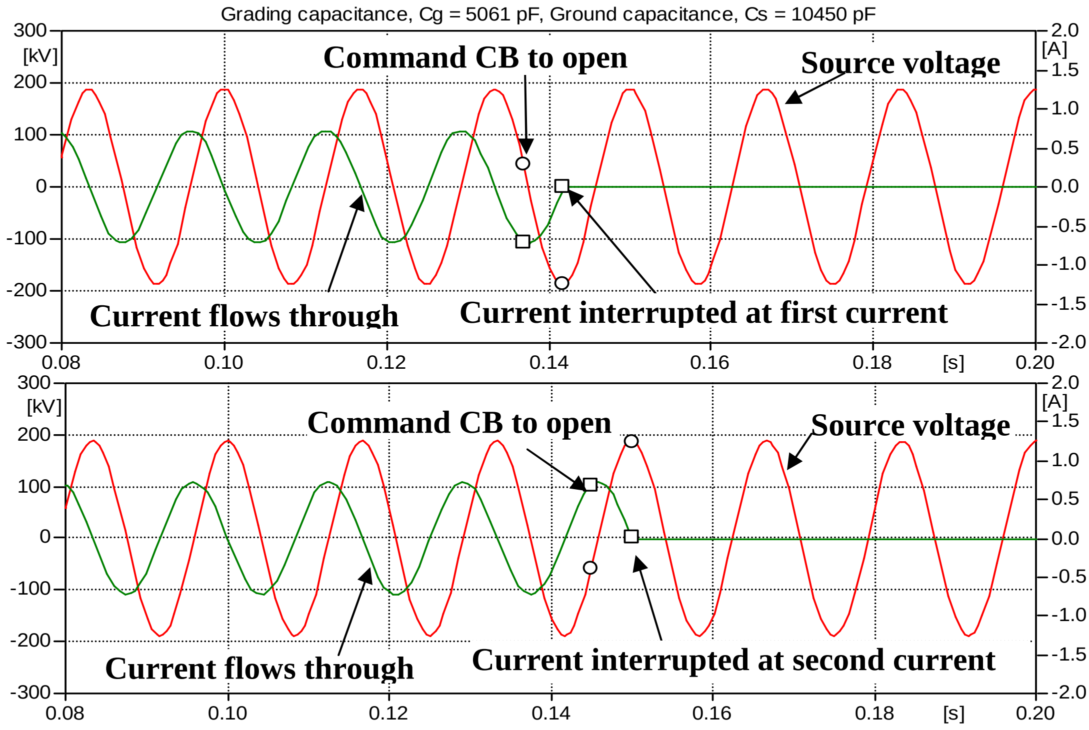

Figure 3.7: Top - Current interrupted at first current zero, Bottom – second current zero

The current waveforms of Figure 3.7 have been generated according to the base values of parameters as defined in Figure 3.1. The waveforms suggest that the circuit is purely capacitive because the current waveform leads the supply voltage by 90°.

3.4.1 Grading Capacitance (C_g)

Circuit breakers employing series-connected interrupting chambers are served for the purpose of providing better breaking capability. The use of the grading capacitor connected across the chamber is to provide improvement of balance of voltage distribution across the chambers in a series arrangement [32]. In spite of their usefulness, this capacitance on the other hand can produce the likelihood of occurrence of ferroresonance phenomena.

In order to look into the effect of this capacitance on the circuit, let us look at a wider view by having the grading capacitance, C_g varied from 1000 pF up to 8000 pF, against a wide spectrum of ground capacitance, C_s spreading from 1000 pF up to 10,450 pF. The result of the findings is presented as shown in Figure 3.8 showing the x-axis being the grading capacitance while the y-axis represents the ground capacitance. The small circle represents the types of responses that have been induced, with the blue representing the subharmonic mode and the red one the sustained fundamental mode. The one without any indication in the figure is when the system has been responded to a normal state, that is the final steady state which is characterised by either a 60 Hz sinusoidal with reduced amplitude.

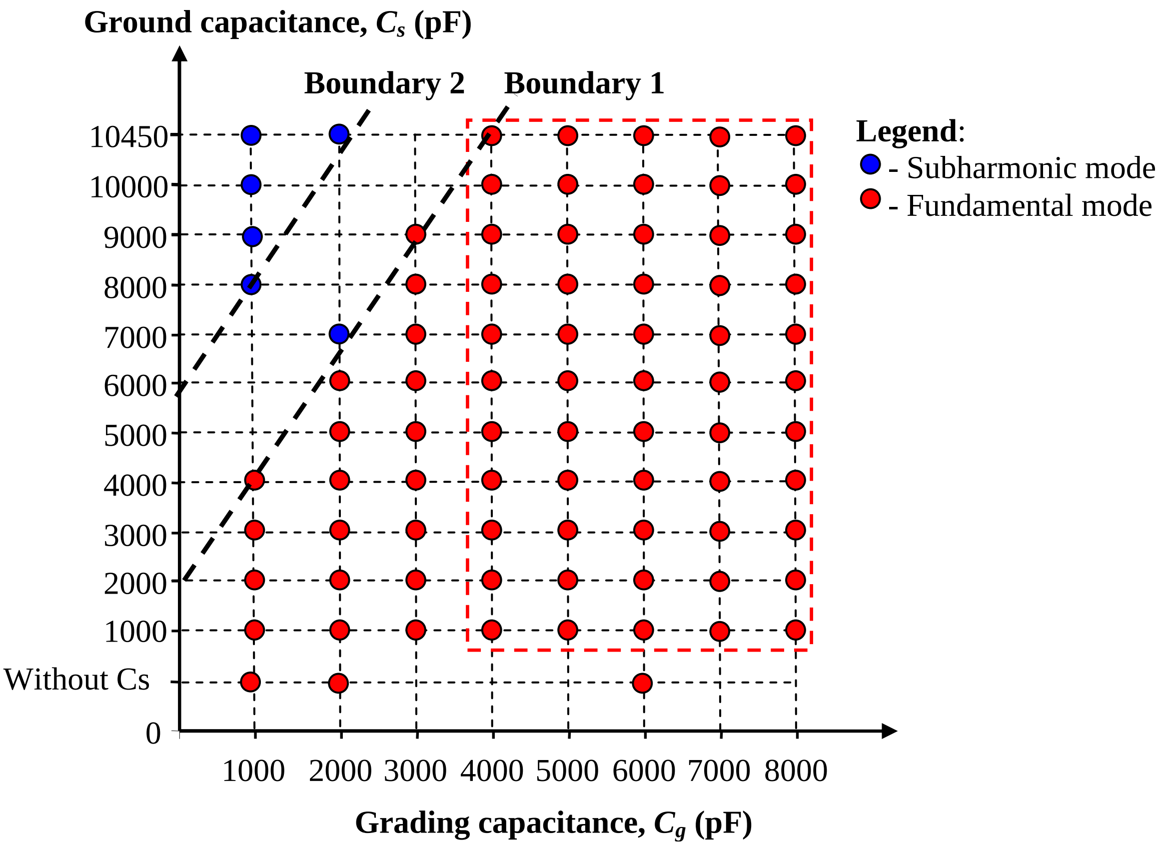

Figure 3.8: Overall system responses to change of grading capacitances

A glimpse on Figure 3.8 shows that there is a boundary region where the fundamental mode, subharmonic mode and normal state operated. Fundamental and subharmonic modes are more likely to occur below and above Boundary 1 and 2 respectively, while the normal state is operated in between the two boundaries. The result suggests that sustained fundamental mode ferroresonance (i.e. Period-1) is more prone to occur as the grading capacitances is increased against the ground capacitances. In fact, the most influence range is from 4000 pF to 8000 pF because this response is able to be induced widely for the whole range of ground capacitance (as shown in broken red line). On the other hand, subharmonic mode has also been induced but this occurs for the lowest value of grading capacitance (1000 pF), against the highest values of ground capacitances (8000 pF to 10450 pF). The one without the ground capacitance (C_s) shows that Period-1 can still exist.

3.4.2 Ground Capacitance (C_s)

The ground capacitance is mainly due to the bushing, busbar and winding to the tank or core, for example, the capacitances exhibit between the busbar-to-ground with air as an insulation medium. Now, let us look at how the system responses to ferroresonance if the ground capacitance, C_s is varied from 1000 pF up to 10,450 pF, for a wide range of grading capacitances (1000 pF to 8000 pF). The overall result of the findings is presented as shown in Figure 3.9.

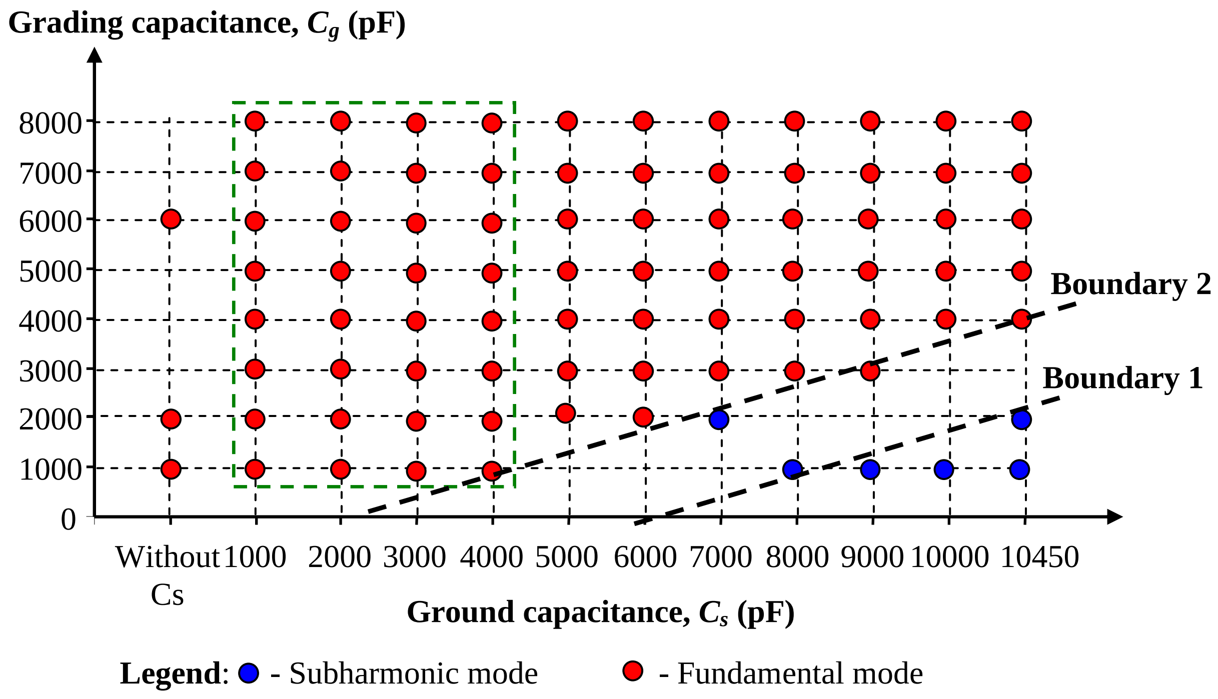

Figure 3.9: Overall system responses to change of capacitances

The overall scaterred diagram of Figure 3.9 shows that both the subharmonic mode and the fundamental mode have been induced in the system but they are operated within the boundary regions as shown in the diagram, as indicated as Boundary 1 and Boundary 2.

From the result, it can be seen that fundamental mode ferroresonance is more pronounce for the grading capacitance working in the range of 1000 pF to 4000 pF against the whole range of ground capacitances (as indicated in broken green line). However, its occurrence becomes less likely to occur as the ground capacitance is increased further, against the lower part of the grading capacitance. A border line marked as Boundary 2 in the diagram is used to indicate the limit where Period-1 occurs. Despite of this, the occurrence of subharmonic modes begins to show up for the highest part of ground capacitance but this only happened against the lowest value of grading capacitance of 1000 pF. The operating limit for the occurrence of subharmonic mode is marked as Boundary 1. In between the two boundaries, is a region where normal state occurs in the system. In contrast, it is also found that the fundamental mode ferroresonance is still able to be initiated into the system even without the presence of ground capacitance but its occurrence is more likely at the lower range of grading capacitances from 1000 pF to 2000 pF. The time-domain voltage waveforms of different kinds are shown in Figure 3.10.

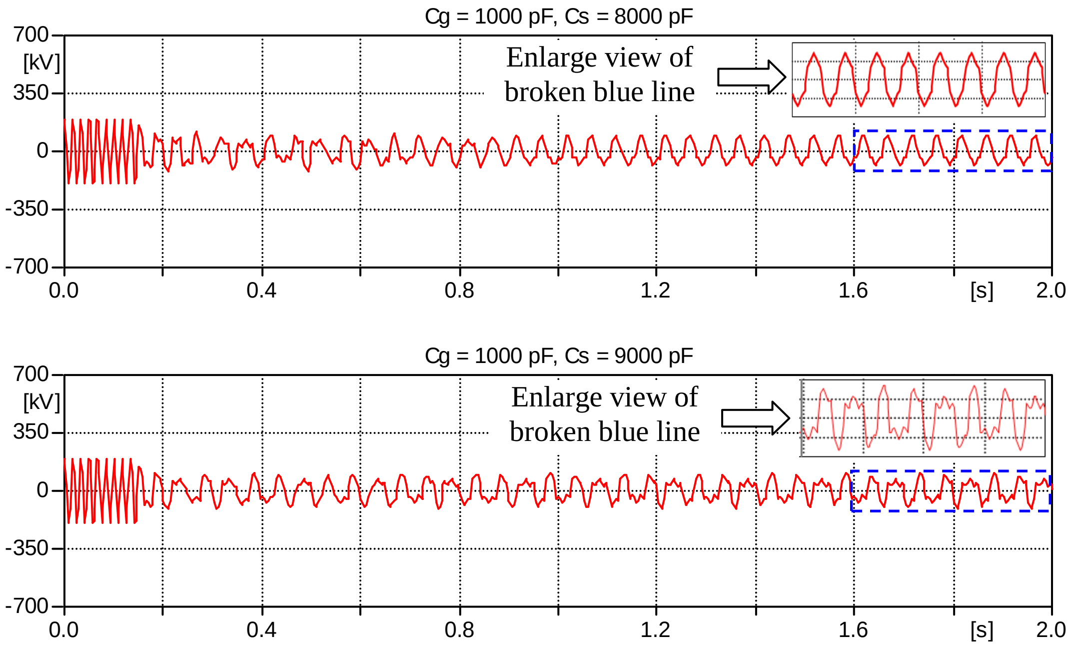

Continue….

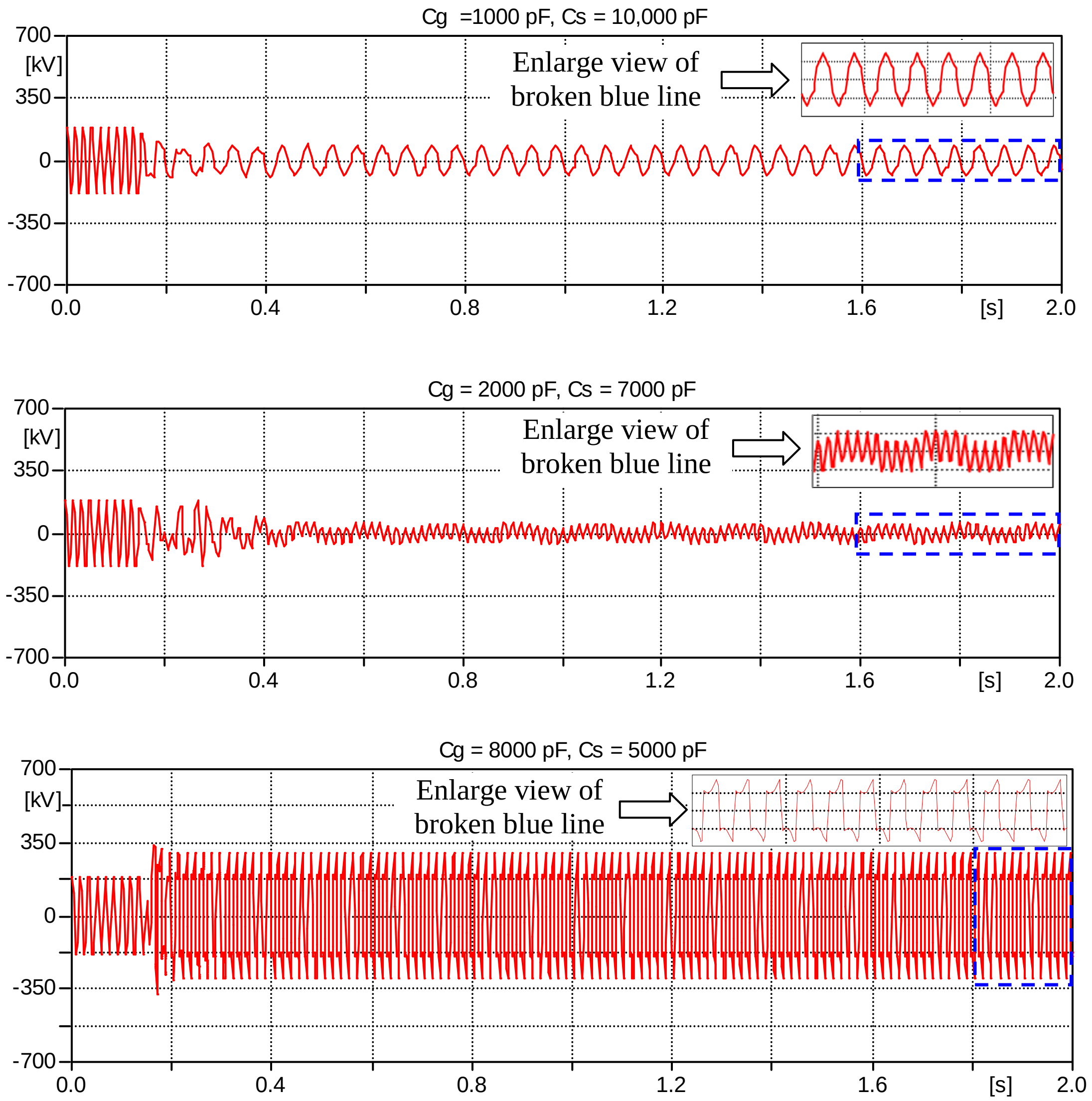

Figure 3.10: Time-domain voltage waveforms

The frequency contents of the sustained steady-state voltage waveforms of Figure 3.10 are analysed by using FFT,

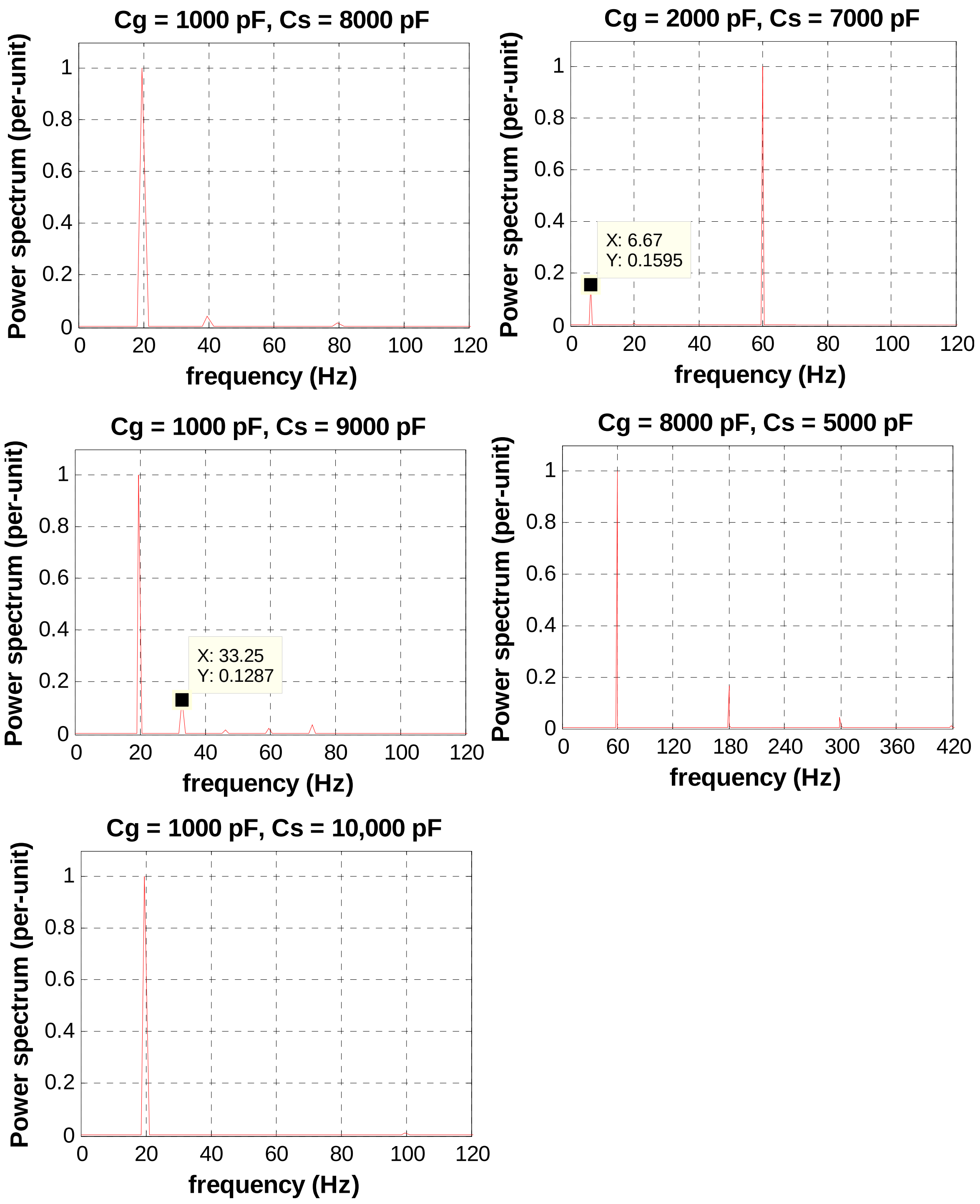

Figure 3.11: FFT plots of the time-domian voltage waveforms of Figure 3.10

The characteristics of the FFT plots corresponding to the voltage waveforms of Figure 3.10 are explained as follows:

(1) Voltage waveform with Cg = 1000 pF, Cs = 8000 pF

The FFT plot shows that the corresponding voltage waveform is dominated by a 20 Hz frequency and it is also referred to as a period-3 ferroresonance.

(2) Voltage waveform with Cg = 1000 pF, Cs = 9000 pF

The signal has a strong influence of 20 Hz frequency component and superimposed by 33.25 Hz frequency component. This signal is still referred to as period-3 ferroresonance.

(3) Voltage waveform with Cg =1000 pF, Cs = 10,000 pF

The FFT plot shows that the signal consists of only 20 Hz frequency without any other frequency contents. It is a purely period-3 ferroresonance signal.

(4) Voltage waveform with Cg =2000 pF, Cs = 7000 pF

The signal shows a repeatable oscillation with the existence of 6.67 Hz and with a strong influence of 60 Hz frequency component. This signal is referred to as Period-9 ferroresonance of 6.67 Hz subharmonic mode.

(5) Voltage waveform with Cg = 8000 pF, Cs = 5000 pF

The steady-state resonance voltage is 1.61 per-units which is higher than the system amplitude. This signal mainly consists of a strong influence of 60 Hz frequency component followed by the 3rd and 5th higher order harmonics. This phenomenon is referred to as Period-1 ferroresonance or sustained fundamental ferroresonance.

3.4.3 Magnetising Resistance (R_m)

The main function of transformer magnetic core is to provide magnetic flux for the development of transformer action such as to facilitate step-up or step-down of voltages. In this study the core-losses of the transformer is represented by a linear resistance.

The main aim of this study is to investigate the influence of core-losses on ferroresonance, by varying the value of the magnetising resistance, R_m over three different values. In this case the base value of 92 MΩ is varied to 10 MΩ and 5 MΩ. The magnetising plot for each resistance is shown in Figure 3.12 with the narrow loss per-cycle corresponds to the magnetising resistance of 92 MΩ and the one with the widest loss is for the resistance of 5 MΩ.

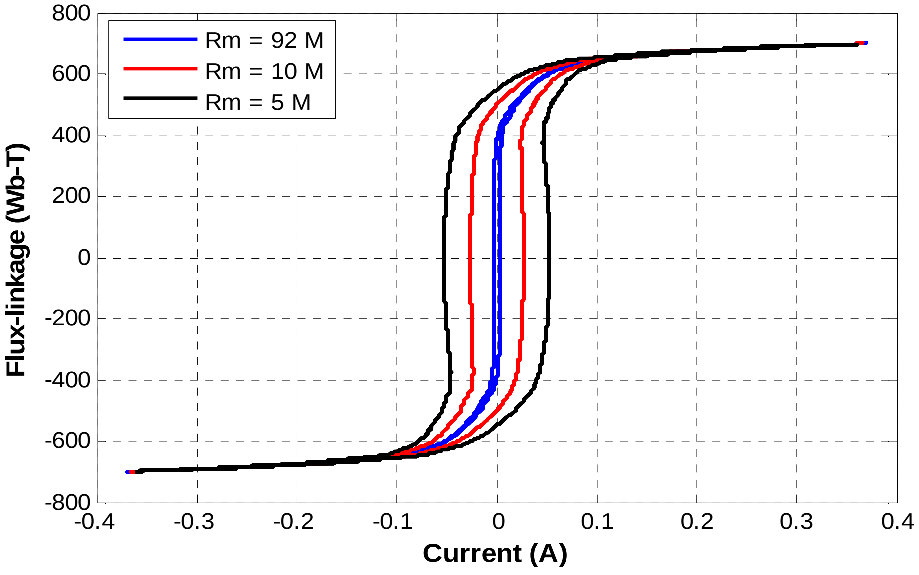

Figure 3.12: Core-losses for R_m = 92 MΩ, 10 MΩ and 5 MΩ

The study is carried out by assuming that C_g = 4500 pF and C_s = 10450 pF. The voltage waveforms across the transformer are recorded as shown in Figure 3.13.

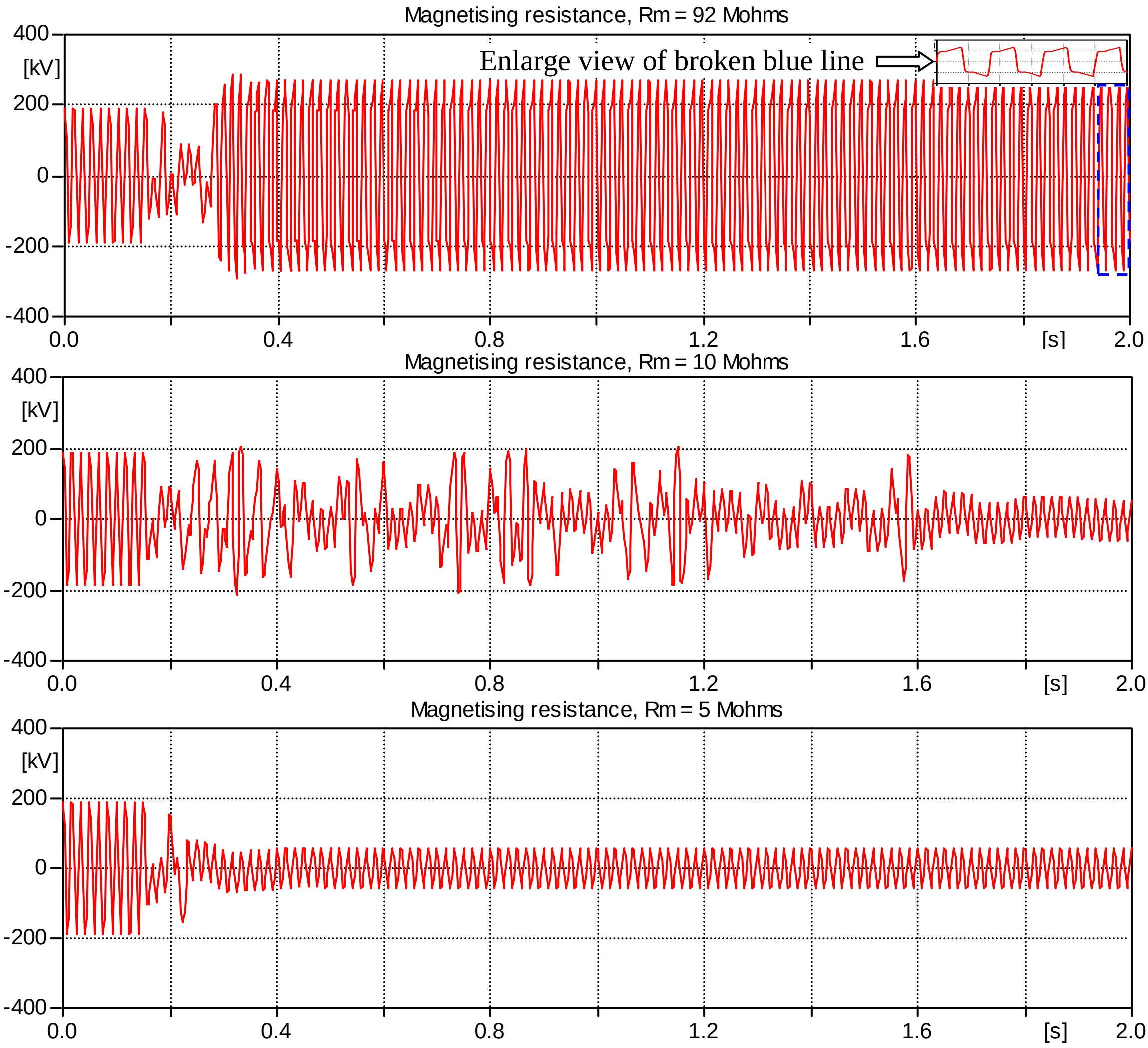

Figure 3.13: Voltage across transformer with variation of core-losses

Initially, with low loss i.e. R_m = 92 MΩ, Period-1 ferroresonance is induced into the system which can be seen in the top diagram of Figure 3.13. As the loss is increased by having R_m = 10 MΩ, the result shows that the transient part takes longer time to settle down, with resonance being damped. However, when the loss is further increased to R_m = 5 MΩ, Period-1 ferroresonance is damped more effectively and ceases to develop. This study suggests that ferroresonance can be damped by using core material with larger loss per cycle, such as soft steel core material.

3.5 Influence of Core Nonlinearity on Ferroresonance

The core characteristic employed in the previous study has a level of nonlinearity as indicated in red line of Figure 3.14.

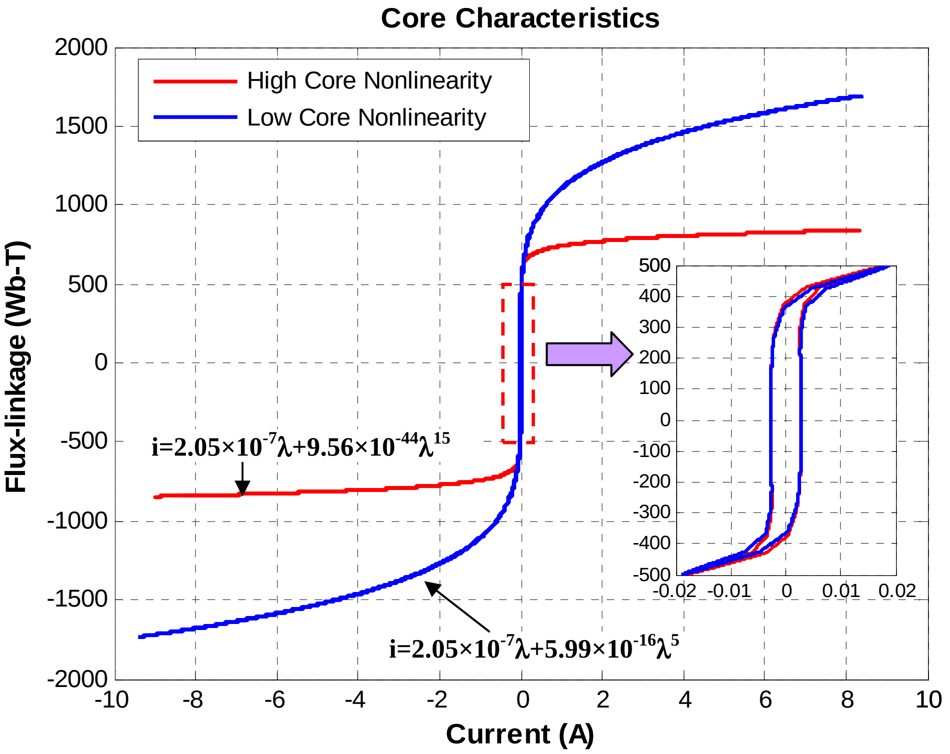

Figure 3.14: Core characteristics

In order to assist further on how both the grading and the ground capacitances can further influence the occurrence of ferroresonance, the degree of nonlinearity of the core characteristic marked in red is adjusted to become less nonlinear as indicated by the blue line shown in Figure 3.14. The adjustment of the degree of nonlinearity of the core characteristic can be accomplished by using the two-terms polynomial equation of $i = A\lambda + B\lambda^n$ [33-35]. The core-losses of the transformer are kept unchanged.

3.5.1 Grading Capacitance (C_g)

Similar to the previous case study, the grading capacitance is varied from 1000 pF up to 8000 pF, with a range of ground capacitances from 10000 pF to 10,450 pF. The result from the simulations is presented in Figure 3.15. With this type of core characteristic, the results suggest that there is more likelihood that subharmonic mode can be induced into the system, particularly a strong influence of Period-3 ferroresonance. In contrary, other type of response such as chaotic mode has also been identified, but its occurrence is at higher value of grading capacitance.

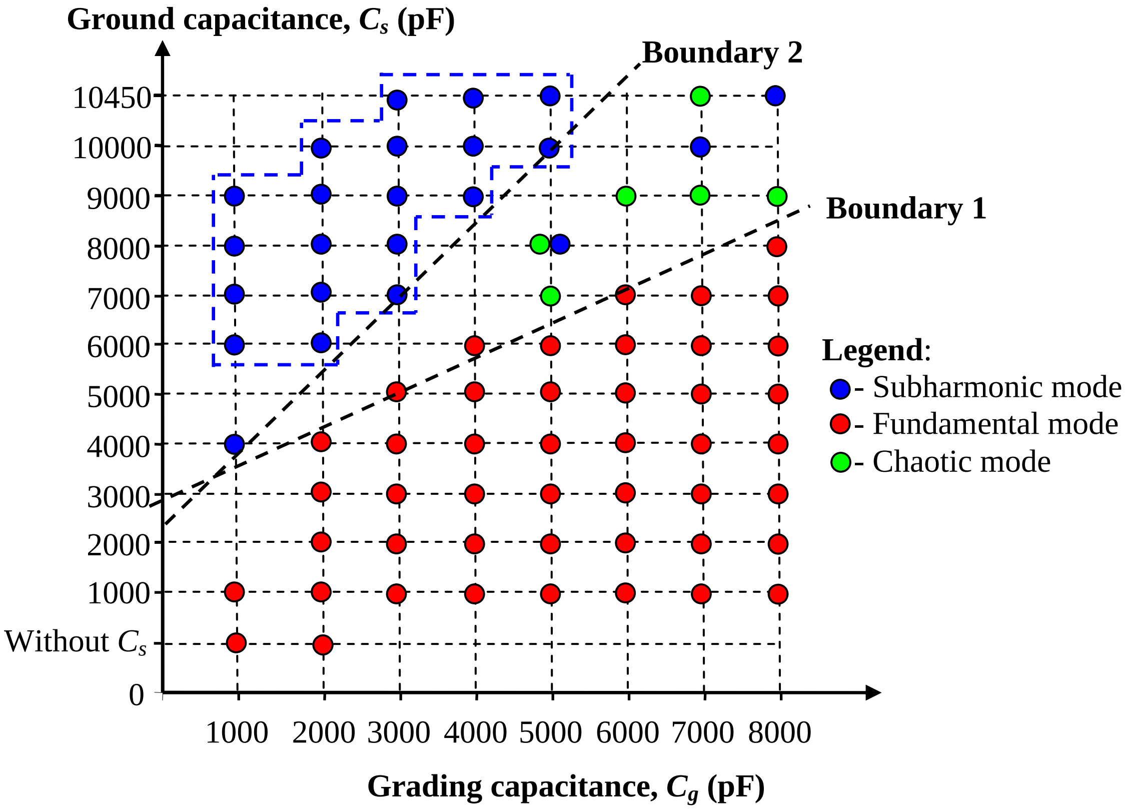

Figure 3.15: Overall responses of the influence of capacitances

The plot suggests that the occurrence of Period-1 ferroresonance is more likely to be induced as the value of grading capacitance is varied from 1000 pF up to 8000 pF, up against escalating values of ground capacitance from 1000 to 8000 pF. In contrary, the likelihood of inducing the subharmonic mode is more widespread at lower range of grading capacitance (1000 pF to 5000 pF) against higher value of the ground capacitance (8000 pF to 10,450 pF), as marked in broken blue line. On the other hand, chaotic mode will also be exhibited but its initiation is more scattered around the high side of the grading and ground capacitances, that is in the region within Boundary 1 and Boundary 2. In addition, the normal state is also operated within these two bundaries.

One interesting observation from the plot is that when the system is operated at C_g = 5000 pF and C_s = 8000 pF, it responded to the chaotic mode when the breaker current is interrupted at negative peak voltage. On the other hand, the system also responded to subharmonic mode when the current is interrupted at positive peak voltage.

3.5.2 Ground Capacitance (C_s)

Similar to the previous characteristic, the overall responses subject to this type of core characteristic is presented as shown in Figure 3.16 with a plot of grading capacitance versus ground capacitance varying over a wide range.

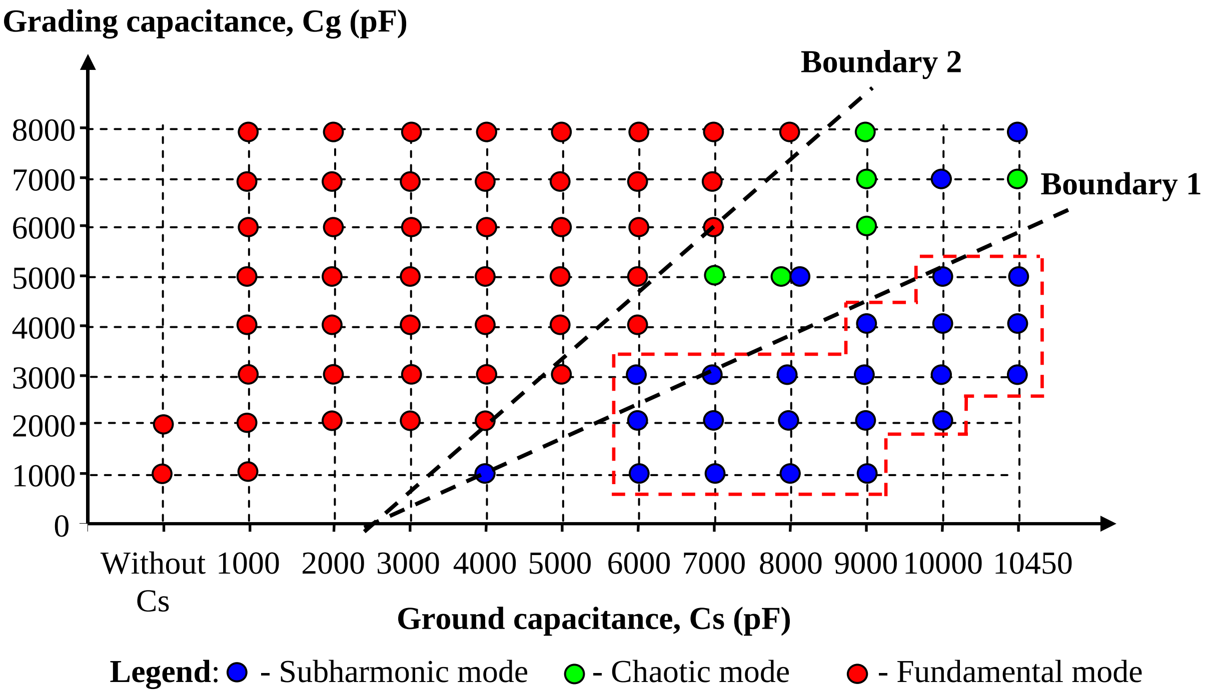

Figure 3.16: Overall responses of the influence of capacitances

The overall responses are explained as follows:

(1) Period-1 ferroresonance is more likely to occur at the lowest part of the ground capacitance i.e. at 1000 pF over the whole range of the grading capacitances.

(2) Period-1 ferroresonance becomes less frequent as the grading capacitance is in the range from 1000 pF up to 8000 pF, against the lower range of grading capacitance. However, this response is in fact becoming less susceptible as the grading capacitance is increased further, the likelihood of occurrence of subharmonic mode on the other hand is more pronounced, favoring at the lower range of grading capacitance (as indicated in broken red line).

(3) Without exception, Period-1 ferroresonance will also occur without the ground capacitance connected to the system but this only happened at the lower value of grading capacitance.

(4) Chaotic mode and normal state is operated within the region between Boundary 1 and Boundary 2 but chaotic mode is more pronounced at higher range of ground capacitance.

The time-domain waveforms and their corresponding FFT plots are shown in Figure 3.17 and 3.18 respectively.

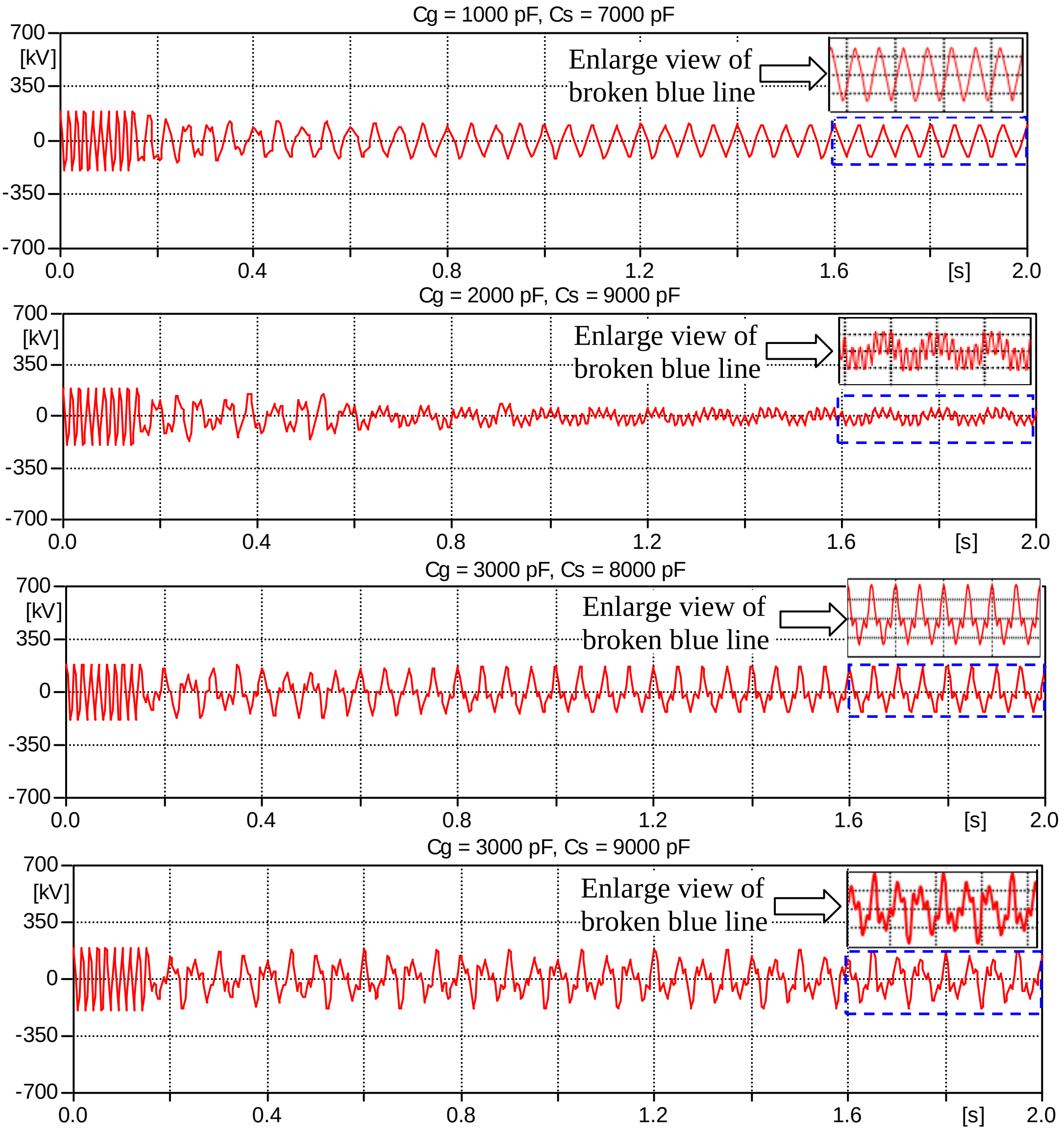

Continue…

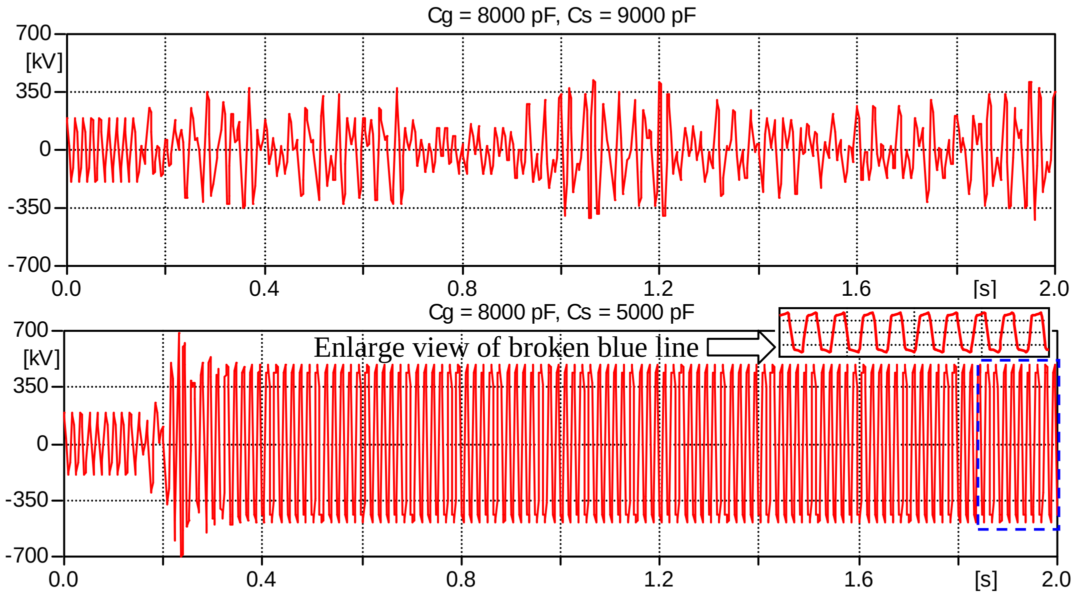

Figure 3.17: Time-domain voltage waveforms

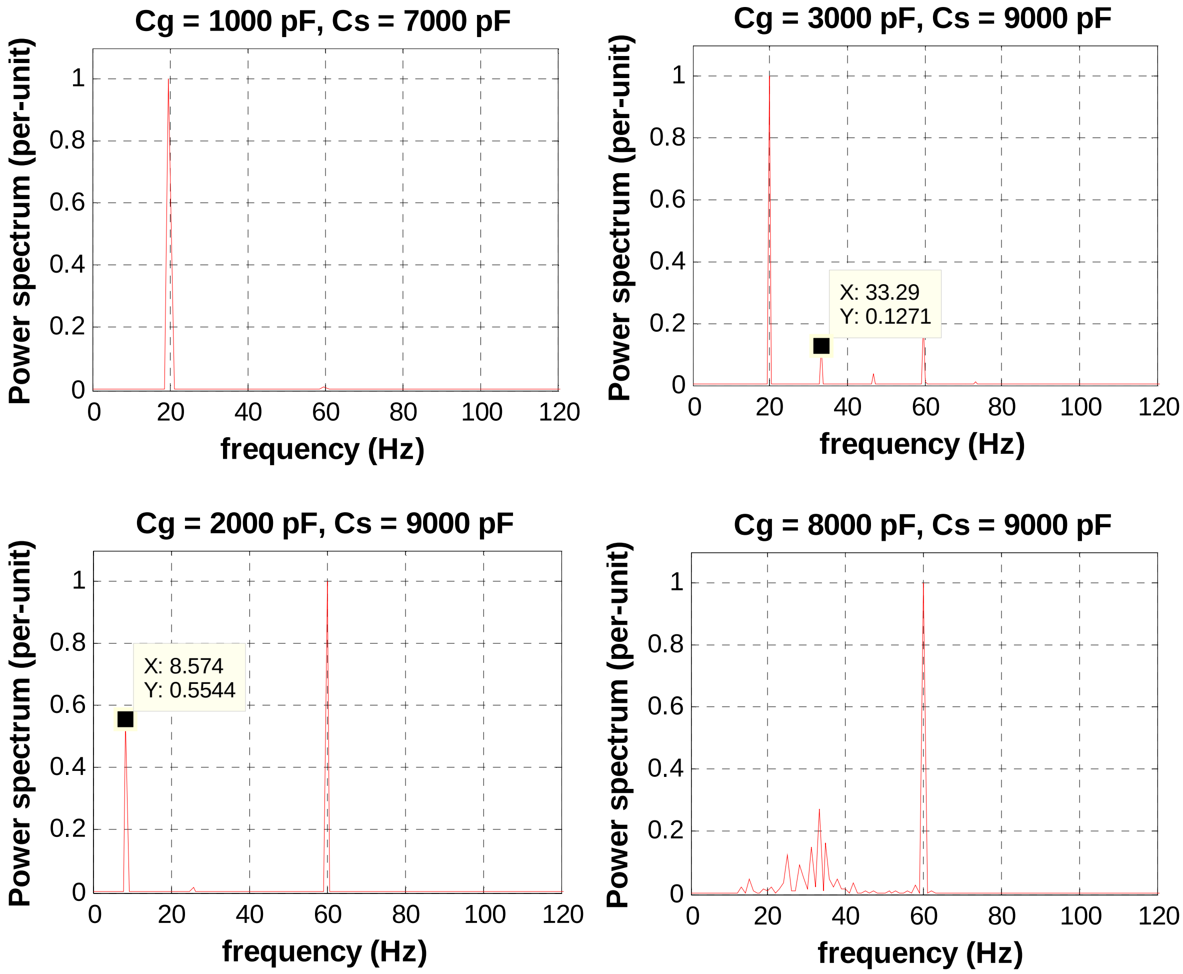

Continue…

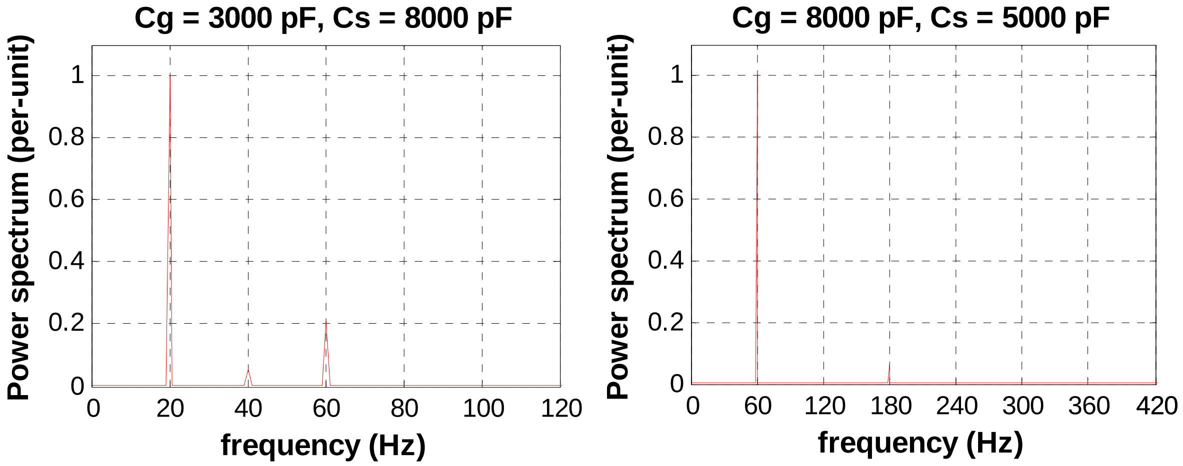

Figure 3.18: FFT plot of the time-domain waveforms of Figure 3.17

The characteristics of the FFT plots corresponding to the voltage waveforms are explained as follows:

(1) Voltage waveform with Cg = 1000 pF, Cs = 7000 pF

The FFT plot shows that there is a strong nomination of a 20 Hz frequency component contained in the signal which is called a Period-3 or a 20 Hz subharmonic ferroresonance.

(2) Voltage waveform with Cg = 2000 pF, Cs = 9000 pF

The response shows repeatable oscillation of 8.5 Hz with the strong influence of 60 Hz frequency component. This signal is called a 8.5 Hz subharmonic mode or a Period-7 ferroresonance.

(3) Voltage waveform with Cg = 3000 pF, Cs = 8000 pF

The FFT plot shows that the signal consists of strong influence of 20 Hz frequency, therefore it can be considered as a Period-3 or 20 Hz subharmonic ferroresonance.

(4) Voltage waveform with Cg = 3000 pF, Cs = 9000 pF

This type of signal is Period-3 or 20 Hz subharmonic mode because the signal contains mainly the 20 Hz frequency component.

(5) Voltage waveform with Cg = 8000 pF, Cs = 9000 pF

The time-domain waveform shows that the amplitude is randomly varied with time, oscillating at different frequencies. The FFT plot suggests that there is evidence of continuous frequency spectrum spreading in the region of 20 Hz and 60 Hz. This type of signal is categorised as chaotic mode.

(6) Voltage waveform with Cg = 8000 pF, Cs = 5000 pF

The sustained amplitude of this signal is 1.45 per-unit which is higher than the system voltage amplitude. The content of this signal is mainly 60 Hz followed by higher odd order harmonic of 180 Hz. The phenomenon is referred to as Period-1 ferroresonance or sustained fundamental ferroresonance.

3.6 Comparison between Low and High Core Nonlinearity

In the previous sections, the study of ferroresonance accounts for the variation of both the grading and ground capacitances and the degrees of core nonlinearity have been carried out. For comparison between the two characteristics, they are then presented as shown in Figure 3.19.

(1) High Core Nonlinearity

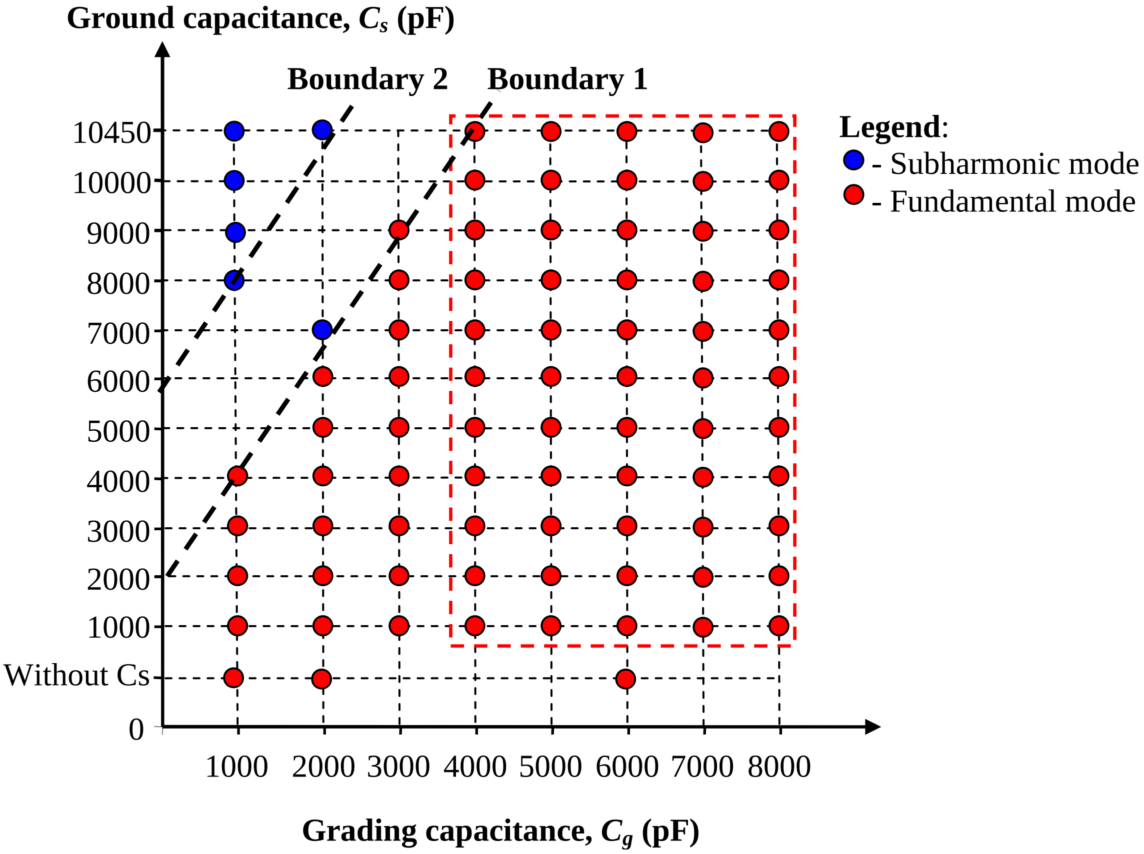

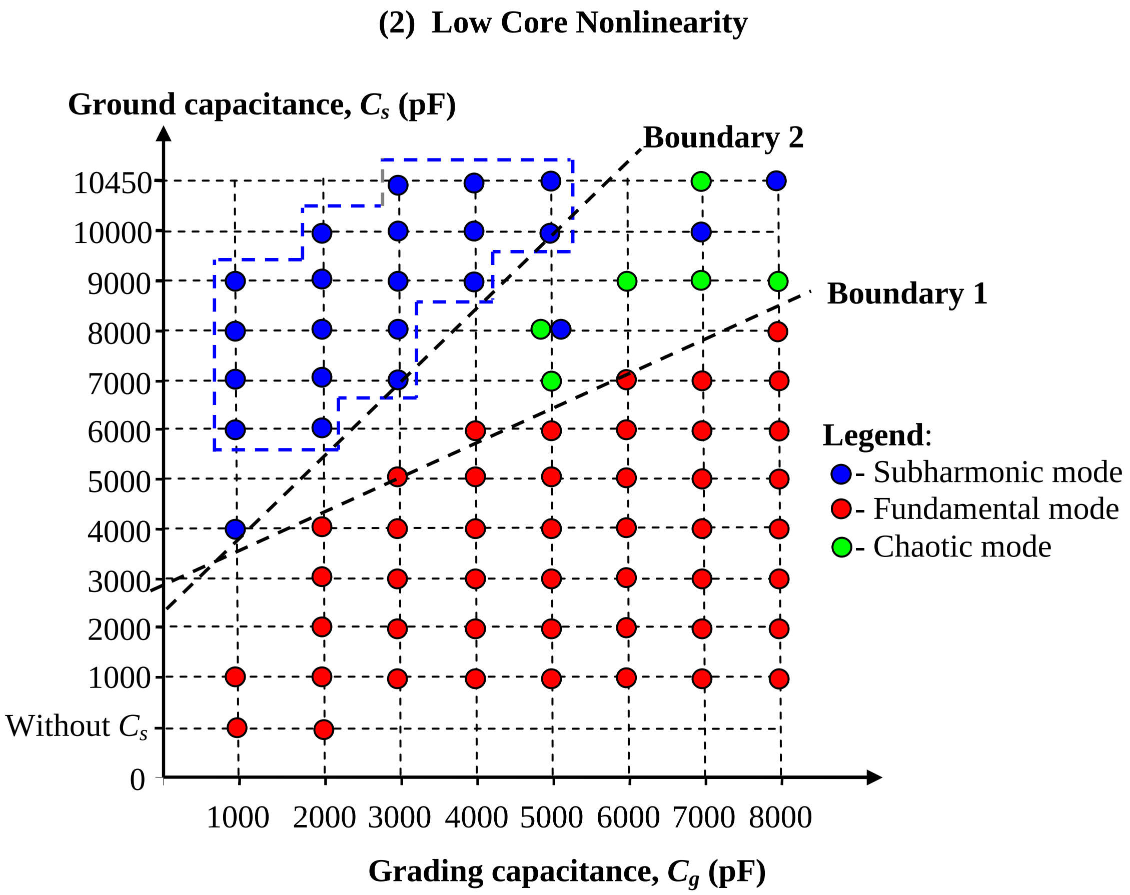
(2) Low Core Nonlinearity

Figure 3.19: Top: High core nonlinearity, Bottom: Low core nonlinearity

3.7 Analysis and Discussion

From Figure 3.19, it can be seen that both types of core nonlinearities have a great influence on the occurrence of a Period-1 ferroresonance when the value of the grading capacitance is increased. The main reason can be explained by a graphical diagram of Figure 3.21. The equation of the ferroresonance circuit of is given as

$$V_{Lm} = E_{Thev.} + V_C \tag{3.1}$$

where Thevenin’s voltage at terminals X-Y, $E_{Thev.} = E \times \dfrac{C_{series}}{C_{series} + C_{shunt}}$ and Thevenin’s capacitance at terminals X-Y, $C = C_{series} + C_{shunt}$

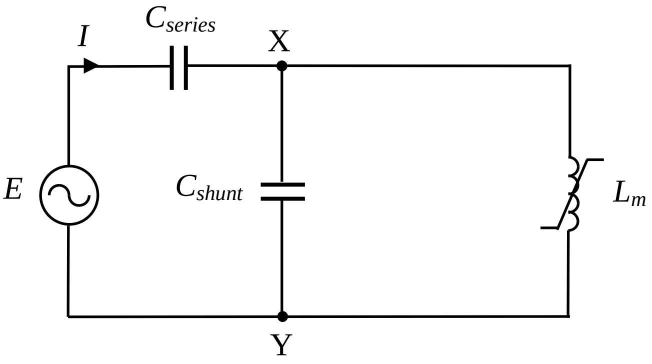

Figure 3.20: Single-phase ferroresonance circuit

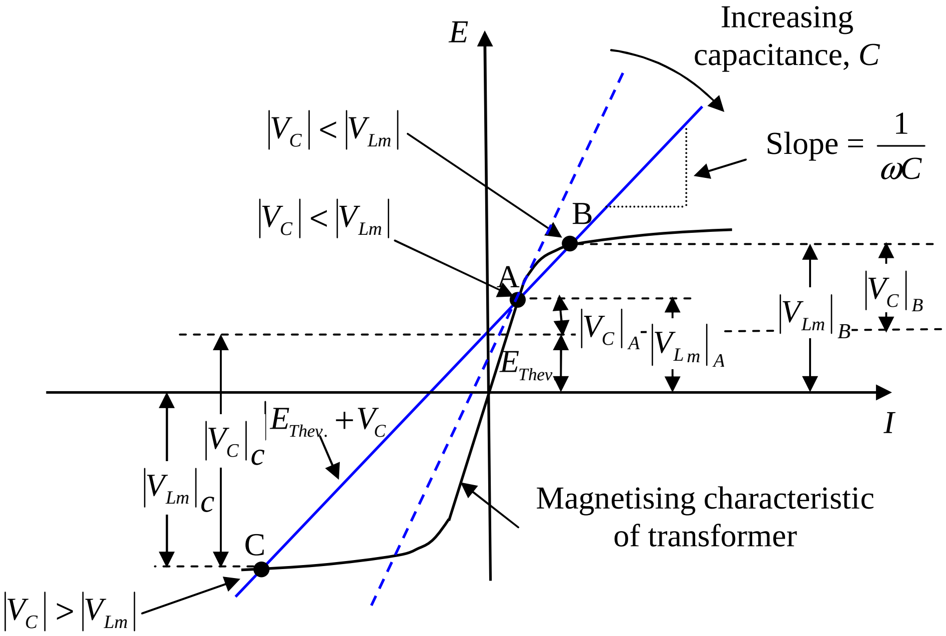

Where $E_{Thev.}$ = Thevenin's voltage source, V_{Lm} = voltage across transformer (L_m), V_C = voltage across capacitance (C), ω = frequency of the supply voltage

Figure 3.21: Graphical view of ferroresonance

As can be seen from Figure 3.21, the straight line represents the *V-I* characteristic across the transformer [36-42]. On the other hand, the s-shape curve represents the *V-I* magnetising characteristic of the core. The intersection of the supply voltage across L_m i.e. the straight line with the magnetising curve of the voltage transformer is to provide the operating point of the system behaviour. From the graph, it can be seen that there are three possible operating points of this circuit for a given value of X_C. Point A in the positive quadrant of the diagram corresponds to normal operation in the linear region, with flux and excitation current within the design limit. This point is a stable solution and it is represented by the steady state voltage that appears across the voltage transformer terminals therefore ferroresonance would not take place. Point C is also a stable operating point where V_C is greater than V_{Lm} which corresponds to the ferroresonance conditions charaterised by flux densities beyond the design value of the transformer, and a large excitation current. Point B, which is in the first quadrant, is unstable. The instability of this point can be seen by increasing the source voltage ($E_{Thev.}$) by a small amount follows a current decrease which is not possible. Therefore a mathematic solution at this point does not exist [24].

Moreover, the presence of the grading capacitance suggests that core characteristic with high nonlinearity has a high probability of inducing sustained ferroresonance as compared to the low one. The reason is because of core characteristic with high degree of nonlinearity has an approximate constant saturable slope (see Figure 3.22) which can cause the core to be driven into deep saturation if there is only a small increase of voltage impinging upon the transformer.

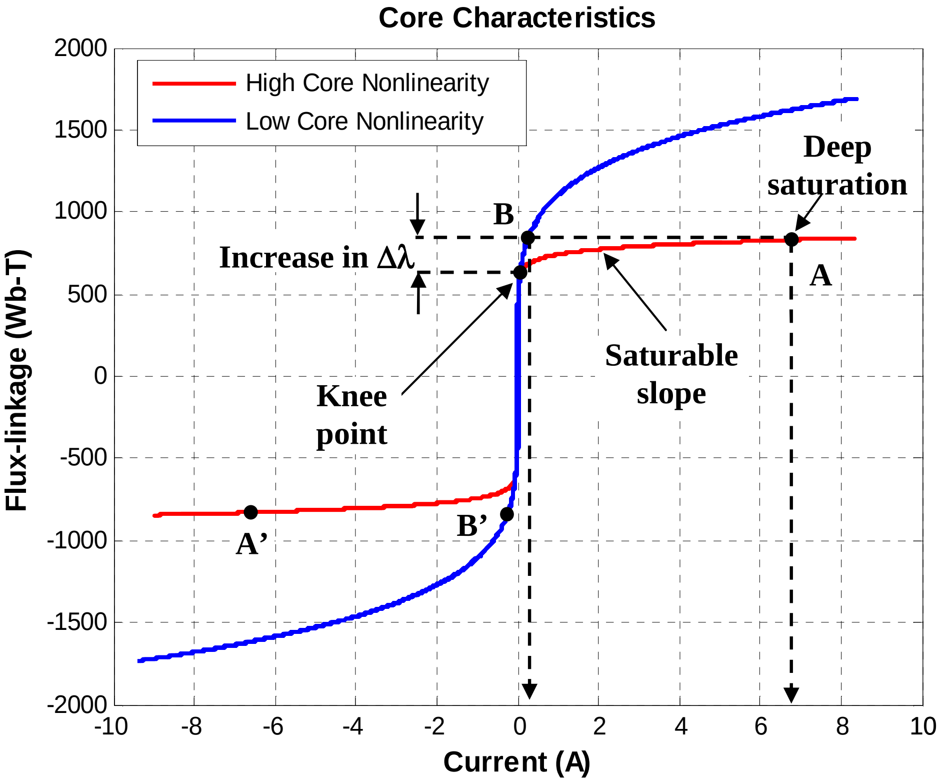

Figure 3.22: Top-High core nonlinearity, Bottom-Low core nonlinearity

In order to study the effect of degree of core nonlinearity on ferroresonance, let us consider an example by looking into a particular working point at C_s = 10450 pF and C_g = 4000 pF as indicated in broken line of Figure 3.19. The energisation of Period-1 ferroresonance using high core nonlinearity has the voltage and current characteristics as shown in Figure 3.23.

The sustained ferroresonance voltage of Figure 3.23 has a magnitude of 1.40 per-unit which has an increase of voltage of 40%. This change of voltage will over-excite the transformer and then pushes the core into profound saturation therefore withdrawing a high peaky current from the system (bottom diagram of Figure 3.23). The sustained amplitude oscillates between point A and A' along the magnetising characteristic of Figure 3.22, marked in red.

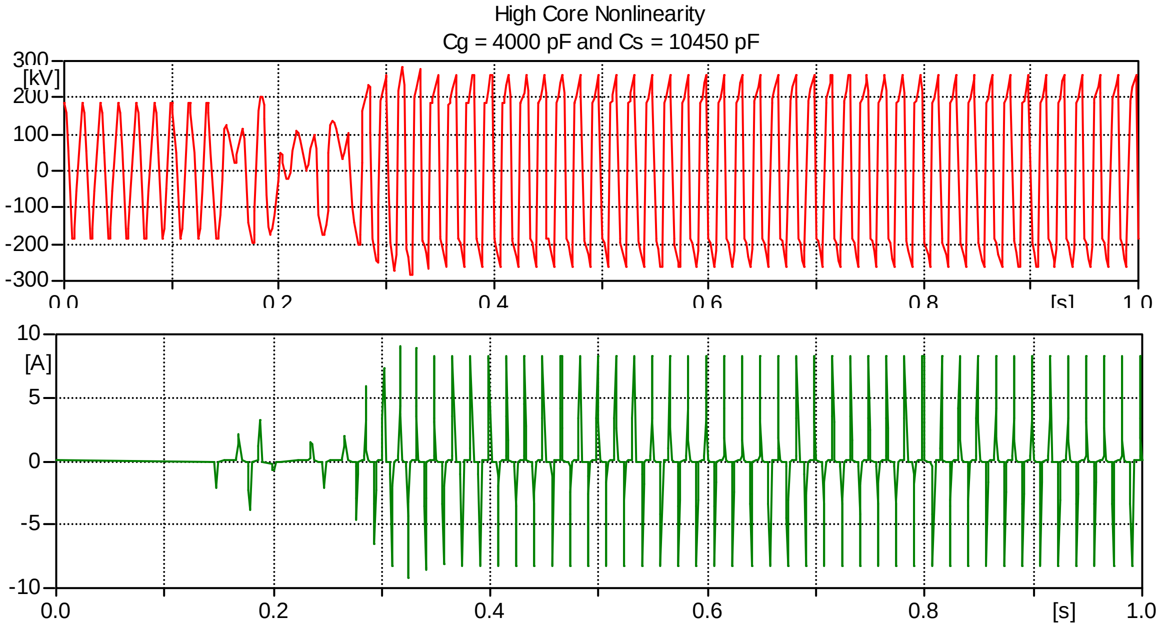
High Core Nonlinearity
Cg = 4000 pF and Cs = 10450 pF

Figure 3.23: Top-Voltage waveform, Bottom-Current waveform

In contrary, the employment of low degree of core nonlinearity has generated totally different types of voltage and current responses as shown in Figure 3.24.

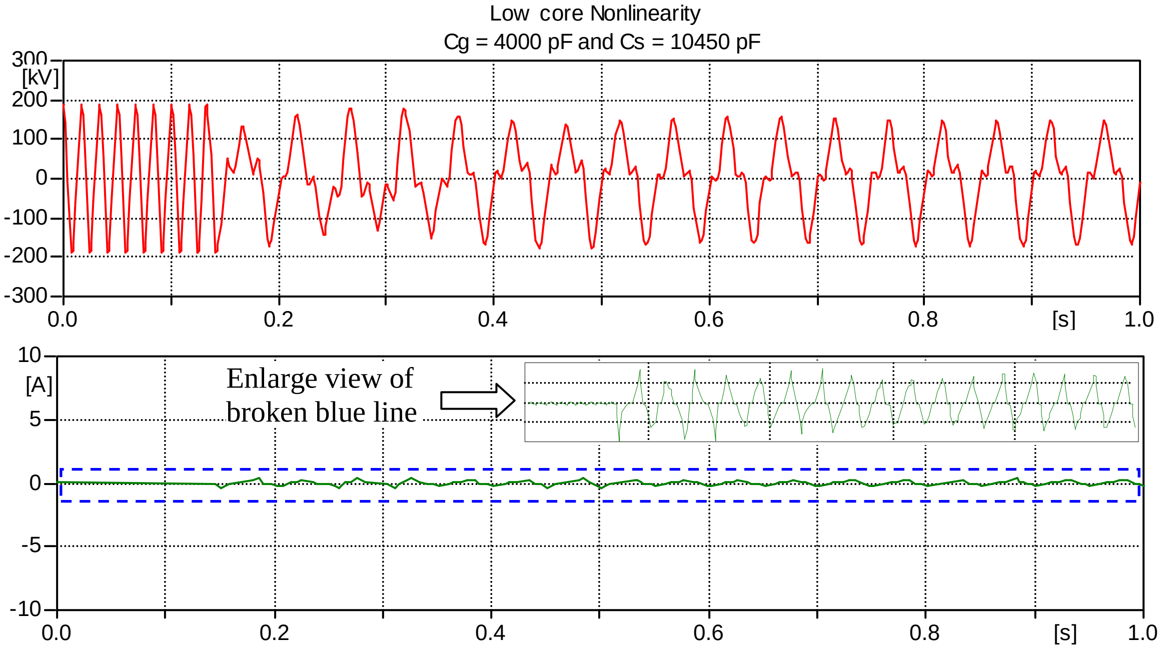
Low core Nonlinearity
Cg = 4000 pF and Cs = 10450 pF

Figure 3.24: Top-Voltage waveform, Bottom-Current waveform

The results show that low current Period-3 ferroresonance has been induced into the system. This observation suggests that the transformer has been working around the knee point i.e. at point B of the core characteristic as marked in blue of Figure 3.25. Since the response oscillates between point B and B’ at a rate of 20 Hz, therefore core characteristic with this kind requires larger change of voltage in order for the transformer to induce Period-1 ferroresonance. The reason that the transformer operating around the knee point when it is impinged by a subharmonic mode response can be explained as follows.

Dividing equation (3.1) by frequency, ω then it becomes

$$V_{Lm} = \omega.F\left(I\right) = \frac{E_{Thev.}}{\omega} + \frac{V_C}{\omega} = \frac{E_{Thev.}}{\omega} + \frac{I}{\omega^2 C} \tag{3.2}$$

then

$$F\left(I\right) = \frac{E_{Thev.}}{\omega} + \frac{I}{\omega^2 C} \tag{3.3}$$

Equation (3.3) represents the straight line marked in blue and green of Figure 3.25, but the position and the gradient of the line changes greatly with frequency [43]. For high frequency at ω_1, the gradient of the line is less steep therefore intersects the magnetising characteristic on the negative branch at point A. On the other hand, with lower frequency, ω_2 the gradient of the line is steeper as indicated in blue line hence crossing at point B against the magnetising characteristic.

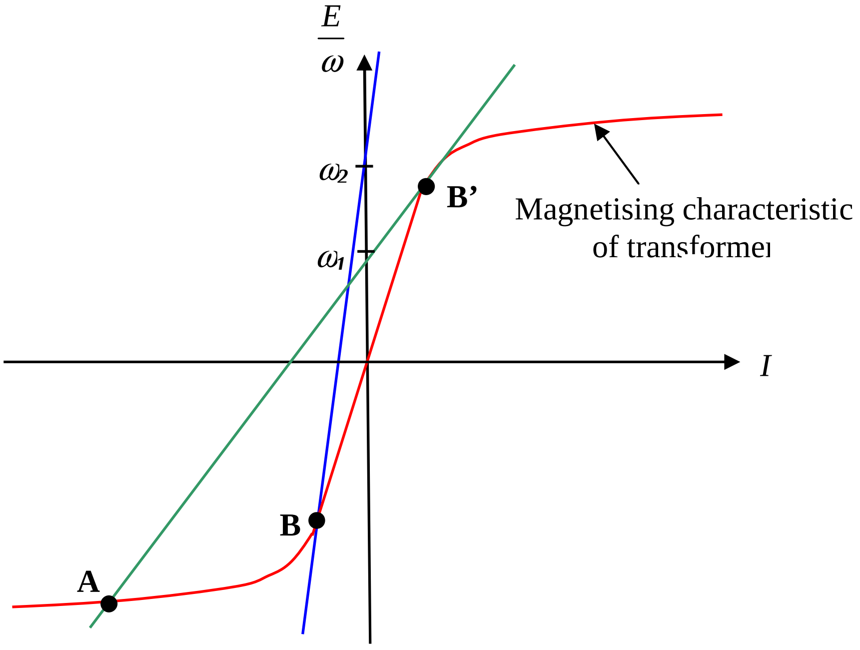

Figure 3.25: Effect of frequency on magnetic characteristic

Lower frequency such as the response having the characteristic of subharmonic mode is more likely to operate around the knee point region of the core characteristic, inducing low current in magnitude.

3.8 Summary

Two case studies employing two different types core of characteristics to investigate how the grading and ground capacitances can influence the types of ferroresonant modes have been performed in the preceding sections. The comparison between the two is summarised as shown in Table 3.1.

Table 3.1: Comparison between high and low core nonlinearity

Core characteristic	**Types of responses**		
	Fundamental mode	**Subharmonic mode**	**Chaotic mode**
(A) High Nonlinearity			
	- More likely to occur at high Cg	- Less likely to occur - Prone at high Cs & low Cg	- Not available
(B) Low Nonlinearity			
	- Less likely to occur - More likely at high Cg but limited at higher range of Cs	- More likely to occur - Likely at high Cs & low Cg	- Likely to occur - More likely to occur at high Cs & high Cg

In summary, Period-1 ferroresonance is more susceptible to occur for core characteristic with high degree of nonlinearity as compared to the low one, covering a wide range of grading capacitances against ground capacitances. However, this type of core characteristic has a less likelihood of initiating subharmonic mode. In fact the occurrence of this subharmonic response is only limited at high value of grading capacitance against low value of ground capacitance. Other type of response such as chaotic mode has not occurred for high degree nonlinear core characteristic.

One of the main observations throughout this study is that the ground capacitance has in effect provided a wider range of grading capacitance for Period-1 to be more frequently occur, particularly for the core characteristic with high degree of nonlinearity. The grading capacitance on the other hand acts as a key parameter for the initiation of ferroresonance.

This is because Period-1 response is still able to be induced without the presence of the ground capacitance.

In contrast, core characteristic employing low degree of nonlinearity has a less chance for the Period-1 ferroresonance to occur. Instead this type of response occurs in a confined range of high ground capacitance against high value of grading capacitance. Subsequently, it is more pronounced for subharmonic mode to be induced, confining at high ground capacitance and low value of grading capacitances. Furthermore, chaotic mode can also be exhibited but restricted around high ground and grading capacitances.

The overall study from the above can thus provide an overall glimpse on how a system network responds to ferroresonance for the variation of the following parameters; the grading capacitance, the ground capacitance, the core-losses and the use of different degree of nonlinearity of core characteristics.

CHAPTER 4

4. SYSTEM COMPONENT MODELS FOR FERRORESONANCE

4.1 Introduction

In the preceding chapter, the study of a single-phase ferroresonance circuit has been carried out to investigate the fundamental behaviours of the phenomenon when the parameters are varied.

One of the main aims of this thesis is to determine the best possible predefined models in ATPDraw so that each of the components can be suitably represented for modeling the real case circuit which has experienced ferroresonance. It is therefore the objective of this chapter to firstly introduce the technical aspects of the power system components, and to identify the best possible model for the study of ferroresonance that are available in ATPDraw. As ferroresonance is classified as a low frequency transient, much attention is then concentrated on the circuit breaker, the transmission line and the power transformer which are concerned. The criteria to be used for determining the suitability of each of the predefined models are taken in relation to the modeling guidance proposed by CIGRE and are explained accordingly.

4.2 400-kV Circuit Breaker

A circuit breaker is a mechanical switching device, regardless of its location in the power system network, it is required for controlling purposes by switching a circuit in, by carrying load currents and by switching a circuit off under manual or automatic supervision. In its simplistic term, the main function of the circuit breaker is to act as a switch capable of making, carrying, and breaking currents under the normal and abnormal conditions.

There are five basic types of switch models [44] available in ATPDraw namely: the time-controlled switch, the gap switch, diode switch, the thyristor switch and the measuring switch. The only one relevant to the circuit breaker is the time-controlled switch which is an ideal switch that can be employed for opening and closing operations. The way in which it is operated is explained by referring to Figure 4.1.

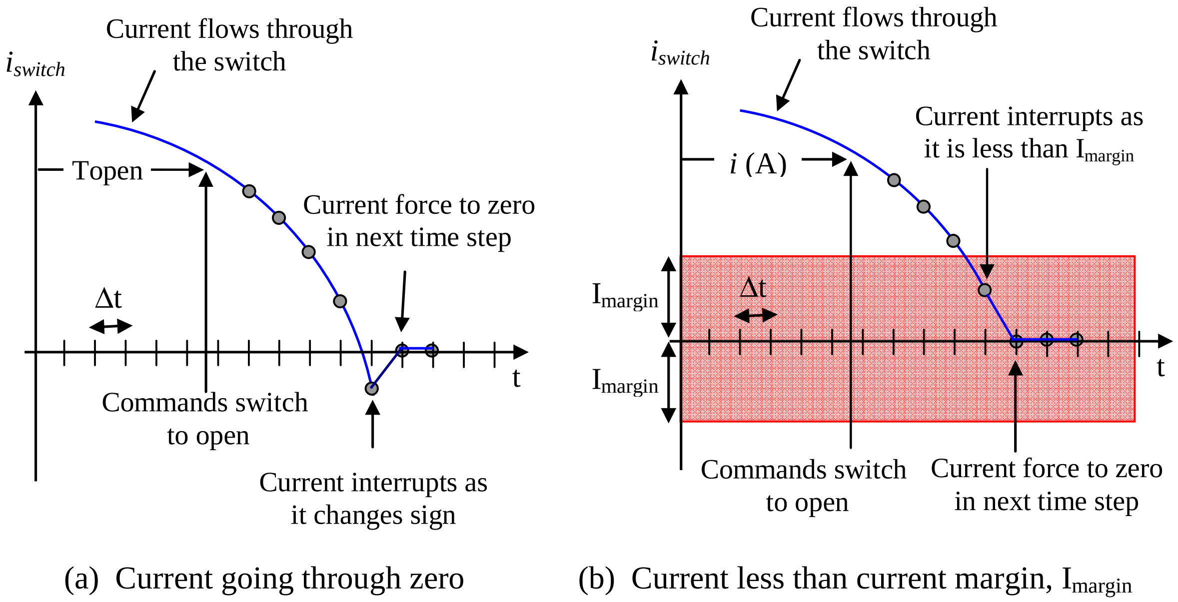

(a) Current going through zero (b) Current less than current margin, I_{margin}

Figure 4.1: Circuit breaker opening criteria

(a) No current margin ($I_{margin}= 0$)

If the circuit breaker is assumed to have no current margin and it is commanded to open at Topen, the breaker will not open if t <Topen. However, it will open as soon as the current goes through zero by detecting changes in current sign when t >Topen. Once the current is interrupted successfully, the breaker will remain open. The detailed switching process is shown in Figure 4.1(a). Note that T_{open} is the idealized time commanding the opening of the circuit breaker before full current interruption, simply for simulation purpose.

(b) With current margin ($I_{margin}\neq 0$)

With current margin (I_{margin}) defined as a value which is less than the peak current, the breaker will open if the current is within the region of predefined current margin as soon as the breaker is commanded to open (i.e. t>Topen). The detailed switching process is shown in Figure 4.1(b). I_{margin} is actually the current chopping which relates to real circuit breaker operation.

From the above, the criterion employed by the time-controlled switch to command the opening of the circuit breaker considers ideal breaking action without taking account of arc and restrike characteristics. Are these characteristics really needed and what level of model complexity for a circuit breaker is required for ferroresonance study? For ferroresonance study, the circuit breaker with its simplistic form is sufficient because of the following:

- In respect to the Thorpe-Marsh/Brinsworth system, prior to the reconfiguration of the system the current passing through the circuit breaker involved the line charging current and the current for the affected power transformer (SGT1) which is at no-load with a small cable charging current at the secondary. Therefore, modeling circuit breaker with its arc mechanism is not required as this is only applicable for high current interruption such as a short-circuit current.
- Circuit breaker's restrike characteristic representation is normally employed in a situation where high frequency current interruption of breaker occurs, typically in a frequency range from 10 kHz up to 3 MHz [2, 45, 46]. Therefore, modeling to account for this behaviour is not required as ferroresonance is a low frequency phenomenon which has a range of frequency from 0.1 Hz up to 1 kHz [45]. Indeed, 50 Hz and 16.67 Hz ferroresonance have been induced in the Thorpe-Marsh/Brinsworth system [47].

In addition to the above, the model criteria as described in Table 4.1 [45] have not recommended any but the mechanical pole spread under the category of the Low Frequency Transient to which ferroresonance falls into.

Table 4.1: Modeling guidelines for circuit breakers proposed by CIGRE WG 33-02

OPERATION	**Low Frequency Transient**	**Slow Front Transient**	**Fast-Front Transient**	**Very Fast-Front Transient**
Closing				
Mechanical pole spread	Important	Very important	Negligible	Negligible
Prestrikes (decrease of sparkover voltage versus time)	Negligible	Important	Important	Very important
Opening				
High current interruption (arc equation)	Important only for interruption capability studies	Important only for interruption capability studies	Negligible	Negligible
Current chopping (arc instability)	Negligible	Important only for interruption of small inductive currents	Important only for interruption of small inductive currents	Negligible
Restrike characteristic (increase of sparkover voltage versus time)	Negligible	Important only for interruption of small inductive currents	Very important	Very important
High frequency current interuption	Negligible	Important only for interruption of small inductive currents	Very important	Very important

It is therefore suggested that for modeling circuit breaker's opening operation, 3-phase time-controlled switches are employed in ferroresonance study.

4.3 Power Transformer

Electrical power produced from generation stations has to be delivered over a long distance for consumption. To enable a large amount of power to be transmitted through small conductors while keeping the losses small the use of very high transmission voltages is required. Therefore, a step-up transformer is employed to increase the voltage to a very high level. In the distribution level, the high voltages are then step-down for distribution to customers.

Transformers are considered to be one of the most universal components employed in power transmission and distribution networks. Their complex structures mainly consist of electromagnetic circuits. They are operating in a linear region of their magnetic characteristic, drawing transformation of steady state sinusoidal voltages and currents. However, there are instances the operating linear region is breached when the transformer is subjected to the influence of an abnormal event. This incident could eventually lead to one of the low frequency transient events, a phenomenon known as ferroresonance.

High peaky current will be drawn from the system once transformers are impinged upon by ferroresonance. In view of this, transformers are constrained in their performance by the magnetic flux limitations of the core. Core materials cannot support infinite magnetic flux densities: they tend to "saturate" at a certain level, meaning that further increases in magnetic field force (m.m.f) do not result in proportional increases in magnetic field flux (Φ). In this regard, the transformer cores become nonlinear and they have to be modeled correctly to characterise saturation effect. Saturation effect introduces distortion of the excitation current when the cores are under the influence of nonlinearity.

In modeling the nonlinear core of transformer, core saturation effect can be represented by either a single-value curve alone or with loss to account for major hysteresis curve. Both representations are studied to differentiate their variations in generating the excitation currents. In addition, the harmonic contents of the excitation currents operating along the core characteristic are also studied.

Two mathematical approaches based on [35, 48, 49] are used to characteristic core saturation; they are the single-value curve (without loss) and the major hysteresis curve (with loss), and each of them is presented in the following section.

4.3.1 The Anhysteretic Curve

The anhysteretic curve is the core characteristic without taking any loss into account and it is represented by the dotted curve labelled as '*gob*' which is situated in the first and third quadrants of λ-i plane of Figure 4.2. The curve is also called the "true saturation part" or "single-value curve", which gives the relationship between peak values of flux linkage (λ) and peak values of magnetising current (i). This curve is represented by a nonlinear inductance, L_{m}.

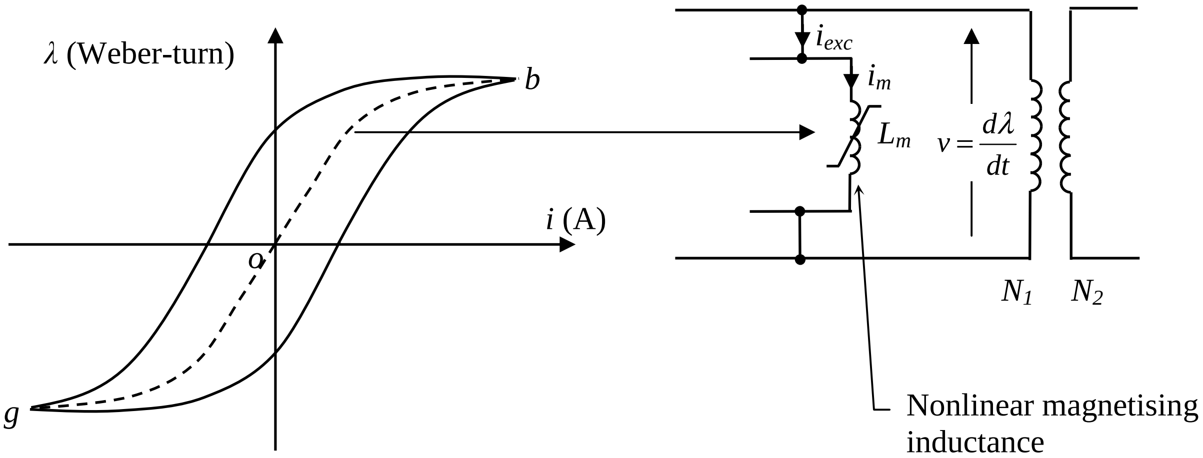

Figure 4.2: Hysteresis loop

The curve is represented by a p^{th} order polynomial which has the following form:

$$i_m = A\lambda + B\lambda^p \tag{4.1}$$

where $p = 1, 3, 5 \ldots$ and the exponent p depends on the degree of saturation.

The core characteristic of a 1000 MVA, 400 kV/275 kV/13 kV derived from equation (4.1) is shown in Figure 4.3, where $p = 27$.

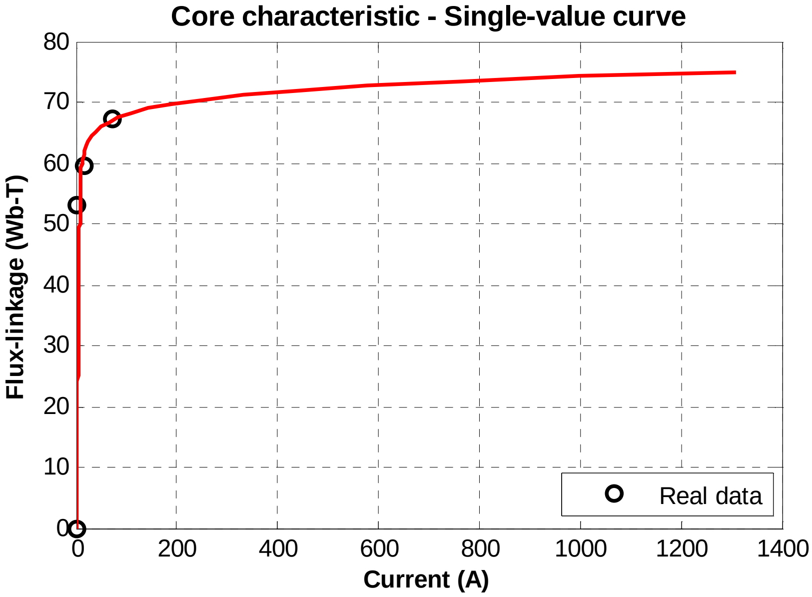

Figure 4.3: λ-i characteristic derived from $i_m=A\lambda+B\lambda^p$

With a sinusoidal voltage e_1 applied to the transformer, the flux linkage will be sinusoidal in nature and it is given as

$$\lambda = \lambda_m\, sin\left(\omega t\right) \tag{4.2}$$

Substitute (4.2) into (4.1) and rearranging, the following is obtained:

$$i_m = A\left[\lambda_m \sin\left(\omega t\right)\right] + B\left[\lambda_m \sin\left(\omega t\right)\right]^p \tag{4.3}$$

With the exponent, p = 27, then the expansion of $\sin^{27}(\omega t)$ is carried out using Bromwich formula (4.4) [50] of,

$$\begin{aligned}\sin\left(n\alpha\right) = nx - \frac{n\left(n^2-1^2\right)x^3}{3!} + \frac{n\left(n^2-1^2\right)\left(n^2-3^2\right)x^5}{5!} \\ - \frac{n\left(n^2-1^2\right)\left(n^2-3^2\right)\left(n^2-5^2\right)x^7}{7!} \ldots\ldots\ldots\ldots\ldots\ldots\ldots\ldots \textit{for n odd}\end{aligned} \tag{4.4}$$

Where $x = \sin\alpha$

The outcome of the expansion reveals as the following:-

$$\sin^{27}(\omega t) = \frac{1}{b}\begin{pmatrix} a_1 \sin(\omega t) - a_3 \sin(3\omega t) + a_5 \sin(5\omega t) \\ -a_7 \sin(7\omega t) + a_9 \sin(9\omega t) - a_{11} \sin(11\omega t) \\ +a_{13} \sin(13\omega t) - a_{15} \sin(15\omega t) + a_{17} \sin(17\omega t) \\ -a_{19} \sin(19\omega t) + a_{21} \sin(21\omega t) - a_{23} \sin(23\omega t) \\ +a_{25} \sin(25\omega t) - a_{27} \sin(27\omega t) \end{pmatrix} \tag{4.5}$$

where the constants are found to be:

b = 67108864; a_1 = 20058300; a_3 = 17383860; a_5 = 13037895; a_7 = 8436285; a_9 = 4686825; a_{11} = 2220075; a_{13} = 888030; a_{15} = 296010; a_{17} = 80730; a_{19} = 17550; a_{21} = 2925; a_{23} = 351; a_{25} = 27; a_{27} = 1;

Substituting (4.5) into (4.3)

$$i_m = A'\sin\left(\omega t\right) + B'\left\{\frac{1}{b}\begin{pmatrix} a_1\sin(\omega t) - a_3\sin(3\omega t) + a_5\sin(5\omega t) \\ -a_7\sin(7\omega t) + a_9\sin(9\omega t) - a_{11}\sin(11\omega t) \\ +a_{13}\sin(13\omega t) - a_{15}\sin(15\omega t) + a_{17}\sin(17\omega t) \\ -a_{19}\sin(19\omega t) + a_{21}\sin(21\omega t) - a_{23}\sin(23\omega t) \\ +a_{25}\sin(25\omega t) - a_{27}\sin(27\omega t) \end{pmatrix}\right\} \tag{4.6}$$

Where $A' = A\lambda_m$, $B' = B\lambda_m^{27}$

Finally, the general equation of magnetising current in the time domain without the hysteresis effect is derived as,

$$\begin{aligned} i_m = {} & \hat{I}_1\sin\left(\omega t\right) + \hat{I}_3\sin\left(3\omega t\right) + \hat{I}_5\sin(5\omega t) + \hat{I}_7\sin(7\omega t) + \hat{I}_9\sin(9\omega t) \\ & + \hat{I}_{11}\sin(11\omega t) + \hat{I}_{13}\sin(13\omega t) + \hat{I}_{15}\sin(15\omega t) + a_{17}\sin(17\omega t) \\ & + \hat{I}_{19}\sin(19\omega t) + \hat{I}_{21}\sin(21\omega t) + \hat{I}_{23}\sin(23\omega t) + \hat{I}_{25}\sin(25\omega t) + \hat{I}_{27}\sin(27\omega t) \end{aligned} \tag{4.7}$$

Where

$$\hat{I}_1 = A' + \frac{a_1}{b}B',\ \hat{I}_3 = -\frac{a_3}{b}B',\ \hat{I}_5 = \frac{a_5}{b}B',\ \hat{I}_7 = -\frac{a_7}{b}B',\ \hat{I}_9 = \frac{a_9}{b}B',\ \hat{I}_{11} = -\frac{a_{11}}{b}B',$$

$$\hat{I}_{13} = \frac{a_{13}}{b}B',\ \hat{I}_{15} = -\frac{a_{15}}{b}B',\ \hat{I}_{17} = \frac{a_{17}}{b}B',\ \hat{I}_{19} = -\frac{a_{19}}{b}B',\ \hat{I}_{21} = \frac{a_{21}}{b}B',$$

$$\hat{I}_{23} = -\frac{a_{23}}{b}B',\ \hat{I}_{25} = \frac{a_{25}}{b}B',\ \hat{I}_{27} = -\frac{a_{27}}{b}B'$$

The magnetising current, i_m together with its harmonic contents up to 27th can be plotted using *MATLAB*. The magnetising currents, i_m operating along the core λ-i characteristic labeled as A, B, C, D and E of Figure 4.4 are studied.

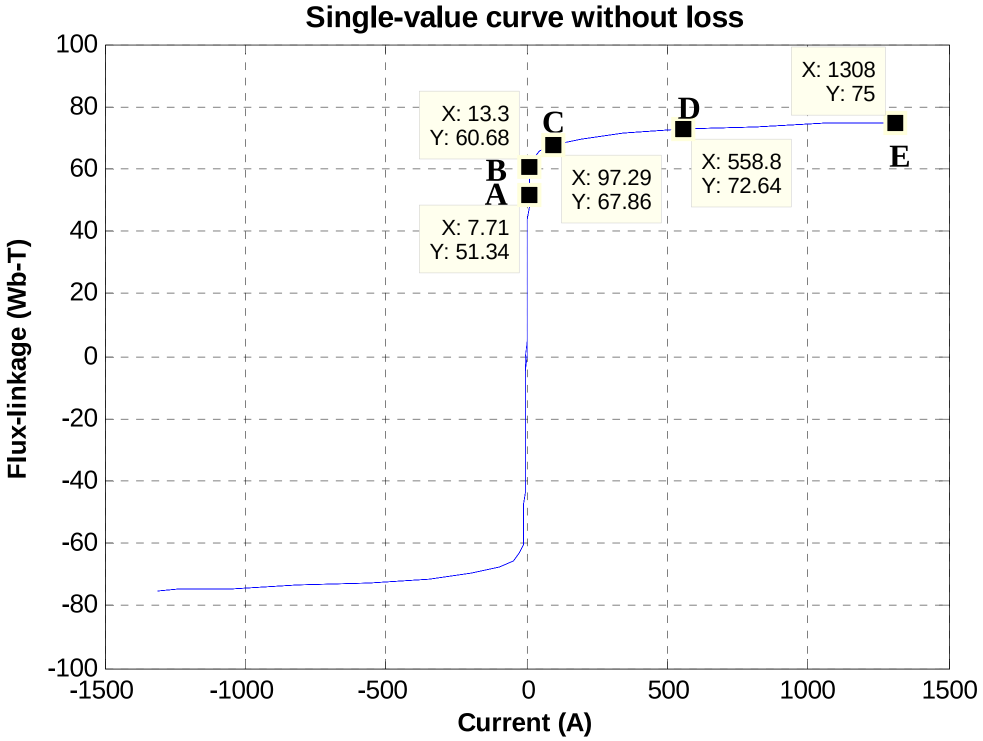

Figure 4.4: *λ-i* characteristic

The magnetising currents operating at points A, B, C, D and E along the core characteristic of Figure 4.5 are depicted accordingly as shown in Figure 4.5 to Figure 4.9.

Legends:

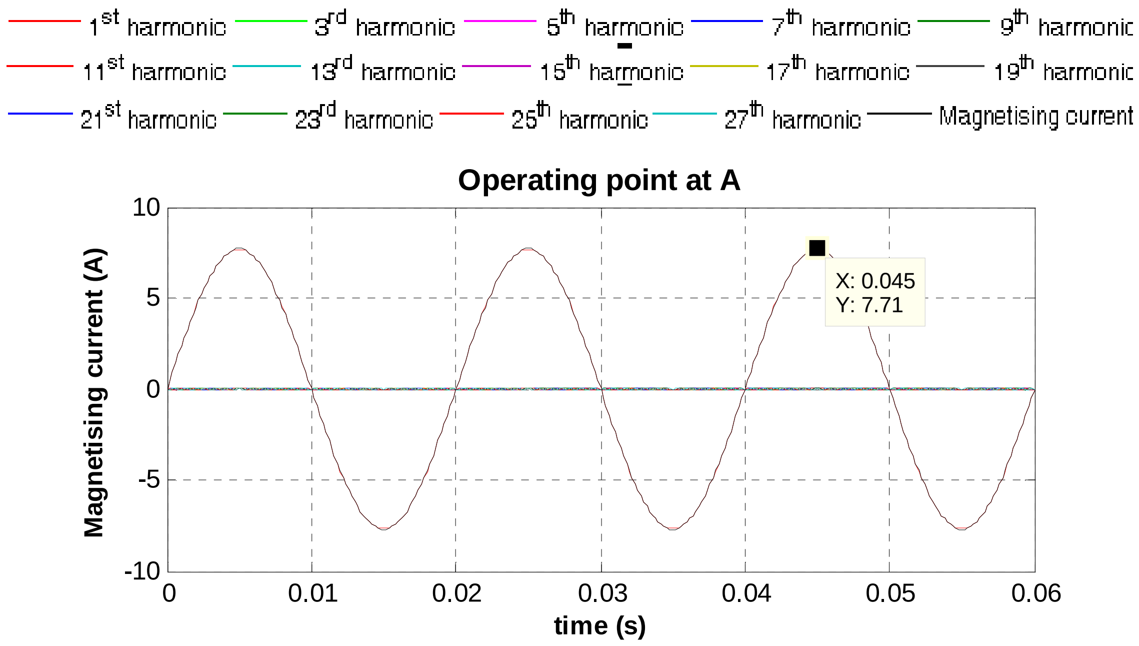

Figure 4.5: Generated current waveform at operating point A

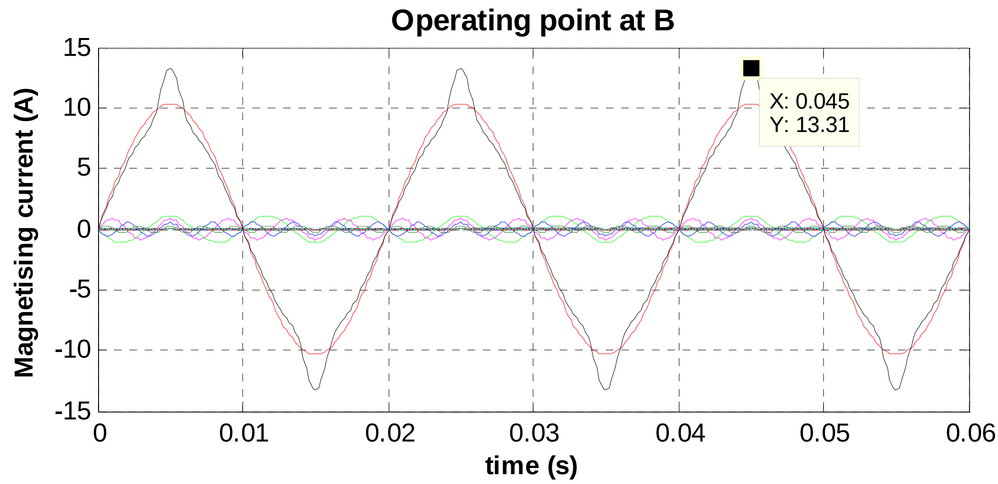

Figure 4.6: Generated current waveform at operating point B

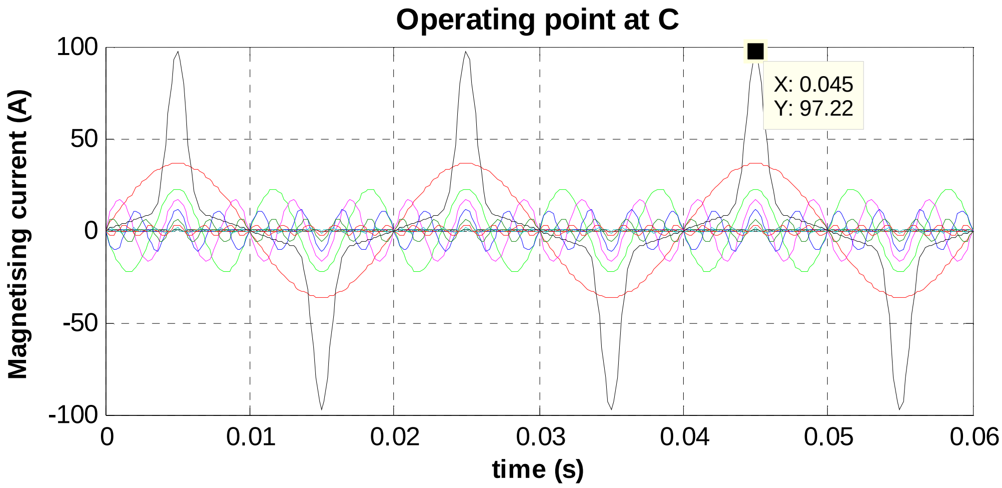

Figure 4.7: Generated current waveform at operating point C

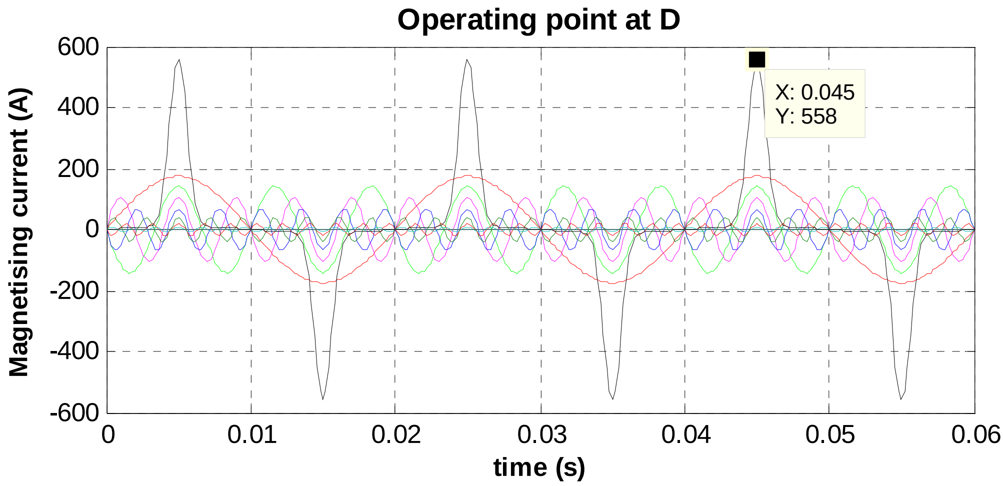

Figure 4.8: Generated current waveform at operating point D

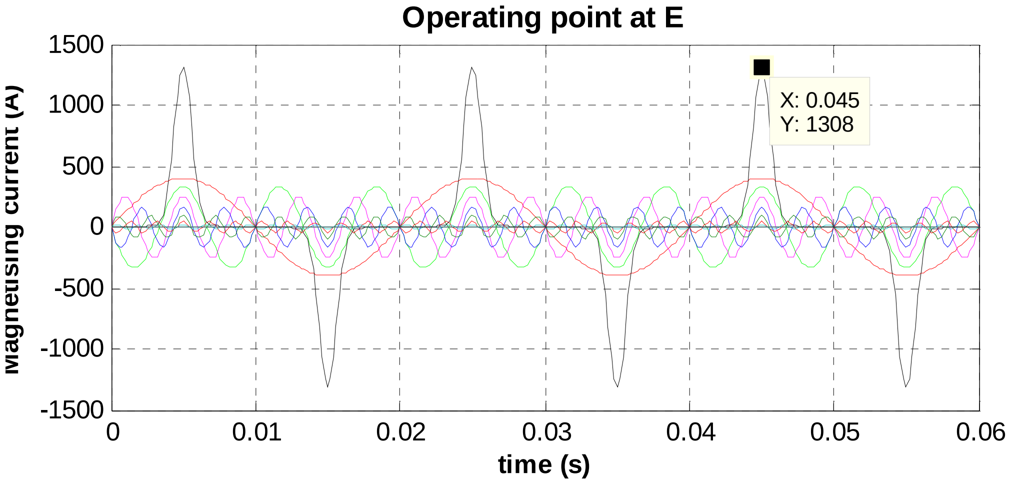

Figure 4.9: Generated current waveform at operating point E

Operating point A lies in the linear region of the λ-i characteristic as shown in Figure 4.5. The magnetising current is expected to be in sinusoidal fashion. Core operating at this point has its magnetising current equal to the fundamental component with all other harmonics negligible in amplitudes.

Operating point B is in the actual operating point i.e. near the knee point, the magnetising current is not sinusoidal but slightly distorted in shape because the amplitudes of the 3rd, 5th and 7th harmonic contents are very small but are present in the magnetising current.

Operating point C is slightly above the knee point. The magnetising current is not sinusoidal but peaky in shape as a result of introducing higher amplitudes of the harmonic contents.

Operating point D is at the middle of the core characteristic. The current waveform becomes much more peaky in shape. The magnitudes of the harmonic contents increase further causing the relative reduction in the magnitude of fundamental current.

Operating point E is in the deep saturation region of the λ-i characteristic, the magnetising current generated is high in magnitude and peaky in shape as a result of higher amplitude of harmonic current being generated.

The main observation in this study suggests that much higher amplitudes of harmonic signals are generated, particularly the 3rd, 5th and 7th harmonics when the core is driven into deep saturation.

4.3.2 Hysteresis Curve

Based on the investigation from the preceding section, the magnetising branch can be represented by a non-linear inductance, L_m which is used to characterise the saturation effect without hysteresis effect.

In order to represent saturation with hysteresis effect (i.e. hysteresis loop) in the core, a parameter called a loss function is introduced in Figure 4.10 by drawing a distance of '*ae*' in the hysteresis loop. This corresponds to adding a resistor, R_C connected in parallel with the nonlinear inductor, L_m. Base on [33], the loss function is given as,

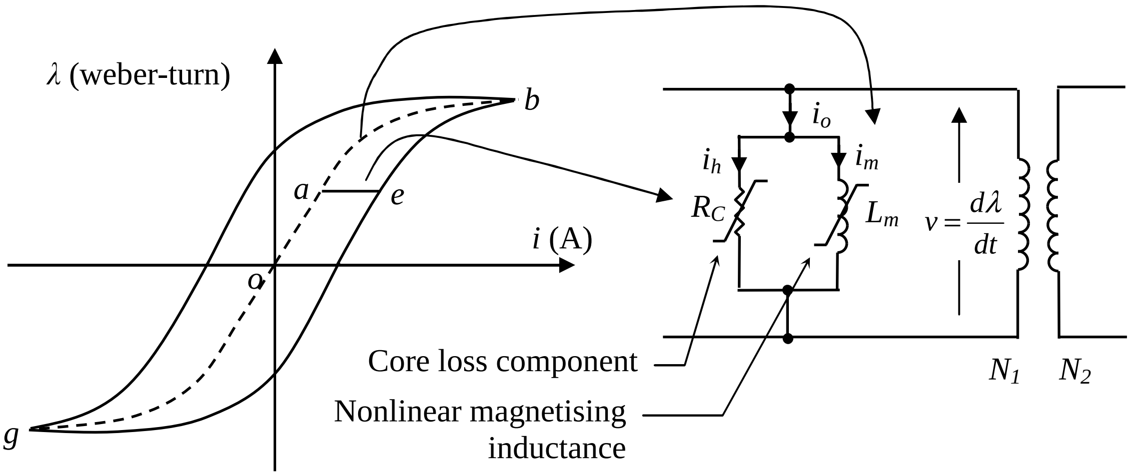

Figure 4.10: Single-phase equivalent circuit with dynamic components

$$f\left(\dot{\lambda}\right) \text{ where } \dot{\lambda} = \frac{d\lambda}{dt} \tag{4.8}$$

Incorporating the loss function to the true saturation characteristic, the mathematical expression for the hysteresis loop is

$$i_o = A\lambda + B\lambda^p + f\left(\dot{\lambda}\right) \tag{4.9}$$

The loss function which represents the loss part is approximately determined by a q^{th} even order polynomial and it is expressed as

$$f\left(\dot{\lambda}\right) = \left[C + D\left(\frac{d\lambda}{dt}\right)^q\right]\frac{d\lambda}{dt} \qquad q = 2, 4, 6 \ldots \tag{4.10}$$

The total no-load current is

$$\begin{aligned} i_o &= i_m + i_h \\ &= \left[A\lambda + B\lambda^p\right] + \left[C + D\left(\frac{d\lambda}{dt}\right)^q\right]\frac{d\lambda}{dt} \end{aligned} \qquad (4.11)$$

where i_m is the magnetising current due to magnetic core inductance, and i_h is the resistive current due to hysteresis loss.

The flux linkage is expressed as $\lambda = \lambda_m \sin(\omega t)$, then $\frac{d\lambda}{dt} = \lambda_m\, \omega\cos(\omega t)$ and substituting into (4.11) then

$$\begin{aligned} i_o &= i_m + i_h \\ &= \left\{A\left[\lambda_m \sin(\omega t)\right] + B\left[\lambda_m \sin(\omega t)\right]^p\right\} + \left\{C\left[\lambda_m\, \omega\cos(\omega t)\right] + D\left[\lambda_m\, \omega\cos(\omega t)\right]^{q+1}\right\} \\ &= \left[A'\sin(\omega t) + B'\sin^P(\omega t)\right] + \left[C'\cos(\omega t) + D'\cos^{q+1}(\omega t)\right] \end{aligned} \qquad (4.12)$$

where $A' = A\lambda_m,\ B' = B\lambda_m{}^p,\ C' = C\lambda_m\omega,\ D' = D(\lambda_m\omega)^{q+1}$

The true saturation characteristic is approximated by 27th order polynomial and the loss part $f\left(\dot{\lambda}\right)$ is approximated by the q^{th} order polynomial which will be determined by curve fitting using the power loss equation. The area of the hysteresis loop which determines the power loss per cycle is given as

$$\begin{aligned} P_{losses} &= \frac{1}{2\pi}\int_0^{2\pi}\left[v_{(t)}.i_{h(t)}\right]d(\omega t) \\ &= \frac{1}{2\pi}\int_0^{2\pi}\left\{\left[V_m \cos(\omega t)\right].\left[C'\cos(\omega t) + D'\cos^{q+1}(\omega t)\right]\right\}d(\omega t) \\ &= \frac{V_m}{2\pi}\int_0^{2\pi}\left[C'\cos^2(\omega t) + D'\cos^{q+2}(\omega t)\right]d(\omega t) \\ &= \frac{V_m}{2\pi}\left\{\int_0^{2\pi} C'\cos^2(\omega t)\,d(\omega t) + \int_0^{2\pi} D'\cos^{q+2}(\omega t)\,d(\omega t)\right\} \end{aligned} \qquad (4.13)$$

For the first term, since $\cos^2\theta = \frac{1}{2}\left[\cos(2\theta) + 1\right]$ and solving it yields,

$$\begin{aligned}
First\ term:\ \frac{V_m}{2\pi}\int_0^{2\pi} C'\cos^2(\omega t)\,d(\omega t) &= \frac{V_m C'}{2(2\pi)}\int_0^{2\pi}\left[\cos(2\omega t)+1\right]d(\omega t)\\
&= \frac{V_m C'}{2(2\pi)}\left[\frac{1}{2}\sin(2\omega t)+\omega t\right]_0^{2\pi}\\
&= \frac{V_m C'(2\pi)}{2(2\pi)}\\
&= \frac{C'V_m}{2}\\
&= \frac{CV_m^2}{2}
\end{aligned}$$

$$\begin{aligned}
Second\ term:\frac{V_m}{2\pi}\int_0^{2\pi} D'\cos^{q+2}(\omega t)\,d(\omega t) &= \frac{V_m D'}{2\pi}\int_0^{2\pi} D'\cos^{n}(\omega t)\,d(\omega t)\\
&= \frac{V_m D'}{2\pi}\left[\frac{1}{n}\cos^{n-1}(\omega t)\sin(\omega t)\right]_0^{2\pi} + \frac{n-1}{n}I_{n-2}\\
&= \frac{V_m D'}{2\pi}\left[\frac{n-1}{n}I_{n-2}\right]\\
&= \frac{DV_m^{q+2}}{2\pi}\left[\frac{(n-1)(n-3)(n-5)...}{n(n-2)(n-4)...}\times 2\pi\right]
\end{aligned}$$

where $n = q+2$, $I_{n-2} = \int_0^{2\pi}\cos^{n-2}(\omega t)\,d(\omega t)$

Note: $I_0 = \int_0^{2\pi}\cos^0(\omega t)\,d(\omega t) = 2\pi$

Finally, the general core loss is expressed as,

$$P_{losses} = \frac{CV_m{}^2}{2} + DV_m{}^{q+2}\left[\frac{(q+1)(q-1)(q-3)(q-5)(q-7)...}{(q+2)(q)(q-2)(q-4)(q-6)...}\right] \tag{4.14}$$

To confirm the correctness of equation (4.14), an example is carried out by deriving the power equation without using equation (4.14). It is assumed that in a modern transformer, the true saturation characteristic is approximated by a fifth order polynomial and the loss part $f(\dot{\lambda})$ approximation by the cubic order, i.e. p = 5 and q = 2. Then,

$$\begin{aligned}
P_{losses} &= \frac{1}{2\pi}\int_0^{2\pi}\left[v_{(t)}.i_{h(t)}\right]d\left(\omega t\right)\\
&= \frac{1}{2\pi}\int_0^{2\pi}\left\{\left[V_m\cos\left(\omega t\right)\right].\left[C'\cos\left(\omega t\right)+D'\cos^{2+1}\left(\omega t\right)\right]\right\}dt\\
&= \frac{V_m}{2\pi}\int_0^{2\pi}\left[C'\cos^2\left(\omega t\right)+D'\cos^{2+2}\left(\omega t\right)\right]d\left(\omega t\right)\\
&= \frac{V_m}{2\pi}\left\{\int_0^{2\pi}C'\cos^2\left(\omega t\right)d\left(\omega t\right)+\int_0^{2\pi}D'\cos^4\left(\omega t\right)d\left(\omega t\right)\right\}
\end{aligned}\tag{4.15}$$

For the first term, since $\cos^2\theta=\frac{1}{2}\left[\cos\left(2\theta\right)+1\right]$ and solving yields,

$$\begin{aligned}
\textit{First term}:\frac{V_m}{2\pi}\int_0^{2\pi}C'\cos^2\left(\omega t\right)d\left(\omega t\right) &= \frac{V_mC'}{\left(2\pi\right)2}\int_0^{2\pi}\left[\cos\left(2\omega t\right)+1\right]d\left(\omega t\right)\\
&= \frac{V_mC'}{2\left(2\pi\right)}\left[\frac{1}{2}\sin\left(2\omega t\right)+\omega t\right]_0^{2\pi}\\
&= \frac{C'V_m\left(2\pi\right)}{2\left(2\pi\right)}\\
&= \frac{CV_m{}^2}{2}
\end{aligned}$$

$$\begin{aligned}
\textit{Second term}:\frac{V_m}{2\pi}\int_0^{2\pi}D'\cos^4\left(\omega t\right)d\left(\omega t\right) &= \frac{V_mD'}{\left(2\pi\right)4}\int_0^{2\pi}\left\{\left[\cos\left(2\omega t\right)+1\right]\left[\cos\left(2\omega t\right)+1\right]\right\}d\left(\omega t\right)\\
&= \frac{V_mD'}{\left(2\pi\right)4}\int_0^{2\pi}\left\{\frac{1}{2}\cos\left(4\omega t\right)+\frac{1}{2}+2\cos\left(2\omega t\right)+1\right\}d\left(\omega t\right)\\
&= \frac{V_mD'}{\left(2\pi\right)4}\left[\frac{1}{8}\sin\left(4\omega t\right)+\frac{1}{2}\omega t+\sin\left(2\omega t\right)+\omega t\right]_0^{2\pi}\\
&= \frac{3DV_m{}^4}{8}
\end{aligned}$$

Finally, the core-loss is expressed as,

$$\begin{aligned}
P_{losses} &= \frac{V_m}{2\pi}\left\{\int_0^{2\pi}C'\cos^2\left(\omega t\right)d\left(\omega t\right)+\int_0^{2\pi}D'\cos^4\left(\omega t\right)d\left(\omega t\right)\right\}\\
&= \frac{1}{2}CV_m{}^2+\frac{3}{8}DV_m{}^4
\end{aligned}\tag{4.16}$$

The power-loss which has been derived in equation (4.16) is proved to be mathematically correct with the power loss equation (4.14) by using the previous assumptions of $p=5$ and $q=2$ then

$$P_{losses} = \frac{CV_m^{\ 2}}{2} + DV_m^{\ q+2}\left[\frac{(q+1)(q-1)}{(q+2)(q)}\right]$$

then

$$P_{losses} = \frac{CV_m^{\ 2}}{2} + DV_m^{\ 2+2}\left[\frac{(2+1)(1)}{(2+2)2}\right]$$

$$= \frac{CV_m^{\ 2}}{2} + \frac{3}{8}DV_m^{\ 4}$$

which is the same as equation (4.16)

As can be seen from the power-loss equation, the core loss is dependent on the voltage across the transformer. *C* and *D* are constants that need to be obtained by curve fitting over the open-circuit test data of the transformer.

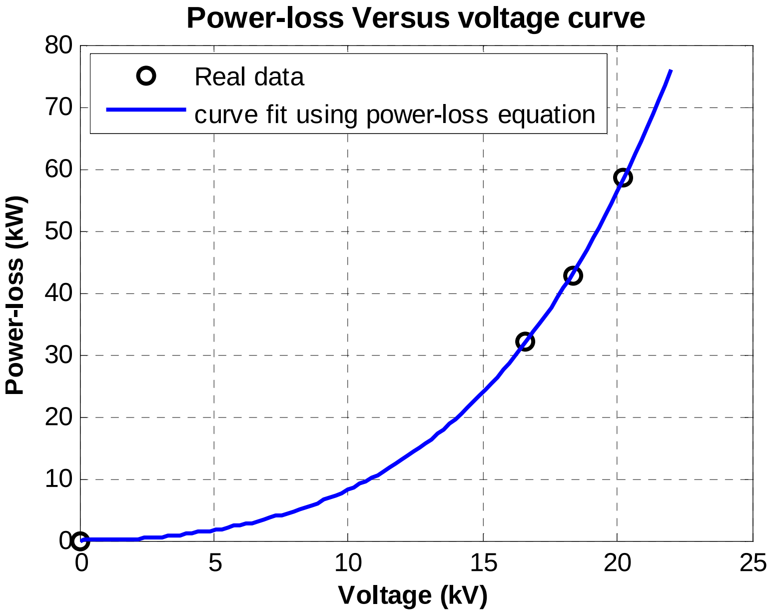

Figure 4.11: Power-loss data and curve fit curve

Once all the constants have been determined, the next step is to develop a saturation characteristic with hysteresis effect (i.e. the hysteresis loop) based on equation (4.12). Then

$$\begin{aligned} i_o &= i_m + i_h \\ &= \left\{A\left[\lambda_m \sin(\omega t)\right] + B\left[\lambda_m \sin(\omega t)\right]^p\right\} + \left\{C\left[\lambda_m \cos(\omega t)\right] + D\left[\lambda_m \cos(\omega t)\right]^{q+1}\right\} \\ &= \left[A'\sin(\omega t) + B'\sin^P(\omega t)\right] + \left[C'\cos(\omega t) + D'\cos^{q+1}(\omega t)\right] \end{aligned} \tag{4.17}$$

where $A' = A\lambda_m$, $B' = B\lambda_m^{\ p}$, $C' = C\lambda_m\omega$, $D' = D(\lambda_m\omega)^{q+1}$

Expanding the above equation using $p = 27$ and $q = 2$,

$$i_o = A'\sin\left(\omega t\right) + B'\left\{ \frac{1}{b}\left(\begin{array}{l} a_1\sin(\omega t) - a_3\sin(3\omega t) + a_5\sin(5\omega t) \\ -a_7\sin(7\omega t) + a_9\sin(9\omega t) - a_{11}\sin(11\omega t) \\ +a_{13}\sin(13\omega t) - a_{15}\sin(15\omega t) + a_{17}\sin(17\omega t) \\ -a_{19}\sin(19\omega t) + a_{21}\sin(21\omega t) - a_{23}\sin(23\omega t) \\ +a_{25}\sin(25\omega t) - a_{27}\sin(27\omega t) \end{array} \right) \right\} \\ + \left[C'\cos\left(\omega t\right) + D'\cos^{q+1}\left(\omega t\right) \right] \tag{4.18}$$

Rearranging in the fundamental of sin(ωt) and cos(ωt), and the third harmonics of sin(3ωt) and cos(3ωt) terms yields,

$$\begin{aligned} i_o = {} & \sqrt{\left(A\lambda_m + \frac{a_1}{b}B\lambda_m^{27} \right)^2 + \left(C\lambda_m\omega + \frac{3}{4}D\lambda_m^3\omega^3 \right)^2}\,\sin\left(\omega t + \tan^{-1}\frac{\left(C\lambda_m\omega + \frac{3}{4}D\lambda_m^3\omega^3 \right)}{\left(A\lambda_m + \frac{a_1}{b}B\lambda_m^{27} \right)} \right) \\ & + \sqrt{\left(-\frac{a_3}{b}B\lambda_m^{27} \right)^2 + \left(\frac{1}{4}D\lambda_m^3\omega^3 \right)^2}\,\sin\left(3\omega t + \tan^{-1}\frac{\left(\frac{1}{4}D\lambda_m^3\omega^3 \right)}{\left(-\frac{a_3}{b}B\lambda_m^{27} \right)} + \pi \right) \\ & + B\lambda_m^{27}\left\{ \frac{1}{b}\left[a_5\sin\left(5\omega t\right) - a_7\sin\left(7\omega t\right) + a_9\sin\left(9\omega t\right) \ldots + a_{27}\sin\left(27\omega t\right) \right] \right\} \end{aligned} \tag{4.19}$$

Using *MATLAB*, the single-value with loss characteristic as shown in Figure 4.12 is determined using equation (4.19) and $\lambda = \lambda_m \sin\left(\omega t\right)$.

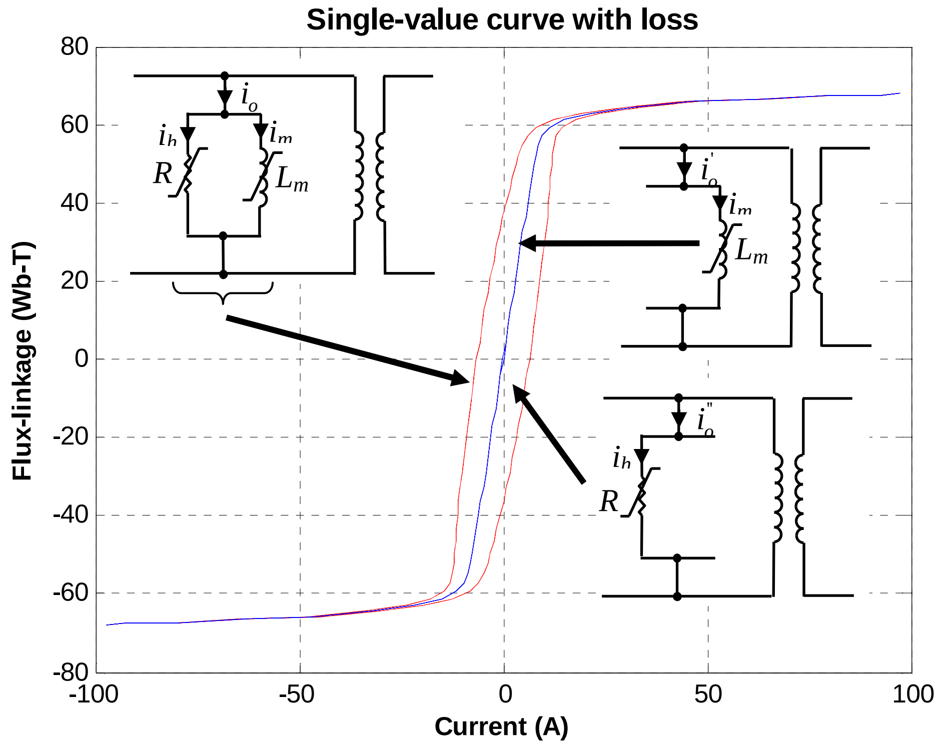

Figure 4.12: Effect of introducing the loss function

With the effect of the hysteresis, the currents operating at points as labeled similarly in the previous study i.e. A, B, C, D and E along the curve are plotted as shown in Figure 4.13 to Figure 4.17.

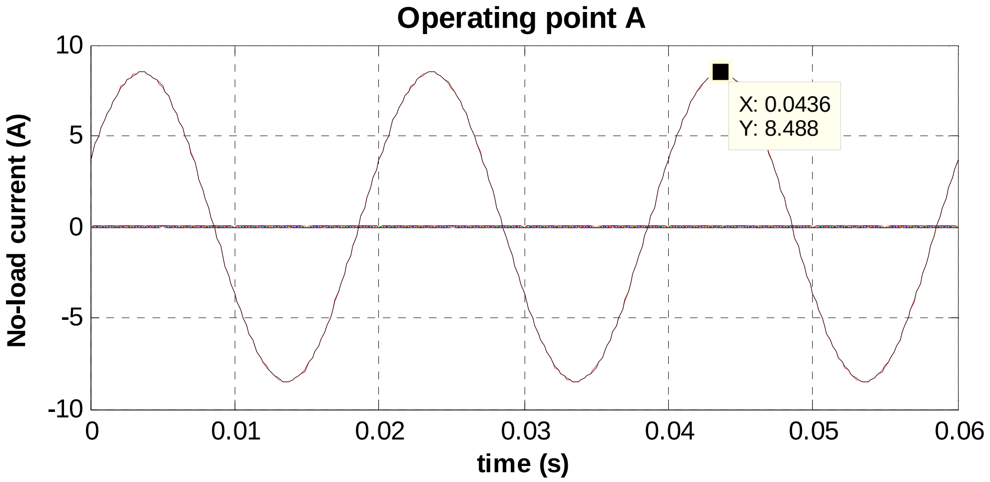

Figure 4.13: With loss function - current waveform at point A

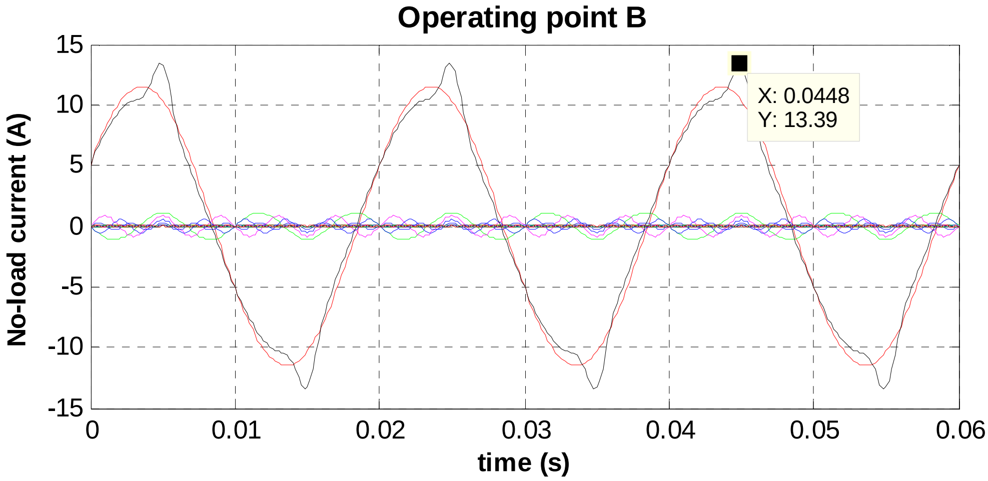

Figure 4.14: With loss function **-** current waveform at point B

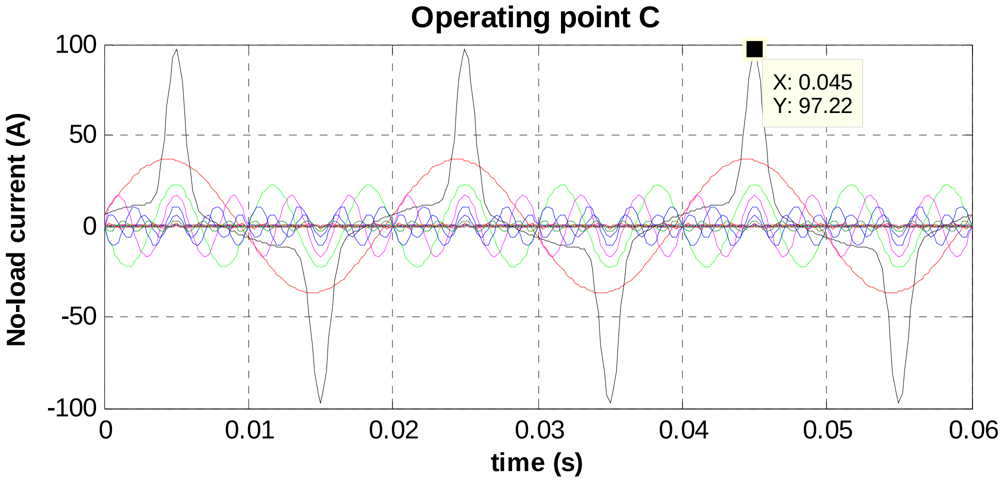

Figure 4.15: With loss function **-** current waveform at point C

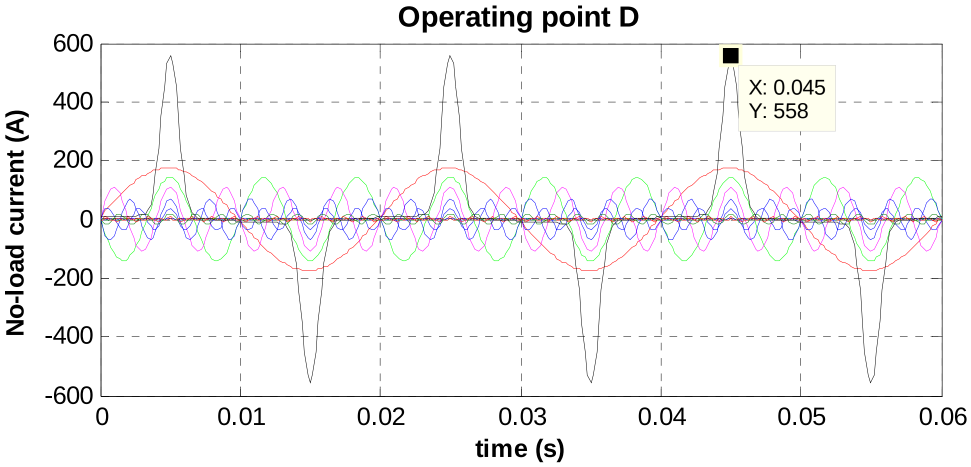

Figure 4.16: With loss function **-** current waveform at point D

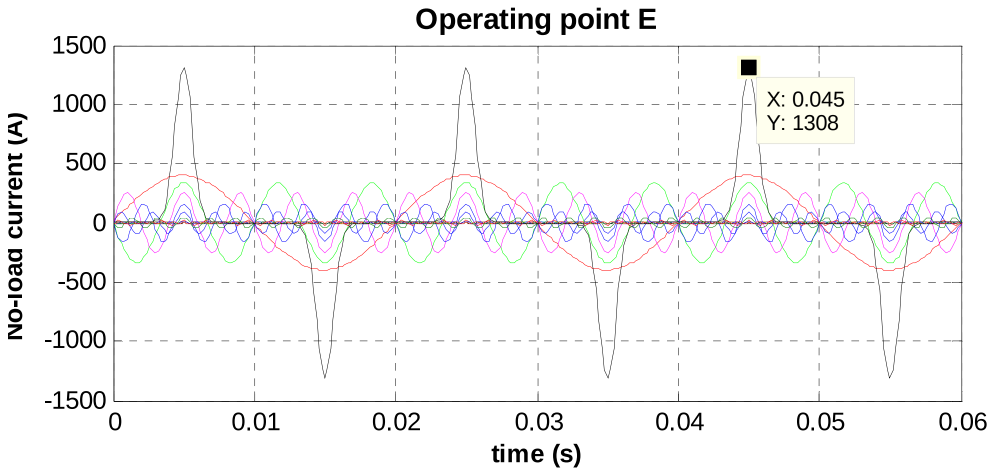

Figure 4.17: With loss function - current waveform at point E

The current waveforms as shown in Figure 4.13 to Figure 4.17 suggest that there is an influence of the loss on the shape of the current waveform, particularly around the knee point region. A comparison between the anhysteretic and the hysteresis curves is taken in Figure 4.18 when the core is operating at point C.

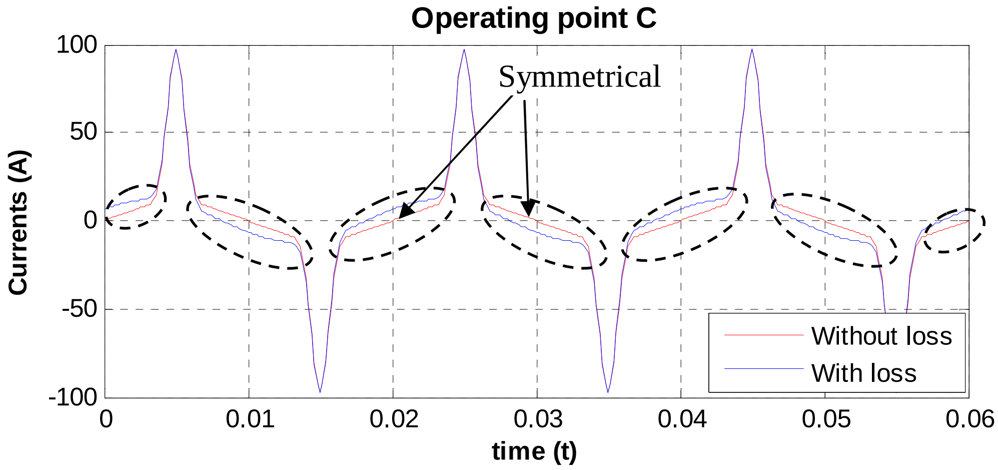

Figure 4.18: Comparison between loss and without loss – around knee region

The influence of the loss on the waveform of the current is noticeable as indicated by the dotted line, the current without the loss as shown in the diagram has a symmetrical shape against the vertical axis. However, the one with the loss, the current (blue colour) as indicated in broken line shifted slightly. Depending on the loss, the greater the area of the loss, the higher the shift will be. On the other hand, when the core is driven into deep saturation, the influence of the loss is not significant on the waveform anymore and the comparison can be seen in Figure 4.19.

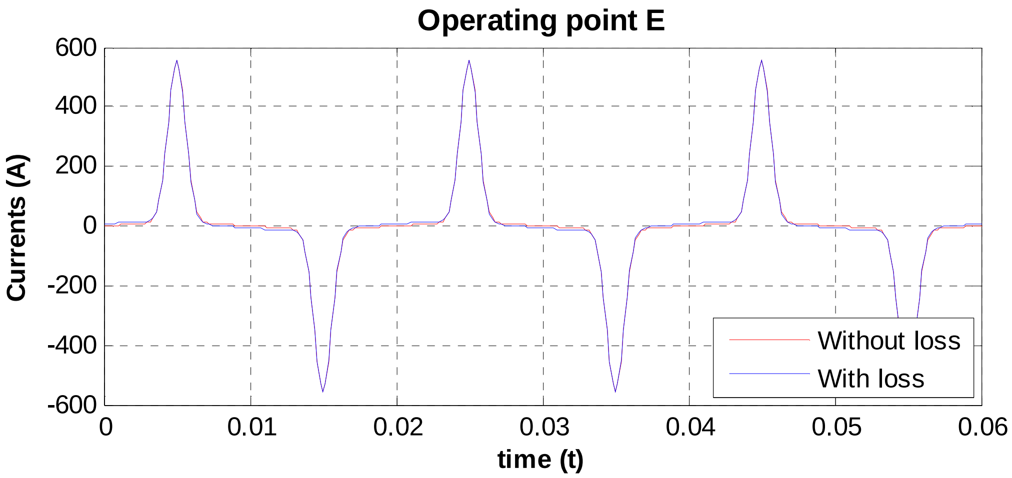

Figure 4.19: Comparison between loss and without loss – deep saturation

Figure 4.19 suggests that similar current amplitudes and shapes have been produced by both the cases with and without loss when the core is driven into deep saturation.

In view of the above, it is therefore suggested that the participation of the loss in modeling the core is necessary as ferroresonance can induce the subharmonic modes which are believed to operate around the knee region of the core characteristic. However, for the generation of high peaky current such as the one in the fundamental mode (Period-1), the loss can be disregarded and the core can be represented by only a single-value nonlinear inductor.

Now, let us look at the types of predefined transformer models which are offered in ATPDraw for the study of ferroresonance.

4.3.3 Transformer Models for Ferroresonance Study

The characteristics of power transformers can be complex when they are subjected to transient phenomena because of their complicated structure which account for the variations of magnetic core behaviour and windings. In view of this, detailed modeling of power transformer to account for such factors is difficult to achieve therefore CIGRE WG 33-02 [51] have come up with four groups of classifications aimed for providing the types of transformer model valid for a specific frequency range of transient phenomena. The classifications are shown in Table 4.2.

Table 4.2: *CIGRE* modeling recommendation for power transformer

Parameter/Effect	**Low Frequency Transients**	**Slow Front Transients**	**Fast Front Transients**	**Very Fast Front Transients**
Short-circuit impedance	***Very important***	Very important	Important	Negligible
Saturation	***Very important***	Very important(1)	Negligible	Negligible
Iron Losses	***Important(2)***	Important	Negligible	Negligible
Eddy Current	***Very important***	Important	Negligible	Negligible
Capacitive coupling	***Negligible***	Important	Very important	Very important

(1) Only for transformer energisation phenomena, otherwise important
(2) Only for resonance phenomena

As ferroresonance is having a frequency range varying from 0.1 Hz to 1 kHz [20] which falls under the category of low frequency transients, the parameters/effect which have been highlighted in Table 4.2 are necessary to be taken into account when modeling a power transformer for ferroresonance study.

Two types of predefined transformer models in ATPDraw have been taken into consideration for ferroresonance. They are namely the BCTRAN+ and the HYBRID transformer models. The detailed representations of each of the models are explained in the following sections.

4.3.3.1 BCTRAN+ Transformer Model

BCTRAN transformer model [44, 52-56] can be found in the component selection menu of the Main window in ATPDraw. The derivation of the matrix is supported by the BCTRAN supporting routine in EMTP which required both the open- and short-circuit test data, at rated frequency. The routine supports transformers with two or three windings, configuring in either wye, delta or auto connection and as well as supporting all possible phase shifts.

The formulation to describe a steady state single-phase multi-winding transformer is represented by a linear branch impedance matrix which has the following form,

$$\begin{bmatrix} V_1 \\ V_2 \\ . \\ . \\ . \\ V_N \end{bmatrix} = \begin{bmatrix} Z_{11} & Z_{12} & . & . & . & Z_{1N} \\ Z_{21} & Z_{22} & . & . & . & Z_{2N} \\ . & . & . & . & . & . \\ . & . & . & . & . & . \\ . & . & . & . & . & . \\ Z_{N1} & Z_{N2} & . & . & . & Z_{NN} \end{bmatrix} \begin{bmatrix} I_1 \\ I_2 \\ . \\ . \\ . \\ I_N \end{bmatrix} \qquad (4.20)$$

For a three-phase transformer, the formulation can be extended by replacing any element of $[Z]$ in equation (4.20) by a 3×3 submatrix of

$$\begin{bmatrix} Z_s & Z_m & Z_m \\ Z_m & Z_s & Z_m \\ Z_m & Z_m & Z_s \end{bmatrix} \qquad (4.21)$$

where Z_s = the self-impedance of a phase and Z_m is the mutual impedance among phases.

For transient solution such as ferroresonance, equation (4.20) is represented by the following matrix equation,

$$\frac{d}{dt}\begin{bmatrix} i_1 \\ i_2 \\ . \\ i_N \end{bmatrix} = \begin{bmatrix} L_{11} & L_{12} & . & L_{1N} \\ L_{21} & L_{22} & . & L_{2N} \\ . & . & . & . \\ L_{N1} & L_{N2} & . & L_{NN} \end{bmatrix}^{-1} \begin{bmatrix} v_1 \\ v_2 \\ . \\ v_N \end{bmatrix} + \begin{bmatrix} L_{11} & L_{12} & . & L_{1N} \\ L_{21} & L_{22} & . & L_{2N} \\ . & . & . & . \\ L_{N1} & L_{N2} & . & L_{NN} \end{bmatrix}^{-1} \begin{bmatrix} R_{11} & R_{12} & . & R_{1N} \\ R_{21} & R_{22} & . & R_{2N} \\ . & . & . & . \\ R_{N1} & R_{N2} & . & R_{NN} \end{bmatrix} \begin{bmatrix} i_1 \\ i_2 \\ . \\ i_N \end{bmatrix} \qquad (4.22)$$

where $[L]$ is the inductance matrix, $[R]$ is the resistance matrix, $[v]$ is a vector of terminal voltages, and $[i]$ is the current vector.

The complete transformer models for either 2- or 3-winding configuration employing BCTRAN, with an externally connected simplistic nonlinear inductive core element are shown in Figure 4.20 and Figure 4.21 respectively. This model is named BCTRAN+ transformer model.

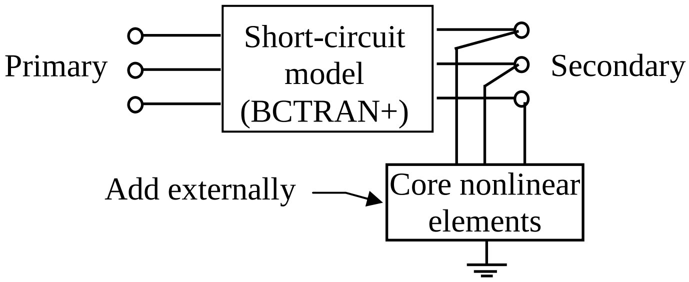

Figure 4.20: BCTRAN+ model for 2 winding transformer

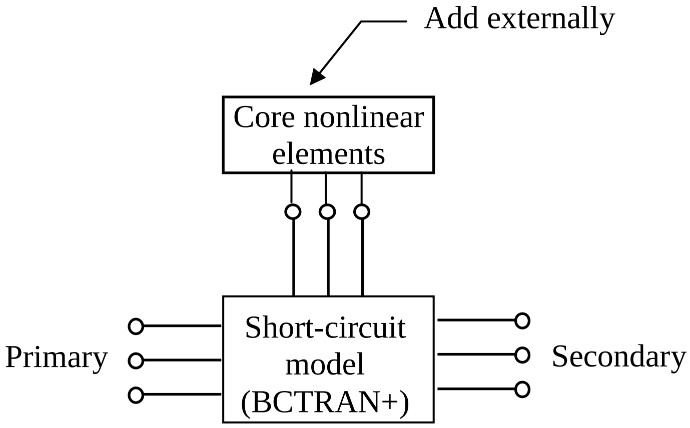

Figure 4.21: BCTRAN+ model for 3-winding transformer

The data from both the open- and short-circuited test are employed to calculate the model parameters. In order to employ the BCTRAN+ model to represent both the magnetic core saturation and losses, the core effects are omitted in the BCTRAN model and replaced by external nonlinear elements. This element is connected to the winding close to the magnetic core of the transformer.

4.3.3.2 HYBRID Transformer Model

[54, 57] described that the drawback of the BCTRAN+ model as not being able to include core nonlinearities to account for deep saturation. Since it can only be modeled externally, multi-limb topology effect on nonlinear core cannot be represented. In view of the limitation, a new transformer model known as HYBRID was then developed where its core representation is derived based on the principle of duality.

The principle is based on the duality between magnetic and electrical circuits, which was originally developed by Cherry [58] in 1949. When making calculations on an electrical circuit especially involving both transformers and electric components, it is frequently desirable to remove the transformers and replaced them by electric components connected to their terminals. With the use of the Principle of Duality, the transformer magnetic circuit can be converted to its equivalent electric circuit, which is then used to model transformers in an electrical circuit.

For the purpose of understanding, a three-phase, three-limbed core-type auto-transformer with its tertiary (T), common (C) and series (S) winding configurations as shown in Figure

4.22 is considered. The HV winding consists of series connection of the common and series windings while the LV winding is the common winding itself.

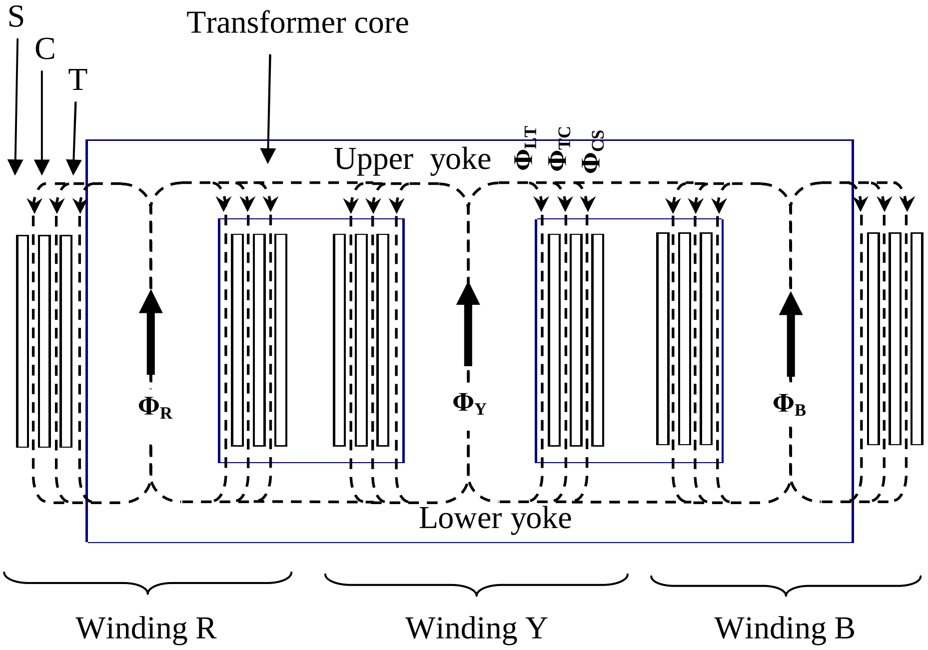

Figure 4.22: Three-phase three-limbed core-type auto-transformer

The way the leakage fluxes are distributed are based on the assumption that not all of the fluxes stay in the core and a small amount will leak out into the airgap between the windings. The fluxes named as Φ_R, Φ_Y, Φ_B and the leakage fluxes marked as Φ_{LT}, Φ_{TC}, Φ_{Cs} are distributed in the main limbs and between the three windings respectively, as shown in Figure 4.22.

The next stage is to derive the equivalent magnetic circuit [59] of the core representation which is shown in Figure 4.23 and then the graphical method of applying the Principle of Duality over the magnetic circuit is carried out.

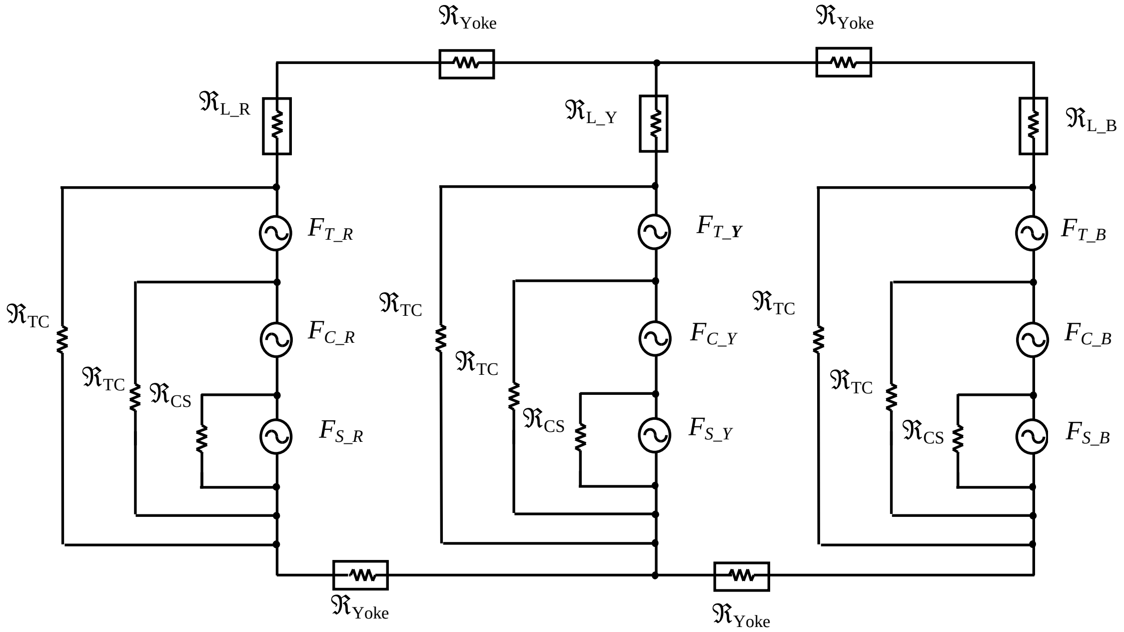

Figure 4.23: Equivalent magnetic circuit

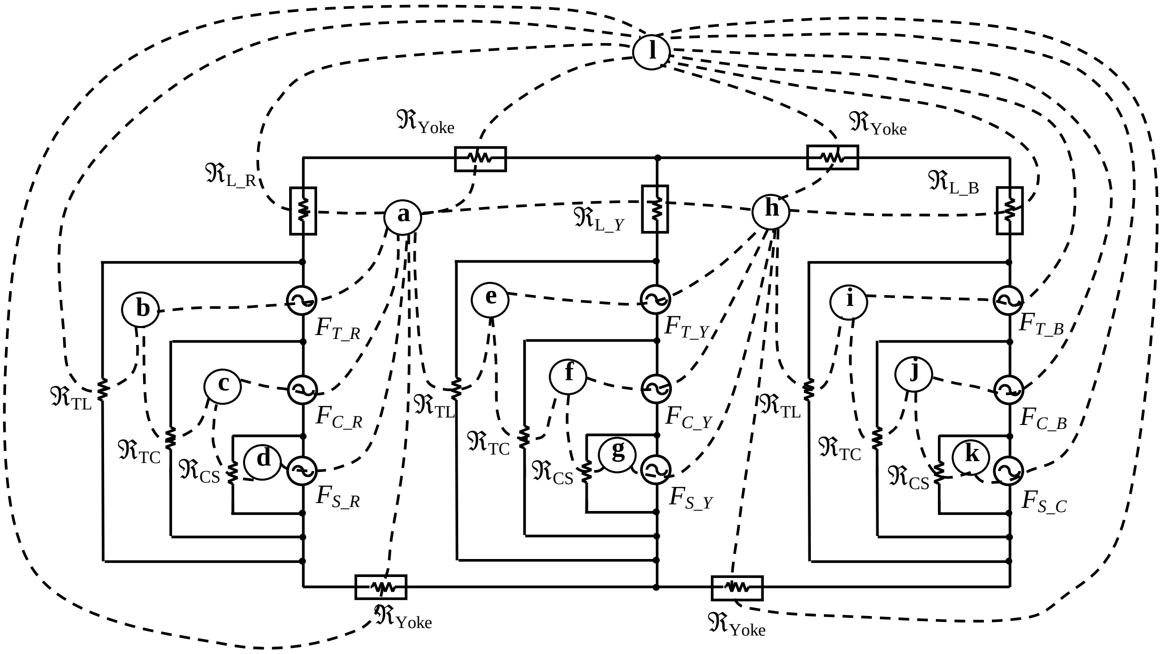

Figure 4.24: Applying Principle of Duality

In the interior of each mesh (loop) of Figure 4.24, a point is given namely a, b, c to l. These points will form the junction points of the new equivalent electric circuit. Each of these points to its neighbour only needs to be joined (see the dotted line). These points become the nodes of the electric circuit and the complete circuit is drawn as shown in Figure 4.25.

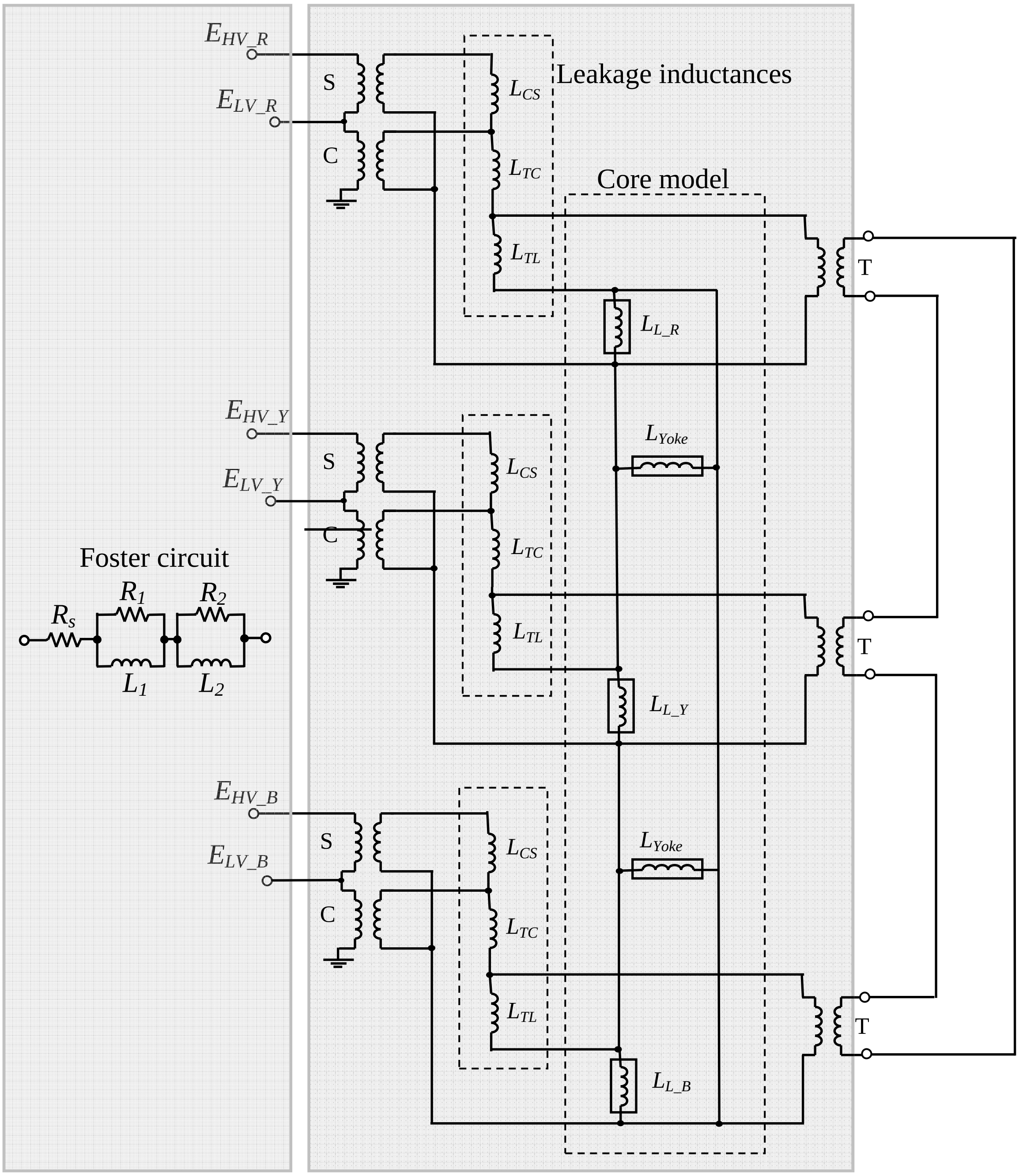

Figure 4.25: Electrical equivalent of core and flux leakages model

HYBRID model consists of the following four main sections which need to be determined in order for a complete transformer to be represented. They are the leakage inductance, the resistances, the capacitances and the core.

(1) Leakage inductances

The leakages fluxes between the windings are represented by linear inductance as L_{CS}, L_{TC} and L_{TL}.

(2) Resistances

The ways the winding resistances are represented in the model are to be added externally at the terminals of the transformer. Moreover, the resistances can be optionally presented as frequency dependent which is derived from the Foster circuit. A Foster circuit [51, 59] is used to represent the resistance of the winding which varies with the frequency of the current, i.e. the change of resistance of the winding due to the skin effects. Skin effect is due to the non-uniformly distribution of current in the winding conductor; as frequency increases, more current flows near the surface of conductor which will increase its resistance.

(3) Capacitances

External and internal coupling capacitive effects of the transformer are taken into consideration in the HYBRID model, they include

- *Capacitances between windings*: primary-to-ground, secondary-to-ground, primary-to-secondary, tertiary-to-ground, secondary-to-tertiary and tertiary-to-primary.
- *Capacitances between phases performed at primary, secondary and tertiary*: Red-to-yellow phase, yellow-to-blue phase and blue-to-red phase.

(4) Core

The core model is developed by fitting the measured excitation currents and losses. The user can specify 9 points on the magnetising characteristic to define the air-core for the transformer.

There are three different sources of data that the HYBRID model can rely on, they are

- *Design parameters* – Winding and core geometries and material properties.
- *Test report* – Standard open- and short-circuited test data from the manufacturers.
- *Typical values* - Typical values based on transformer ratings which can be found in text books. However, care needs to be taken since both design and material properties have changed a lot for the past decades.

The differences between the BCTRAN+ and the HYBRID models have been addressed in previous sections. Let us look at whether each of the representation is able to meet the criteria proposed by CIGRE as listed in Table 4.3 for the study of ferroresonance.

Table 4.3: Comparison between BCTRAN+ and HYBRID models

Parameter/Effect	Low Frequency Transients	BCTRAN+	HYBRID
Short-circuit impedance	***Very important***	√	√
Saturation	***Very important***	√	√
Iron Losses	***Important***$^{(2)}$	√	√
Eddy Current	***Very important***	√	√
Capacitive coupling	***Negligible***	√	√

(1) Short-Circuit Impedance

The way the short-circuit impedance being modeled in both the BCTRAN+ and HYBRID models is based on the short-circuit test carried out on the transformer alone. These data are available from the test report produced by the manufacturer. The main aim of this test is to represent the resistance and inductance of the transformer windings.

(2) Saturation

Detailed analysis concerning the saturations of transformer has been covered in the previous section. The ways both the BCTRAN+ and HYBRID models deal with the saturation effect are explained in the following section.

- BCTRAN+ model

The way the core is being modeled in BCTRAN+ can be referred to Figure 4.26. This model is based on the open-circuit test data of 90%, 100% and 110% and then converted into λ-i characteristic using the supporting routine “SATURA” [44, 51]. The core is then represented by three non-linear inductors connected in delta which are connected externally at the tertiary terminals of the BCTRAN+ model.

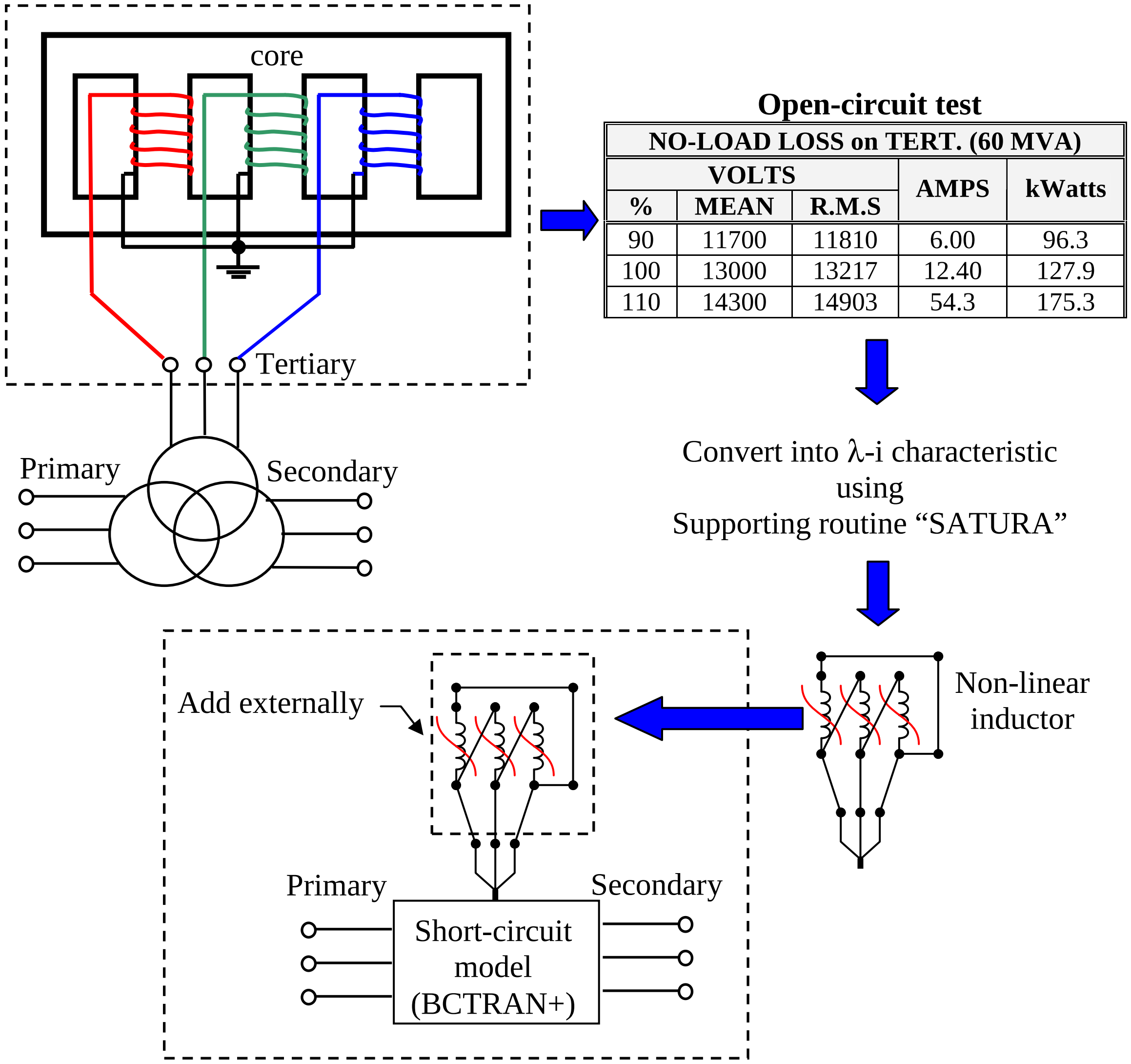

Open-circuit test

NO-LOAD LOSS on TERT. (60 MVA)				
VOLTS			AMPS	kWatts
%	MEAN	R.M.S		
90	11700	11810	6.00	96.3
100	13000	13217	12.40	127.9
110	14300	14903	54.3	175.3

Figure 4.26: Modeling of core in BCTRAN+

The three points which have been converted into λ-i characteristic are not sufficient for the study of ferroresonance therefore deep saturation points to represent air-core is necessary such that peaky current can be drawn from the transformer. The way to determine the air-core is by using the following equation,

$$i = A\lambda + B\lambda^{p} \tag{4.23}$$

- HYBRID model

The core model is developed internally by fitting the 90%, 100% and 110% data from the open-circuit test result based on the following Frolich equation [59],

$$B = \frac{H}{a + b|H|} \tag{4.24}$$

The flux-linkage versus current characteristics of the leg, yoke and outer leg using the following two equations [59] based on core cross-sectional area and core length can be determined,

$$\lambda = BAN \text{ and } i = \frac{Hl}{N} \tag{4.25}$$

where N is the number of turns of the inner winding, A is the cross section of the core, and l is the length of the core.

The air-core point is determined internally via the selection of 9 points of the core characteristic.

(3) Iron-losses

In BCTRAN+, the core loss is represented by dynamic loss which is based on the 90%, 100% and 110% open-circuited test data.

On the other hand, the way the HYBRID represents the loss, R_c consists of the hysteresis loss, R_H eddy current loss, R_E and anomalous loss, R_A. The loss is dynamic which is based on the 90%, 100% and 110% data. The loss representation [57] is shown in Figure 4.27.

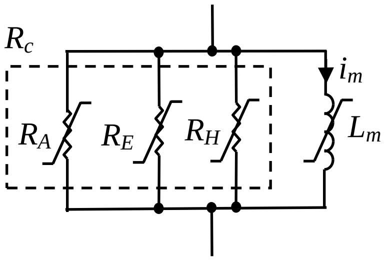

Figure 4.27: Each limb of core

(4) Eddy current

Basically, iron-loss consists of hysteresis and eddy current losses therefore both BCTRAN+ and HYBRID model have taken eddy current loss into consideration.

4.4 Transmission Line

Transmission lines are an important connection or link in power systems for delivering electrical energy. Electricity transmission is either by overhead lines or by underground cables. Overhead lines are of bare conductors made of aluminium with a steel core for strength. The bare conductors are supported on insulators made of porcelain or glass which are fixed to steel lattice towers. All steel lattice towers use suspension insulators. Three phase conductors comprise a single circuit of a three-phase system.

On the other hand, some transient phenomena such as short-circuits (e.g. single-line to ground fault, two-phase-to-ground fault, three-phase to ground fault and line-to-line fault), and lightning impulse are originated in the line. Others are due to switching events in substations creating switching surges which propagates along the lines to other substations. The transmission line when subjected to these phenomena behaves differently because each transient event has its own frequency contents.

4.4.1 Transmission Line Models in ATP-EMTP

There are two classifications of line models [60] which have been readily employed in the ATPDraw and they are shown in Table 4.4.

Table 4.4: Line models available in ATPDraw

Line models	**Time-domain models in ATP-EMTP**		
	Lump-parameter model	**Distributed-parameter model**	
		Constant parameter	**Frequency- dependent parameter**
PI	√	-	-
Bergeron	-	√	-
JMarti	-	-	√
Semlyen	-	-	√
Noda	-	-	√

Some applications and limitations of each of the model have are explained in the following sections.

4.4.1.1 Lump-Parameter Model

The lumped-parameter model is represented by the PI circuit which is the simplest version to represent a transmission line. Basically, the PI circuit is based on the lumped-parameter configuration consisting of a series impedance and two shunt capacitive admittances [61, 62]. Its representation is shown in Figure 4.28.

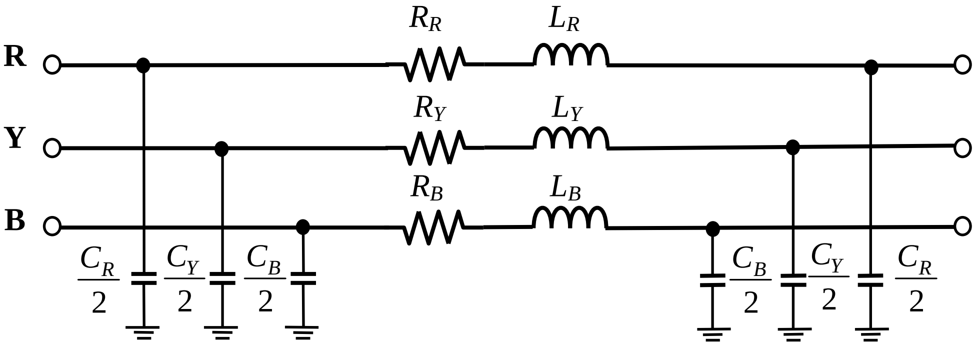

Figure 4.28: Transmission line represents by lumped PI circuit

Transmission lines modeled by lumped parameters (PI) are sufficient for steady state power flow calculations or applications [46] because the values of the lumped elements are accurate around the fundamental frequency.

In order to approximate the distributed character of a long transmission line, a number of sectionalised short PI sections is required, however, this results in longer computation time and less accuracy [63]. PI model is only suitable for transient studies when one needs to save the time so the simulation time step (Δt) can be greater than the travelling-wave time (τ) of the transmission line which needs to be modeled [63]. PI circuit is not generally the best model for transient studies because the distributed-parameter model based on travelling-wave solutions is faster and more accurate [44].

4.4.1.2 Distributed-Parameter Model

Transmission lines represented by distributed-parameter models are the most efficient and accurate because the calculations are based on travelling-wave theory. The parameters of a long transmission line are considered to be evenly distributed and they are not treated as lumped elements. Bergeron, J.Marti, Semlyen and Noda line models are all the representation in the distributed-parameter manner.

(1) The Constant-Parameter Model

The first distributed-parameter line model employed in the ATP-EMTP is the constant-parameter model which is known as the *Bergeron* model [64]. It is a constant frequency method, which is derived from the distributed LC parameter based on the traveling wave theory, with lumped resistance (losses) [44]. Initially, the line is modeled by assuming it is lossless with *L* and *C* elements taken into consideration. This is shown in Figure 4.29.

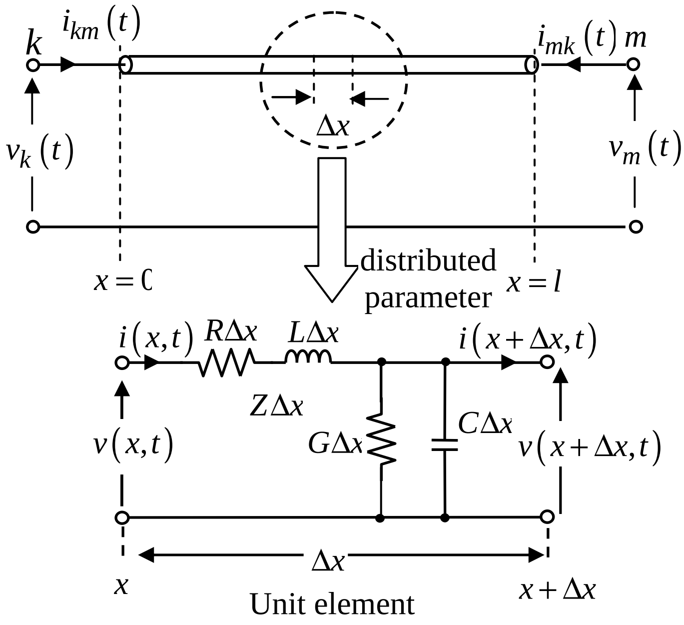

For lossless line, $R=0$ and $G=0$

$v=\frac{1}{\sqrt{LC}}$, $\tau=l.\sqrt{LC}$

$Z_c=\sqrt{\frac{L}{C}}$

Figure 4.29: Distributed parameter of transmission line

The observer leaves node *m* at time $(t-\tau)$ must still be the same when arrives at node *k* at time t and vice versa, then

$$v_m(t-\tau)+Z_c.i_{mk}(t-\tau)=v_k(t)+Z_c.-i_{km}(t) \tag{4.26}$$

$$v_k(t-\tau)+Z_c.i_{km}(t-\tau)=v_m(t)+Z_c.-i_{mk}(t) \tag{4.27}$$

Then $i_{km}(t)=\frac{1}{Z_c}.v_k(t)+I_k(t-\tau)$, where $I_k(t-\tau)=-\frac{1}{Z_c}.v_m(t-\tau)-i_{mk}(t-\tau)$

$i_{mk}(t)=\frac{1}{Z_c}.v_k(t)+I_m(t-\tau)$, where $I_m(t-\tau)=-\frac{1}{Z_c}.v_k(t-\tau)-i_{km}(t-\tau)$

Then finally the single-phase transmission line is modeled as shown in Figure 4.30.

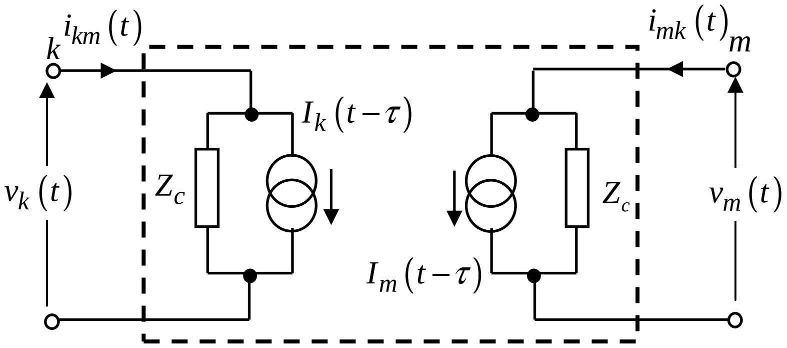

Figure 4.30: Lossless representation of transmission line

In order to gain the usefulness of the travelling wave theory for transient studies, losses are then introduced into the lossless line by simply lumping resistance, *R* in three places along the line. This is carried out by firstly dividing the line into 2 sections and then placing R/4 at both ends of each line [44]. The constant-parameter model (i.e. the Bergeron model) represented in time domain simulation is shown in Figure 4.31.

The transmission line's equations at the sending and receiving-ends are given by the following equations

Sending- end Receiving-end

$$i_{km}(t)=\frac{1}{Z}v_k(t)+I_k^{'}(t-\tau) \qquad\qquad i_{mk}(t)=\frac{1}{Z}v_m(t)+I_m^{'}(t-\tau)$$

Where

$$I_k^{'}(t-\tau)=\frac{(1+h)}{2}\left(-\frac{1}{Z}v_m(t-\tau)-i_{mk}(t-\tau)\right)+\frac{(1-h)}{2}\left(-\frac{1}{Z}v_k(t-\tau)-i_{km}(t-\tau)\right)$$

$$I_m^{'}(t-\tau)=\frac{(1+h)}{2}\left(-\frac{1}{Z}v_k(t-\tau)-i_{km}(t-\tau)\right)+\frac{(1-h)}{2}\left(-\frac{1}{Z}v_m(t-\tau)-i_{mk}(t-\tau)\right)$$

$$h=\frac{Z_c-\frac{1}{4}}{Z_c+\frac{1}{4}}\ ,\ Z=Z_c+\frac{1}{4}\ \text{ and }\ Z_c=\sqrt{\frac{L}{C}}$$

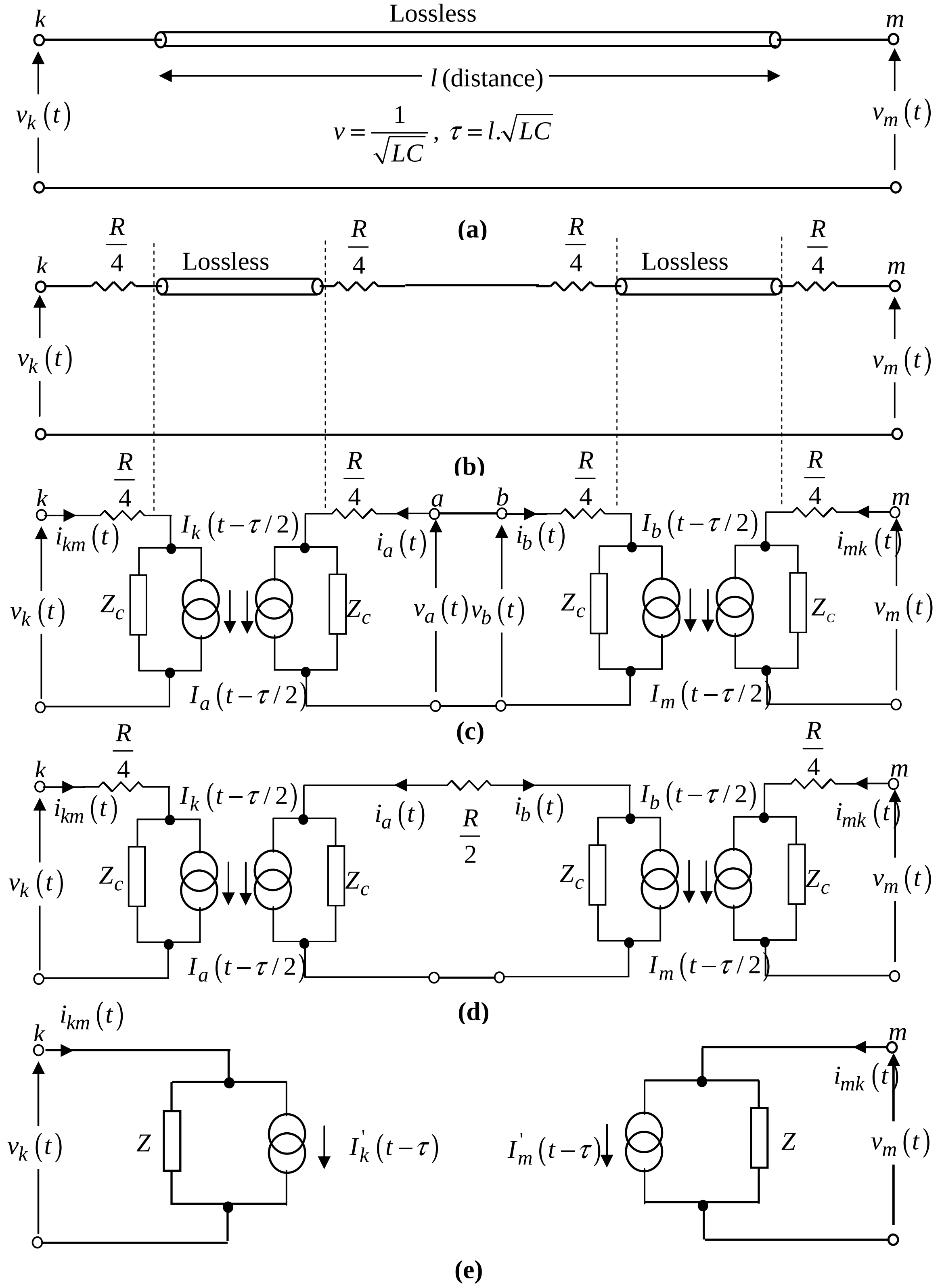

Figure 4.31: Bergeron transmission line model

The limitation of the line model is that the simulation time step, Δt must be less than the travelling time, τ such that the decoupling effect between the end line k and m takes place during the simulation time t [44, 65, 66]. In other words, as long as $\Delta t < \tau$ then a change in voltage and current at one end of the line will appear at the other end until a period τ has passed.

Like the *PI* model, the Bergeron model is also a good choice for simulation studies around the fundamental frequency such as relay studies, load flow, etc. Moreover, it also provides better accuracy if the signal of interest is oscillated near the frequency to which the parameters are calculated and involving positive sequence conditions [63]. The impedances of the line at other frequencies are taken into consideration except that the losses do not change.

However, this model is not adequate to represent a line for a wide range of frequencies that are contained in the response during transient conditions [65]. In addition to that, the lumped resistance is not suitable for high frequencies because it is not frequency-dependent [67]. In addition to that, higher harmonic magnification is produced as a result of distorted waveshapes and exaggerated amplitudes [67].

(2) The Frequency-Dependent Parameter Model

Semlyen model was one of the first frequency-dependent line models and it is the oldest model employed in ATP-EMTP.

The frequency-dependent model considered here is the Marti model. The line is treated as lossy which is represented by *R*, *G*, *L* and *C* elements of Figure 4.30. The frequency domain of the matrix equation of the two port network for a long transmission line is given as [44, 66]:

$$\begin{bmatrix} V_k(\omega) \\ I_{km}(\omega) \end{bmatrix} = \begin{bmatrix} \cosh(\gamma l) & Z_c(\omega)\sinh(\gamma l) \\ \frac{1}{Z_c(\omega)}\sinh(\gamma l) & \cosh(\gamma l) \end{bmatrix} \begin{bmatrix} V_m(\omega) \\ -I_{mk}(\omega) \end{bmatrix} \tag{4.28}$$

where characteristic impedance, $Z_c(\omega)=\sqrt{\frac{Z}{Y}}$, propagation constant, $\gamma(\omega)=\sqrt{Z.Y}$, series impedance, $Z(\omega)=R+j\omega L$, and shunt admittance, $Y(\omega)=G+j\omega C$.

By subtracting $Z_c(\omega)$ multiplies the second row from the first row of equation (4.28), then

$$V_k(\omega)-Z_c(\omega).I_{km}(\omega)=\left[V_m(\omega)+Z_c(\omega).I_{mk}(\omega)\right].e^{-\gamma l}$$

$$V_k(\omega) - Z_c(\omega).I_{km}(\omega) = \left[V_m(\omega) + Z_c(\omega).I_{mk}(\omega)\right].A(\omega) \tag{4.29}$$

$$I_{km}(\omega) = \frac{V_k(\omega)}{Z_c(\omega)} - \left[\frac{V_m(\omega)}{Z_c(\omega)} + I_{mk}(\omega)\right].A(\omega)$$

Similarly for end line at node m,

$$V_m(\omega) - Z_c(\omega).I_{mk}(\omega) = \left[V_k(\omega) + Z_c(\omega).I_{km}(\omega)\right].e^{-\gamma l}$$

$$V_m(\omega) - Z_c(\omega).I_{mk}(\omega) = \left[V_k(\omega) + Z_c(\omega).I_{km}(\omega)\right].A(\omega) \tag{4.30}$$

$$I_{mk}(\omega) = \frac{V_m(\omega)}{Z_c(\omega)} - \left[\frac{V_k(\omega)}{Z_c(\omega)} + I_{km}(\omega)\right].A(\omega)$$

where $A(\omega) = e^{-\gamma l} = e^{-(\alpha + j\beta)l} = e^{-\alpha l}.e^{-j\beta l}$

Equation (4.29) and (4.30) are very similar to Bergeron's method where the expression $[V + ZI]$ is encountered when leaving node m, after having been multiplied with a propagation factor of $A(\omega) = e^{-\gamma l}$, and this is also applied for node k. This is very similar to Bergeron's equation for the distortionless line, except that the factor of $e^{-\gamma l}$ is added into equation (4.18) and (4.19). These equations are in the frequency domain rather than in the time domain as in Bergeron method. The frequency domain of transmission line model is shown in Figure 4.32.

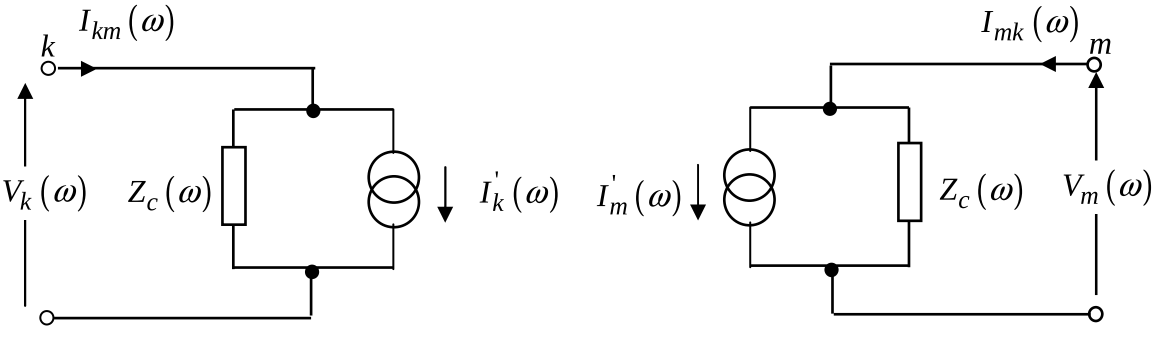

Figure 4.32: Frequency dependent transmission line model

$$I_{km}(\omega) = \frac{V_k(\omega)}{Z_c(\omega)} + I_k^{'}(\omega) \tag{4.31}$$

$$I_{mk}(\omega) = \frac{V_m(\omega)}{Z_c(\omega)} + I_m^{'}(\omega) \tag{4.32}$$

where $I_k^{'}(\omega)=\left[\dfrac{V_m(\omega)}{Z_c(\omega)}+I_{mk}(\omega)\right].A(\omega)$, $I_m^{'}(\omega)=\left[\dfrac{V_k(\omega)}{Z_c(\omega)}+I_{km}(\omega)\right].A(\omega)$,

$A(\omega)=e^{-\gamma l}$

Since time domain solutions are required in the EMTP simulation, therefore the frequency domain of Equation (4.31) and (4.32) are then converted into the time domain by using the convolution integral.

Let,

$$B_k(\omega)=V_k(\omega)-Z_c(\omega).I_{km}(\omega),\ B_m(\omega)=V_m(\omega)-Z_c(\omega).I_{mk}(\omega)$$

$$F_m(\omega)=V_m(\omega)+Z_c(\omega).I_{mk}(\omega),\ F_k(\omega)=V_k(\omega)+Z_c(\omega).I_{km}(\omega)$$

Equation (4.31) and (4.32) become

$$B_k(\omega)=F_m(\omega).A(\omega) \tag{4.33}$$

$$B_m(\omega)=F_k(\omega).A(\omega) \tag{4.34}$$

Applying convolution integral to equation (4.33) and (4.34) then,

$$F_m(\omega).A(\omega) \Leftrightarrow f_m \otimes a(t)=\int_{\tau}^{t} f_m(t-u)\,a(u)\,du$$

$$F_k(\omega).A(\omega) \Leftrightarrow f_k \otimes a(t)=\int_{\tau}^{t} f_k(t-u)\,a(u)\,du$$

However, the above method involves lengthy process of evaluating the convolution integral therefore an alternative approximate approach i.e. a rational function suggested by Marti [66] is best to approximate $A(\omega)=e^{-\gamma l}$ which has the following term,

$$A_{approx}(s)=e^{-\gamma(s)l}=\left\{\frac{k_1}{s+p_1}+\frac{k_2}{s+p_2}+\ .\ .\ .+\frac{k_m}{s+p_m}\right\}e^{-s\tau} \tag{4.35}$$

Then in time-domain form as

$$A_{approx}(t)=k_1e^{-p_1(t-\tau_{\min})}+k_2e^{-p_2(t-\tau_{\min})}+\quad .\quad .\quad .\quad +k_me^{-p_m(t-\tau_{\min})}\quad \text{for } t\geq\tau_{\min}$$

$$=0 \quad \text{for } t\leq\tau_{\min}$$

Similar method is also applied to the characteristic impedance $Z_c(\omega)$ as shown in Figure 4.33. Foster-I R-C network representation was employed to account for frequency-dependence of the characteristic impedance.

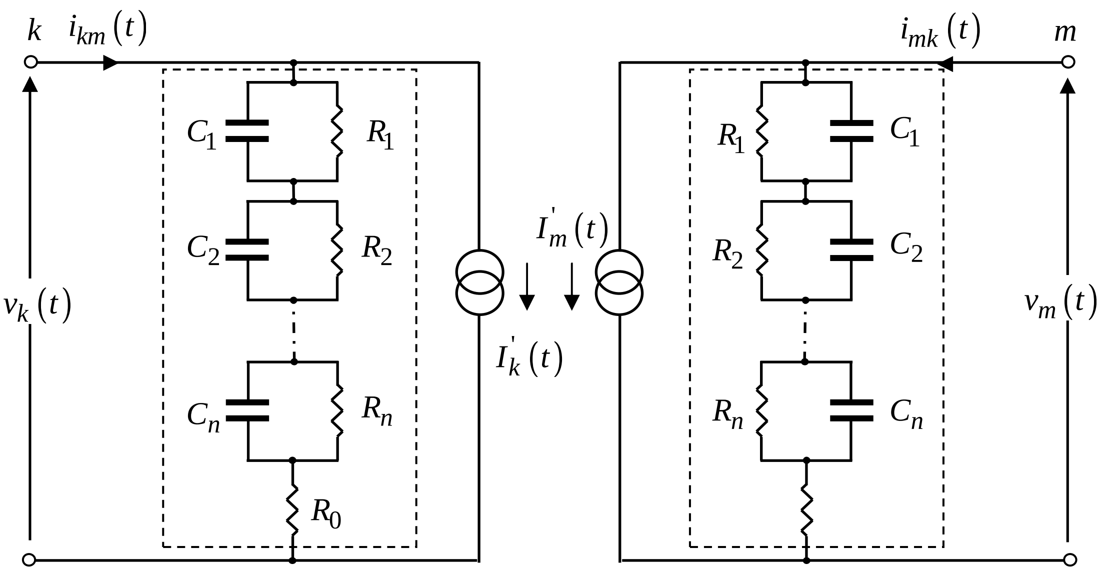

Figure 4.33: Frequency dependent transmission line model

Using the rational function, the characteristic impedance $Z_c(\omega)$ is approximated as

$$Z_{c-approx}(s) = k_0 + \frac{k_1}{s+p_1} + \frac{k_2}{s+p_2} + \ldots + \frac{k_n}{s+p_n}$$ which corresponds to the

R-C network of Figure 4.33, with

$$R_0 = k_0,\ R_i = \frac{k_i}{p_i} \text{ and } C_i = \frac{1}{k_i},\ i = 1, 2, \ldots n$$

This line is accurate to model over a wide range of frequencies from d.c (0 Hz) up to 1 MHz [65]. However, this model has the similar step size constraint as the Bergeron model.

4.4.2 Literature Review of Transmission Line Model for Ferroresonance

There are a number of literatures in which transmission line models are used for ferroresonance studies, some of which are described briefly as follows:

[7] explained that a catastrophic failure of riser pole arrestor occurred when switching operation of disconnector in a 12 kV distribution feeder connected to a station service

transformer has been carried out. The simulation study is modeled using ATP-EMTP. For the component modeling, the overhead line has been modeled as PI model.

[68] mentioned that ferroresonance occurred when a no-load transformer was energised by adjacent live line via capacitive coupling of the double-circuit transmission line. In the simulation model, the transposed transmission line has been modeled by using a frequency dependent line model.

[24] described that a blackout event has occurred at their nuclear power station because of ferroresonant overvoltages being induced into the system. The aim of building a simulation model of the affected system is to determine if the simulation results matched with the actual recording results such that the root cause of the problem can be investigated. The transmission line was modeled by connecting several identical PI divisions to represent an approximate model of distributed parameter line.

[5] explained the modeling work which has been performed to validate the actual ferroresonance field measurements. The transmission line involved in the system is a double-circuit with un-transposed configuration. The type of line modeled in ATP-EMTP has been based on a Bergeron model.

Paper on ‘Modeling and Analysis Guidelines for Slow Transients-Part III: The Study of Ferroresonance’ [69] quoted that either the distributed line or the cascaded PI model for long line can be employed for ferroresonance study.

There is no specific type of line model which has been proposed or suggested for ferroresonance study after surveying some of the literatures. Therefore assessment procedure has been developed to evaluate the type of line model that is suitable for ferroresonance study.

4.4.3 Handling of Simulation Time, Δt

It is important to choose the correct simulation time step before a simulation case study is carried out in ATPDraw to avoid simulation errors. Therefore, the main aim of this section is to aid users to handle the simulation time-step i.e. Δt when either the lumped- or the distributed-parameter transmission lines is chosen for ferroresonance study. A flowchart as shown in Figure 4.34 has been setup for this purpose.

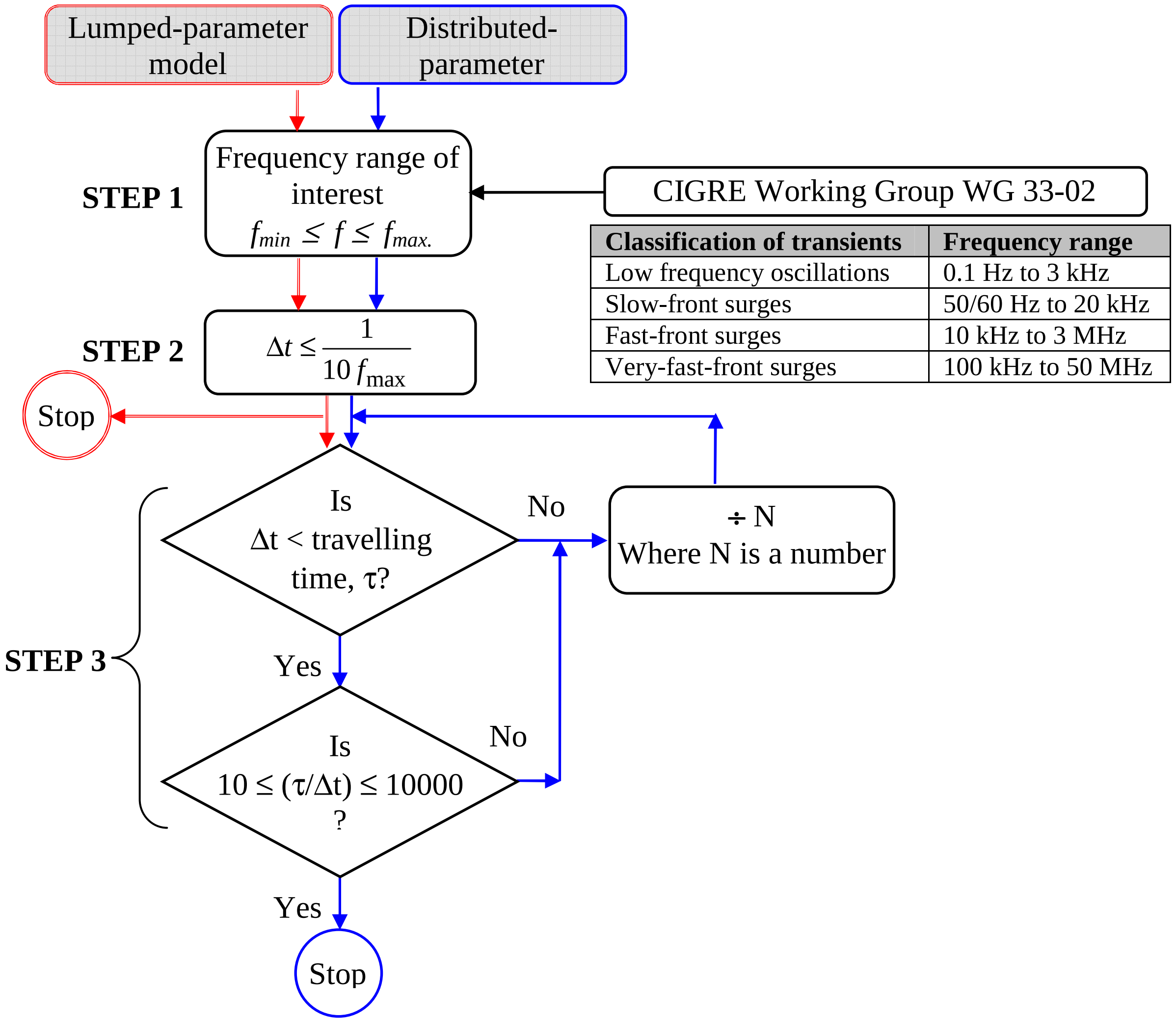

Classification of transients	Frequency range
Low frequency oscillations	0.1 Hz to 3 kHz
Slow-front surges	50/60 Hz to 20 kHz
Fast-front surges	10 kHz to 3 MHz
Very-fast-front surges	100 kHz to 50 MHz

Figure 4.34: Flowchart for transmission line general rule

STEP 1:

Before any simulation is carried out, it is important to firstly identify the frequency range of interest. In the case of ferroresonance, a frequency range from 0.1 Hz to 1 kHz which falls under the category of the Low Frequency Oscillation is suitable. Therefore $f_{max.} = 1$ kHz

STEP 2:

Secondly, it is important to select an appropriate time step (Δt) for generating good and accurate results. As a general rule, the simulation time step is,

$$\Delta t \le \frac{1}{10\, f_{\max}} \quad \text{where } \frac{1}{f_{\max}} \text{ is the period of oscillation of interest}$$

$\Delta t \leq 100\ \mu\text{s}$

If a lumped-parameter such as the PI model is used then Δt = 100 μs is sufficient for the simulation.

STEP 3:

However, if a distributed-parameter is employed, a check of the following is necessary.

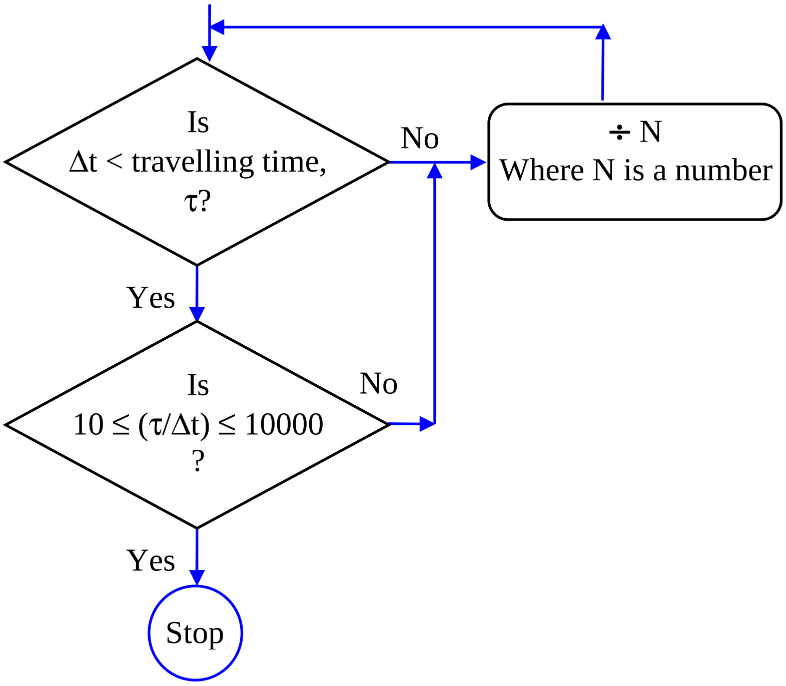

Next, the travelling time, τ along the line needs to be determined. The travelling time is given as

$$\text{Travelling time, } \tau = \frac{l}{c} \text{ (s)}$$

where l = the line length (m) and c = the speed of light, 3×10^{8} m/s

In our case study for the Brinsworth system, the transmission line length is 37 km then the travelling time, τ is calculated as 123 μs which is greater than $\Delta t \leq 100$ μs. Then the next test is to check whether it lies within the 10 and 10000 range and this is presented in the following table.

Simulation time step, Δt (s)	**Propagation time, τ (s)**	**Is $\tau > \Delta t$?**	**Ratio of $\frac{\tau}{\Delta t}$**	Is $10 \leq (\tau/\Delta t) \leq 10000$?
100 μs	123 μs	Yes	1	Not Acceptable
10 μs		Yes	12.33	Acceptable
1 μs		Yes	123.33	Acceptable

A change in the voltage and current at one end of the transmission line will not appear at the other end if Δt is greater than τ. Therefore, simulation time-step of either 10 μs or 1 μs can be preferred

4.4 Summary

In this chapter, the technical aspects of the component models suitable for the study of ferroresonance have been discussed. One of the most important aspects of modeling power system components for ferroresonance is to identify the frequency range of interest so that the parameters are being modeled correctly. Three components which are involved in ferroresonance are circuit breakers, transformers and transmission lines. The criteria in modeling each of the components are explained as follows:

- *Circuit breaker*

As the occurrence of ferroresonance is mainly due to switching events this component has therefore to be considered. Opening/closing of circuit breakers involved transients, i.e. a change of energy takes place and then transient voltages and currents are distributed into a system. The way the circuit breaker is modeled for ferroresonance can be based on the simplistic representation without taking into account of high current interruption, current chopping, restrike characteristic. The reason is that ferroresonance involves only low frequency and low current transients.

- *Power transformer*

The parameters such as the saturation effect, the short-circuit impedance, the iron-loss and the eddy current have to be taken into consideration so that the simulation model can correctly represent the low frequency transients. Two predefined transformer models, the BCTRAN+ and the HYBRID have been looked into to see whether they are capable for ferroresonance study. The review suggests that both models are able to feature the criteria (parameter/effect) for low frequency transients, hence for ferroresonance. In addition BCTRAN+ and HYBRID models are valid for up to 2 kHz and 5 kHz respectively. The only difference between the two is the way in which the core is taken into consideration.

- *Transmission line*

Again, frequency range of interest needs to be determined so that a proper predefined model can be used. The three predefined models, the PI, Bergeron and the Marti are considered to be adequate for modeling ferroresonance. For a short-line up to less than 50 km, a PI model is considered to be adequate for ferroresonance. Bergeron model is a constant frequency method, based on traveling wave theory, and can also be used for ferroresonance study. On the other hand, transmission line represented by the J. Marti model can also be used for ferroresonance study because the parameters of the line are frequency-dependent which can cover up to 1 MHz.

CHAPTER 5

5. MODELING OF 400 KV THORPE-MARSH/BRINSWORTH SYSTEM

5.1 Introduction

In chapter 4, the technical aspects of transformer saturation have been explained. The predefined transformer models in ATPDraw which meet the criteria i.e. the parameters/effects for the study of low frequency transients proposed by CIGRE have been identified. In addition, the differences between the BCTARN+ and the HYBRID models have also been discussed in terms of the way how the core characteristic has been modeled.

On the other hand, different types of predefined transmission line models such as the PI, Bergeron and Marti models have also been introduced. The suitability of each of the model for ferroresonance study is also highlighted.

As much attention has been given to the predefined models as mentioned above, this chapter is allocated with the following aims:

(1) To model the 400 kV Thorpe-Marsh/Brinsworh transmission system,

(2) To validate the transmission line models and power transformers models.

(3) To determine the best possible power system component models, particularly the power transformer and the transmission line models available in ATPDraw that can be used to accurately represent a power system for the study of ferroresonance.

5.2 Description of the Transmission System

The overall circuit configuration of Thorpe-Marsh/Brinsworth 400 kV system [29] is shown in Figure 5.1 where ferroresonance tests have been carried out. The circuit consists of mesh corner substation, a 37 km double-circuit transmission line, Point-on-wave (POW) circuit breaker (X420), two power transformers (SGT1 and SGT2), 170 m cable and load.

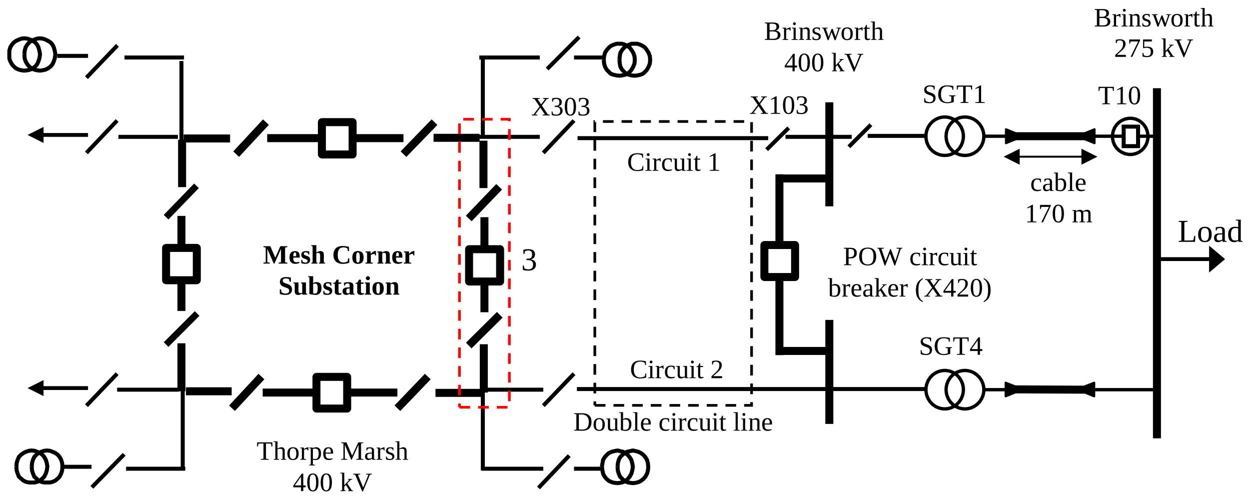

Figure 5.1: Thorpe-Marsh/Brinsworth system

Prior to the test, disconnector (X303) was open, and Mesh corner 3 was restored to service at the Thorpe Marsh 400 kV substation. At the Brinsworth 275 kV substation, circuit breaker (T10) was also open. Moreover, all other disconnectors and circuit breaker (X420) are in service. When testing, the initiation of ferroresonance may occur as a result of opening circuit breaker X420 (Point-on-wave switch).

There have been two types of ferroresonance modes exhibited at the 400 kV side of transformer (SGT1) following the switching events. There are the sustained fundamental frequency ferroresonance and the 16.67 Hz subharmonic ferroresonance. The 3-phase voltages and currents for both the cases are depicted as shown in Figure 5.2 and Figure 5.3 respectively.

The 3-phase ferroresonance voltage and current waveforms of Figure 5.2 have a frequency of $16^{2/3}$ Hz. The recorded field test voltages and currents impinged upon the 400 kV side of the transformer were found to be having peak voltages of approximately +100 kV and -50 kV for R-phase voltage, +100 kV and -100 kV for Y-phase voltage, and +50 kV and -50 kV for B-phase voltage. On the other hand the peak currents are: +50 A and -50 A for R-phase, +50 A and -45 A for Y-phase, and +45 A and -45 A for B-phase. It has been reported that the implication of the initiation of the subharmonic mode ferroresonance has caused the affected transformer to generate a distinct grumbling noise, which can be heard by all the staff on site [29].

Field test recording of Period-3 ferroresonance

(1) 3-phase voltage waveforms

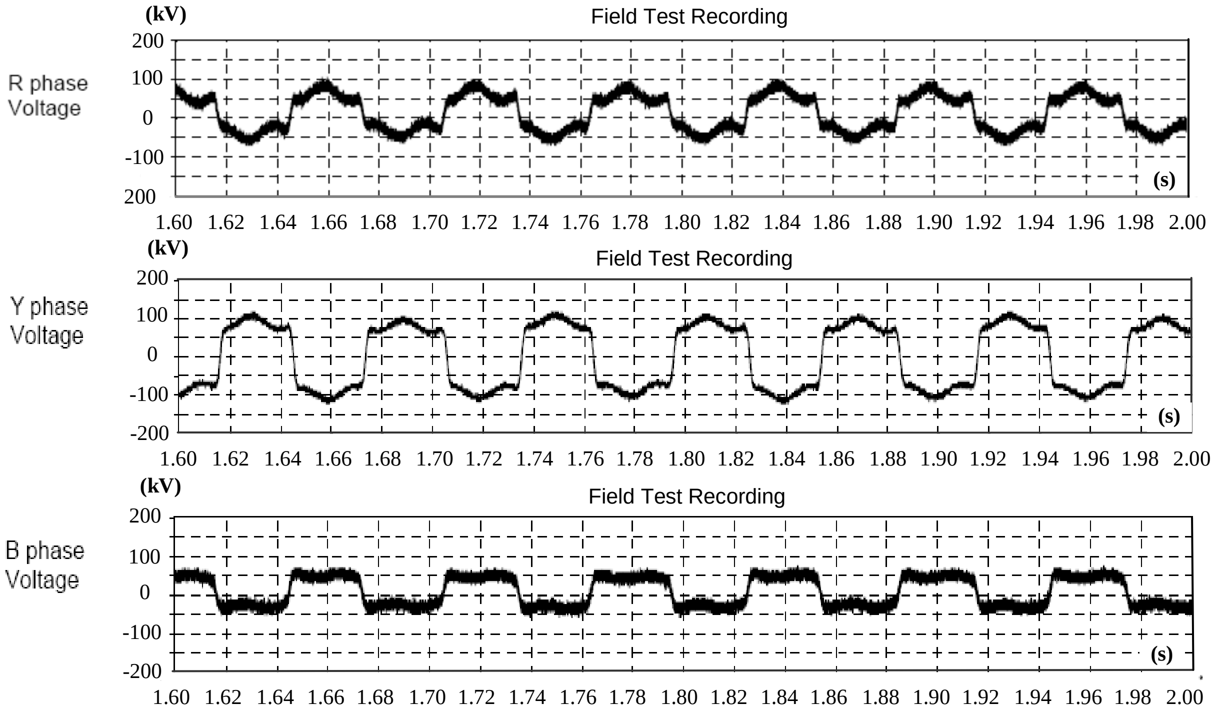

(2) 3-phase current waveforms

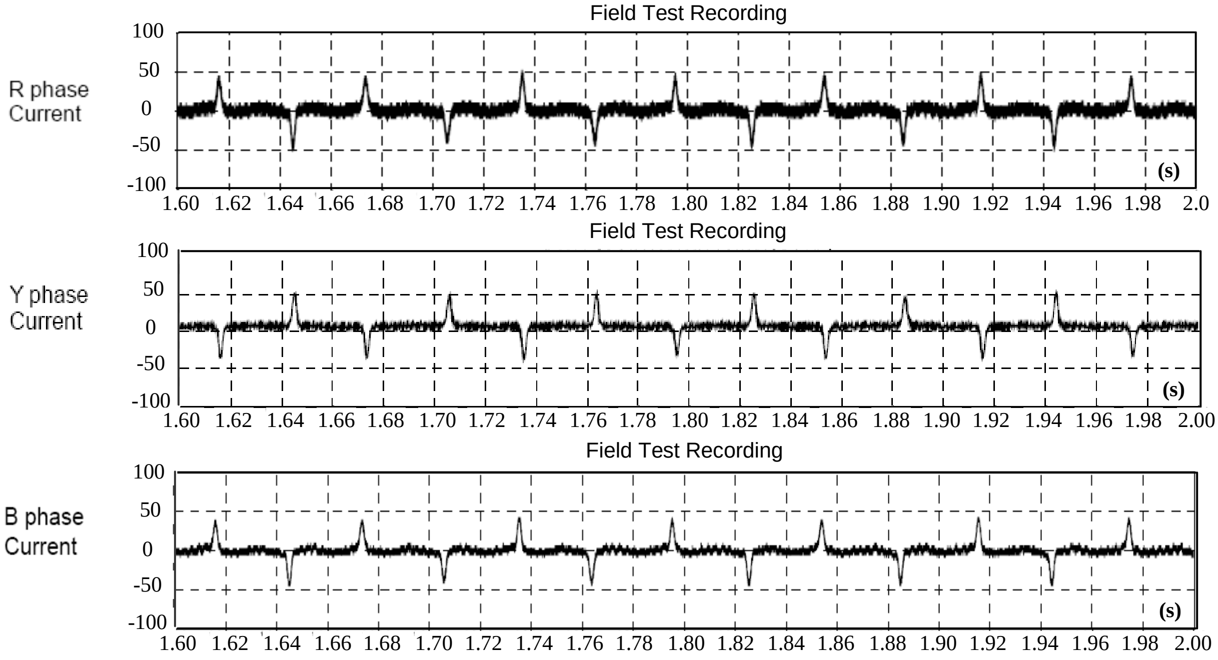

Figure 5.2: Period-3 ferroresonance

On the other hand, the sustained fundamental frequency ferroresonance induced into the system exhibits the voltage and current waveforms as shown in Figure 5.3.

Field test recording of Period-1 ferroresonance

(1) 3-phase voltage waveforms

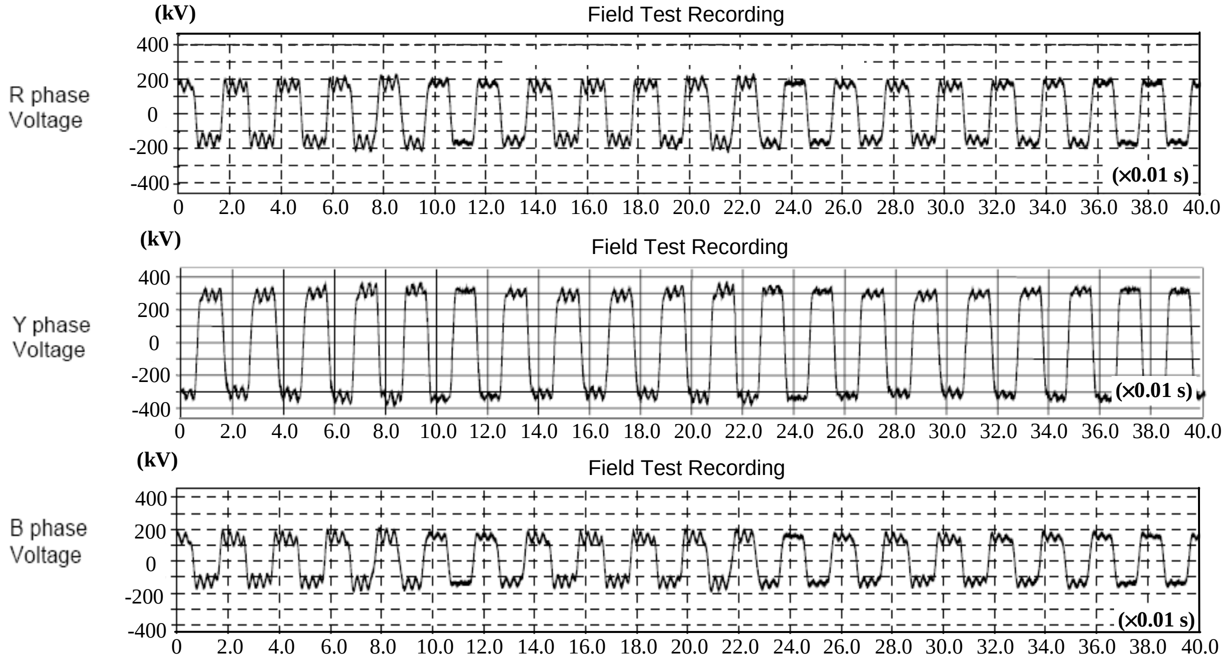

(2) 3-phase current waveforms

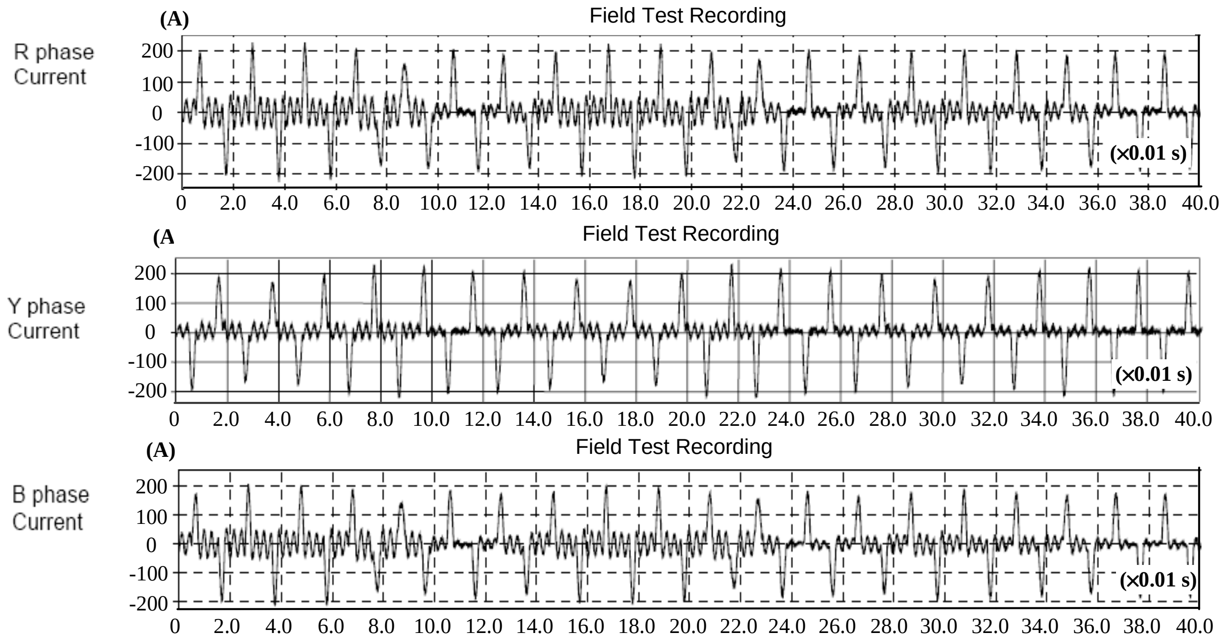

Figure 5.3: Period-1 ferroresonance

The peak voltage and peak current magnitudes recorded from the field test were depicted in Figure 5.3: ±200 kV for the R-phase voltage, ±300 kV for the Y-phase voltage and ±180 kV for the B-phase voltage. The 3-phase currents are ±200 A. The consequence of such phenomenon has resulted the affected transformer to generate a much louder grumbling sound which can be heard by the staff on site a distance of 50 m away from the transformer. In addition, the ferroresonance detection protection which was installed at the Brinsworth substation has not functioned correctly.

5.3 Identification of the Origin of Ferroresonance Phenomenon

The cause of the onset of ferroresonance is the switching event that circuit breaker (X420) is opened. It is evident that this phenomenon occurs when Circuit 1 is energised by the adjacent live line (Circuit 2) via the transmission line's coupling capacitance as a result of opening circuit breaker (X420). The initiation of ferroresonance path is indicated by the dotted line of Figure 5.4 where the power transformer (SGT1) is interacted with the transmission line's coupling capacitor when supplied by the 400 kV mesh corner source.

Network 1 shows in Figure 5.4 acts as the voltage source, however, Network 2 is considered to be the key circuit because of its components being interacted with each other exhibiting ferroresonance phenomenon following the point-on-wave opening of the circuit breaker (X420).

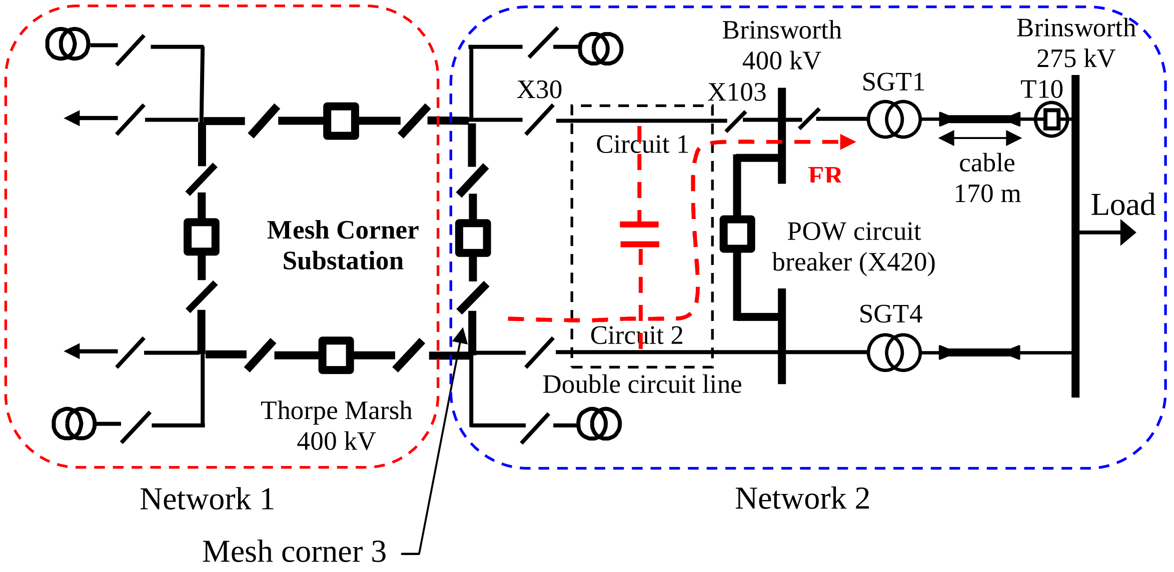

Figure 5.4: Thorpe-Marsh/Brinsworth system

5.4 Modeling of the Transmission System

With Network 1 acting as a voltage source, the circuit of Figure 5.4 can therefore be deduced into a more simplified circuit as depicted in Figure 5.5.

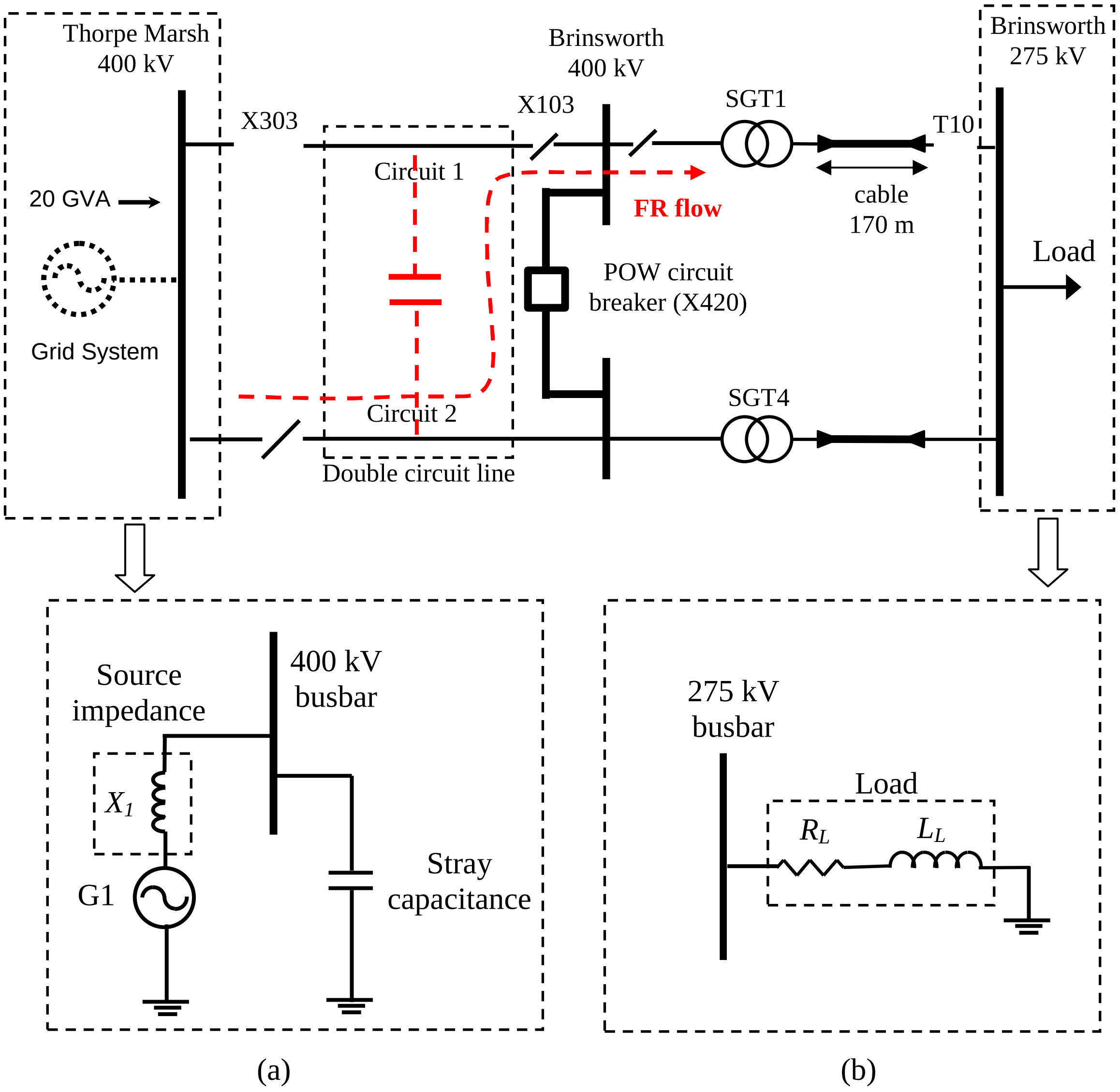

Figure 5.5: Modeling of (a) source impedance (b) load

In order to represent a strong system at the 400 kV substation at Thorpe Marsh, an infinite bus with an assumed fault level of 20 GVA is used. The load connected at the Brinsworth 275 kV side is assumed to draw 30% of 1000 MVA rating, at 80% of power factor. In addition, the stray capacitance to ground of the busbar at both the 400 kV substation is also taken into consideration and its value was estimated at around 10 pF/m [12]. The representation of the equivalent source is presented as shown in Figure 5.5.

5.4.1 Modeling of the Circuit Breakers

Detailed time-controlled switch models employed in ATPDraw have been highlighted in Chapter 4. In addition, the reasons why a simplistic model can be used for ferroresonance study is also explained. The time-controlled switch with no current margin is used throughout this study.

5.4.1.1 Opening of Circuit Breaker at Six Current Zero Crossing

For a single-phase switch, the current interruption takes place twice within a cycle of sinusoidal signal. However, for three-phase currents the interruptions can occur six times within a cycle as indicated in the dotted line frame of Figure 5.6.

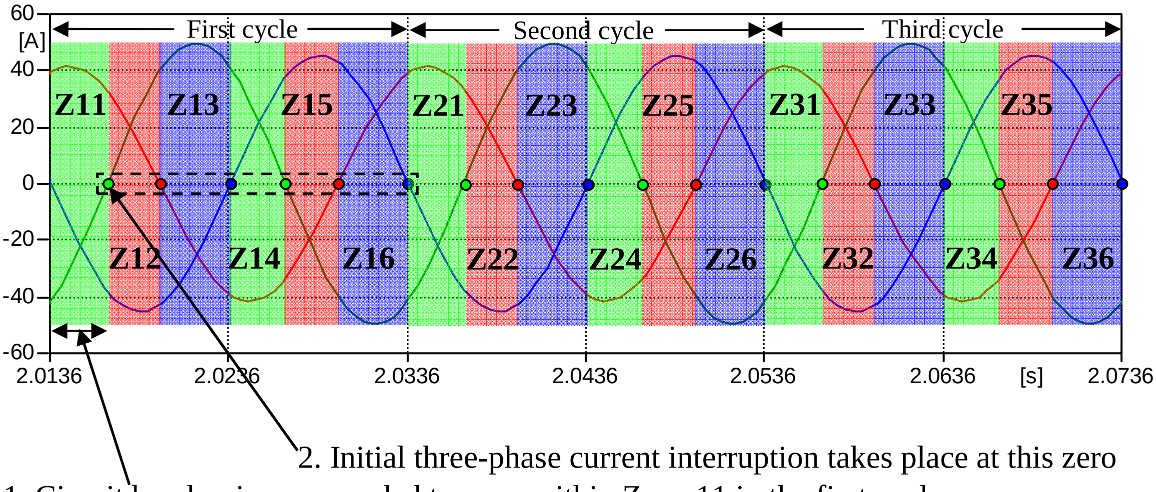

2. Initial three-phase current interruption takes place at this zero

1. Circuit breaker is commanded to open within Zone 11 in the first cycle

Figure 5.6: Six current zero crossing within a cycle

Figure 5.6 shows that there are six zones of pre-zero current crossing within a cycle of the 3-phase currents. If the switch is commanded to open within zone, Z11, the contact of phase yellow will open first, followed by phase red and finally phase blue. The complete sequence of opening the contact corresponding to each zone within the first cycle is shown in Table 5.1.

Table 5.1: Sequence of circuit breaker opening in each phase

Circuit Breaker operations		**Sequence of contact opening at**		
		Red phase	**Yellow phase**	**Blue phase**
First cycle	**Z11**	Second opening	First opening	Third opening
	Z12	First opening	Third opening	Second opening
	Z13	Third opening	Second opening	First opening
	Z14	Second opening	First opening	Third opening
	Z15	First opening	Third opening	Second opening
	Z16	Third opening	Second opening	First opening

In the simulation, the circuit breaker is commanded to open within each zone as indicated in Figure 5.6. The time of opening the circuit breaker in each zone within the respective cycle are shown in Table 5.2. For example, if the circuit breaker is commanded to open at

2.0153 s at zone Z11 within the 1st cycle, the circuit breaker will not open instantly, instead it waits until the first current zero crossing takes place which occurs at phase yellow, follows by current interruptions at red and blue phases.

Table 5.2: Switching time to command the circuit breaker to open

	1st cycle					
	Z11	**Z12**	**Z13**	**Z14**	**Z15**	**Z16**
Time to command CB to open	2.0153 s	2.0181 s	2.0219 s	2.0254 s	2.0283 s	2.0319 s
	2nd cycle					
	Z21	**Z22**	**Z23**	**Z24**	**Z25**	**Z26**
Time to command CB to open	2.0353 s	2.0381 s	2.0419 s	2.0454 s	2.0483 s	2.0519 s
	3rd cycle					
	Z31	**Z32**	**Z33**	**Z34**	**Z35**	**Z36**
Time to command CB to open	2.0553 s	2.0581 s	2.0619 s	2.0654 s	2.0683 s	2.0719 s

Occasionally, the simulations to reproduce the expected waveforms cannot be extended for more than three cycles due to the fact that the initial three-phase currents and voltages at the point of current interruption of each phase are not repetitive from one cycle to another cycle which can be seen in Table 5.3. Although the differences of the initial conditions are small, they determine the initial stored energy in the capacitive and inductive components of the ferroresonant circuit, therefore affect the transient ferroresonant voltages and currents. As we have known, the transient ferroresonance can develop into sustained ferroresonance sometimes and also can decay down into zero.

Table 5.3: Sequence of circuit breaker opening in each phase

Current	**1st Cycle**					
	Z11	**Z12**	**Z13**	**Z14**	**Z15**	**Z16**
Red phase	34.083 A (1.6143E5 V)	Interrupted at 2.0198 s (3.2033E5 V)	-39.647 A (1.2435E5 V)	-33 929 A (-1.6318E5 V)	Interrupted at 2.0298 s (-3.2041E5 V)	39.682 A (-1.2342E5 V)
Yellow phase	Interrupted at 2.0167 s (-3.2194E5 V)	41.222 A (-1.8287E5 V)	40.362 A (1.9468E5 V)	Interrupted at 2.0268 s (3.2193E5 V)	-41.301 A (1.8204E5 V)	-40.253 A (-1.9548E5 V)
Blue phase	-36.731 A (1.6137E5 V)	-42.151 A (-1.373E5 V)	Interrupted at 2.0238 s (-3.1986E5 V)	36.912 A (-1.5961E5 V)	42.092 A (1.3821E5 V)	Interrupted at 2.0338 s 3.1974E5 V)
Current	**2nd Cycle**					
	Z21	**Z22**	**Z23**	**Z24**	**Z25**	**Z26**
Red phase	**34.602 A** (1.5528E5 V)	Interrupted at 2.0398 s (3.2056E5 V)	-39.718 A (1.2249E5 V)	-33.696 A (-1.6578E5 V)	Interrupted at 2.0498 s (-3.2063E5 V)	39.807 A (-1.2062E5 V
Yellow phase	Interrupted at 2.0367 s (-3.2188E5 V)	41.518 A (-1.8036E5 V)	40.139 A (1.9628E5 V)	Interrupted at 2.0468 s (3.2189E5 V)	-41.599 A (1.7953E5 V)	-39.976 A (-1.9788E5 V)
Blue phase	-36.157 A (1.6746E5)	-42.021 A (-1.4004E5 V)	Interrupted at 2.0438 s (-3.1961E5 V)	37.147 A (-1.5697E5 V)	41.967 A (1.4095E5 V)	Interrupted at 2.0538 s (3.1934E5 V)

Continue…

Current	**3rd Cycle**					
	Z31	**Z32**	**Z33**	**Z34**	**Z35**	**Z36**
Red phase	34.383 A (1.5793E5 V)	Interrupted at 2.0598 s (3.1998E5 V)	-39.433 A (1.2899E5 V)	-33.473 A (-1.6836E5 V)	Interrupted at 2.0698 s (-3.1008E5 V)	39.526 A (-1.2714E5 V)
Yellow phase	Interrupted at 2.0567 s (-3.2193E5 V)	40.884 A (-1.8618E5 V)	40.801 A (1.9062E5 V)	Interrupted at 2.0668 s (3.2182E5 V)	-40.97 A (1.8536E5 V)	-40.639 A (-1.9225E5 V)
Blue phase	-36.416 A (1.6486E5 V)	-42.36 A (-1.3362E5 V)	Interrupted at 2.0638 s (-3.2044E5 V)	37.363 A (-1.5431E5 V)	42.31 A (1.3454E5 V)	Interrupted at 2.0738 s (3.2022E5 V)

5.4.2 Modeling of 170 m Cable

The cables which are connected at the 275 kV side of both the SGT1 and SGT4 transformers are 170 m in length and they can be modeled simplistically as a passive capacitor. The values of the capacitance can be determined by referring to the technical cable book [70] as: 275 kV cable: $C = 0.04352\ \mu\text{F}$.

5.4.3 Modeling of the Double-Circuit Transmission Line

The tower design of the line [47] connected between the Thorpe-Marsh and Brinsworth substations is shown in Figure 5.7. Other conductor parameters can be referred to Appendix A.

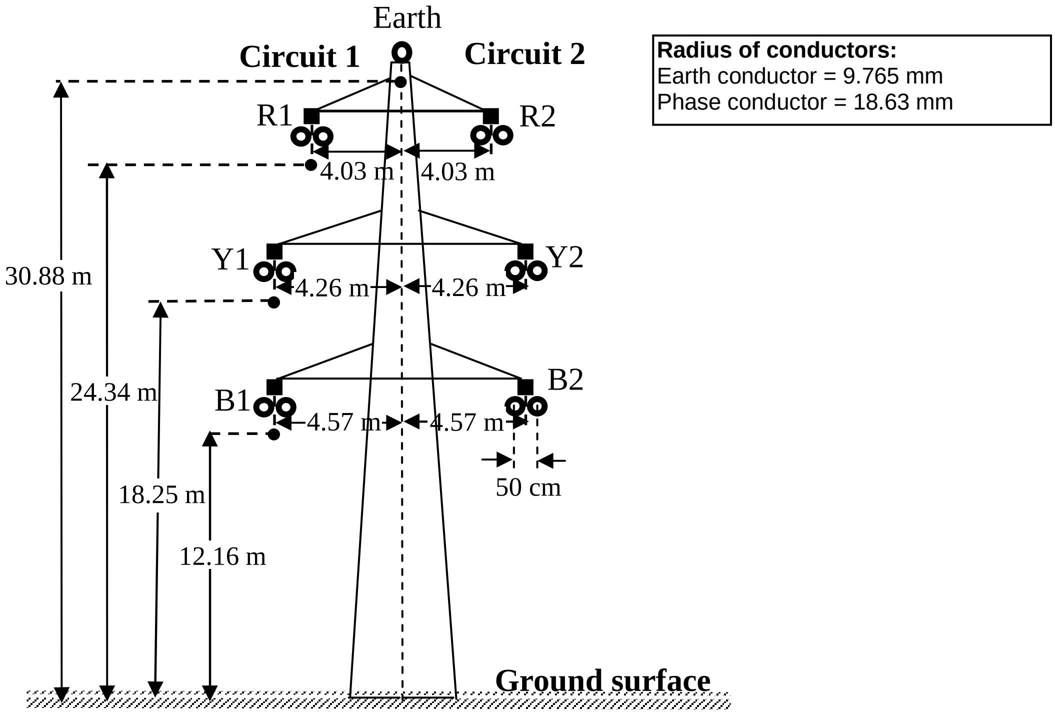

Radius of conductors:
Earth conductor = 9.765 mm
Phase conductor = 18.63 mm

Figure 5.7: Physical dimensions of the transmission line

The line is modeled in ATPDraw using the integrated LCC object according to the available physical dimensions and parameters.

Since the main aim of this chapter is to determine the best possible model for ferroresonance study, therefore, three different types of approaches are put into test to determine their suitability for the purpose.

5.4.3.1 Lumped Parameter Model

Detailed description about the lumped parameter, particularly the PI model has been highlighted in the previous chapter. The double-circuit transmission line is modeled in this representation and the next stage of verifying and checking is shown in Appendix B.

5.4.3.2 Distributed Parameter

Other than the line being modeled in lumped representation, two alternative approaches based on distributed parameter are also considered with an aim to determine the best possible model, the Bergeron and J. Marti models. The detailed of each of them have been explained in the previous chapter.

5.4.4 Modeling of Transformers SGT1 and SGT4

Two power transformers are involved in the transmission system but only SGT1 is affected by ferroresonance therefore it is modeled by using both BCTRAN+ and HYBRID models with an aim to determine the best possible model. On the other hand, SGT4 is not affected by ferroresonance therefore it is only modeled as a steady-state characteristic using BCTRAN. The open- and short-circuit test data obtained from the test report supplying by the manufacturers [71] are shown in Table 5.4. The electrical specification of the SGT1 transformer is 1000 MVA, 400/275/13 kV, Vector: YNa0d11 (5 legs). Zero-sequence data are not available.

Table 5.4: No-load loss data and load-loss data

NO-LOAD LOSS on TERT. (60 MVA)				
VOLTS			AMPS	kWatts
%	MEAN	R.M.S		
			5.25	96.30
90	11700	11810	6.00	
			7.28	
			12.30	127.90
100	13000	13217	12.40	
			14.75	
			55.20	175.30
110	14300	14903	54.30	
			56.80	

LOAD-LOSS on HV				
VOLTS	IMP	AMPS	kWATTS	
			At 20°C	Corrected to 75°C
HV/LV @1000 MVA				
67127	16.78%	1444	1213.10	1383
HV/TERT @ 60 MVA				
29141	7.29%	86.60	62.30	71.90
LV/TERT @ 60 MVA				
16407	5.97%	126	66.10	77.30

The per-unit quantities which are required by both the BCTARN and HYBRID models are calculated as follows:

(1) No-load calculation:

90%:

$$I_{ex}=\frac{\left(5.25+6+7.28\right)}{3}=6.18\,\text{A (line current)}$$

$$I_{ex}(pu)=6.18\times\frac{\sqrt{3}\times11.81\times10^{3}}{1000\times10^{6}}\times100=0.01\%\ \ \text{@1000 MVA}$$

100%:

$$I_{ex}=\frac{\left(12.3+12.4+14.75\right)}{3}=13.15\,\text{A (line current)}$$

$$I_{ex}(pu)=13.15\times\frac{\sqrt{3}\times13.22\times10^{3}}{1000\times10^{6}}\times100=0.03\%\ \ \text{@ 1000 MVA}$$

110%:

$$I_{ex}=\frac{\left(55.2+54.3+56.8\right)}{3}=55.43\,\text{A (line current)}$$

$$IEXPOS=55.43\times\frac{\sqrt{3}\times14.90\times10^{3}}{1000\times10^{6}}\times100=0.14\%\ \ \text{@ 1000 MVA}$$

(2) Load loss calculation:

$$Z_{HV-LV}=\frac{67127}{\sqrt{3}\times1444}\frac{1000\times10^{6}}{\left(400\times10^{3}\right)^{2}}\times100=16.77\%\ \ \text{@ 1000 MVA}$$

$$Z_{HV-TV}=\frac{29141}{\sqrt{3}\times86.6}\frac{60\times10^{6}}{\left(400\times10^{3}\right)^{2}}\times100=7.29\%\ \ \text{@ 60 MVA}$$

$$Z_{LV-TV} = \frac{16407}{\sqrt{3}\times 126}\frac{60\times 10^{6}}{\left(275\times 10^{3}\right)^{2}}\times 100 = 5.97\% \text{ @ 60 MVA}$$

Once all the data are entered into predefined models, they are then checked on whether they are able to reproduce the expected data. The open- and short-circuit simulation tests are performed on the model and the results are tabulated as shown in Table 5.5 and Table 5.6.

Table 5.5: Comparison of open-circuit test results between measured and BCTRAN and HYBRID models

Vrms [kV]	Measured		BCTRAN		HYBRID	
	Irms [A]	P [kW]	Irms [A]	P [kW]	Irms [A]	P [kW]
11.7 (90%)	6.180	96.30	6.15	100.21	6.35	99.40
13 (100%)	13.15	127.90	11.77	123.68	10.36	124.12
14.3 (110%)	55.43	175.30	46.41	149.50	58.83	151.30

Table 5.6: Comparison of load loss test results between measured and BCTRAN+ and HYBRID models

Vrms [V]	Measured		BCTRAN		HYBRID	
	Irms [A]	P [kW]	Irms [A]	P [kW]	Irms [A]	P [kW]
HV/LV @1000 MVA						
67127	1444	1383	1444.40	1443.50	1443.50	1383.30
HV/TERT @ 60 MVA						
29141	86.6	71.90	86.55	72.50	86.55	71.84
LV/TERT @ 60 MVA						
16407	126	77.30	125.89	77.66	125.89	77.23

The results show that the data reproduced from the open- and short-circuited tests using both the BCTRAN and HYBRID models are generally in good agreement with the test reports although magnetizing current at 100% and iron loss at 110% for open-circuit tests are lower than the test results. This suggests that the predefined transformer models have been reasonably set up.

Much attention has been allocated in this chapter aiming to determine the best possible power system component models available in ATPDraw that can be used to accurately represent a power system for the study of ferroresonance. The way the developed simulation model is recognised as the best possible model is by comparing the simulation results produced from all the listed combination in Table 5.7 with the field recording waveforms. Particularly, comparisons have to be made for the three-phase sustained ferroresonant voltages and currents.

Table 5.7: Combination of power transformer and transmission line models

	Power Transformer model	**Transmission line model**
Case Study 1	BCTRAN+	PI
Case Study 2	BCTRAN+	Bergeron
Case Study 3	BCTRAN+	Marti
Case Study 4	HYBRID	PI
Case Study 5	HYBRID	Bergeron
Case Study 6	HYBRID	Marti

5.5 Simulation of the Transmission System

5.5.1 Case Study 1: Transformer - BCTRAN+, Line - PI

In this section, BCTRAN+ and PI models are employed to model the SGT1 power transformer and the 37 km double-circuit transmission line. The BCTRAN+ model required the core characteristic to be modeled as nonlinear inductor externally connected at the tertiary winding in a delta configuration. Externally delta-connected core characteristic employed by the BCTRAN+ model required the use of three nonlinear inductors, based on the 90%, 100% and 110% open circuit test data. These data are then converted into flux-linkage, λ versus current, i characteristic using SATURA supporting routine [44] which is available in Appendix C.

The three-point data for the SGT1 transformer indicated as real data are shown in Figure 5.8 with the various converted core curves. However, this core representation which accounts for the saturation effect is not sufficient for the reproduction of the ferroresonant currents under the tests. The air-core (fully saturated) inductance is needed by curve fitting through the three points and extrapolating by using the n^{th} order polynomial which has the following equation,

$$i_m = A\lambda + B\lambda^n \tag{5.1}$$

where $n = 1, 3, 5 \ldots$ and the exponent n depends on the degree of saturation.

With equation (5.1), a sensitivity study has been carried out by assessing the degrees of saturation from n=13 up to 27 in order to determine the best possible core characteristic.

The outcome from the evaluation suggests that the degree of saturation with *n*=27 is the best representation to be employed as the core characteristic for the BCTRAN+ transformer model. All the degrees of saturation are depicted in Figure 5.8.

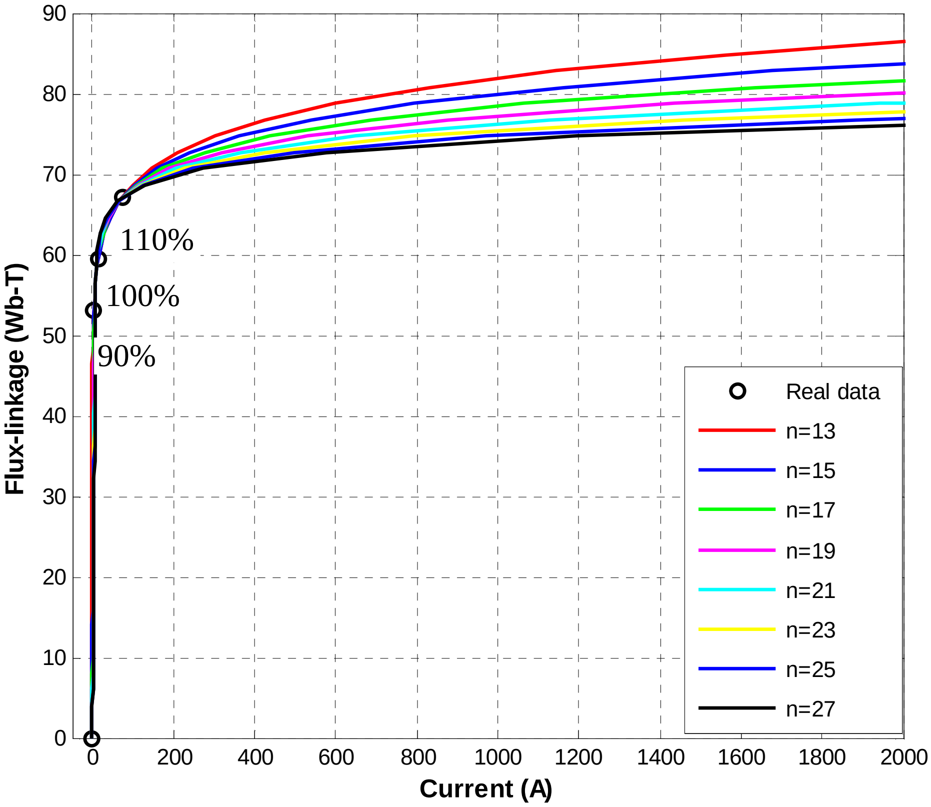

Figure 5.8: Magnetising characteristic

The simulation results employing this model are shown in Figure 5.9 to Figure 5.20. Note that the sustained ferroresonant waveforms obtained from the simulation are determined at a time after both the steady-state and transient parts have passed.

3-phase Fundamental Mode Ferroresonance Voltages (Period-1)

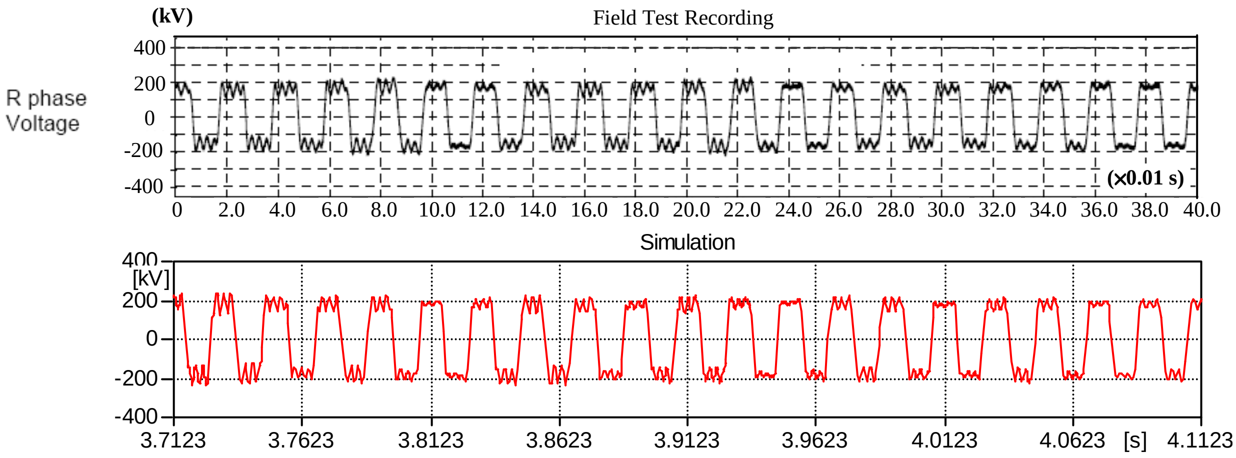

Figure 5.9: Period-1 voltage waveforms – Red phase

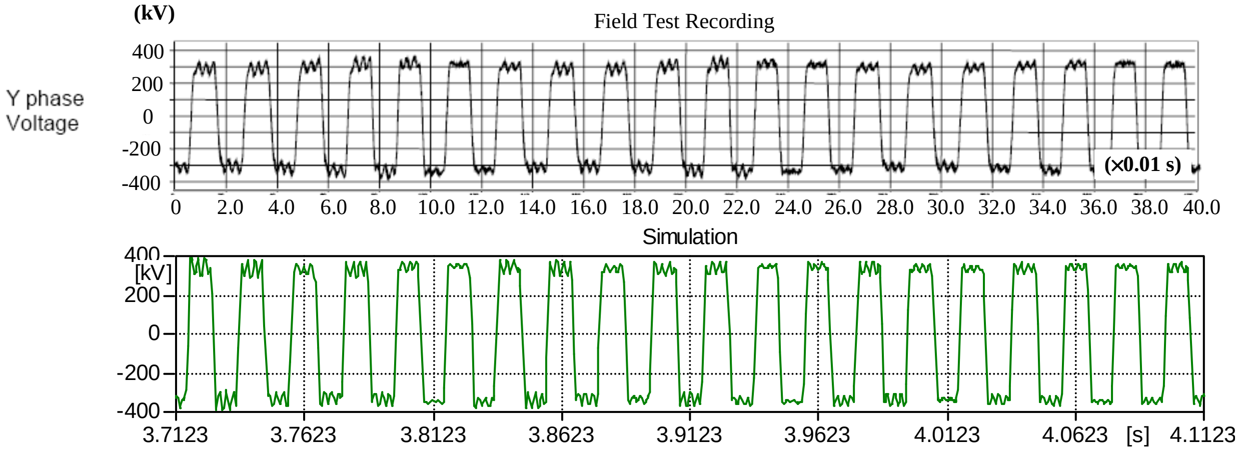

Figure 5.10: Period-1 voltage waveforms – Yellow phase

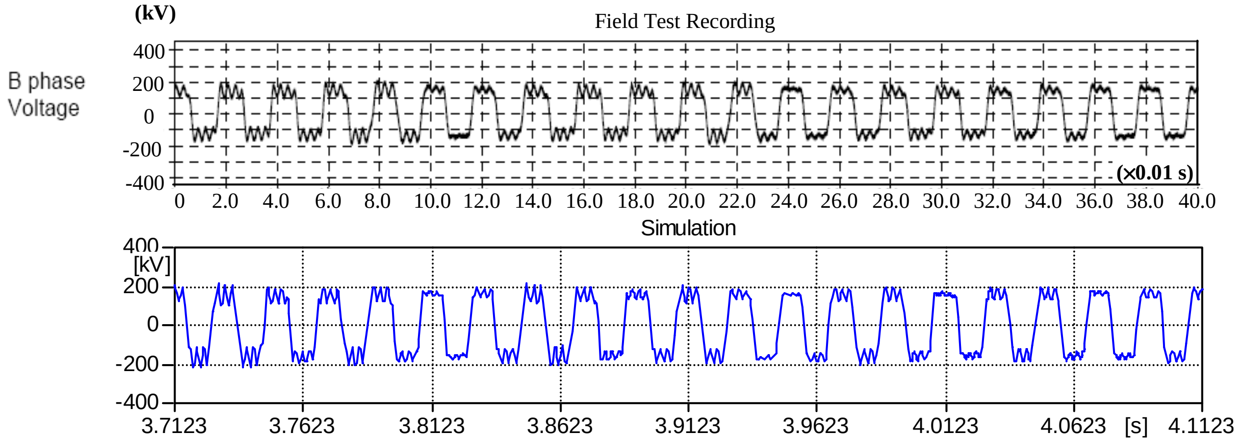

Figure 5.11: Period-1 voltage waveforms – Blue phase

Comparison between the field recorded and simulation results are as follows:

	R-phase voltage	**Y-phase voltage**	**B-phase voltage**
Field recorded	±200 kV	±300 kV	±180 kV
Simulations	±200 kV	±380 kV	±190 kV

3-phase Fundamental Mode Ferroresonance Currents (Period-1)

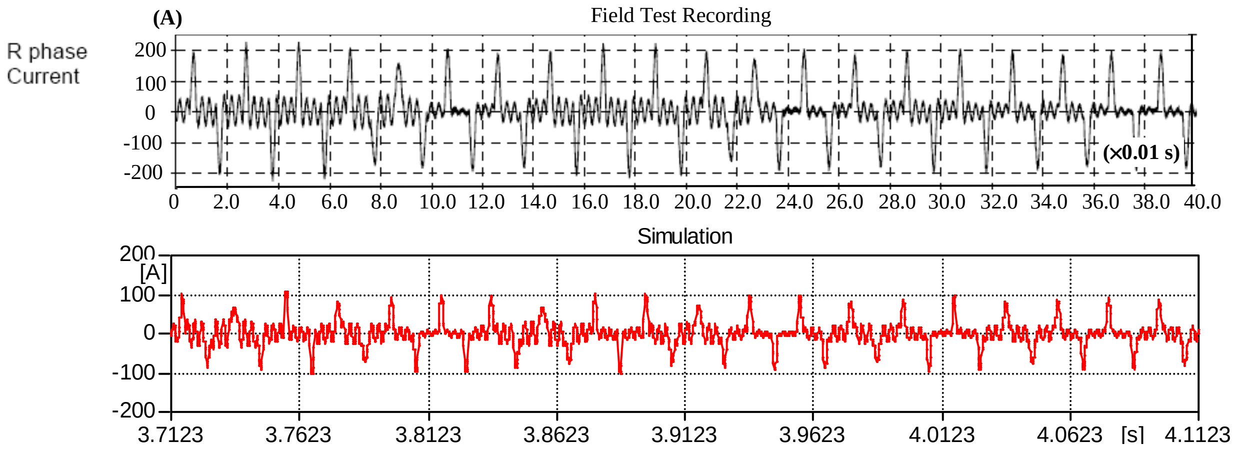

Figure 5.12: Period-1 current waveforms – Red phase

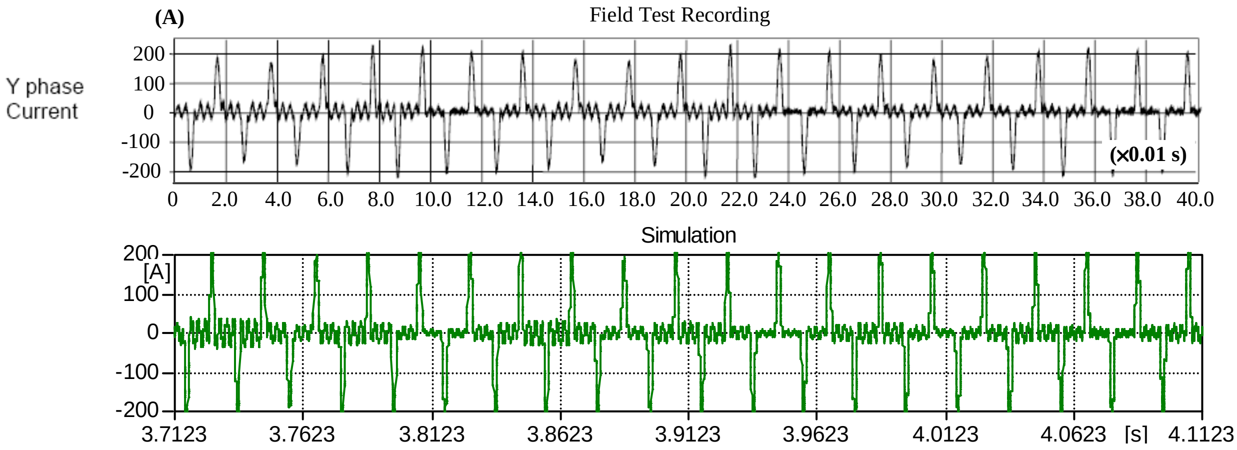

Figure 5.13: Period-1 current waveforms – Yellow phase

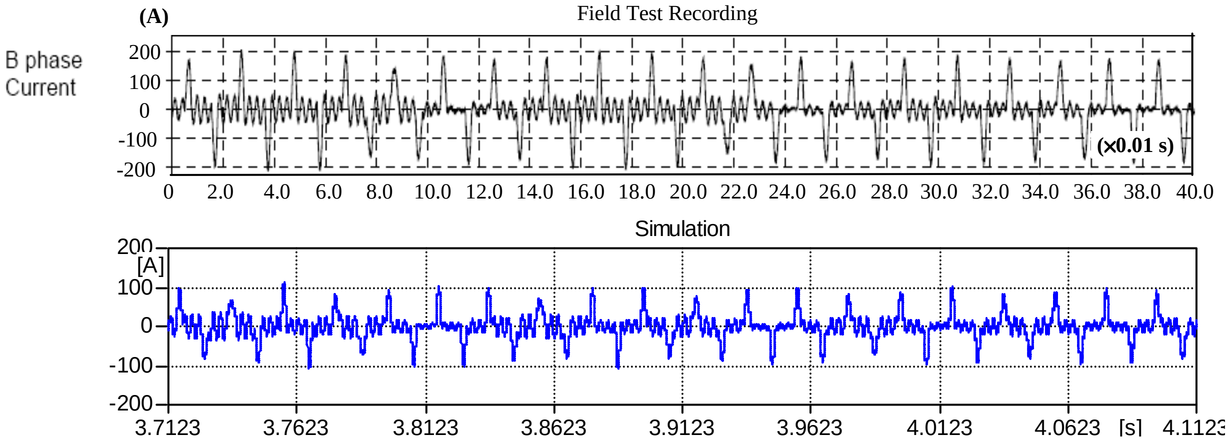

Figure 5.14: Period-1 current waveforms – Blue phase

Comparison between the field recorded and simulation results are as follows:

	R-phase current	**Y-phase current**	**B-phase current**
Field recorded	±200 A	±200 A	±200 A
Simulations	±100 A	±200 A	±100 A

3-phase Subharmonic Mode Ferroresonance Voltages (Period-3)

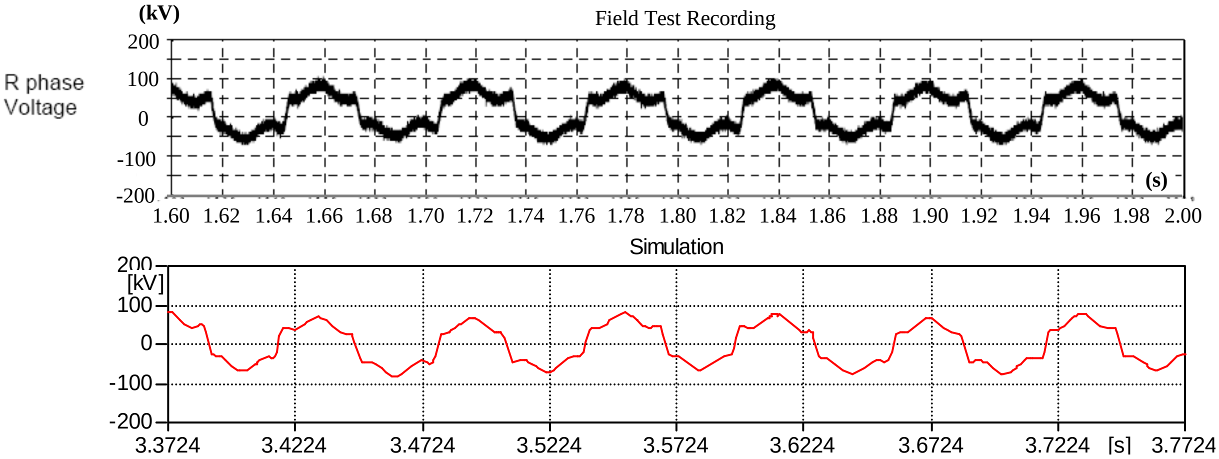

Figure 5.15: Period-3 voltage waveforms – Red phase

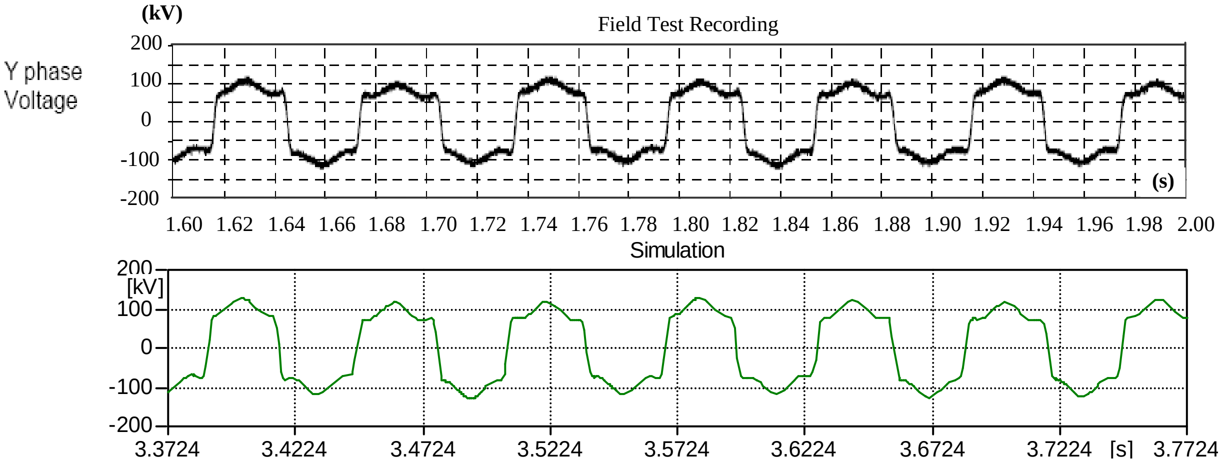

Figure 5.16: Period-3 voltage waveforms – Yellow phase

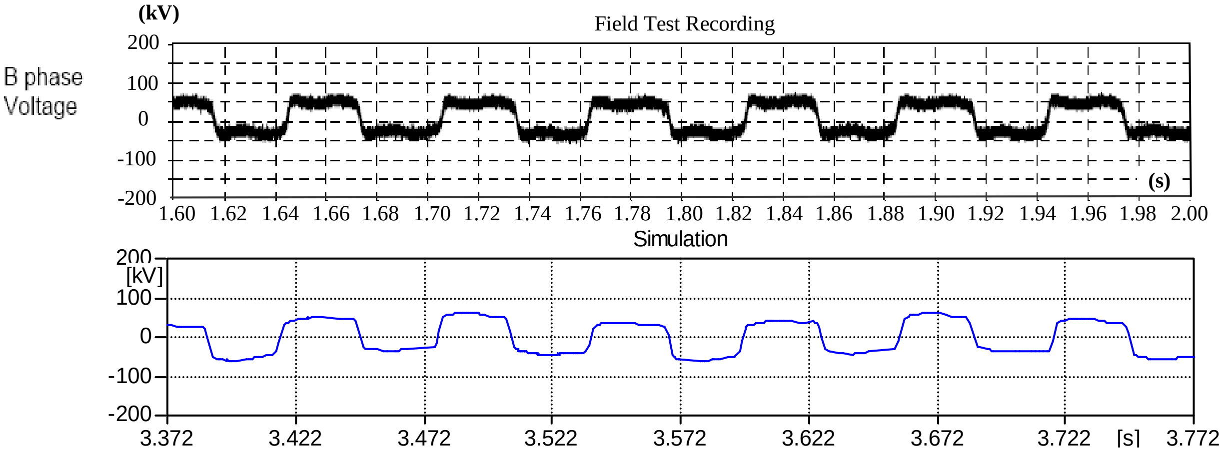

Figure 5.17: Period-3 voltage waveforms – Blue phase

Comparison between the field recorded and simulation results are as follows:

	R-phase voltage	**Y-phase voltage**	**B-phase voltage**
Field recorded	+100 kV, -50 kV	±100 kV	±50 kV
Simulations	+80 kV, - 50kV	±110 kV	±48 kV

3-phase Subharmonic Mode Ferroresonance Currents (Period-3)

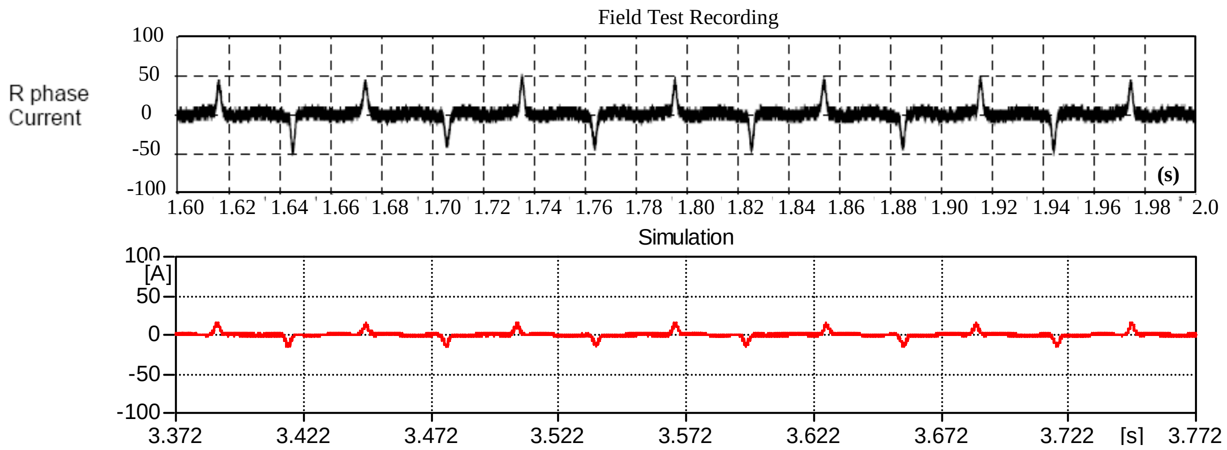

Figure 5.18: Period-3 current waveforms – Red phase

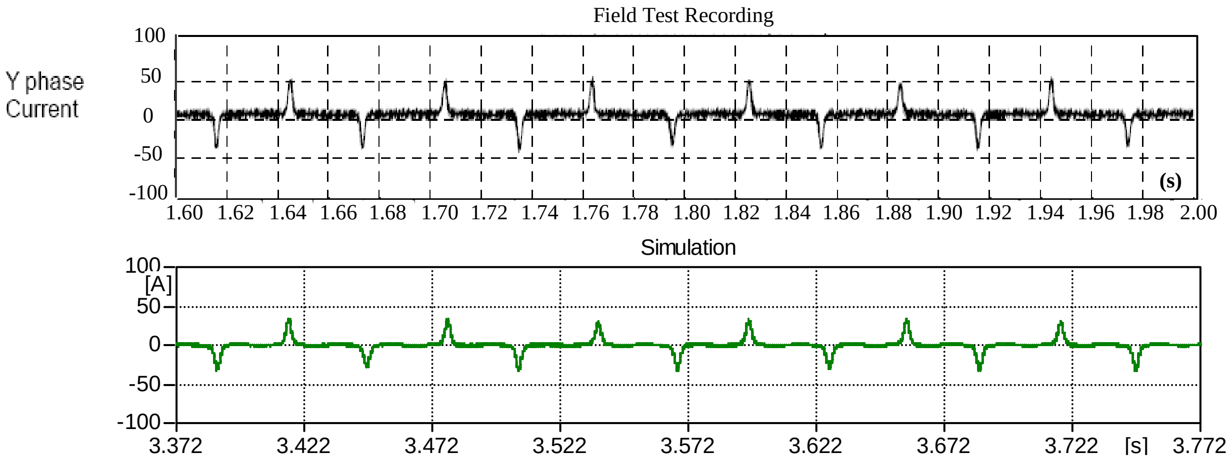

Figure 5.19: Period-3 current waveforms – Yellow phase

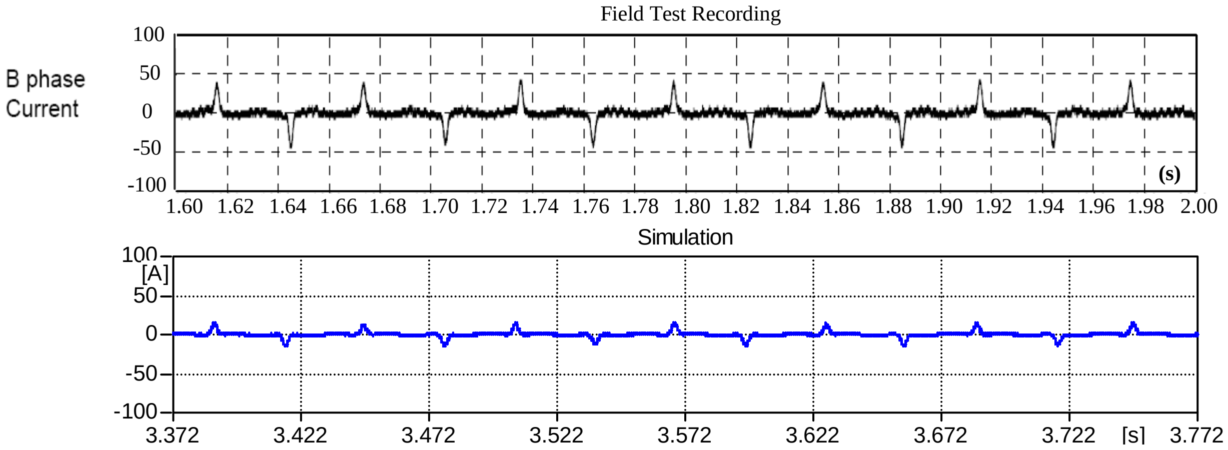

Figure 5.20: Period-3 current waveforms – Blue phase

Comparison between the field recorded and simulation results are as follows:

	R-phase current	**Y-phase current**	**B-phase current**
Field recorded	±50 A	+50 A, -45 A	±45 A
Simulations	±20 A	+38 A, -35A	±20 A

5.5.2 Case Study 2: Transformer - BCTRAN+, Line - BERGERON

In Section 5.5.1, the transformer BCTRAN+ model employing various degrees of saturations with *n*=13, 15, 17, 19, 21, 23, 25 and 27 together with the PI transmission line model have been used in the simulation. In this section, the only change in the simulation model is that Bergeron transmission line model is considered. The results after a number of simulations are presented in Figure 5.21 to Figure 5.32.

3-phase Fundamental Mode Ferroresonance Voltages (Period-1)

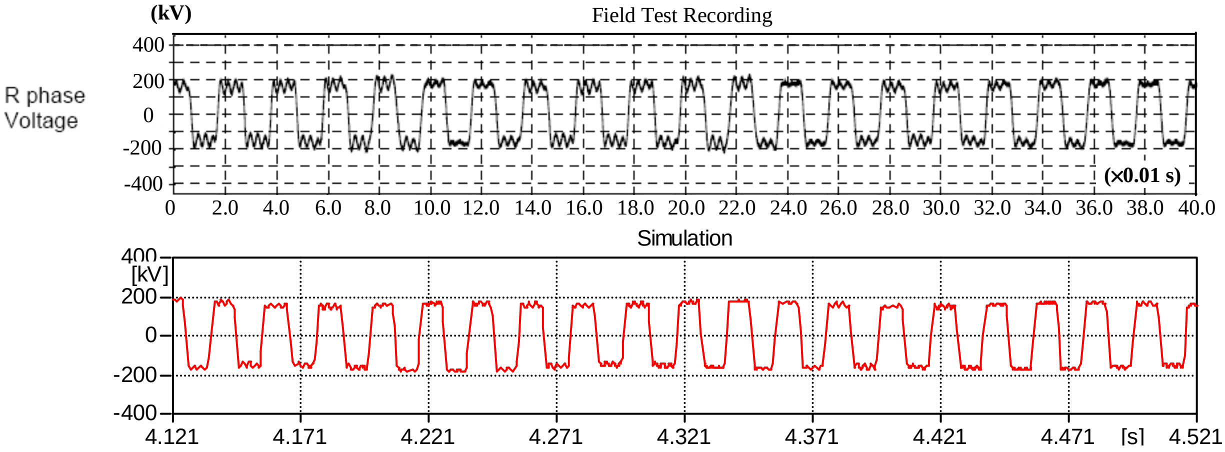

Figure 5.21: Period-1 voltage waveforms – Red phase

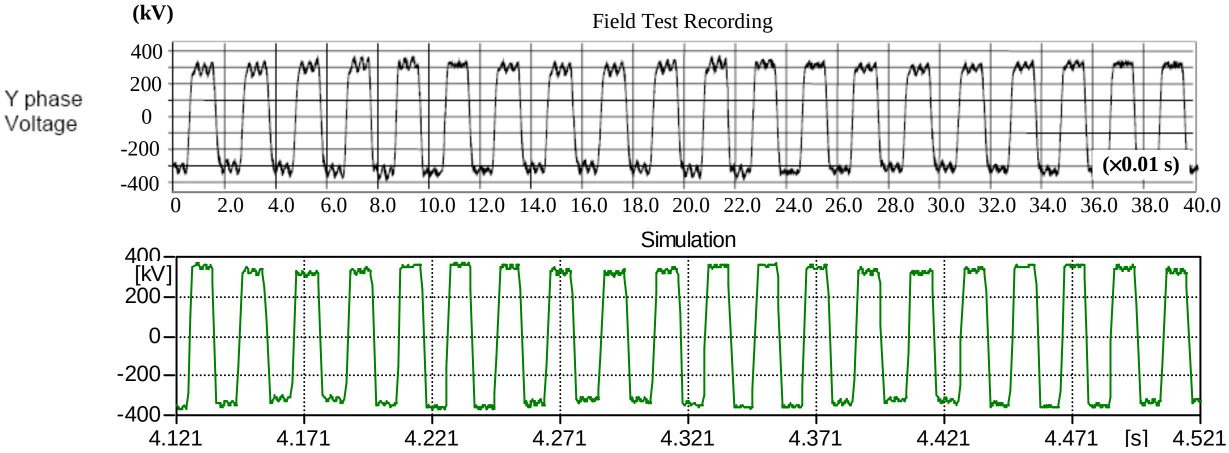

Figure 5.22: Period-1 voltage waveforms – Yellow phase

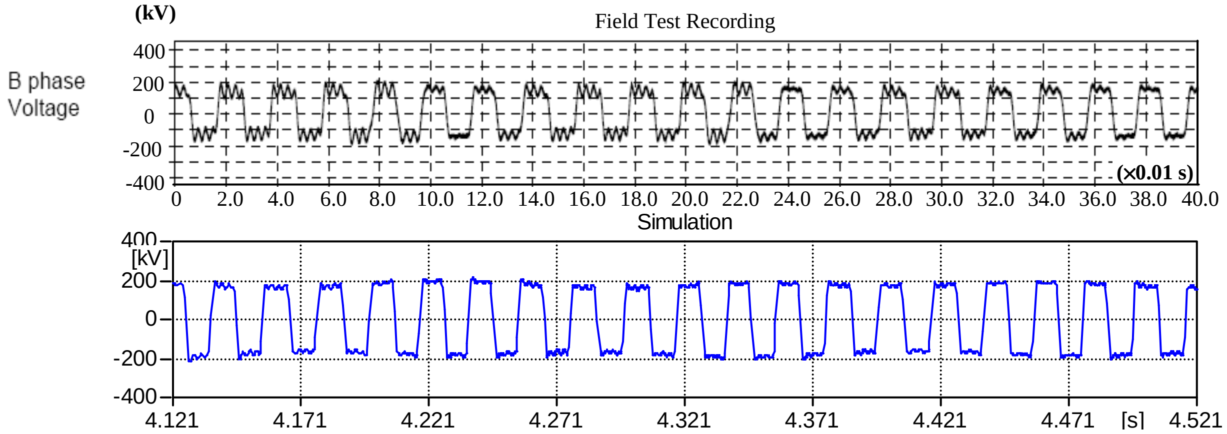

Figure 5.23: Period-1 voltage waveforms – Blue phase

Comparison between the field recorded and simulation results are as follows:

	R-phase voltage	**Y-phase voltage**	**B-phase voltage**
Field recorded	±200 kV	±300 kV	±180 kV
Simulations	±190 kV	±360 kV	±200 kV

3-phase Fundamental Mode Ferroresonance Currents (Period-1)

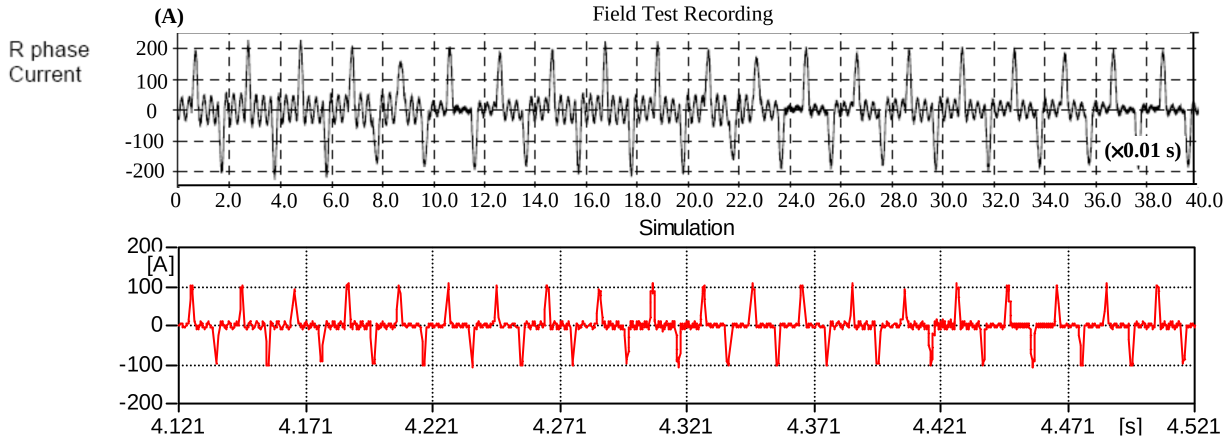

Figure 5.24: Period-1 current waveforms – Red phase

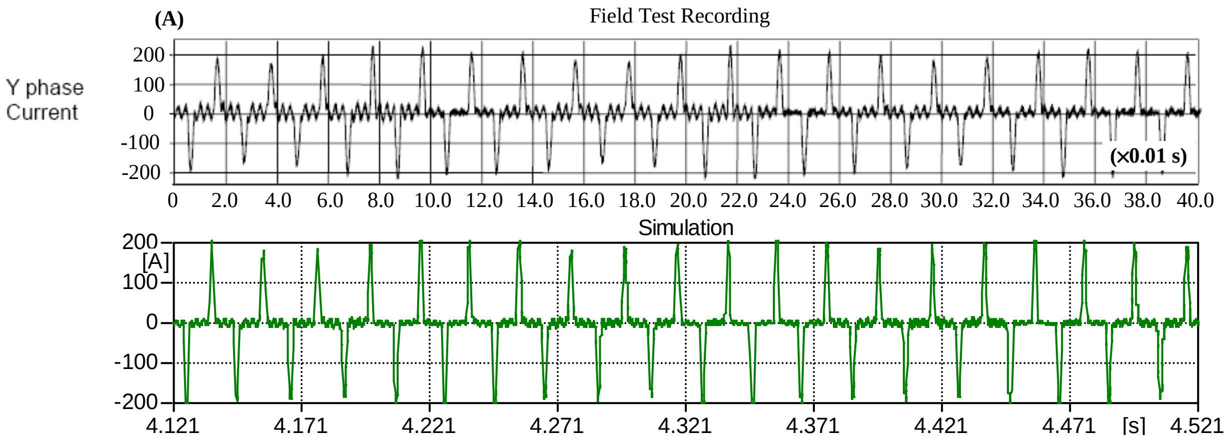

Figure 5.25: Period-1 current waveforms – Yellow phase

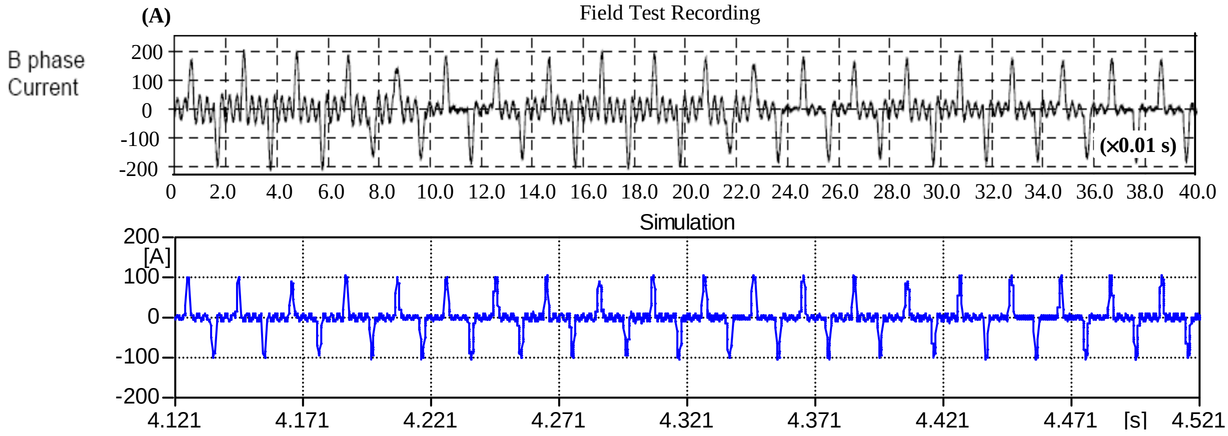

Figure 5.26: Period-1 current waveforms – Blue phase

Comparison between the field recorded and simulation results are as follows:

	R-phase current	**Y-phase current**	**B-phase current**
Field recorded	±200 A	±200 A	±200 A
Simulations	±100 A	±200 A	±100 A

3-phase Subharmonic Mode Ferroresonance voltages (Period-3)

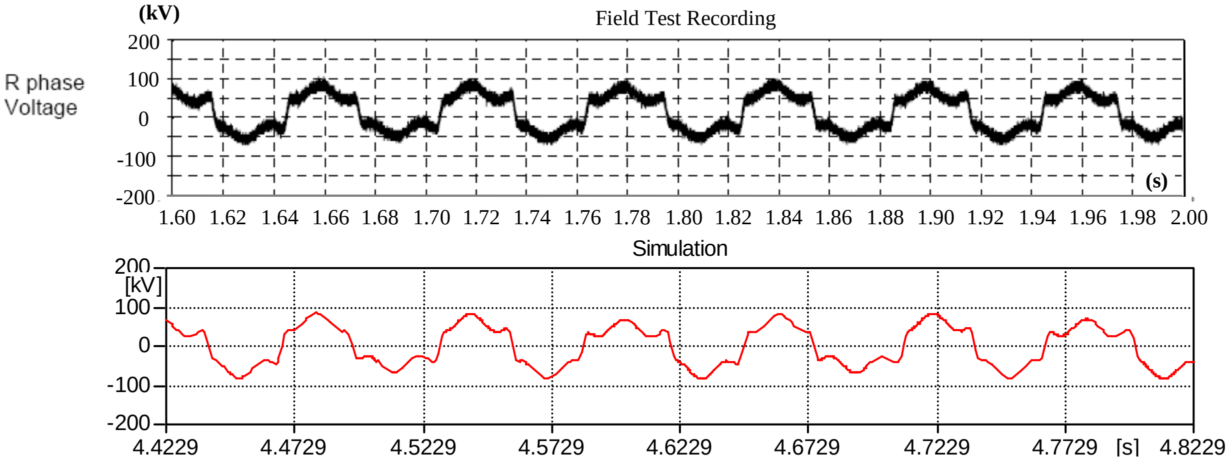

Figure 5.27: Period-3 voltage waveforms – Red phase

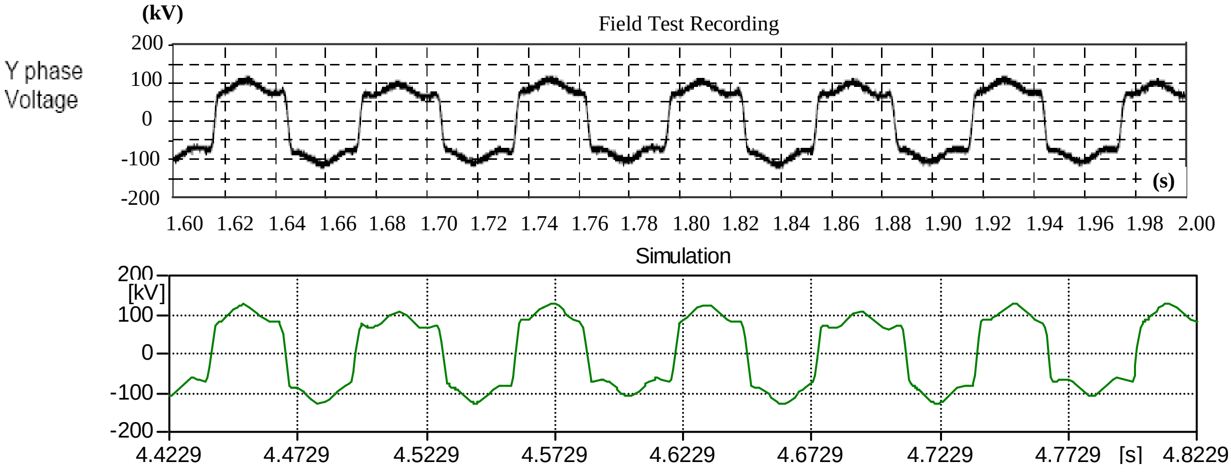

Figure 5.28: Period-3 voltage waveforms – Yellow phase

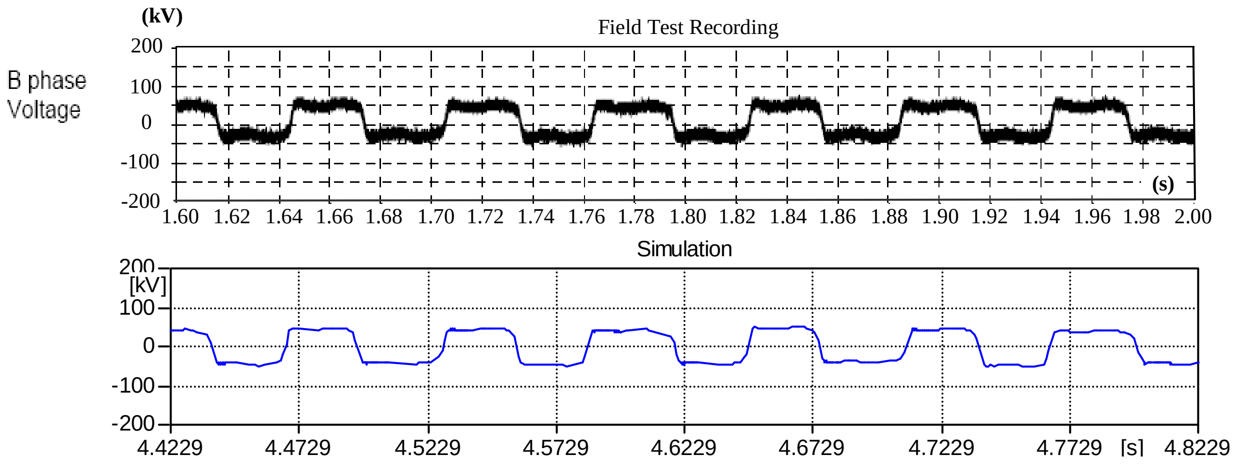

Figure 5.29: Period-3 voltage waveforms – Blue phase

Comparison between the field recorded and simulation results are as follows:

	R-phase voltage	Y-phase voltage	B-phase voltage
Field recorded	+100 kV, -50 kV	±100 kV	±50 kV
Simulations	+80 kV, - 70kV	±110 kV	±48 kV

3-phase Subharmonic Mode Ferroresonance Currents (Period-3)

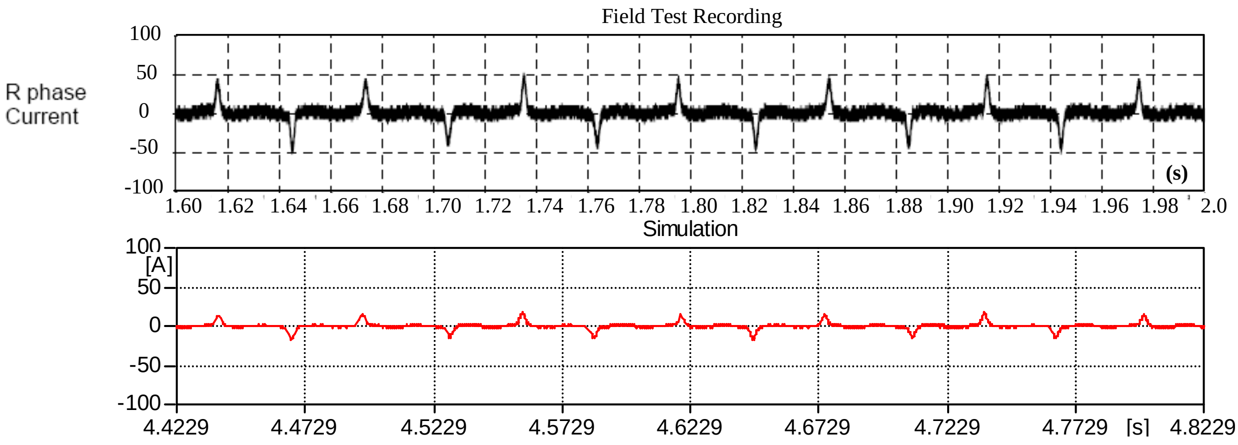

Figure 5.30: Period-3 current waveforms – Red phase

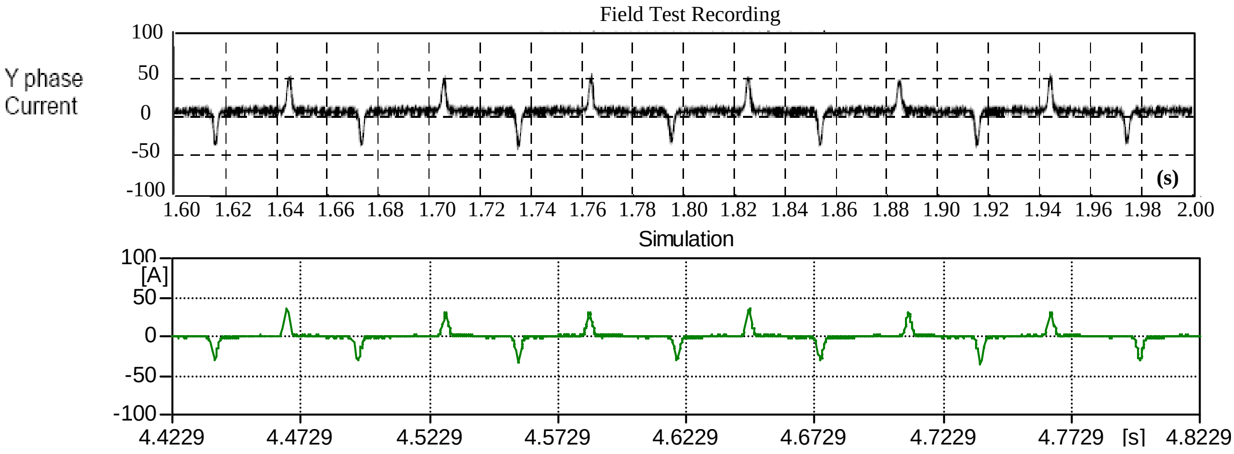

Figure 5.31: Period-3 current waveforms – Yellow phase

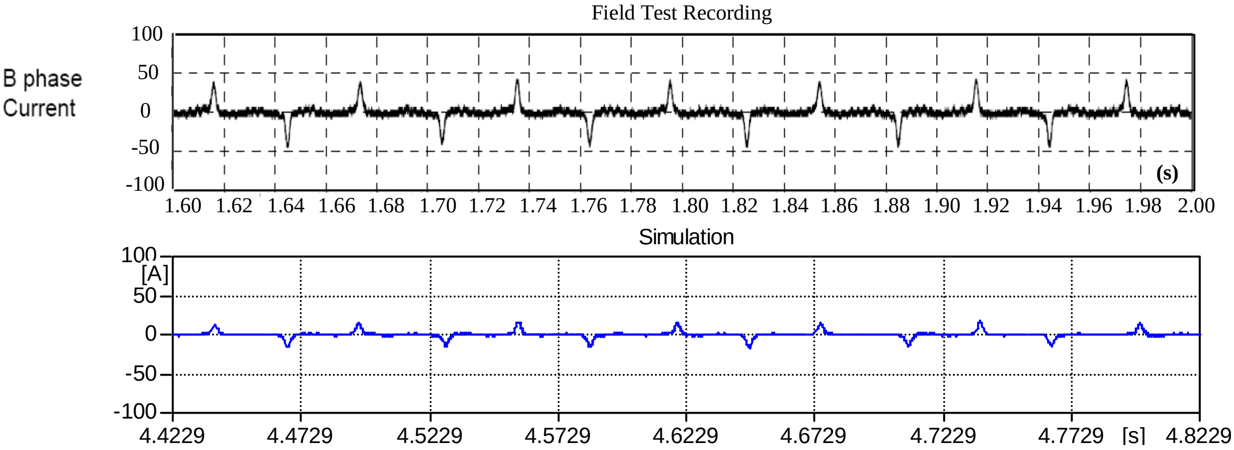

Figure 5.32: Period-3 current waveforms – Blue phase

Comparison between the field recorded and simulation results are as follows:

	R-phase current	Y-phase current	B-phase current
Field recorded	±50 A	+50 A, -45 A	±45 A
Simulations	±18 A	+39 A, -32A	±19 A

5.5.3 Case Study 3: Transformer - BCTRAN+, Line – MARTI

Transmission line models employing PI and Bergeron have been studied in the preceding sections. In this section, another distributed parameter line model which takes into account of frequency dependent loss has been used. The simulation results are presented in Figure 5.33 to Figure 5.44.

<u>3-phase Fundamental Mode Ferroresonance Voltages (Period-1)</u>

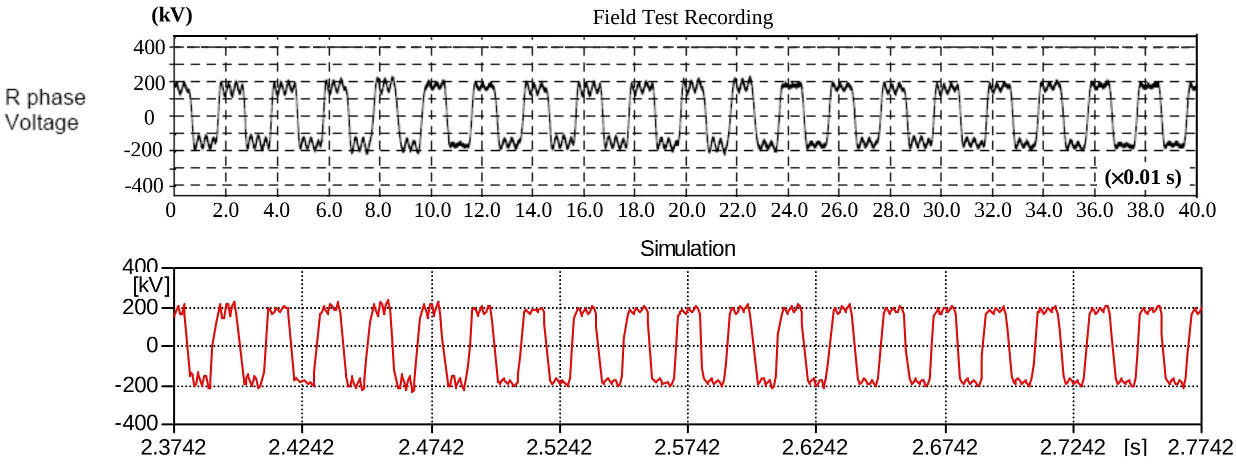

Figure 5.33: Period-1 voltage waveforms – Red phase

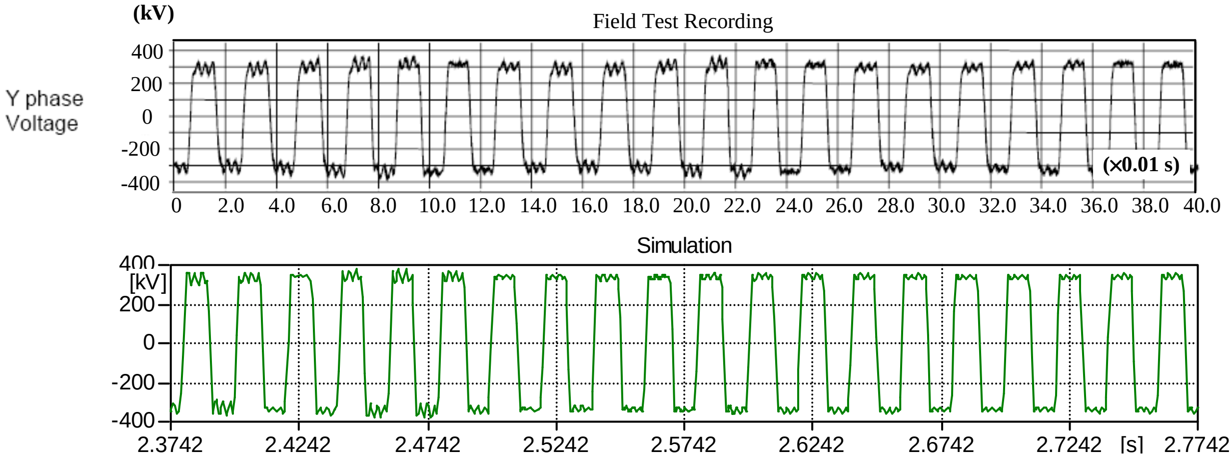

Figure 5.34: Period-1 voltage waveforms – Yellow phase

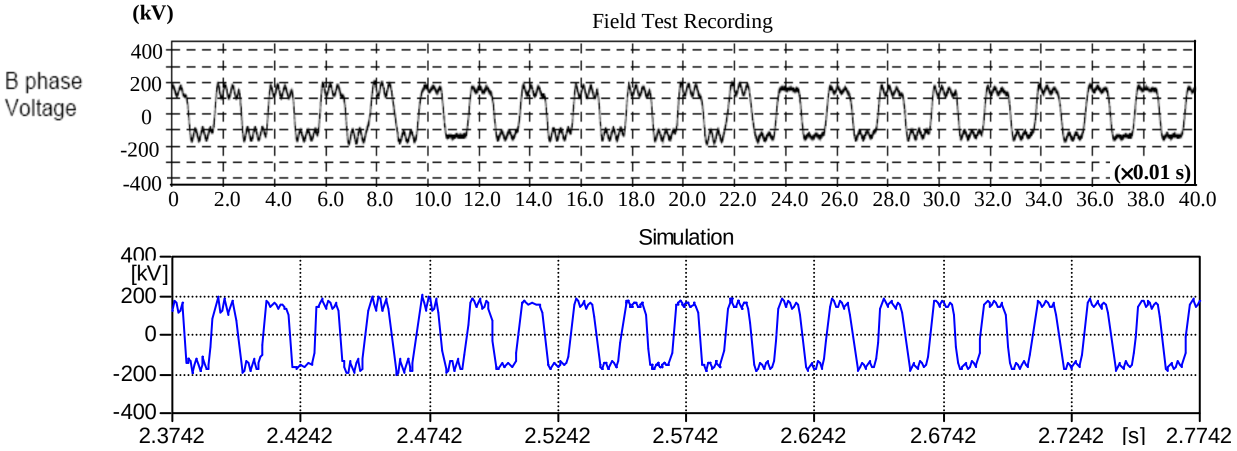

Figure 5.35: Period-1 voltage waveforms – Yellow phase

Comparison between the field recorded and simulation results are as follows:

	R-phase voltage	**Y-phase voltage**	**B-phase voltage**
Field recorded	±200 kV	±300 kV	±180 kV
Simulations	±200 kV	±375 kV	±180 kV

3-phase Fundamental Mode Ferroresonance Currents (Period-1)

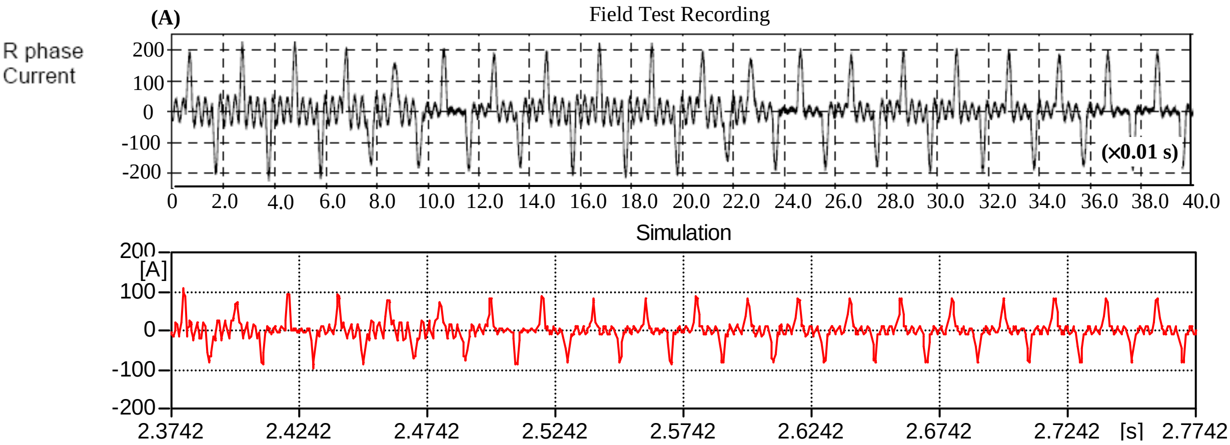

Figure 5.36: Period-1 current waveforms – Red phase

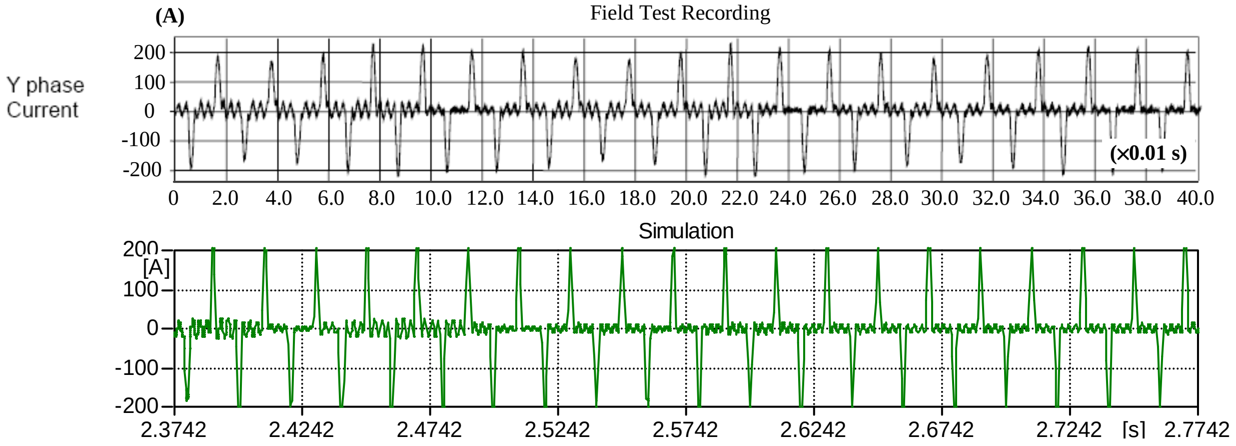

Figure 5.37: Period-1 current waveforms – Yellow phase

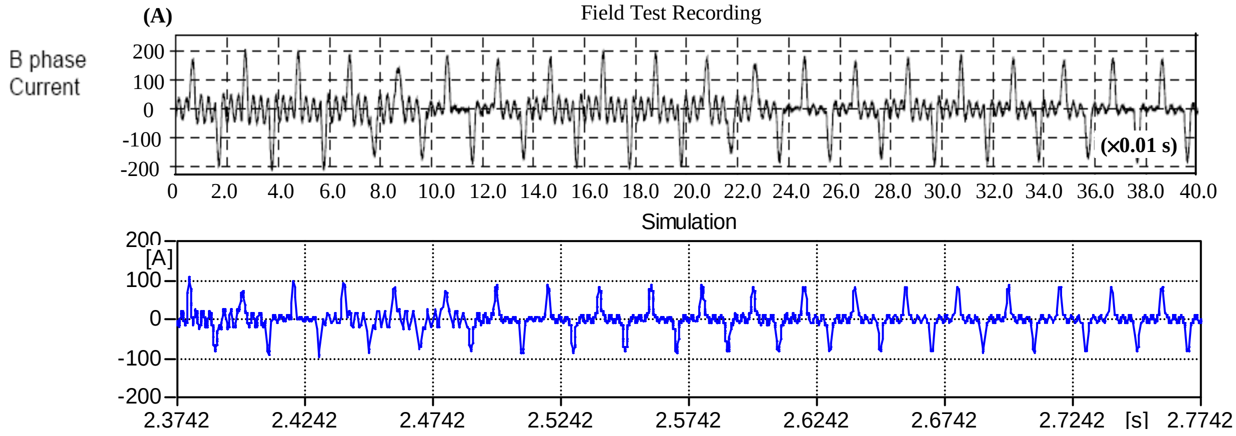

Figure 5.38: Period-1 current waveforms – Blue phase

Comparison between the field recorded and simulation results are as follows:

	R-phase current	**Y-phase current**	**B-phase current**
Field recorded	±200 A	±200 A	±200 A
Simulations	±90 A	±200 A	±90 A

3-phase Subharmonic Mode Ferroresonance Voltages (Period-3)

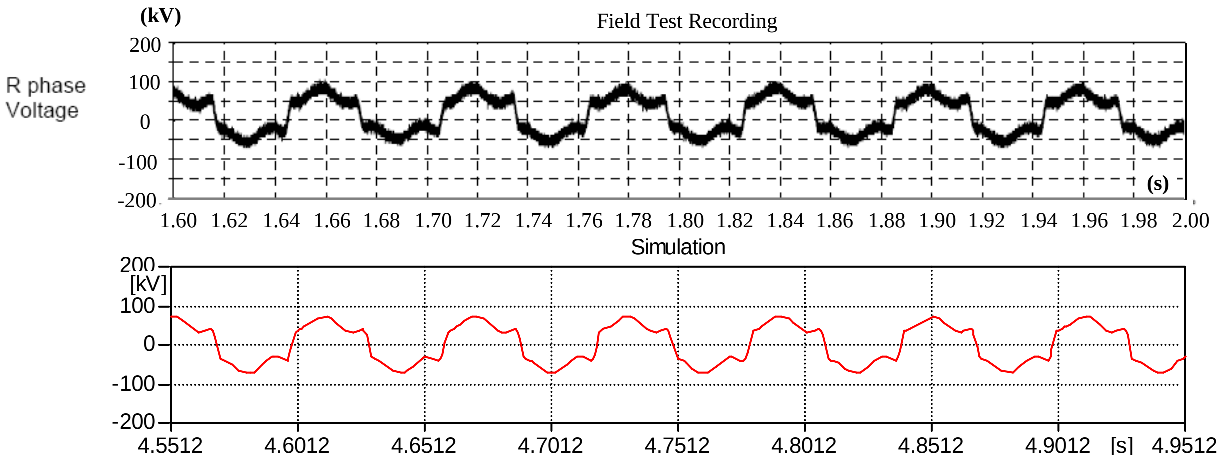

Figure 5.39: Period-3 voltage waveforms – Red phase

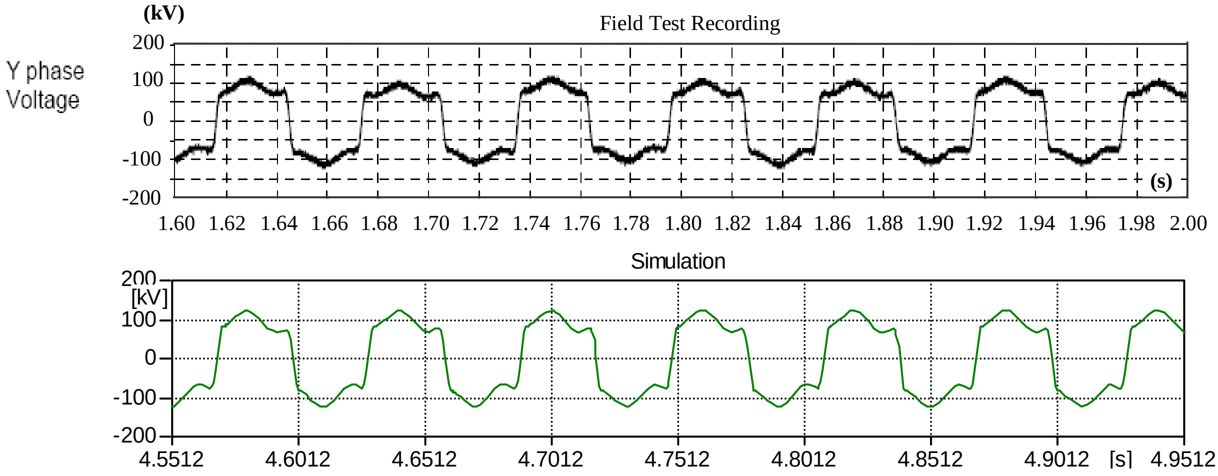

Figure 5.40: Period-3 voltage waveforms – Yellow phase

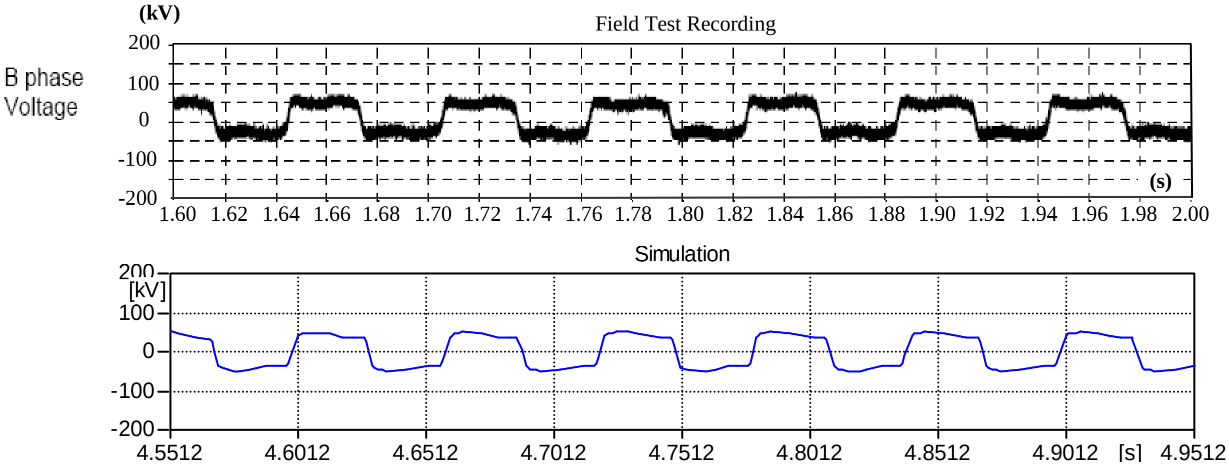

Figure 5.41: Period-3 voltage waveforms – Blue phase

Comparison between the field recorded and simulation results are as follows:

	R-phase voltage	Y-phase voltage	B-phase voltage
Field recorded	+100 kV, -50 kV	±100 kV	±50 kV
Simulations	+75 kV, - 75kV	±110 kV	±49 kV

3-phase Subharmonic Mode Ferroresonance Currents (Period-3)

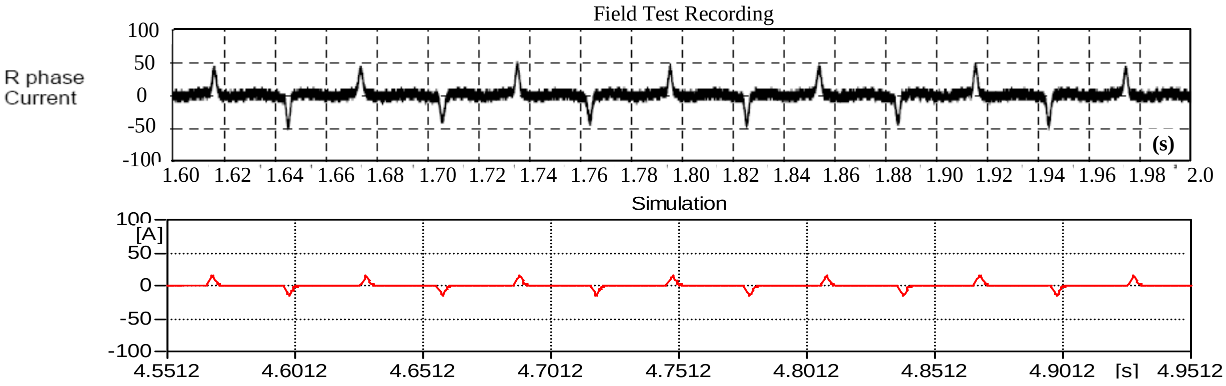

Figure 5.42: Period-3 current waveforms – Red phase

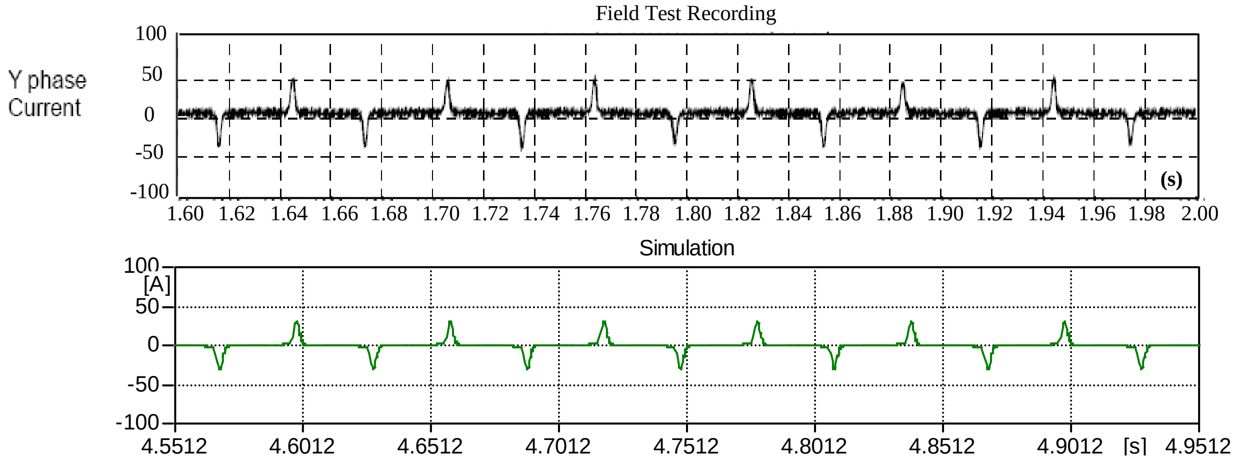

Figure 5.43: Period-3 current waveforms – Yellow phase

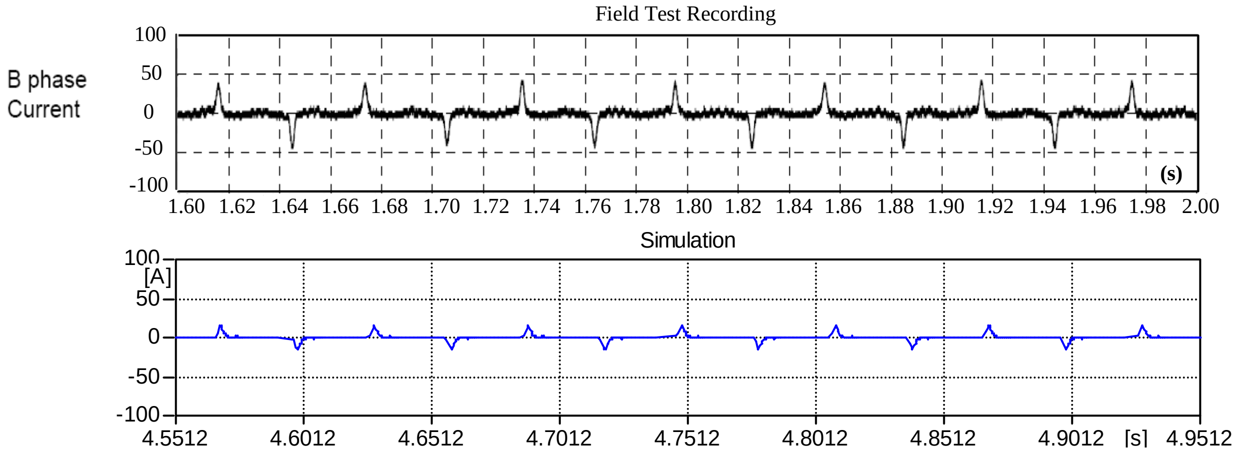

Figure 5.44: Period-3 current waveforms – Blue phase

Comparison between the field recorded and simulation results are as follows:

	R-phase current	**Y-phase current**	**B-phase current**
Field recorded	±50 A	+50 A, -45 A	±45 A
Simulations	±19 A	+39 A, -32A	±19 A

- **Summary of Case Study 1, 2 and 3**

After evaluating the three case studies above, that is by using the BCTRAN+ transformer model with three different types of transmission line models, the simulation results show that each of them is equally able to produce both the Period-1 and Period-3 ferroresonance.

From the results, a number of observations have been noted in order to replicate the field recording waveforms in terms of their three phase voltage/current magnitudes. They are commented as follows:

(1) Period-1 ferroresonance

	Case Study 1	**Case Study 2**	**Case Study 3**
Voltage amplitude	There is a similarity in the voltage magnitude produced by all the three case studies; no significant difference between them.		
Voltage waveshape	All the three cases produce the same voltage pattern which is rectangular in shape but slight differences exist in the voltage ripple at both the positive and negative peak voltages.		
Current amplitude	The current magnitudes are moderately similar. The results show that the magnitudes of both the red and the blue phases are only half of the field test recording ones. However, the magnitude produced by the yellow phase is most comparable to the recording.		
Current waveshape	All the three cases are able to produce the peaky shape currents but slight deviations are in the magnitudes of current ripples which appear around the zero current magnitude of the waveforms.		

From the observation, it can be suggested that Case Study 1 which employed BCTRAN+ model for transformer and Pi model for the transmission line are most similar to the measured ones.

(2) Period-3 ferroresonance

	Case Study 1	**Case Study 2**	**Case Study 3**
Voltage amplitude	The voltage magnitudes for all the three phases produced from all the cases are comparable to the real recording waveforms.		
Voltage waveshape	All the three cases are able to reproduce almost the same patterns as the measured three phase voltage waveforms. However, the high frequency oscillatory ripple does not reproduce itself at the peak of the waveforms.		
Current amplitude	In term of the current magnitudes, the simulation showed that both the simulated red and blue phases are about 60% less that the measured ones while the yellow phase is about 20% less.		
Current waveshape	The currents are peaky in shape which match with the real ones but high frequency oscillatory ripples oscillation appearing around the zero current magnitudes are missing in the simulations.		

From the observation, it suggested that the simulation results produced by Case Study 1 are most similar to the measured ones.

In summary, it has been observed that all the three case studies have produced almost the similar characteristics to one and another. The magnitudes and waveshapes gained from the models are not distinctively different from one and another. In addition, they are able to replicate the real recording waveforms in a reasonable fashion for both the Period-1 and Period-3 ferroresonance. In view of the above, a decision to choose the best simulation model for the representation of the Brinsworth system on ferroresonance is difficult. Therefore, it has been decided that all the models are acceptable for the study of ferroresonance. The use of BCTRAN+ model to represent the power transformer and the employment of either the PI, the Bergeron or the J. Marti to model a transmission line can be taken.

It has been found that modeling of core characteristic employing the BCTRAN+ model is time consuming because the limitation the predefined model has is such that the users needs to “trial and error” to pick up the best possible nonlinear inductor element, it is therefore decided to look into an alternative transformer model where its air-core (deep saturation) inductance of core characteristic can be determined via the build-in calculation.

5.5.4 Case Study 4: Transformer - HYBRID, Line – PI

In this section, instead of using BCTRAN+, a HYBRID model is employed to represent the transformer where the core characteristic is modeled based on the principle of duality.

Unlike the BCTRAN+ model, where the core characteristic has been evaluated via sensitivity study on different degrees of saturation in order for the simulation model to replicate the field test recording waveforms with good accuracy, the HYBRID model no longer requires such evaluation as this type of model is able to generate its own characteristic including the air-core inductance based on the build-in Frolich equation and core dimension embedded in itself.

The results of simulations are shown in Figure 5.45 to Figure 5.56.

3-phase Fundamental Mode Ferroresonance Voltages (Period-1)

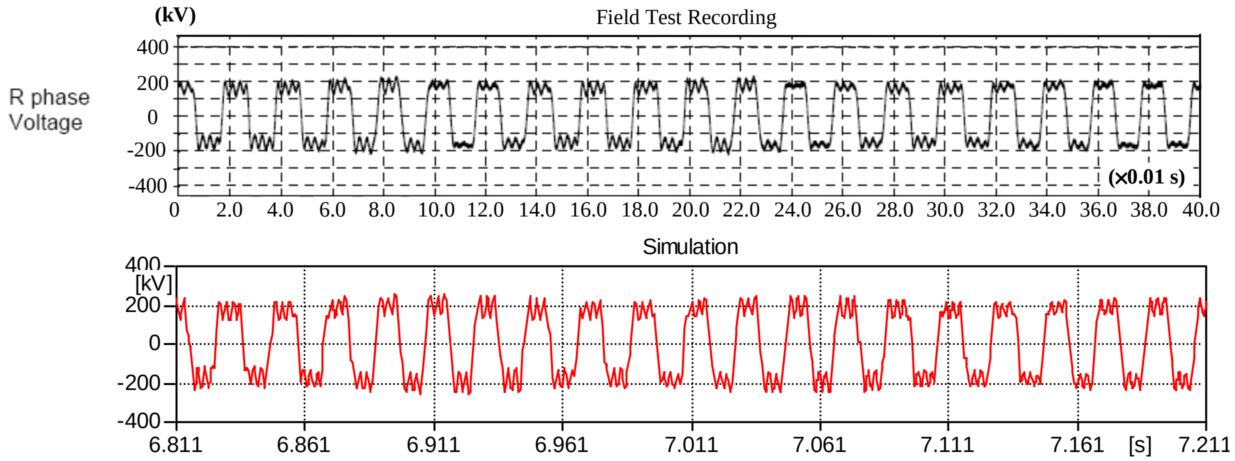

Figure 5.45: Period-1 voltage waveforms – Red phase

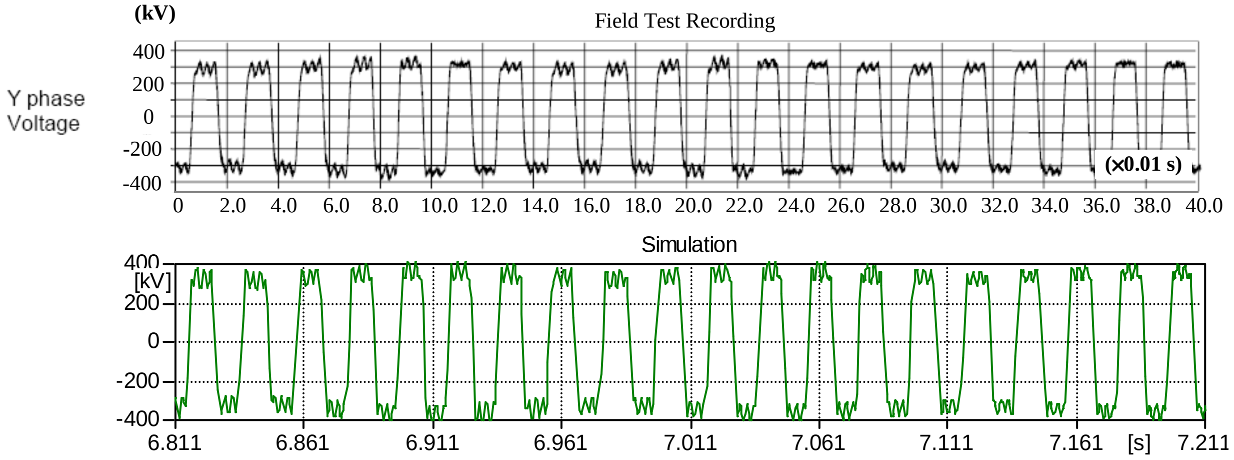

Figure 5.46: Period-1 voltage waveforms – Yellow phase

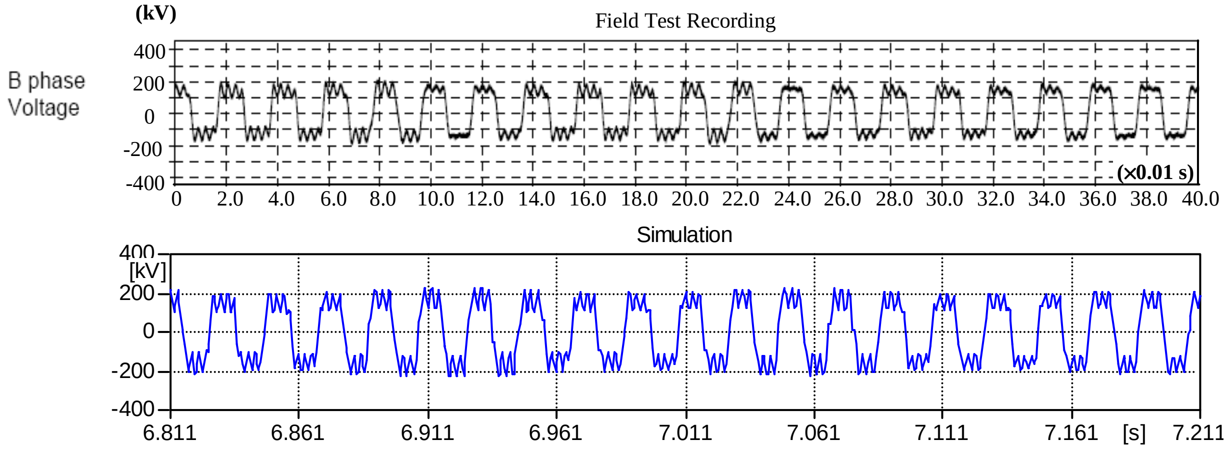

Figure 5.47: Period-1 voltage waveforms – Blue phase

Comparison between the field recorded and simulation results are as follows:

	R-phase voltage	**Y-phase voltage**	**B-phase voltage**
Field recorded	±200 kV	±300 kV	±180 kV
Simulations	±200 kV	±390 kV	±200 kV

3-phase Fundamental Mode Ferroresonance Currents (Period-1)

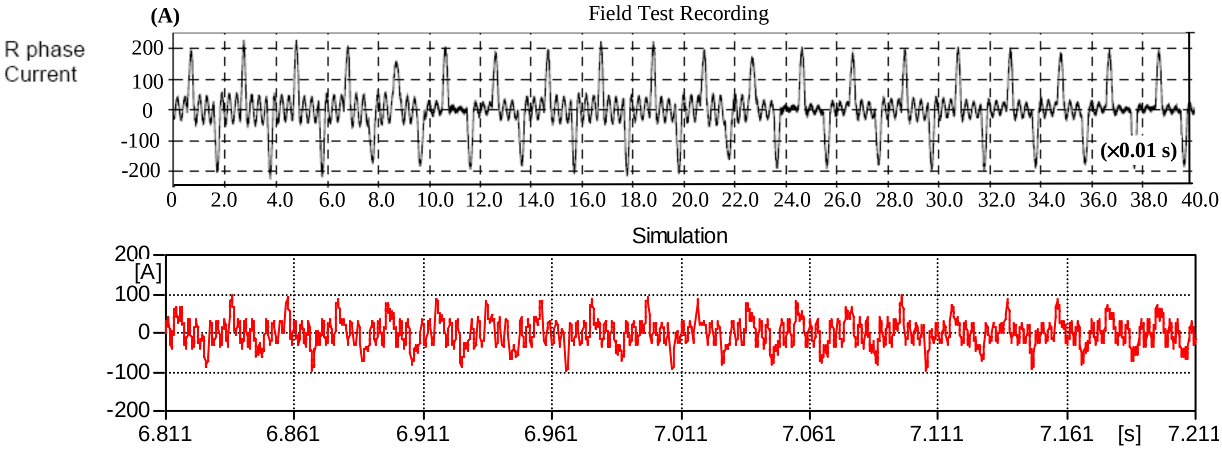

Figure 5.48: Period-1 current waveforms – Red phase

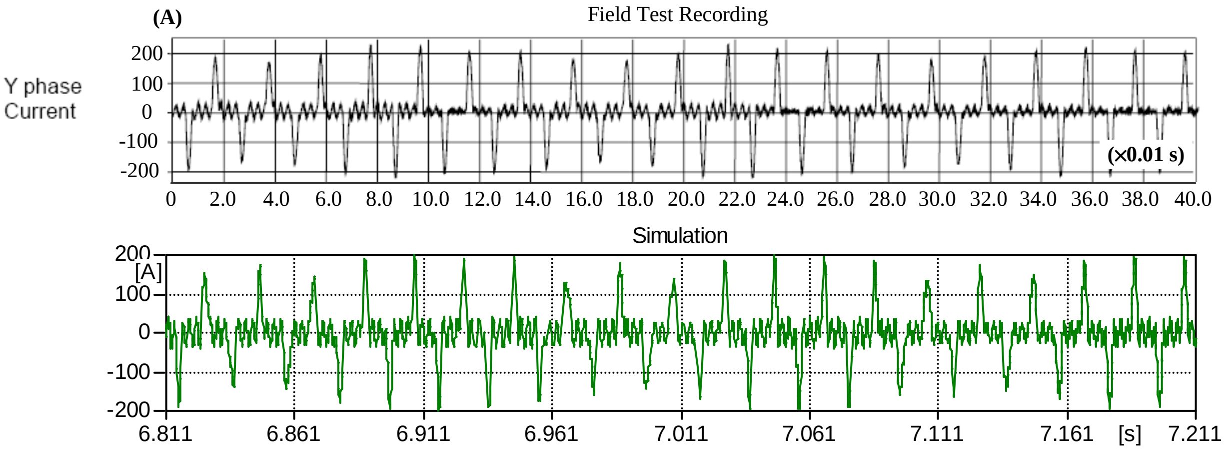

Figure 5.49: Period-1 current waveforms – Yellow phase

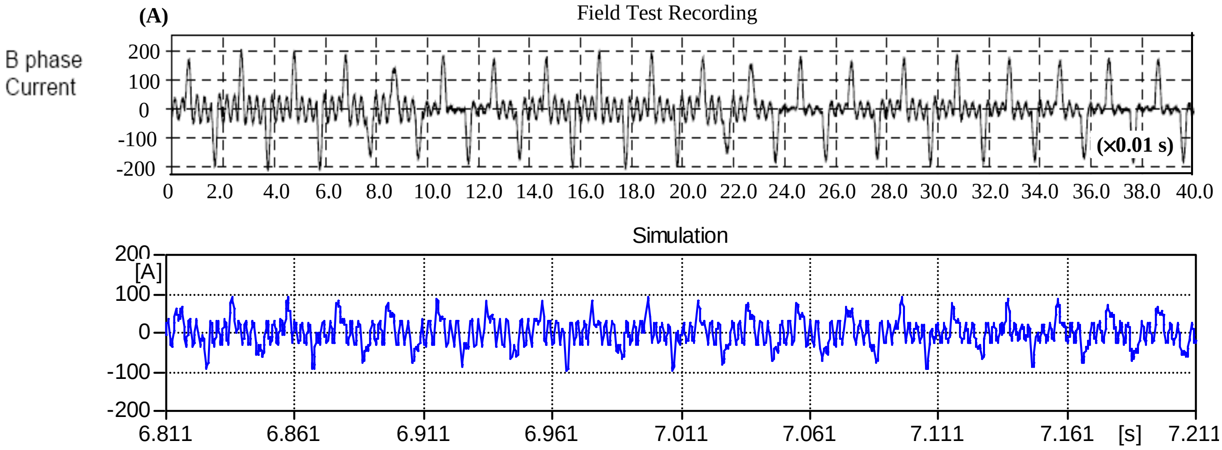

Figure 5.50: Period-1 current waveforms – Blue phase

Comparison between the field recorded and simulation results are as follows:

	R-phase current	**Y-phase current**	**B-phase current**
Field recorded	±200 A	±200 A	±200 A
Simulations	±90 A	±190 A	±90 A

3-phase Subharmonic Mode Ferroresonance Voltages (Period-3)

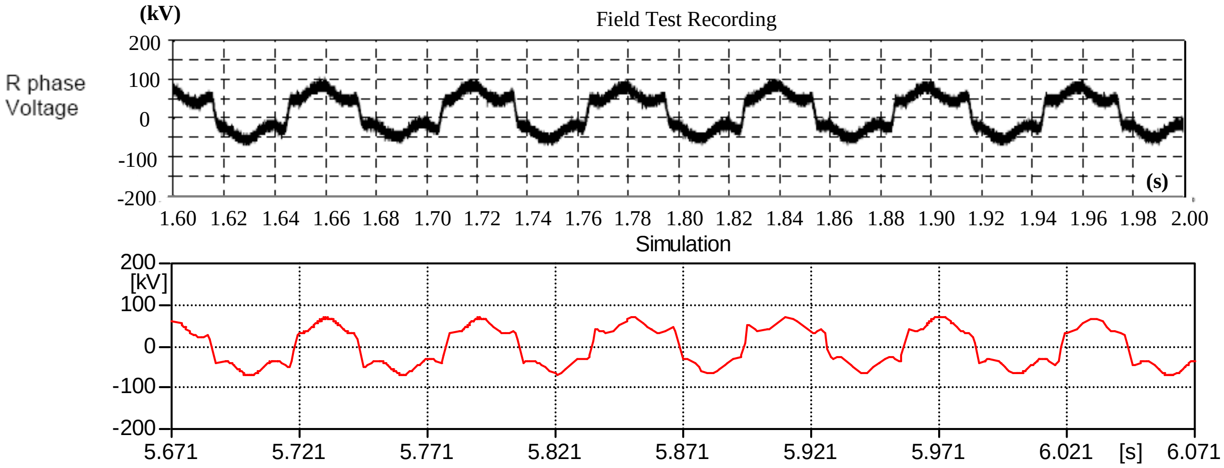

Figure 5.51: Period-3 voltage waveforms – Red phase

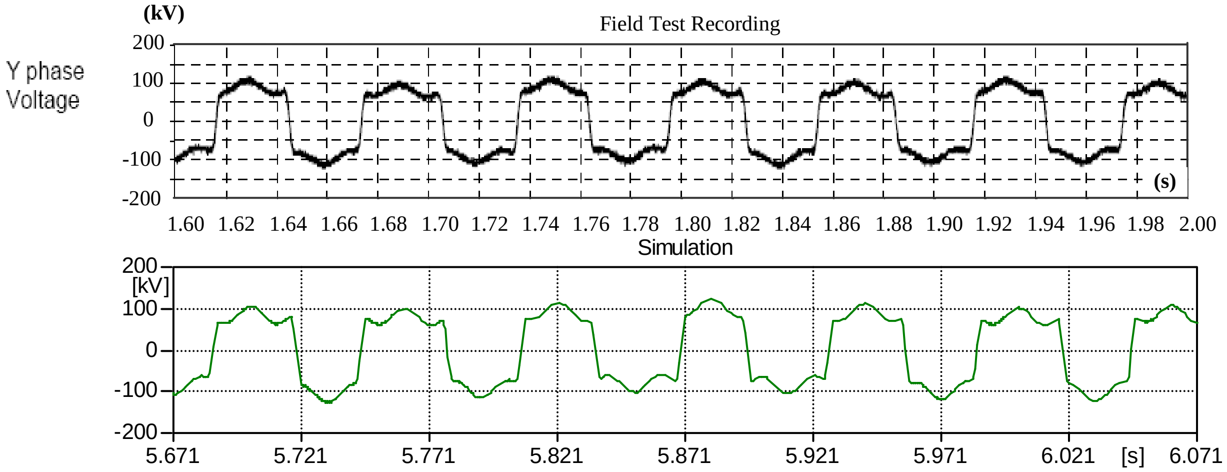

Figure 5.52: Period-3 voltage waveforms – Yellow phase

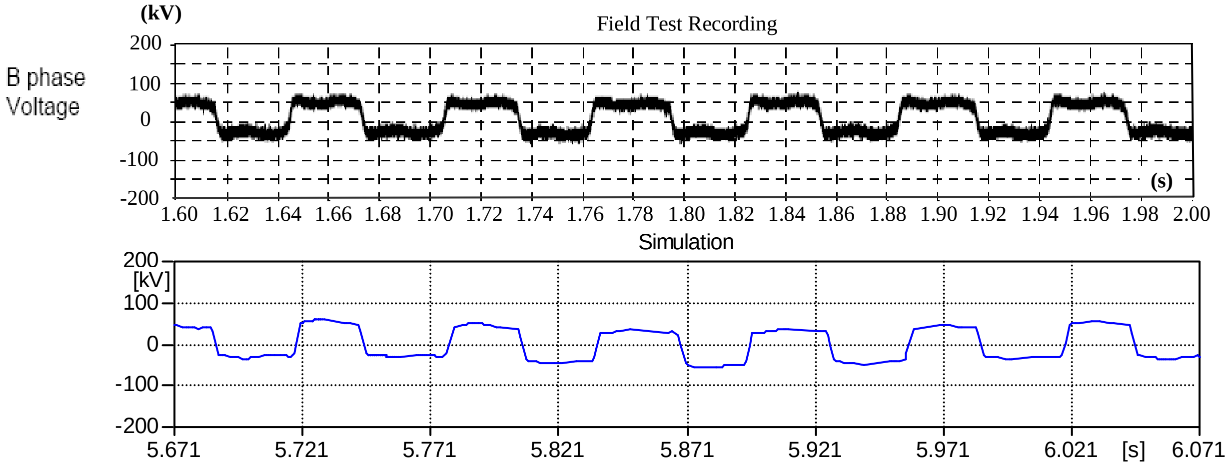

Figure 5.53: Period-3 voltage waveforms – Blue phase

Comparison between the field recorded and simulation results are as follows:

	R-phase voltage	**Y-phase voltage**	**B-phase voltage**
Field recorded	+100 kV, -50 kV	±100 kV	±50 kV
Simulations	+75 kV, - 75kV	±100 kV	±48 kV

3-phase Subharmonic Mode Ferroresonance Currents (Period-3)

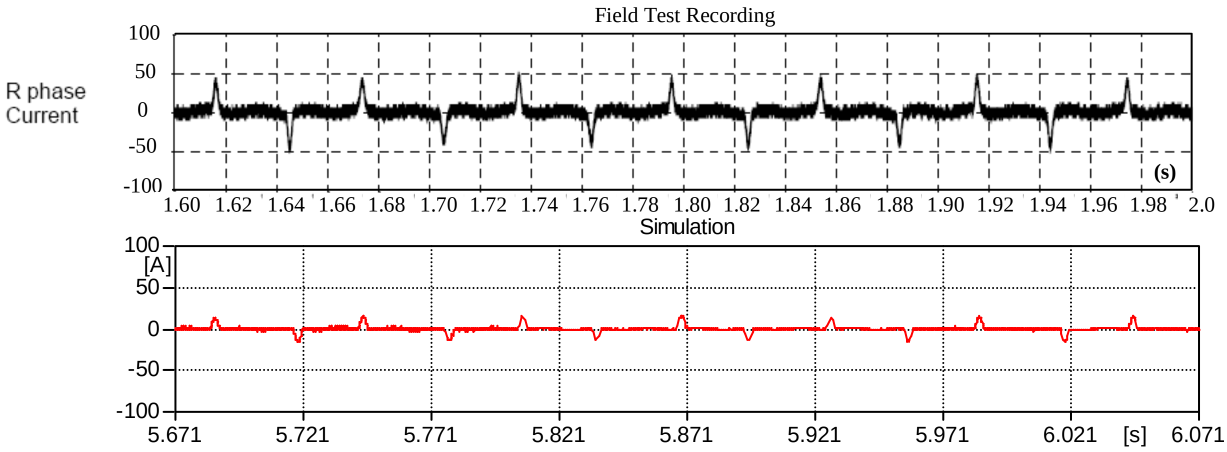

Figure 5.54: Period-3 current waveforms – Red phase

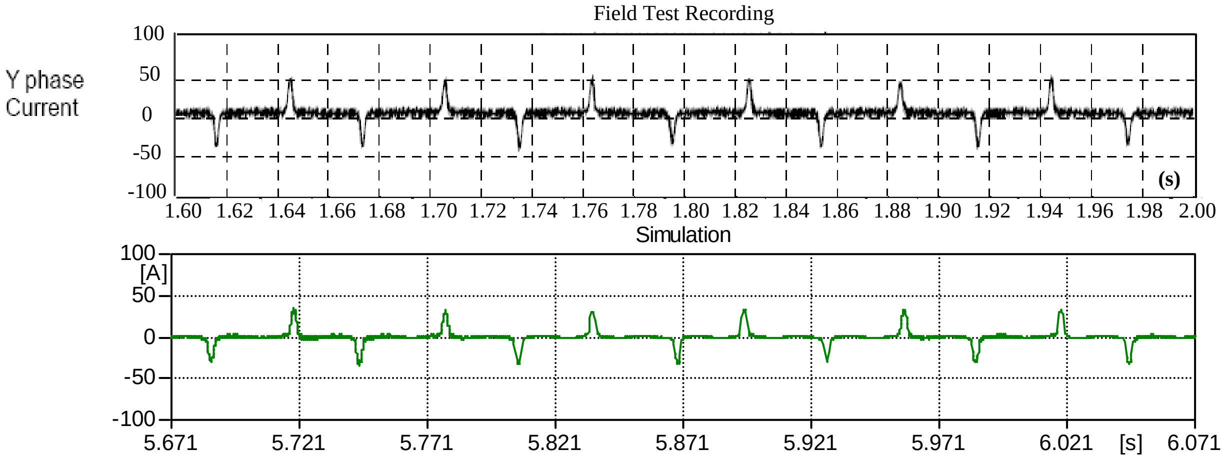

Figure 5.55: Period-3 current waveforms – Yellow phase

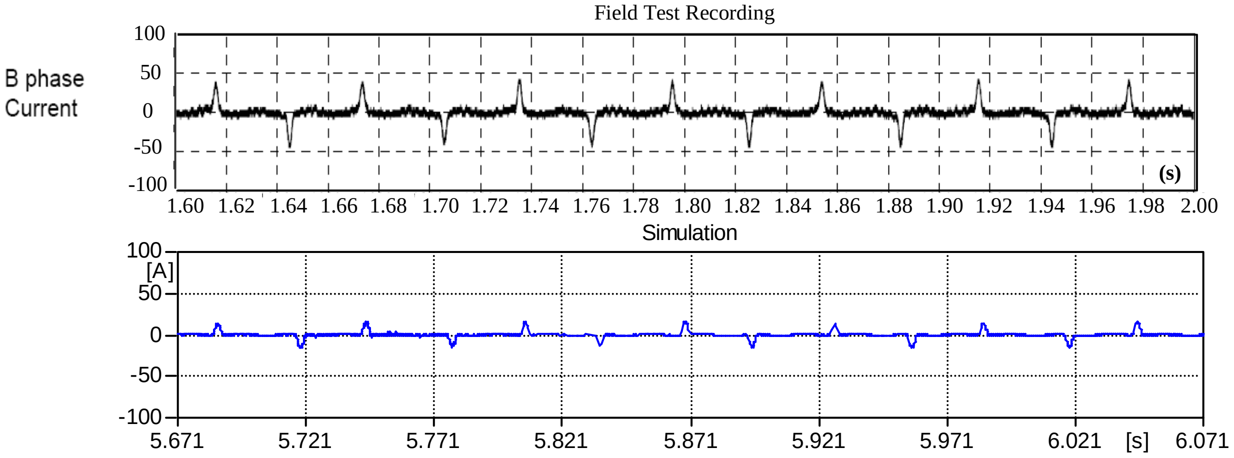

Figure 5.56: Period-3 current waveforms – Blue phase

Comparison between the field recorded and simulation results are as follows:

	R-phase current	**Y-phase current**	**B-phase current**
Field recorded	±50 A	+50 A, -45 A	±45 A
Simulations	±19 A	+40 A, -40A	±19 A

5.5.5 Case Study 5: Transformer - HYBRID, Line – BERGERON

To see if there are any changes by employing the Bergeron model for the representation of the transmission line, the transformer model is kept unchanged, still using the HYBRID model.

The waveforms obtained from the simulations for both Period-1 and Period-3 ferroresonance are shown in Figure 5.57 to Figure 5.68.

3-phase Fundamental Mode Ferroresonance Voltages (Period-1)

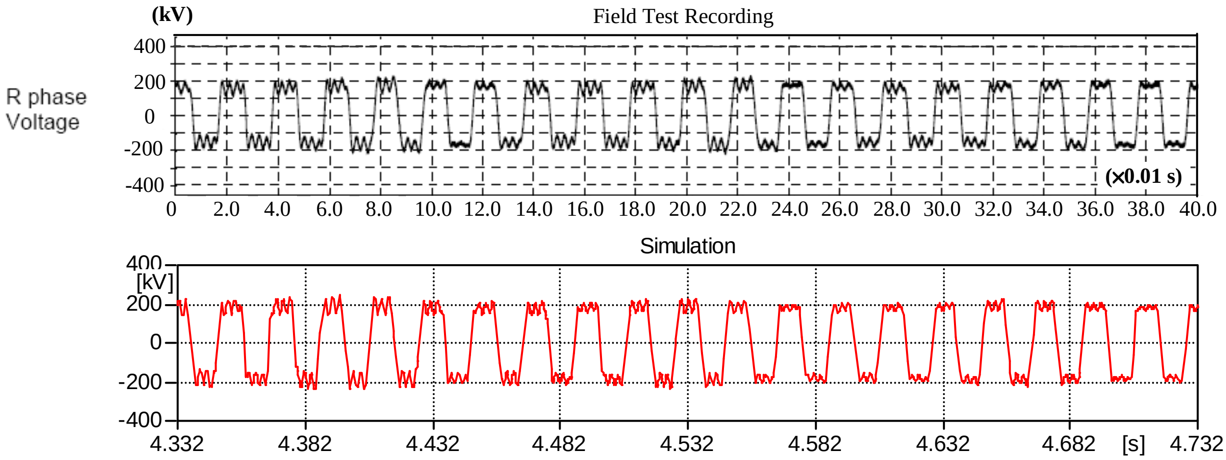

Figure 5.57: Period-1 voltage waveforms – Red phase

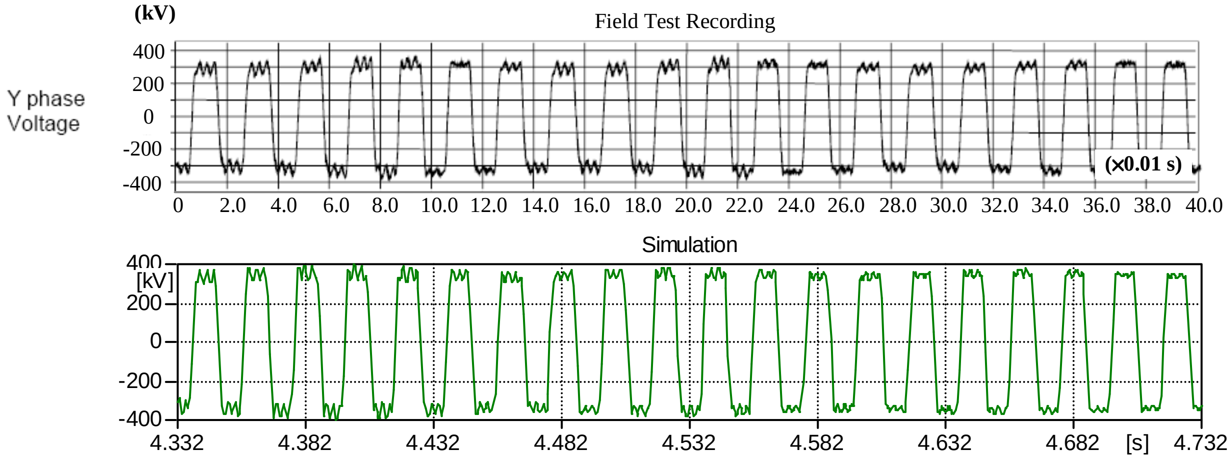

Figure 5.58: Period-1 voltage waveforms – Yellow phase

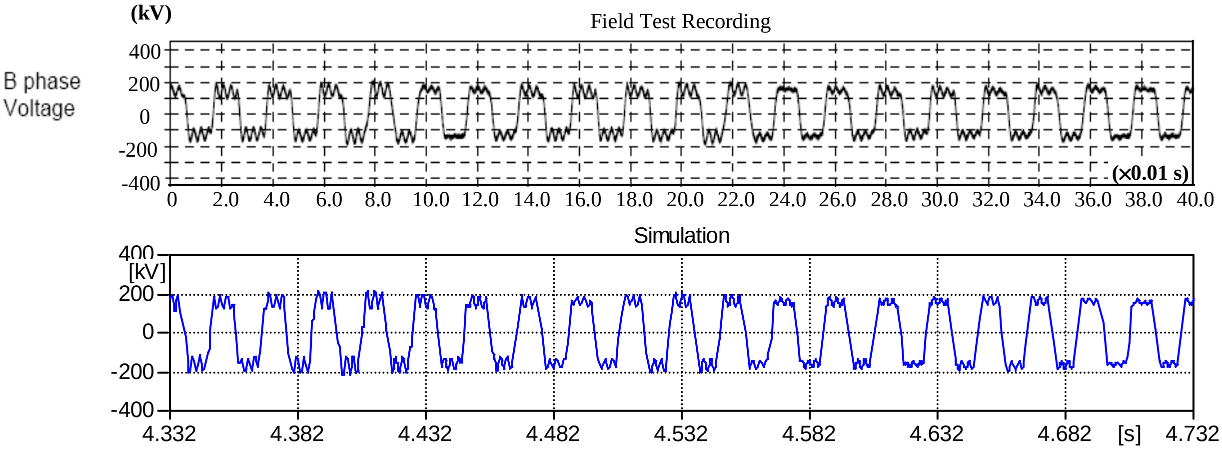

Figure 5.59: Period-1 voltage waveforms – Blue phase

Comparison between the field recorded and simulation results are as follows:

	R-phase voltage	**Y-phase voltage**	**B-phase voltage**
Field recorded	±200 kV	±300 kV	±180 kV
Simulations	±200 kV	±380 kV	±190 kV

3-phase Fundamental Mode Ferroresonance Currents (Period-1)

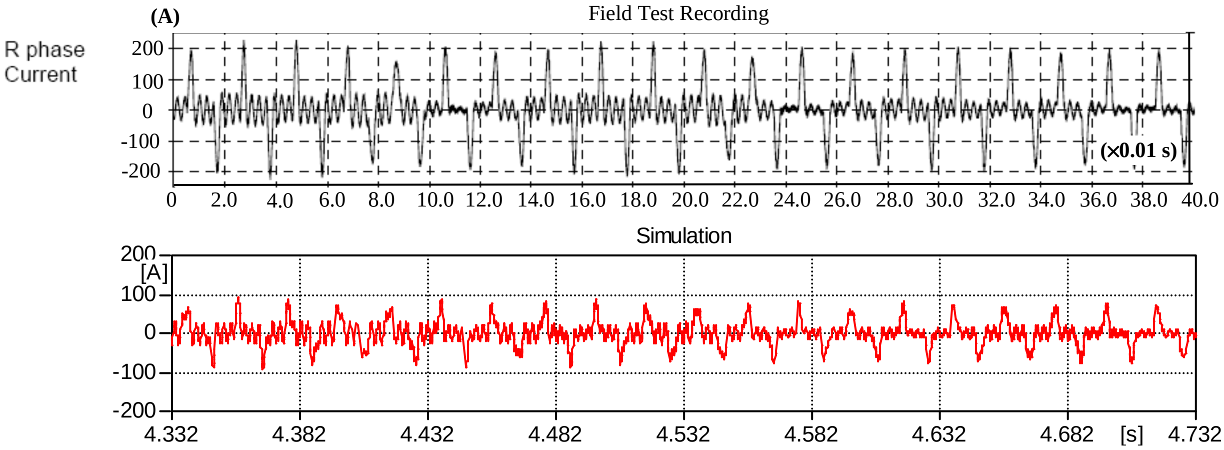

Figure 5.60: Period-1 current waveforms – Red phase

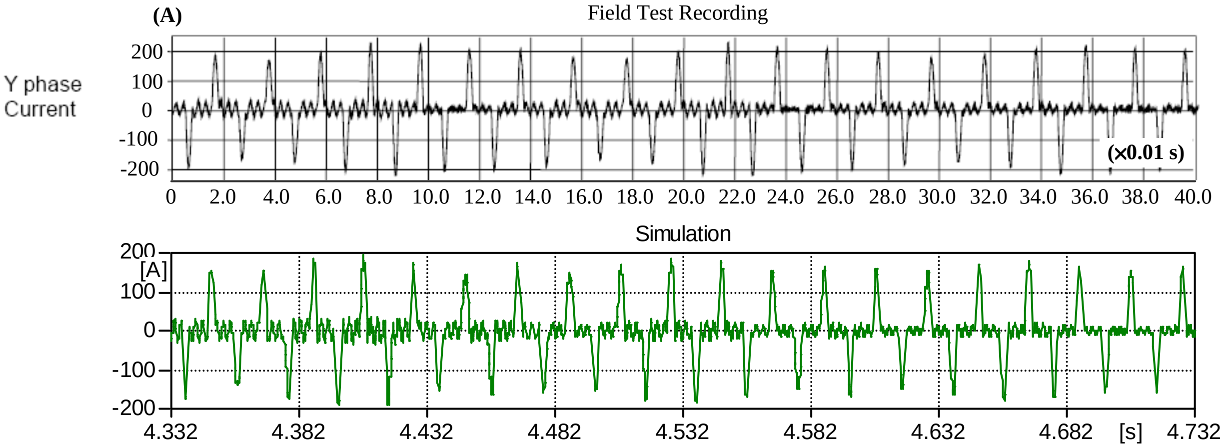

Figure 5.61: Period-1 current waveforms – Yellow phase

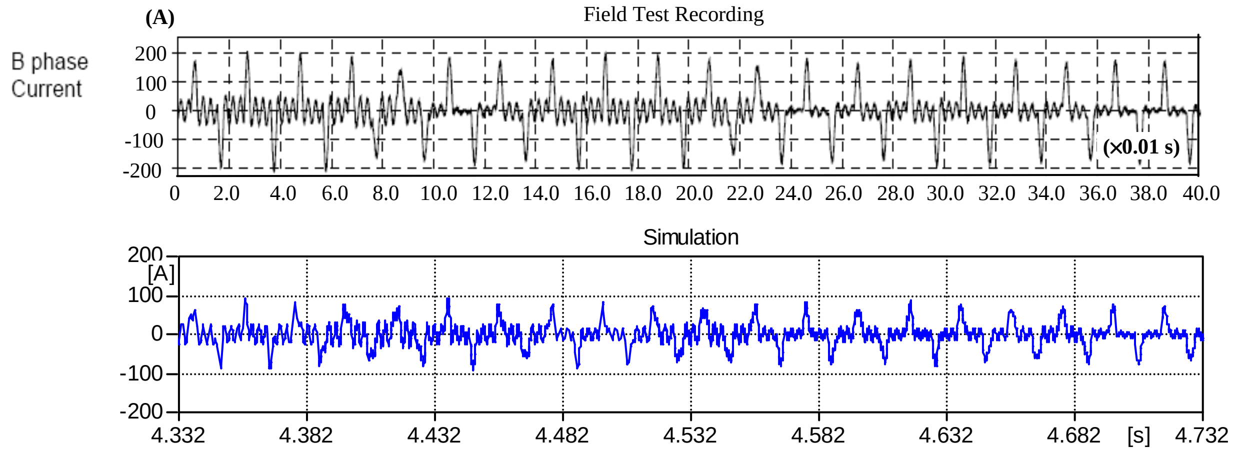

Figure 5.62: Period-1 current waveforms – Blue phase

Comparison between the field recorded and simulation results are as follows:

	R-phase current	**Y-phase current**	**B-phase current**
Field recorded	±200 A	±200 A	±200 A
Simulations	±90 A	±180 A	±90 A

3-phase Subharmonic Mode Ferroresonance Voltages (Period-3)

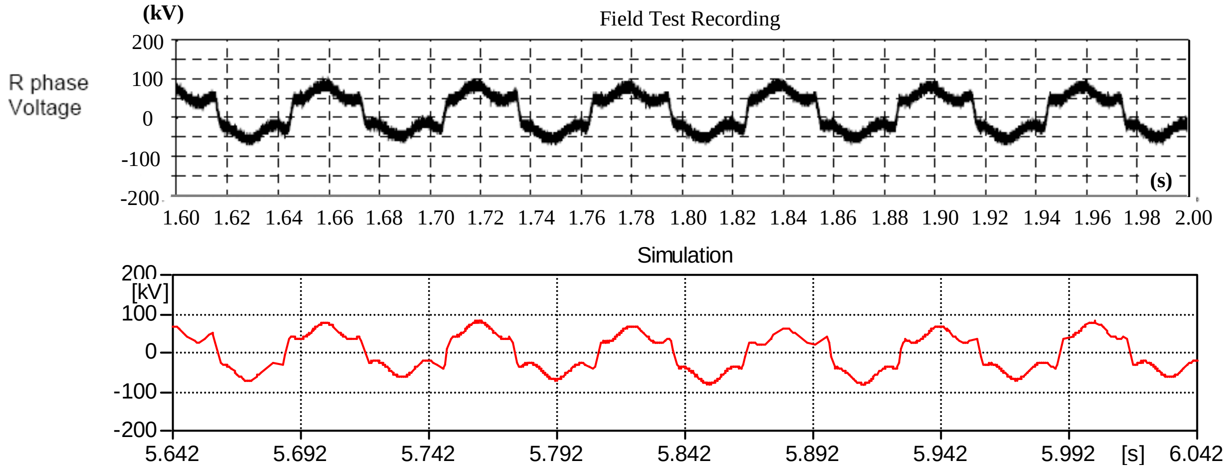

Figure 5.63: Period-3 voltage waveforms – Red phase

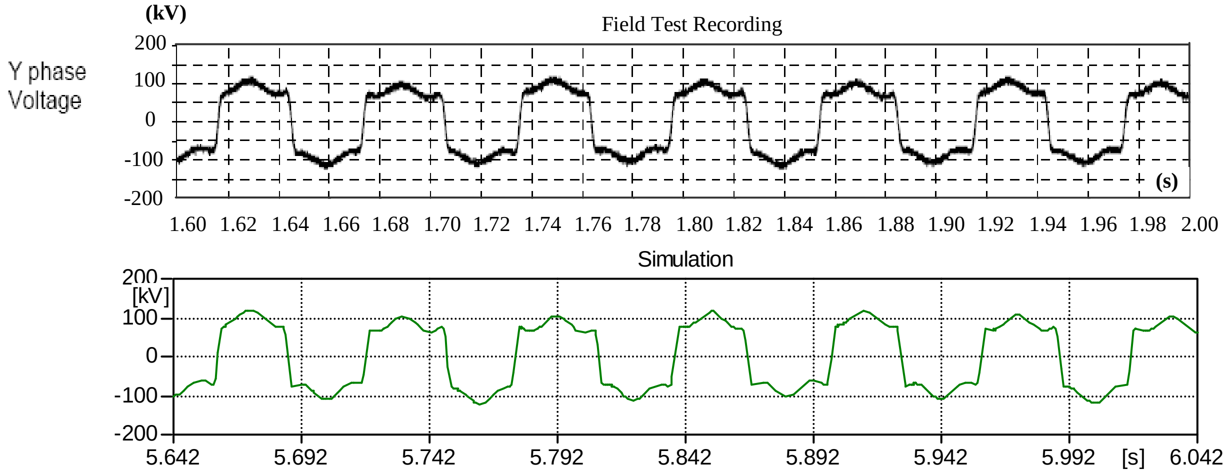

Figure 5.64: Period-3 voltage waveforms – Yellow phase

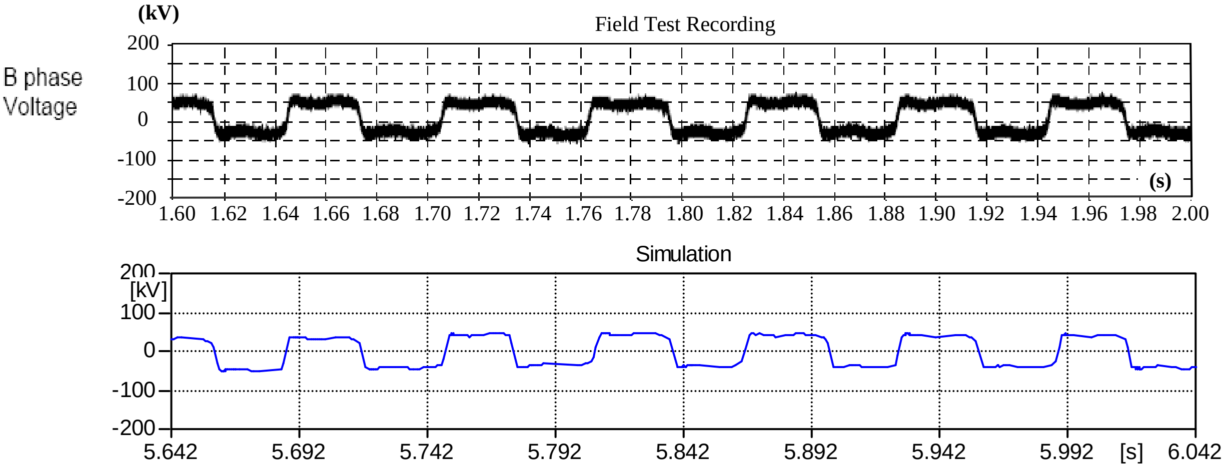

Figure 5.65: Period-3 voltage waveforms – Blue phase

Comparison between the field recorded and simulation results are as follows:

	R-phase voltage	Y-phase voltage	B-phase voltage
Field recorded	+100 kV, -50 kV	±100 kV	±50 kV
Simulations	+75 kV, - 75kV	±100 kV	±48 kV

3-phase Subharmonic Mode Ferroresonance Currents (Period-3)

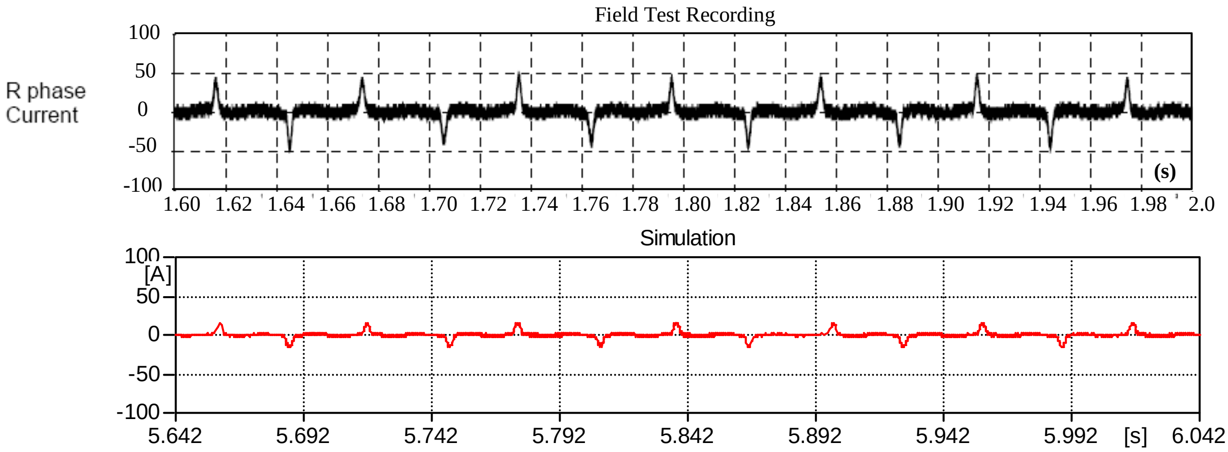

Figure 5.66: Period-3 current waveforms – Red phase

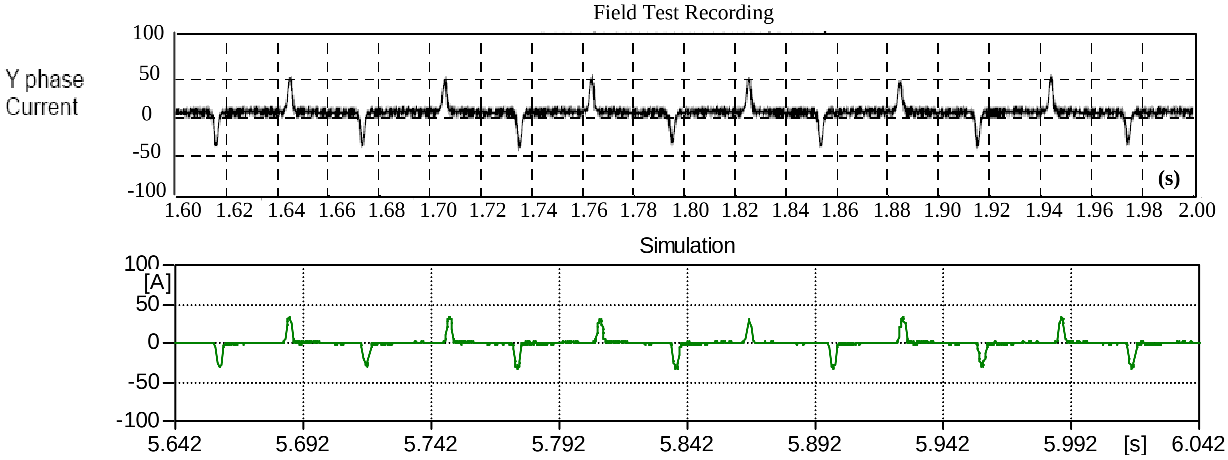

Figure 5.67: Period-3 current waveforms – Yellow phase

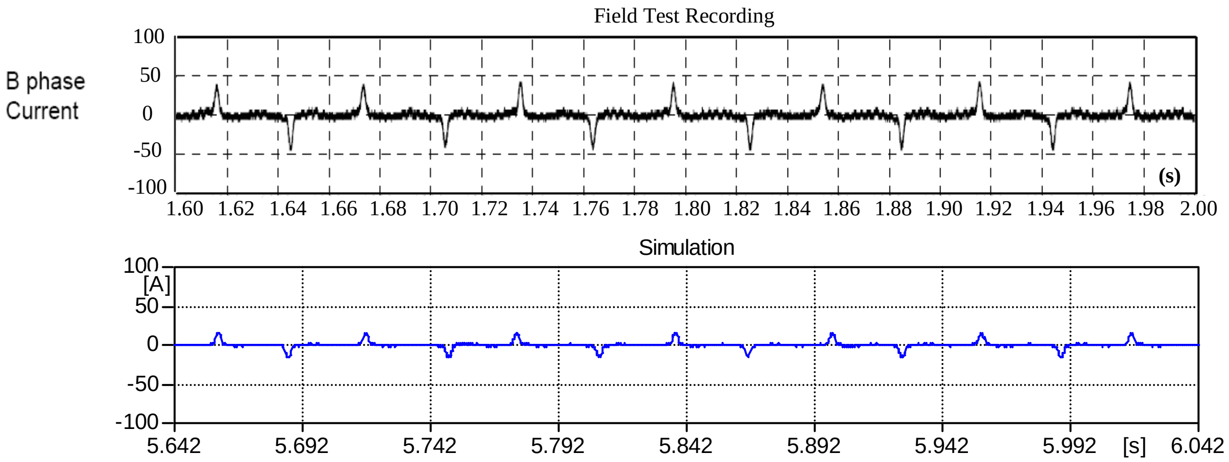

Figure 5.68: Period-3 current waveforms – Blue phase

Comparison between the field recorded and simulation results are as follows:

	R-phase current	Y-phase current	B-phase current
Field recorded	±50 A	+50 A, -45 A	±45 A
Simulations	±19 A	+40 A, -40A	±19 A

5.5.6 Case Study 6: Transformer - HYBRID, Line – MARTI

Finally, a frequency dependent Marti model is employed for the representation of the transmission line. Again, the transformer model is kept unchanged, using the HYBRID model. The waveforms reproduced from the simulations for both Period-1 and Period-3 ferroresonance are shown in Figure 5.69 to Figure 5.80.

3-phase Fundamental Mode Ferroresonance Voltages (Period-1)

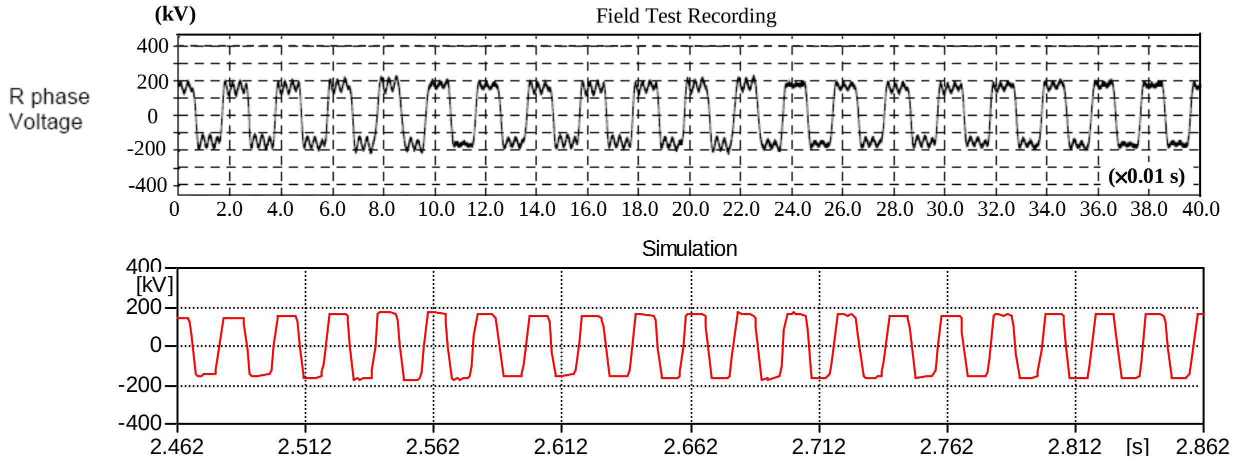

Figure 5.69: Period-1 voltage waveforms – Red phase

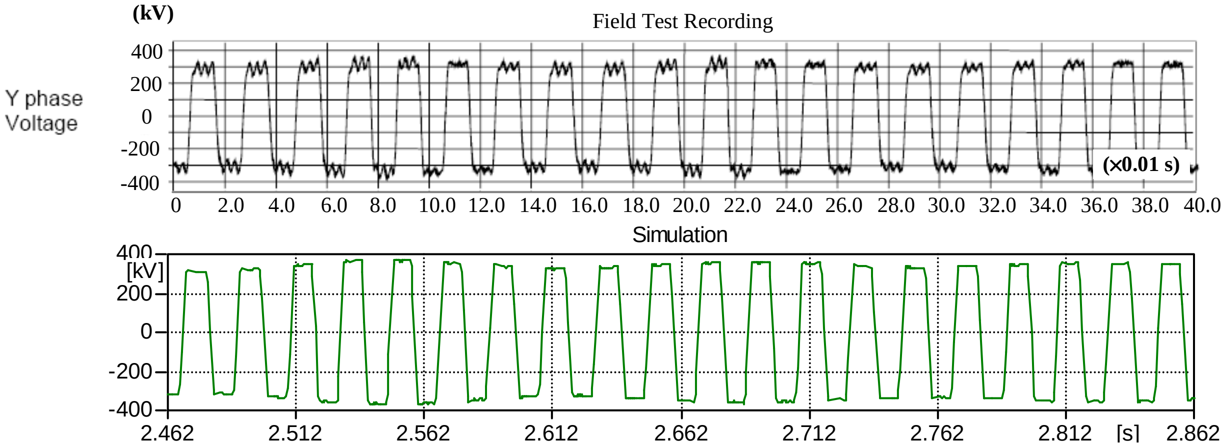

Figure 5.70: Period-1 voltage waveforms – Yellow phase

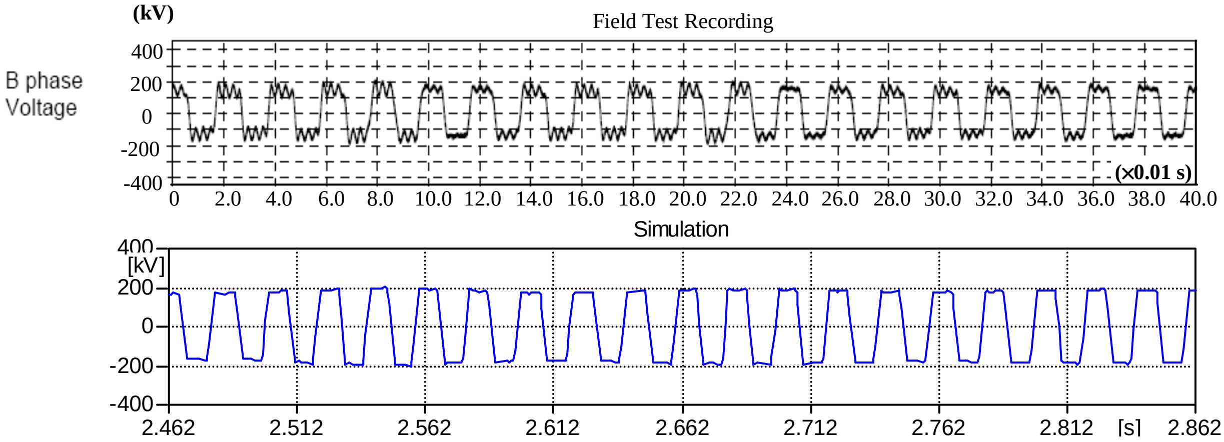

Figure 5.71: Period-1 voltage waveforms – Blue phase

Comparison between the field recorded and simulation results are as follows:

	R-phase voltage	Y-phase voltage	B-phase voltage
Field recorded	±200 kV	±300 kV	±180 kV
Simulations	±175 kV	±375 kV	±190 kV

3-phase Fundamental Mode Ferroresonance Currents (Period-1)

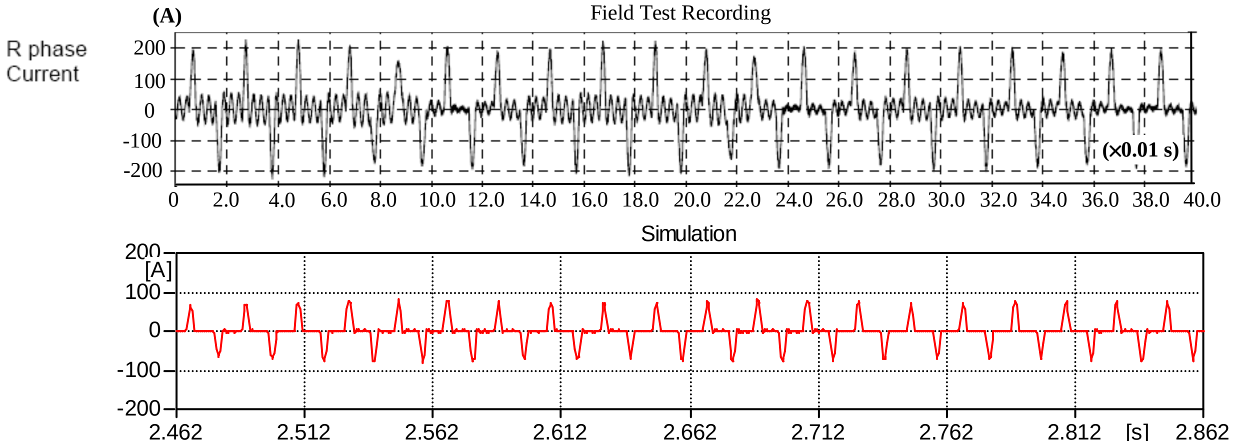

Figure 5.72: Period-1 current waveforms – Red phase

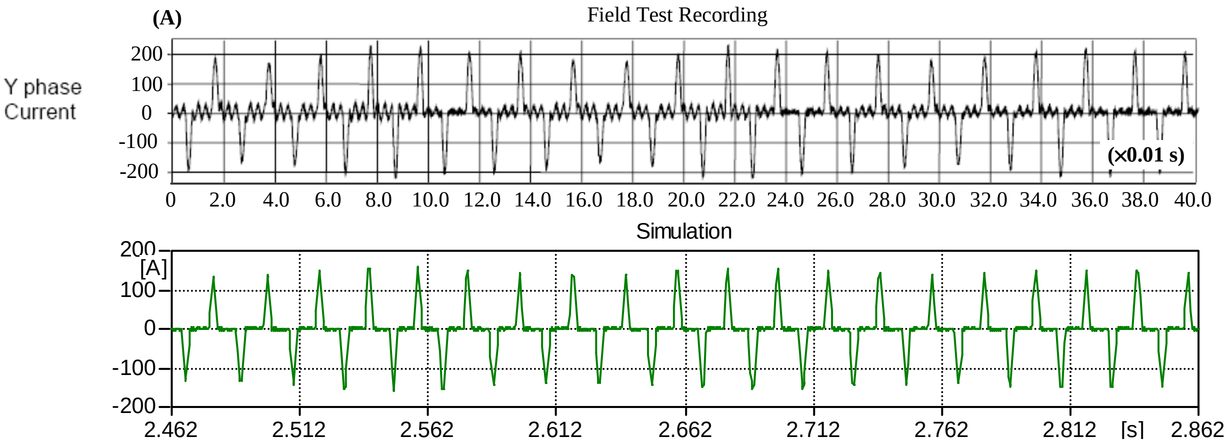

Figure 5.73: Period-1 current waveforms – Yellow phase

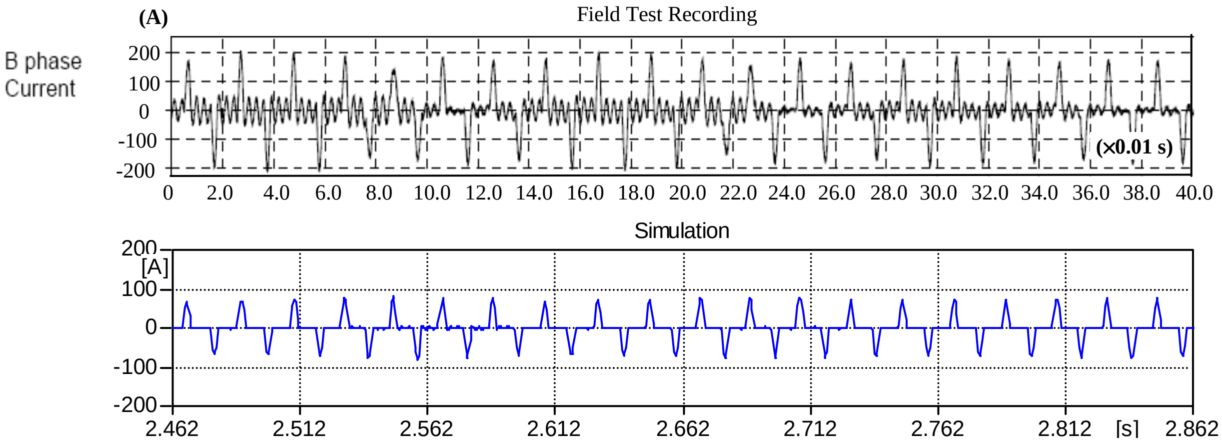

Figure 5.74: Period-1 current waveforms – Blue phase

Comparison between the field recorded and simulation results are as follows:

	R-phase current	Y-phase current	B-phase current
Field recorded	±200 A	±200 A	±200 A
Simulations	±90 A	±180 A	±90 A

3-phase Subharmonic Mode Ferroresonance Voltages (Period-3)

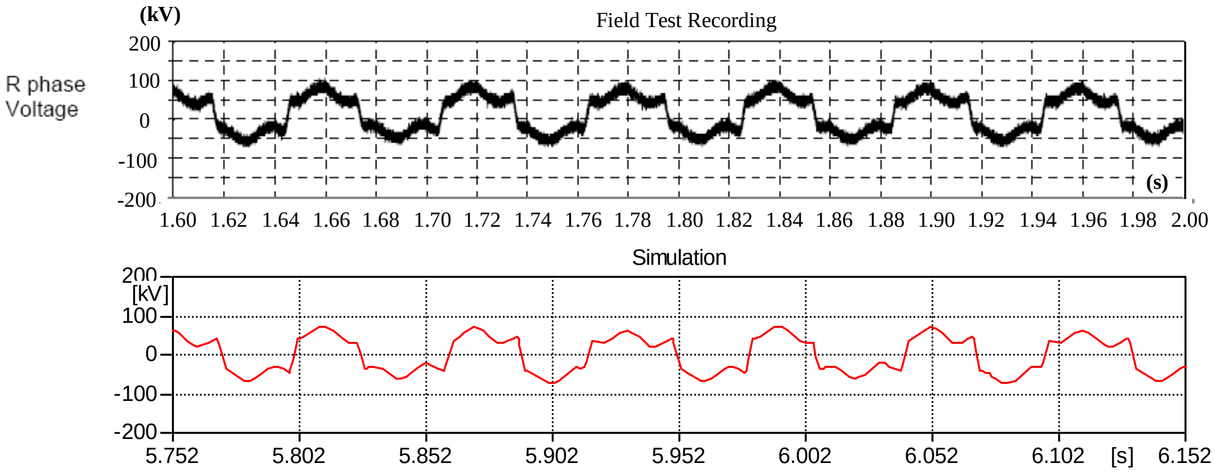

Figure 5.75: Period-3 voltage waveforms – Red phase

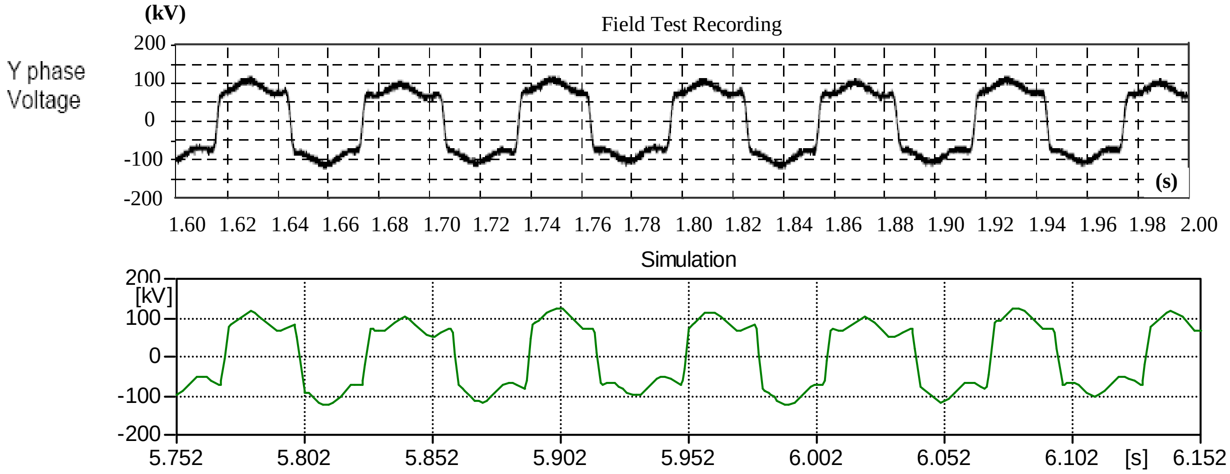

Figure 5.76: Period-3 voltage waveforms – Yellow phase

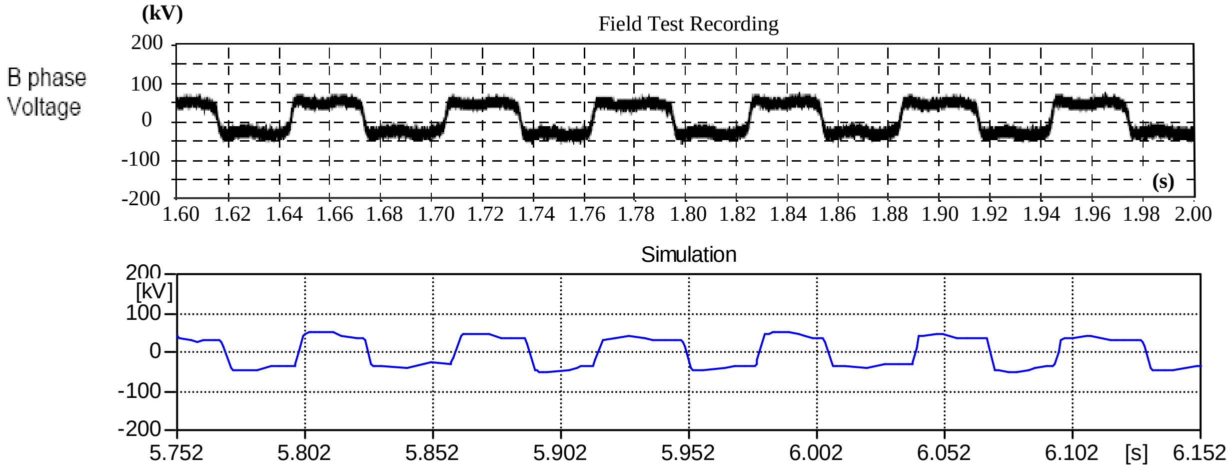

Figure 5.77: Period-3 voltage waveforms – Blue phase

Comparison between the field recorded and simulation results are as follows:

	R-phase voltage	Y-phase voltage	B-phase voltage
Field recorded	+100 kV, -50 kV	±100 kV	±50 kV
Simulations	+75 kV, - 75kV	±100 kV	±48 kV

3-phase Subharmonic Mode Ferroresonance Currents (Period-3)

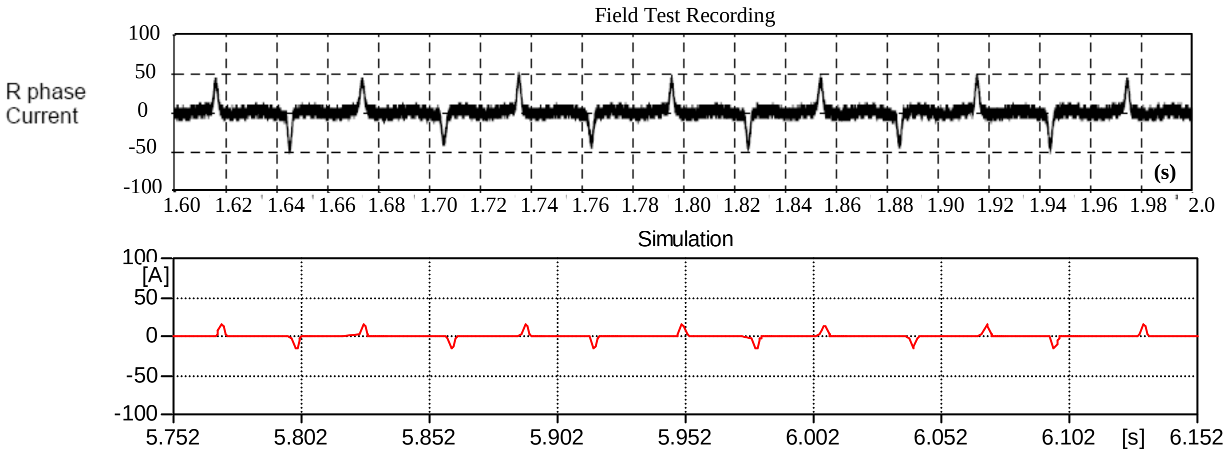

Figure 5.78: Period-3 current waveforms – Red phase

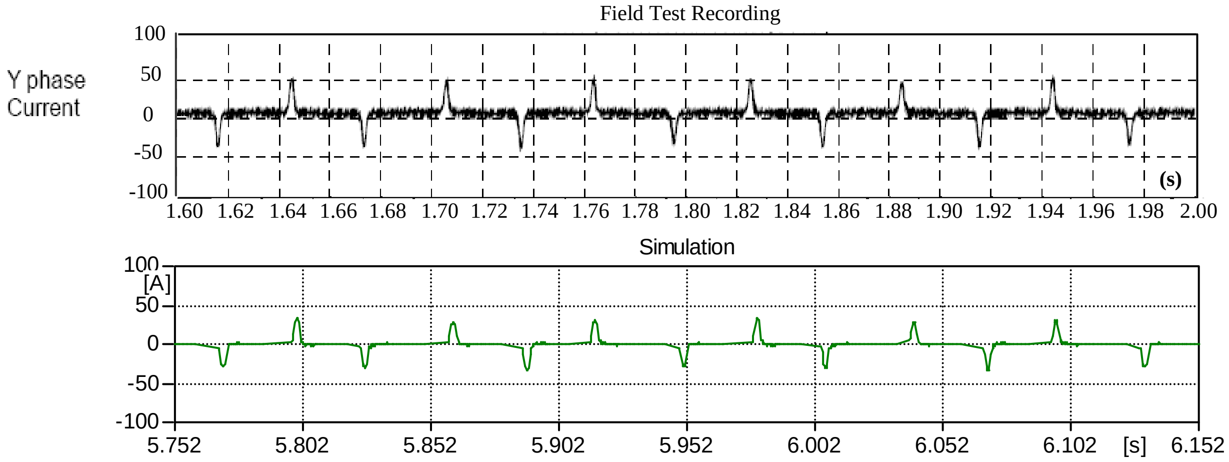

Figure 5.79: Period-3 current waveforms – Yellow phase

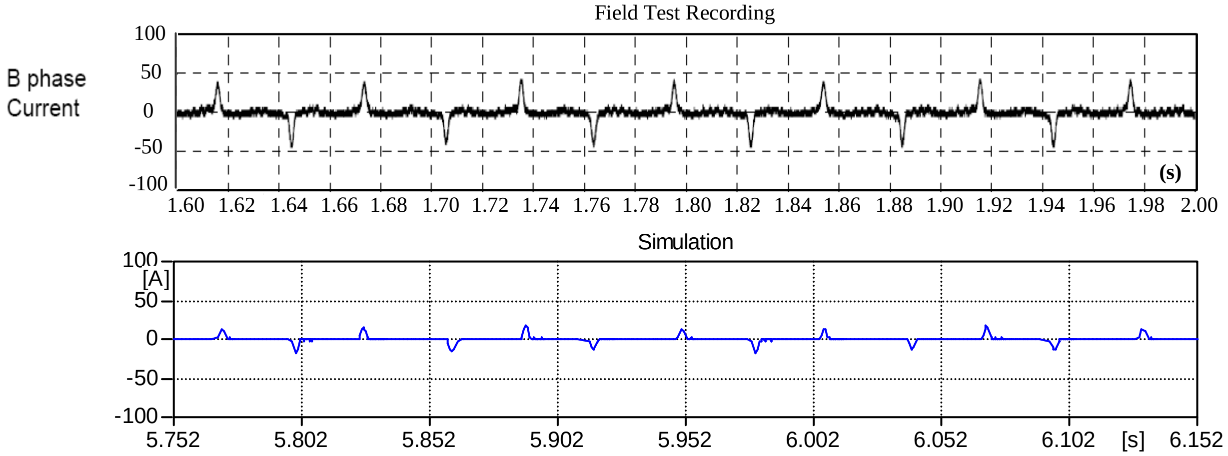

Figure 5.80: Period-3 current waveforms – Blue phase

Comparison between the field recorded and simulation results are as follows:

	R-phase current	Y-phase current	B-phase current
Field recorded	±50 A	+50 A, -45 A	±45 A
Simulations	±19 A	+38 A, -38A	±19 A

- **Summary of Case Study 4, 5 and 6**

In general, the simulation models developed based on all the case studies have been able to produce both the Period-1 and Period-3 ferroresonance.

Some deviations have been identified in the waveforms reproduced from the simulation models when they are compared side by side with the test recording case ones and the difference are described in the following;

(1) Period-1 ferroresonance

	Case Study 4	Case Study 5	Case Study 6
Voltage amplitude	The three-phase voltages and currents obtained from these three simulation models are not significantly different among them in terms of their amplitudes and waveshapes. However, by comparing with the real case ones, the current magnitudes are low for the red and blue phases. This is similar to the previous case studies employing the BCTRAN+ model.		
Voltage waveshape			
Current amplitude			
Current waveshape			

(2) Period-3 ferroresonance

	Case Study 4	Case Study 5	Case Study 6
Voltage amplitude	There are not a great deal of differences among the simulation results produced by the simulation models. Nevertheless, the only deviation when comparing to the test recordings are the low magnitudes of three-phase currents and the non-existence of high frequency voltage/current ripples. This is similar to the previous cases employing the BCTRAN+ model.		
Voltage wave shape			
Current amplitude			
Current wave shape			

Based on the simulation results, it has been observed that both the Period-1 and Period-3 responses produced from each of the six simulation models are relatively similar to one and another, both in the voltage/current magnitudes and waveshapes. Moreover, the simulation have been able to replicate the field test recording waveforms in good agreement.

After the evaluation of all the six simulation models, the following observations have been noticed;

The occurrence of Period-1 and Period-3 ferroresonance is not repeatable from one cycle to another successive cycle upon the opening of circuit breaker. This behaviour occurs due to the fact that the initial voltages upon the interruption of current are different from one cycle to another and this suggests that there have been different values of initial conditions being applied to the system. The system is triggered with different voltage points which can be sensitive for the initiation of different responses. This kind of behaviour has also been experienced by [13, 14] in which different steady state responses can be induced simply due to small changes in system parameters or initial conditions. In view of this behaviour, there have been a great deal of simulations being carried out in order for the system to be able to exhibit the type of required ferroresonant response. That is the reason that a large amount of simulations lasting for a few cycles are sometimes required for the determination of both the Period-1 and Period-3 responses. Furthermore, from the UK perspective as quoted in [72], the onset of this type of phenomena has been considered as random or stochastic which is dependent on system parameters. In addition, [11] mentioned that the nonlinear system of ferroresonance condition is extremely susceptible to changes in system parameters and initial conditions. The system can induce different responses upon a small change of system voltage, capacitance or losses. [17] described that ferroresonance phenomena relied on (1) the degree of transformer’s residual flux, (2) the initial charge of the capacitive elements and (3) the point on the voltage wave.

The major limitations that all the six simulation models have are explained as follows;

(1) Period-1 ferroresonance

	Case Study 1, 2, 3, 4, 5 and 6
Limitation	The magnitudes of the red and blue phase currents that have been reproduced from all the simulation models are only 50% of the measurement ones.

(2) Period-3 ferroresonance

	Case Study 1, 2, 3, 4, 5 and 6
Limitation	The magnitudes of the three-phase currents reproduced from the simulation models are relatively small as compared to the real case ones. Furthermore, both the voltages and currents that have been reproduced do not contain any high frequency ripples as expected from the real ones.

Due to the limitations of the simulation models therefore the next step is to improve one of the six models by looking into a possible way to modify the parameter of either the transformer or the transmission line models. The following questions arise before modification takes place.

(1) Which simulation model out of six is the best choice to be employed for improvement?

(2) Which component model needs to be modified for improvement? Is it the transformer or the transmission line model?

(3) Based on what criterion a parameter has been chosen for the purpose of model improvement?

5.6 Improvement of the Simulation Model

In the previous sections, six different types of simulation models have been assessed in order to determine the best model for the study of ferroresonance. The simulation results produced by each of them are comparable with one another, in terms of the voltage/current magnitudes and waveshapes. The deficiency that the simulation results have calls for improvement of the model so that such limitation can be removed.

5.6.1 Selection of the Simulation Model

There have been six possible predefined transformer and transmission line models that are qualified to be considered in modeling any circuits for the study of ferroresonance. Which model or case study is to be taken into consideration for the improvement? The selection of the best preference is explained as follows:

Case Study	**Transformer + Transmission line**	**Observation**
1	**BCTRAN+ + PI**	Modeling of a transformer using the BCTRAN+ model requires additional effort on curve fitting through the 90%, 100% and 110% of the core characteristic and then extrapolating into air-core inductance (deep saturation). In addition, a sensitivity study on the degree of saturation has to be carried out in order to select the best core representation for the study of ferroresonance. On the other hand, the transmission line based on PI representation is considered to be fairly accurate and simplistic which does not require any attention on defining the simulation time step to be less than the propagation time of the transmission line.
2	**BCTRAN+ + Bergeron**	
3	**BCTRAN+ + Marti**	

4	**HYBRID** **+** **PI**	Representing a transformer employing the HYBRID model does not require the same attention as the way the BCTRAN+ model. Instead the core behaviour including its deep saturation has been internally dealt with based on the Frolich equation. The transmission line modeled in PI can be worthy taken into account as the reasons being given previously.
5	**HYBRID** **+** **Bergeron**	
6	**HYBRID** **+** **J. Marti**	

In view of the above, Case Study 4 is considered to be the best option to be employed for improvements.

The predefined component model that requires a great deal of attention in the simulation model is for the transformer instead of the transmission line; the reason is that its magnetic circuit has a greater influence on transient studies, particularly ferroresonance. The core characteristic that has been developed in the HYBRID model is determined according to the 90%, 100% and 110% open-circuit test data and then processed by the build-in Frolich equation for the flux-linkage/current relationship. This representation of determining the core characteristic is not fully correct when ferroresonance condition is considered, since the magnetic circuit of transformer under this condition fringes out into the air-gap for example passing through the metallic butt ends of the cores [43]. These air-fluxes passing through the air-gap has an effect of increasing the reluctance thus reducing the inductance of the effective core circuit.

Since this type of core characteristic is not available and is impossible to obtain at the moment, therefore the way to deal with this shortfall is to modify the core characteristic. This is carried out by lowering down the 110% open-circuit test point and the outcome after the modification of the core characteristic is shown in Figure 5.81.

It can be seen in Figure 5.81 that there is a down shift in the core characteristic after the 110% point has been lowered down. This change suggests that there would be a small amount of increase in the magnetising current as expected; previously the current was at point ‘A’ and it is now at point ‘B’ after the modification takes place, the current at this point has been increased. In addition, there is also a slight change occurred for the outer-leg and yoke relationships.

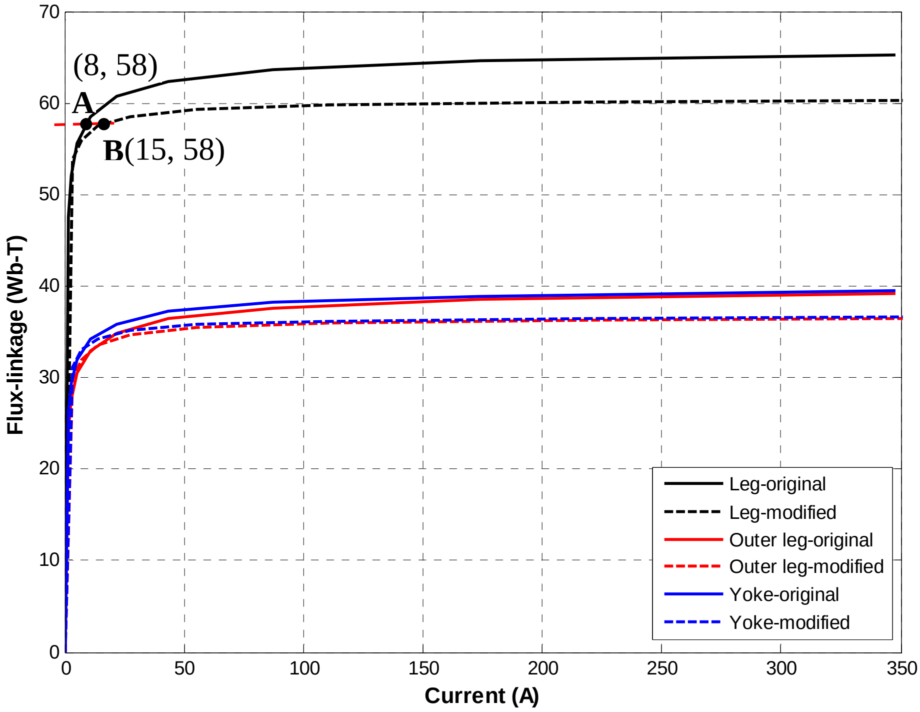

Figure 5.81: Modified core characteristic

The simulation results employing this type of modified core characteristic for both the Period-1 and Period-3 ferroresonance are presented in Figure 5.82 to Figure 5.93.

<u>3-phase Fundamental Mode Ferroresonance Voltages (Period-1)</u>

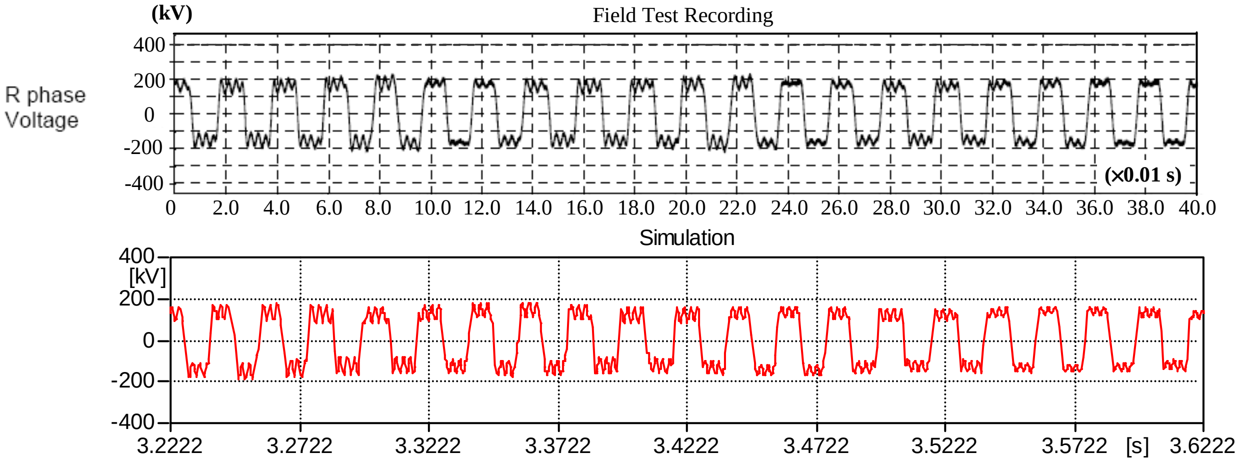

Figure 5.82: Period-1 voltage waveforms – Red phase

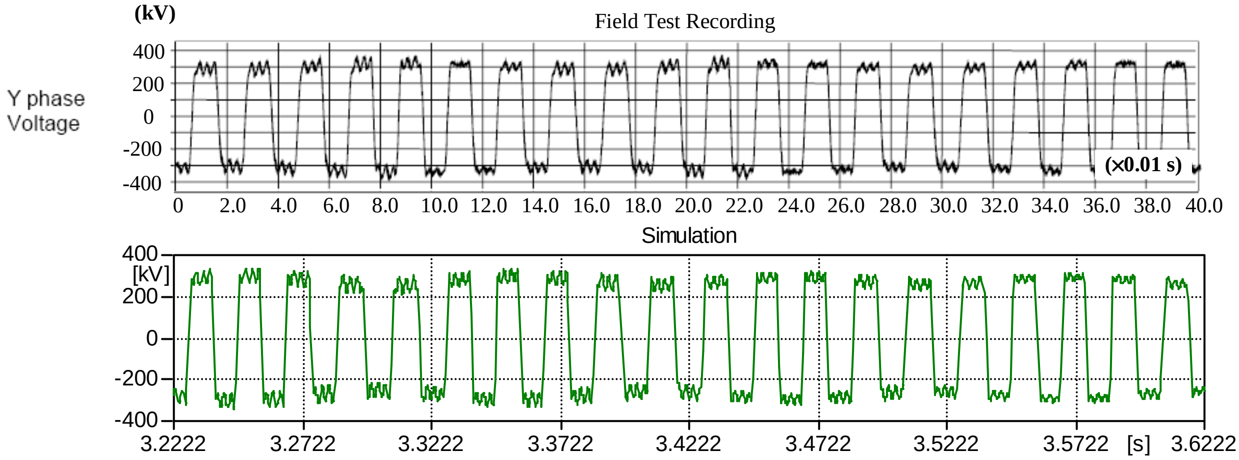

Figure 5.83: Period-1 voltage waveforms – Yellow phase

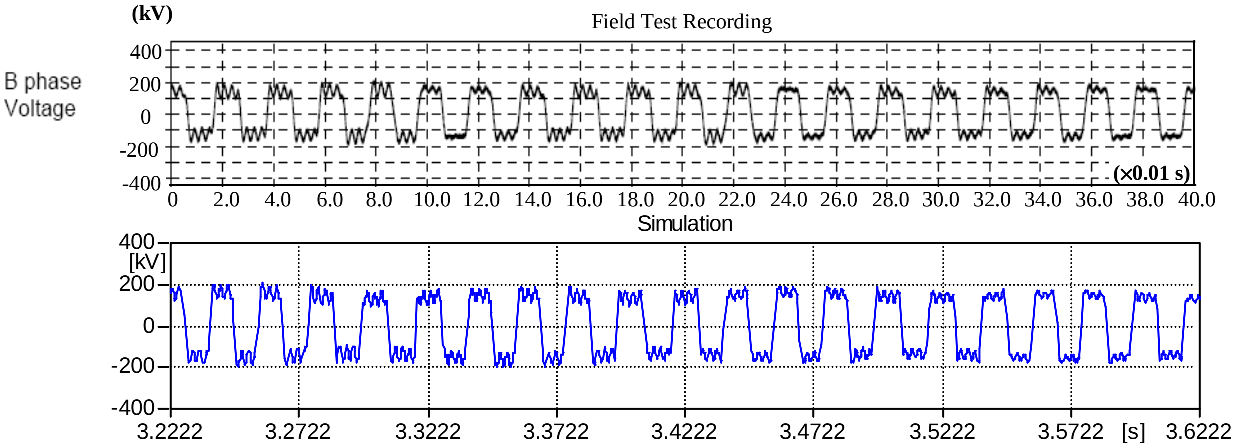

Figure 5.84: Period-1 voltage waveforms – Blue phase

Comparison between the field recorded and simulation results are as follows:

	R-phase voltage	**Y-phase voltage**	**B-phase voltage**
Field recorded	±200 kV	±300 kV	±180 kV
Simulations	±175 kV	±300 kV	±180 kV

Simulations results show that there is slight improvement on the magnitude of the Y-phase voltage.

3-phase Fundamental Mode Ferroresonance Currents (Period-1)

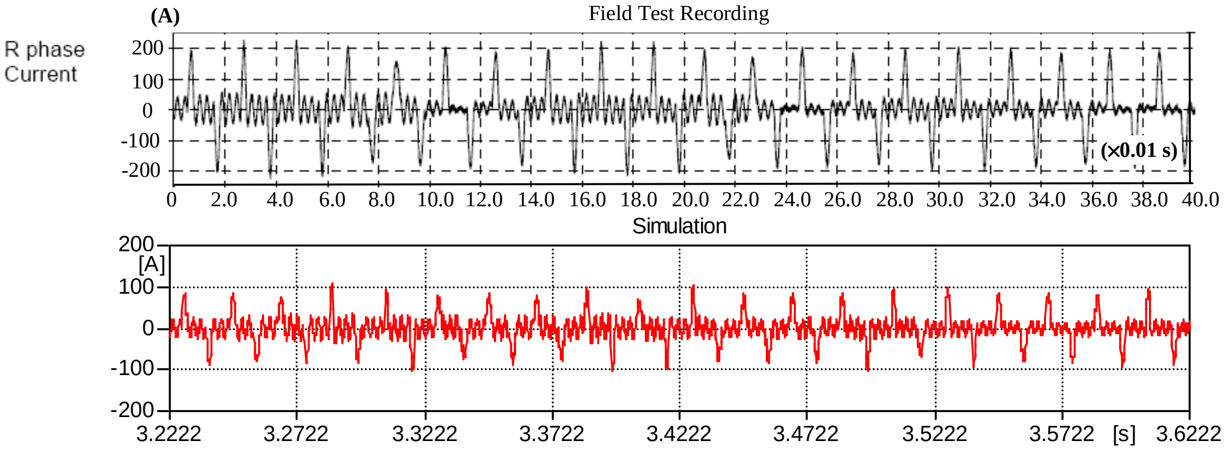

Figure 5.85: Period-1 current waveforms – Red phase

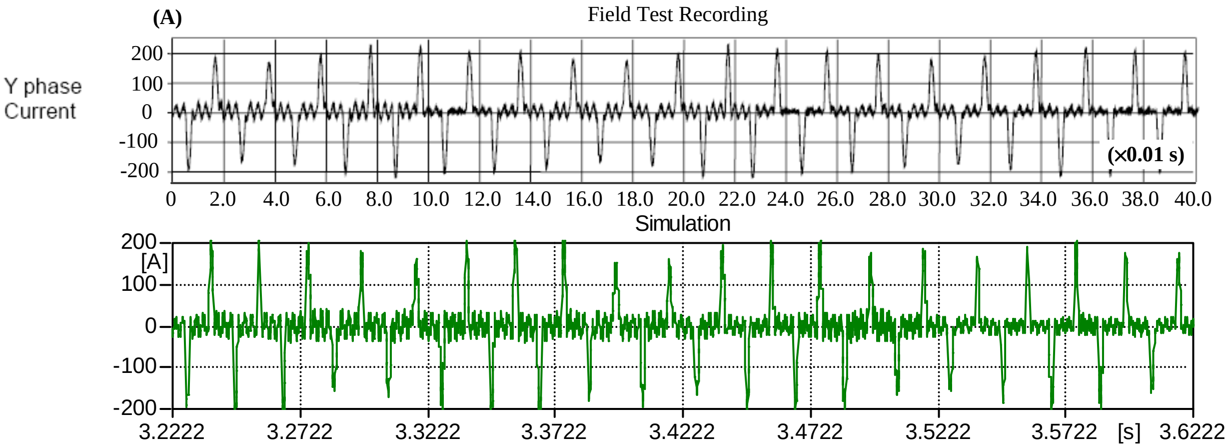

Figure 5.86: Period-1 current waveforms – Yellow phase

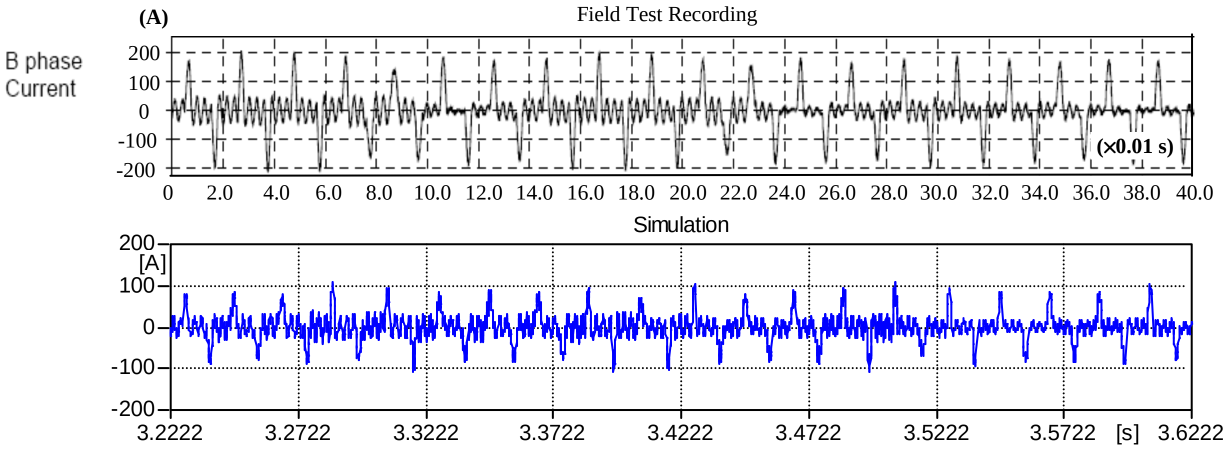

Figure 5.87: Period-1 current waveforms – Blue phase

Comparison between the field recorded and simulation results are as follows:

	R-phase current	**Y-phase current**	**B-phase current**
Field recorded	±200 A	±200 A	±200 A
Simulations	±100 A	±200 A	±100 A

For the Period-1 ferroresonance, no improvement has been occurred on the current magnitude with this core characteristic; the reason is due to the fact that the deep saturation region has not been affected by the modified core characteristic.

3-phase Subharmonic Mode Ferroresonance Voltages (Period-3)

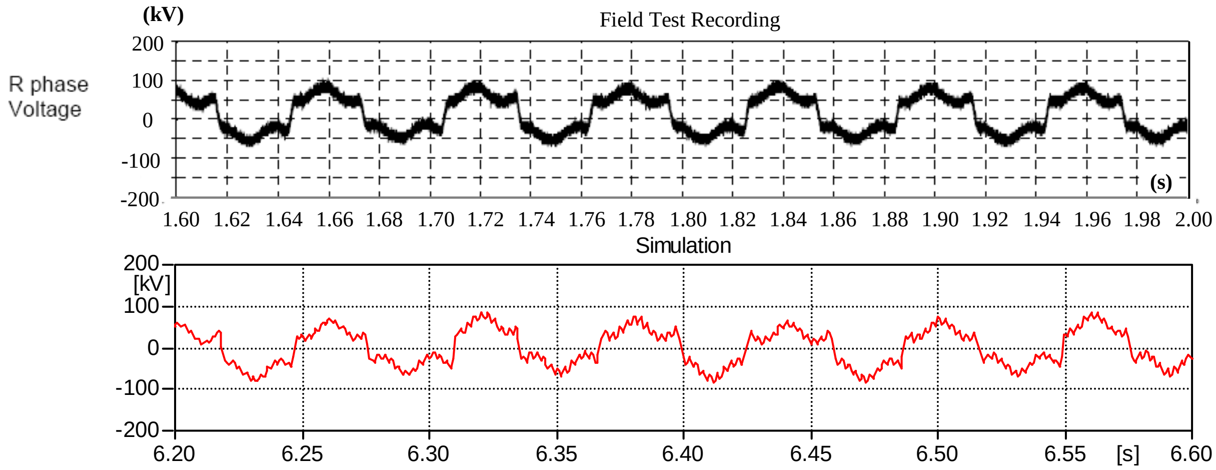

Figure 5.88: Period-3 voltage waveforms – Red phase

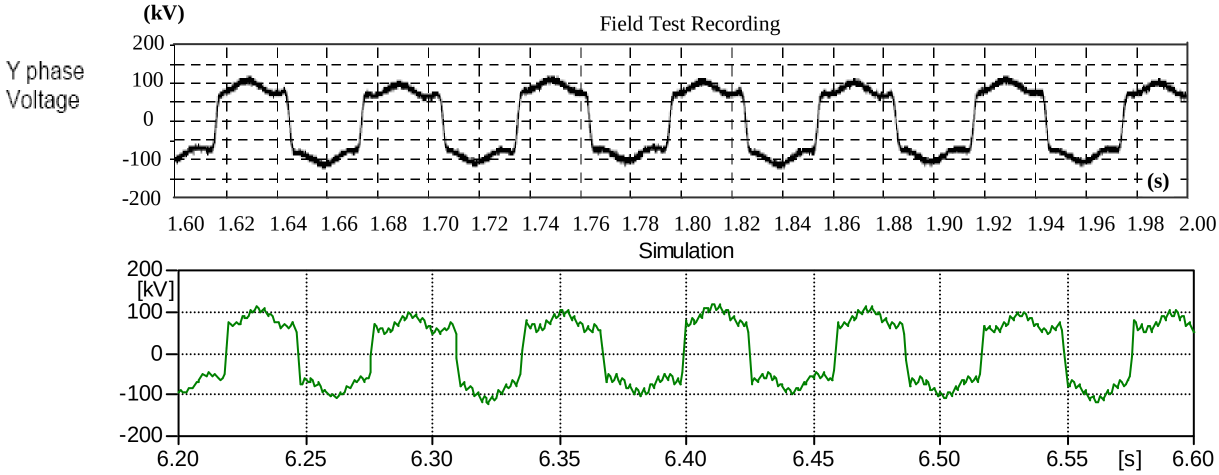

Figure 5.89: Period-3 voltage waveforms – Yellow phase

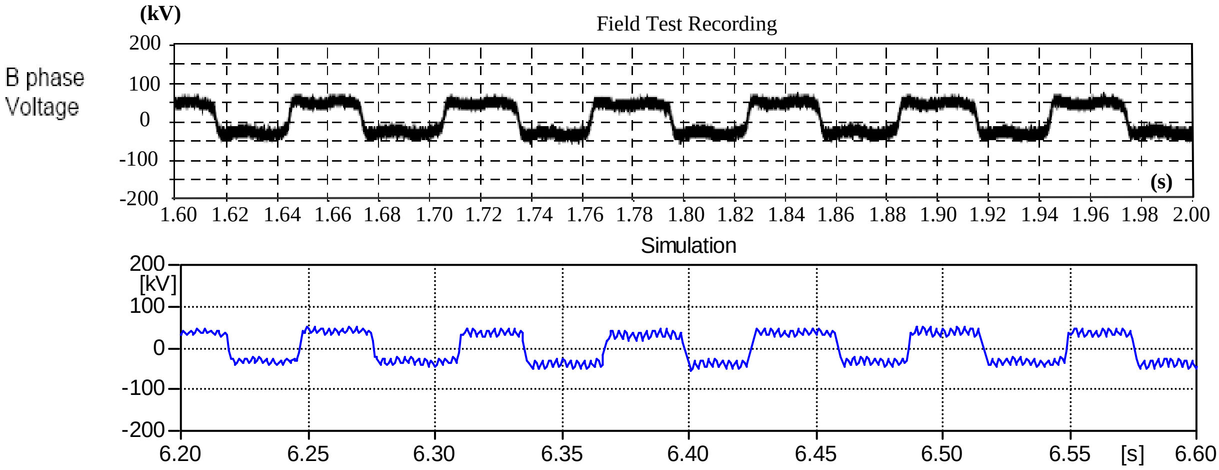

Figure 5.90: Period-3 voltage waveforms – Blue phase

Comparison between the field recorded and simulation results are as follows:

	R-phase voltage	**Y-phase voltage**	**B-phase voltage**
Field recorded	+100 kV, -50 kV	±100 kV	±50 kV
Simulations	+75 kV, - 75kV	±100 kV	±48 kV

Simulation results show that high frequency ripples have been introduced in all the 3-phase voltage waveforms.

3-phase Subharmonic Mode Ferroresonance Currents (Period-3)

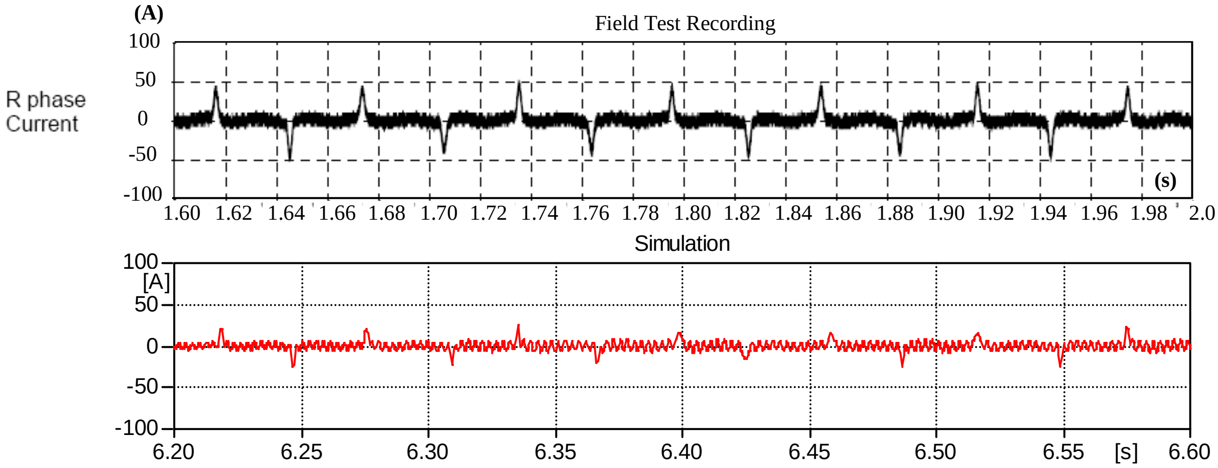

Figure 5.91: Period-3 current waveforms – Red phase

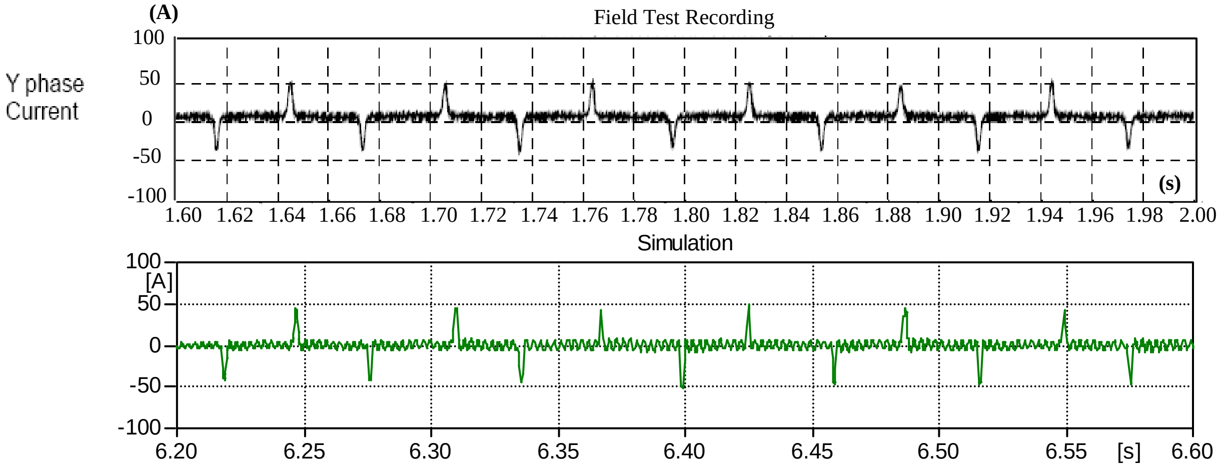

Figure 5.92: Period-3 current waveforms – Yellow phase

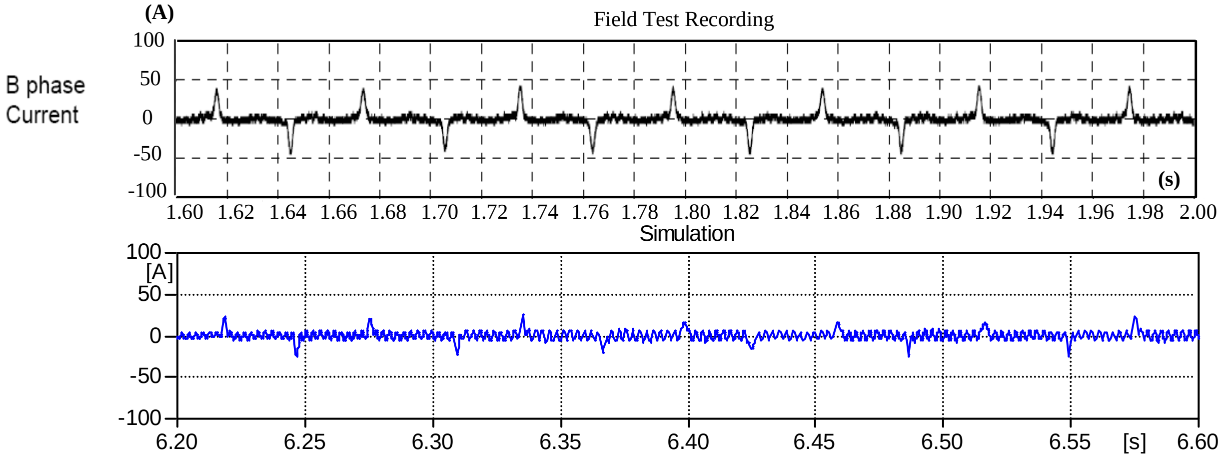

Figure 5.93: Period-3 current waveforms – Blue phase

Comparison between the field recorded and simulation results are as follows:

	R-phase current	**Y-phase current**	**B-phase current**
Field recorded	±50 A	+50 A, -45 A	±45 A
Simulations	±20 A	+50 A, -48A	±30 A

Major improvement in the simulation results are the high frequency ripples being introduced into the waveforms. In addition, the magnitude of the Y-phase current has improved significantly.

From the simulation results, it can be seen that the magnitude of the yellow phase current has been drastically improved only for the Period-3 ferroresonance, the reason is because this resonance does oscillate around the knee point region (see Chapter 3), the region where the magnetising current has been augmented. In term of the high frequency ripples, both the 3-phase voltages and currents have been able to replicate the recording ones. The reason is because the natural frequency in relation to the modified core inductance around the knee point has been excited.

5.7 Key Parameters Influence the Occurrence of Ferroresonance

In this section the parameters are evaluated with an aim to determine which of them has a great influence for the occurrence of ferroresonance. There are two types of ferroresonance that have been impinged upon the system; the Period-1 and Period-3 ferroresonance. Period-1 ferroresonance can induce damaging overvoltages and overcurrents which can pose a potential risk to the affected transformer and the nearby power system components. In view of this, attention has been drawn to look into the parameters that would influence the occurrence of this phenomenon. The parameters that are likely to contribute to this type of phenomenon are listed as follows;

(1) the coupling capacitances of the power transformer (SGT1)

(2) the 170 m length cable connected at the secondary side of the transformer (SGT1)

(3) the coupling capacitances of the 37 km length double-circuit transmission line

5.7.1 The Coupling Capacitances of the Power Transformer

The effect from the coupling capacitances of the transformer on the occurrence of ferroresonance can be checked by removing them from the model; they are the primary-to-ground capacitance, the secondary-to-ground capacitance, the tertiary-to-ground capacitance, the primary-to-secondary capacitance and finally the secondary-to-tertiary capacitance.

Transformer coupling capacitance	***C* (nF)**
Primary-to-ground capacitance (P-G)	4
Secondary-to-ground capacitance (S-G)	0.5
Tertiary-to-ground capacitance (T-G)	3
Primary-to-secondary capacitance (P-S)	5
Secondary-to-tertiary capacitance (S-T)	4

After a number of simulations, it can be seen in Figure 5.94 that Period-1 ferroresonance has been induced into the system and this clearly suggests that the occurrence of the phenomenon does not depend on the coupling capacitances of the transformer. This means that the presence of the capacitances is as seen to be negligible which does not influence the interaction of exchanging the energy between the capacitances and the saturable core inductance.

Similar characteristics of Period-1 ferroresonance have been reproduced under the assumption that the coupling capacitances of the transformer have been removed. The three-phase voltages show they are rectangular in shape with their ripple around the voltage peaks. Nevertheless, the currents are peaky in shape with a magnitude of about 200 A peak.

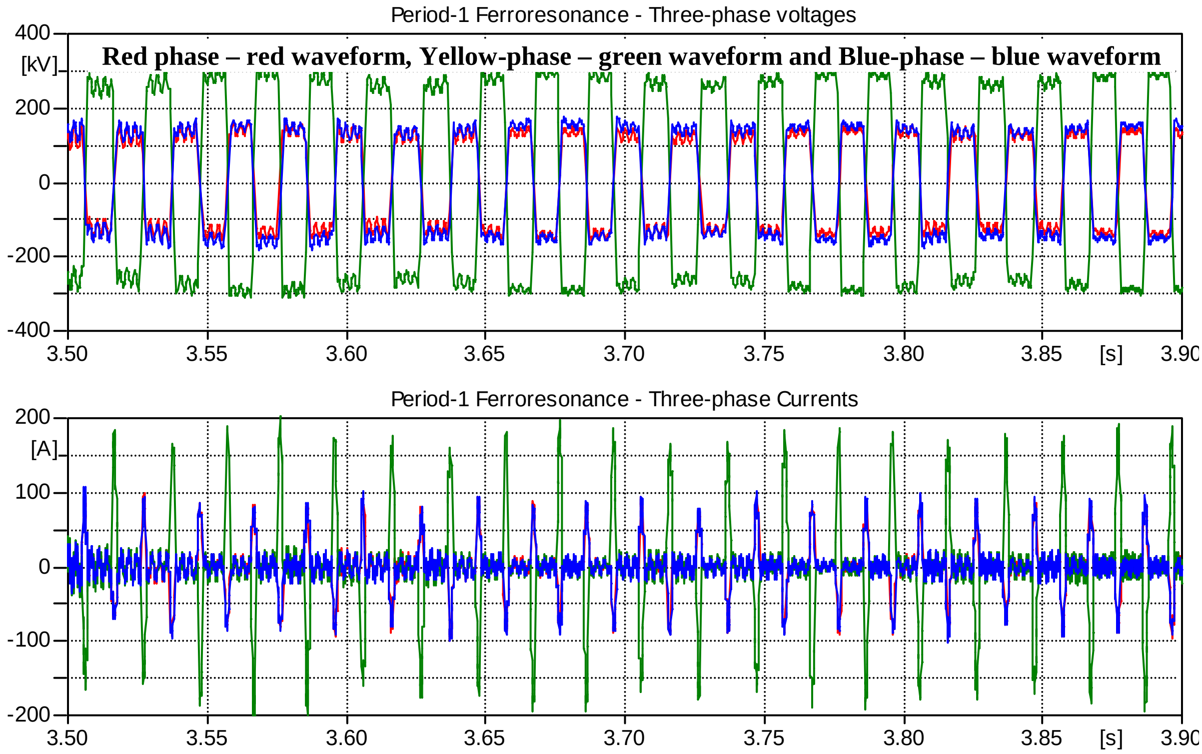

Figure 5.94: Period-1 - without transformer coupling capacitances

5.7.2 The 170 m length Cable at the Secondary of the Transformer

Previous study shows that the system can initiate the Period-1 ferroresonance without the coupling capacitances of the transformer connected into the system. It is therefore in this section to look into whether the existence of the short cable would affect this type of phenomenon. Three-phase capacitances are used to model the cable which is equal to 0.04352 μF/phase.

The results from the simulation without the presence of cable are shown in Figure 5.95, similar characteristics of Period-1 ferroresonance have been preserved without the presence of the cable capacitance. It is evident that Period-1 ferroresonance is still able to occur into the system even though both the transformer coupling capacitances and the cable are not participating the system. This observation suggests that these two parameters do not contribute significantly for the initiation of Period-1 ferroresonance. The main reason is that the value of this capacitance is not significant enough to interact with the deep saturation of the transformer core characteristic. In view of this, the only possible capacitances that would interact with the saturable inductance of the transformer in the configuration would be no doubt originated from the double-circuit transmission line.

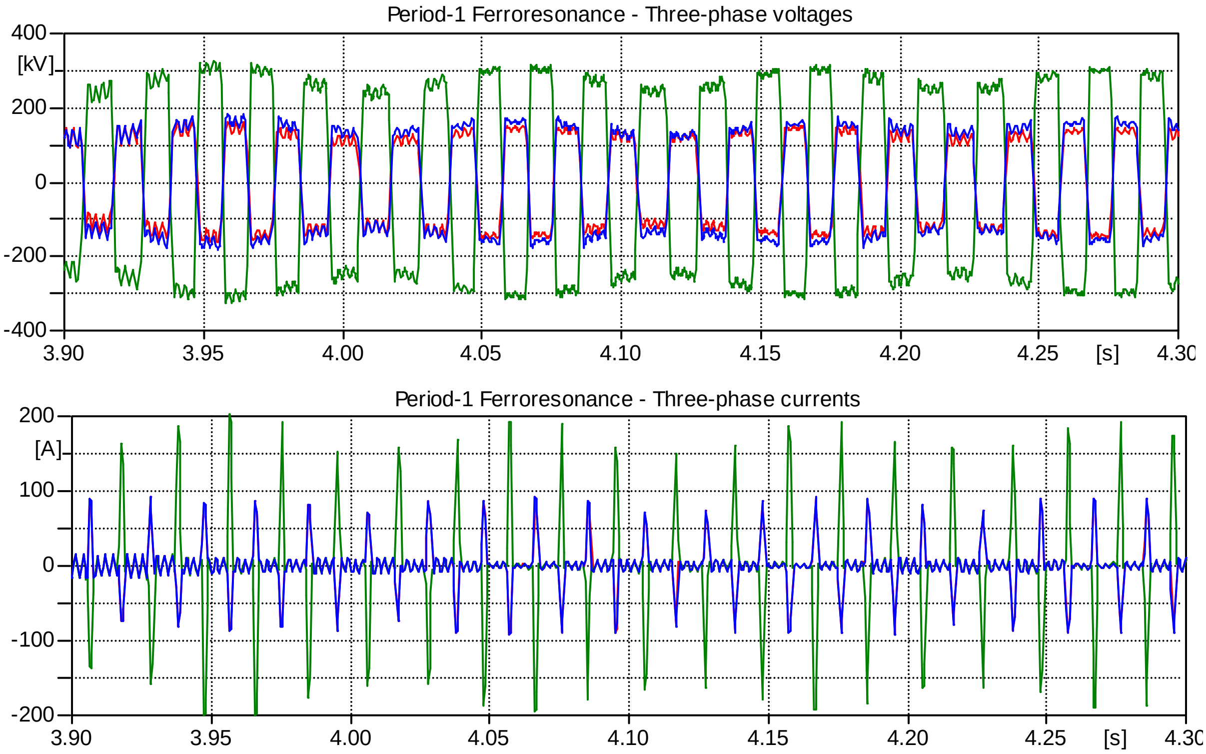
Period-1 Ferroresonance - Three-phase voltages

Period-1 Ferroresonance - Three-phase currents

Figure 5.95: Period-1 - without cable

5.7.3 The Transmission Line's Coupling Capacitances

The configuration of the transmission line that is connected into the system is shown in Figure 5.96. It consists of two circuits namely Circuit 1 and 2 with each of them having the phase conductors of R1, Y1, B1, R2, Y2 and B2. In addition, because the line is less than 50 km therefore the line is classified as a short line and it is un-transposed. Due to the close proximity of the phase conductors it is expected that the line consists of coupling capacitances which play an important role in inducing the Period-1 phenomenon. In order to identify the key capacitance the transmission line has to be modeled as a lumped representation so that each of the coupling capacitances can be separately assessed.

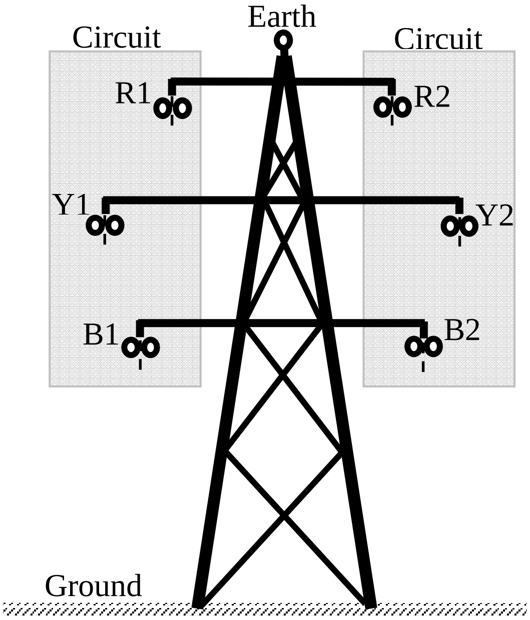

Figure 5.96: Double-circuit transmission line structure

Owing to the 12 phase conductors and an earth conductor, making up of 13 conductors that have been arranged over the single tower, the lumped elements of the series impedances and the coupling capacitances would consist of 13×13 matrices [44]. The complexity is simplified to 6×6 matrices by using the reduced method which can be seen in the following series impedance,

$$-\frac{d}{dx}\begin{bmatrix} V_{R1} \\ V_{Y1} \\ V_{B1} \\ V_{R2} \\ V_{Y2} \\ V_{B2} \end{bmatrix} = \begin{bmatrix} Z_{R1R1} & Z_{R1Y1} & Z_{R1B1} & Z_{R1R2} & Z_{R1Y2} & Z_{R1B2} \\ Z_{Y1R1} & Z_{Y1Y1} & Z_{Y1B1} & Z_{Y1R2} & Z_{Y1Y2} & Z_{Y1B2} \\ Z_{B1R1} & Z_{B1Y1} & Z_{B1B1} & Z_{B1R2} & Z_{B1Y2} & Z_{B1B2} \\ Z_{R2R1} & Z_{R2Y1} & Z_{R2B1} & Z_{R2R2} & Z_{R2Y2} & Z_{R2B2} \\ Z_{Y2R1} & Z_{Y2Y1} & Z_{Y2B1} & Z_{Y2R2} & Z_{Y2Y2} & Z_{Y2B2} \\ Z_{B2R1} & Z_{B2Y1} & Z_{B2B1} & Z_{B2R2} & Z_{B2Y2} & Z_{B2B2} \end{bmatrix} \begin{bmatrix} I_{R1} \\ I_{Y1} \\ I_{B1} \\ I_{R2} \\ I_{Y2} \\ V_{B2} \end{bmatrix} \qquad (5.2)$$

Similarly, the matrix reduction process is also applicable to the charge of the capacitances of the line as follows,

The 6×6 matrix of the potential coefficients,

$$\begin{bmatrix} q_{R1} \\ q_{Y1} \\ q_{B1} \\ q_{R2} \\ q_{Y2} \\ q_{B2} \end{bmatrix} = \begin{bmatrix} P_{R1R1} & P_{R1Y1} & P_{R1B1} & P_{R1R2} & P_{R1Y2} & P_{R1B2} \\ P_{Y1R1} & P_{Y1Y1} & P_{Y1B1} & P_{Y1R2} & P_{Y1Y2} & P_{Y1B2} \\ P_{B1R1} & P_{B1Y1} & P_{B1B1} & P_{B1R2} & P_{B1Y2} & P_{B1B2} \\ P_{R2R1} & P_{R2Y1} & P_{R2B1} & P_{R2R2} & P_{R2Y2} & P_{R2B2} \\ P_{Y2R1} & P_{Y2Y1} & P_{Y2B1} & P_{Y2R2} & P_{Y2Y2} & P_{Y2B2} \\ P_{B2R1} & P_{B2Y1} & P_{B2B1} & P_{B2R2} & P_{B2Y2} & P_{B2B2} \end{bmatrix}^{-1} \begin{bmatrix} v_{R1} \\ v_{Y1} \\ v_{B1} \\ v_{R2} \\ v_{Y2} \\ v_{B2} \end{bmatrix} \tag{5.3}$$

Finally,

$$\begin{bmatrix} q_{R1} \\ q_{Y1} \\ q_{B1} \\ q_{R2} \\ q_{Y2} \\ q_{B2} \end{bmatrix} = \begin{bmatrix} C_{R1R1} & C_{R1Y1} & C_{R1B1} & C_{R1R2} & C_{R1Y2} & C_{R1B2} \\ C_{Y1R1} & C_{Y1Y1} & C_{Y1B1} & C_{Y1R2} & C_{Y1Y2} & C_{Y1B2} \\ C_{B1R1} & C_{B1Y1} & C_{B1B1} & C_{B1R2} & C_{B1Y2} & C_{B1B2} \\ C_{R2R1} & C_{R2Y1} & C_{R2B1} & C_{R2R2} & C_{R2Y2} & C_{R2B2} \\ C_{Y2R1} & C_{Y2Y1} & C_{Y2B1} & C_{Y2R2} & C_{Y2Y2} & C_{Y2B2} \\ C_{B2R1} & C_{B2Y1} & C_{B2B1} & C_{B2R2} & C_{B2Y2} & C_{B2B2} \end{bmatrix} \begin{bmatrix} v_{R1} \\ v_{Y1} \\ v_{B1} \\ v_{R2} \\ v_{Y2} \\ v_{B2} \end{bmatrix} \tag{5.4}$$

With the capacitance matrix is given as $[C]=[P]^{-1}$

As the capacitances of the line plays an important role for the occurrence of Period-1 ferroresonance, it is therefore suggested that the lumped elements of Figure 5.97 are taken into consideration.

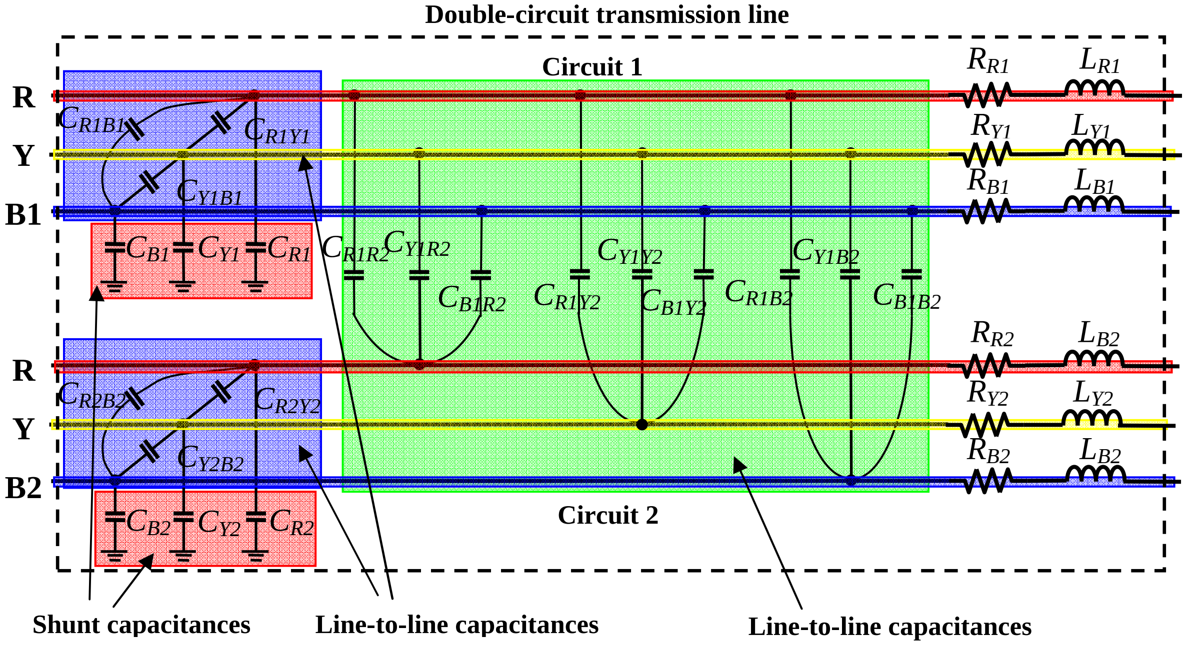

Figure 5.97: Transmission line's lumped elements

The values of the equivalent impedances and the capacitances matrices which have been derived can be referred to Appendix A.

The capacitance matrix is in nodal form which implies that the diagonal elements of C_{ii} is the sum of the capacitances per unit length between conductor i and all other conductors, and the off-diagonal elements of $C_{ik} = C_{ki}$ is negative capacitance per unit length between conductor i and k. The following example illustrating how the ground capacitance C_{R1} is determined,

Capacitance matrix C matrix (Farads for 37 km):

3.7508E-07	-7.3581E-08	-2.3675E-08	-5.5176E-08	-2.6709E-08	-1.4231E-08
-7.3581E-08	3.8735E-07	-7.0921E-08	-2.6709E-08	-2.3100E-08	-1.9884E-08
-2.3675E-08	-7.0921E-08	3.9898E-07	-1.4231E-08	-1.9884E-08	-3.1545E-08
-5.5176E-08	-2.6709E-08	-1.4231E-08	3.7508E-07	-7.3581E-08	-2.3675E-08
-2.6709E-08	-2.3100E-08	-1.9884E-08	-7.3581E-08	3.8735E-07	-7.0921E-08
-1.4231E-08	-1.9884E-08	-3.1545E-08	-2.3675E-08	-7.0921E-08	3.9898E-07

From the definition the value of the shunt capacitance with respect to ground C_{R1} for Circuit 1 is obtained as,

$$C_{R1} = C_{R1R1} - \left(C_{R1Y1} + C_{R1B1} + C_{R1R2} + C_{R1Y2} + C_{R1B2}\right)$$

$$C_{Y1} = C_{Y1Y1} - \left(C_{Y1R1} + C_{Y1B1} + C_{Y1R2} + C_{Y1Y2} + C_{Y1B2}\right)$$

$$C_{B1} = C_{B1B1} - \left(C_{B1R1} + C_{B1Y1} + C_{B1R2} + C_{B1Y2} + C_{B1B2}\right)$$

For Circuit 2,

$$C_{R2} = C_{R2R2} - \left(C_{R2R1} + C_{R2Y1} + C_{R2B1} + C_{R2Y2} + C_{R2B2}\right)$$

$$C_{Y2} = C_{Y2Y2} - \left(C_{Y2R1} + C_{Y2Y1} + C_{Y2B1} + C_{Y2R2} + C_{Y2B2}\right)$$

$$C_{B2} = C_{B2B2} - \left(C_{B2R1} + C_{B2Y1} + C_{B2B1} + C_{B2R2} + C_{B2Y2}\right)$$

On the other hand, the off-diagonal elements are used to represent the line-to-line capacitances and the circuit-to-circuit capacitances.

For the series impedances of each of the circuit, the resistance and the inductance of the line are determined based on the diagonal elements. In addition mutual inductances of the lines are also taken into consideration. The impedance matrix can be referred in Appendix A.

Finally, the double-circuit transmission line is then modeled by PI representation as shown in Figure 5.98. All the capacitance values at the left and right hand sides of the series impedances are divided by 2.

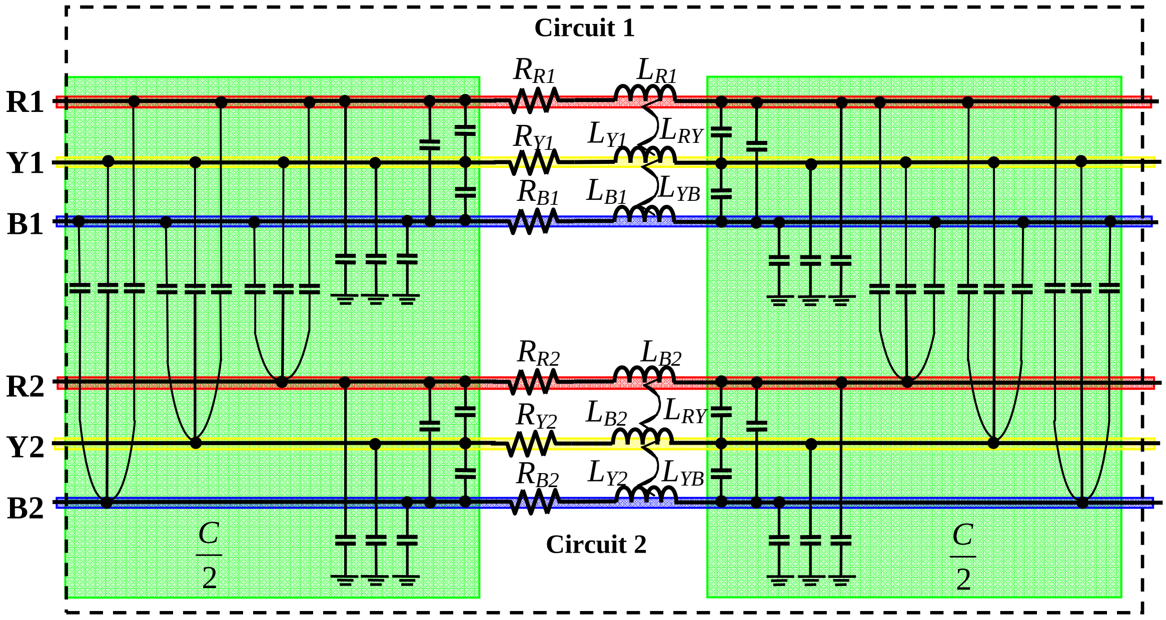

Figure 5.98: Double-circuit transmission line's lumped elements

In order to validate the accuracy of the lumped representation, a frequency scan to measure the input impedance is carried out and compared with the one produced by the predefined build-in model. The comparison between the two is shown in Figure 5.99.

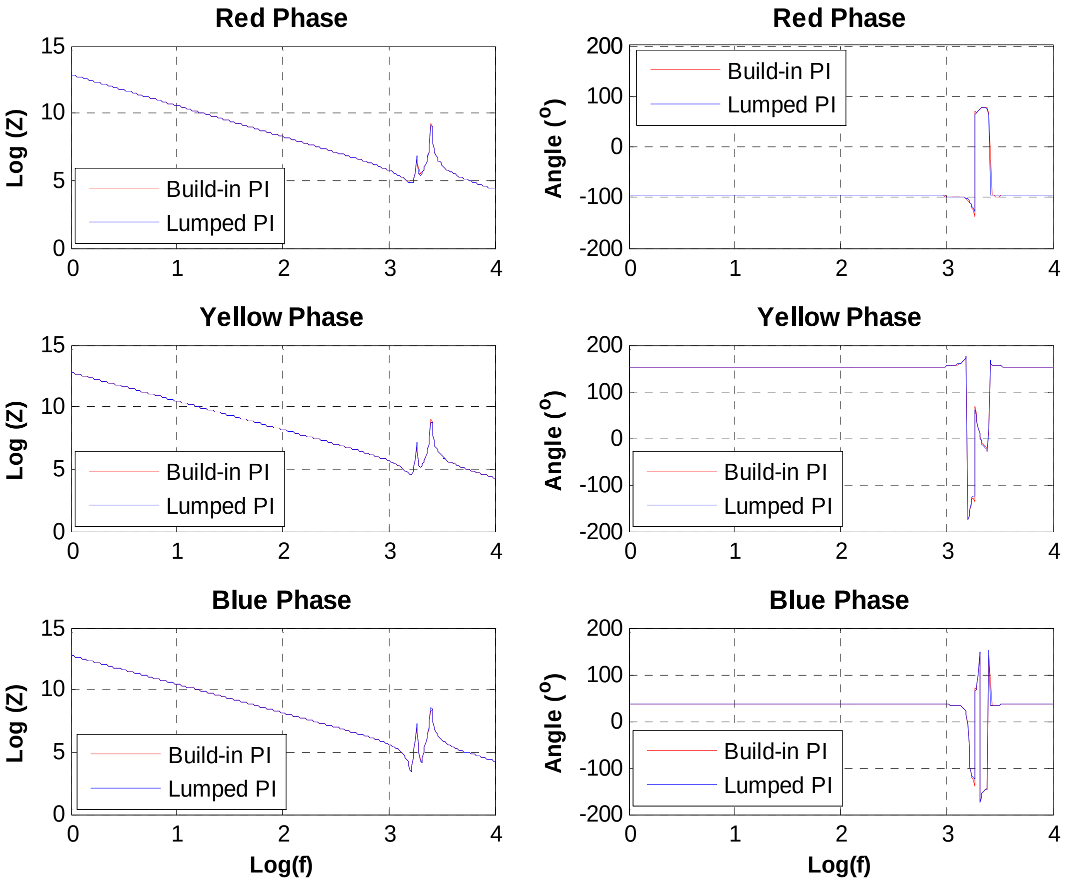

Figure 5.99: Impedance measurement at the sending-end terminals

The results show that the impedances produced by the lumped model are similar to the ones produced by the build-in model and this suggests that the lumped model has been accurately developed based on the individual passive components such as resistors, inductors and capacitors. With the line being modeled by the individual resistance, inductance and capacitance elements, it is then the next task to investigate the key parameter which contributes to the occurrence of ferroresonance.

From the simulations, it has been clearly shown that the model is equally capable to replicate the 3-phase voltage and current ferroresonant waveforms as the ones produced by the predefined models, either the PI, Bergeron or J. Marti. The waveforms are shown in Figure 5.100.

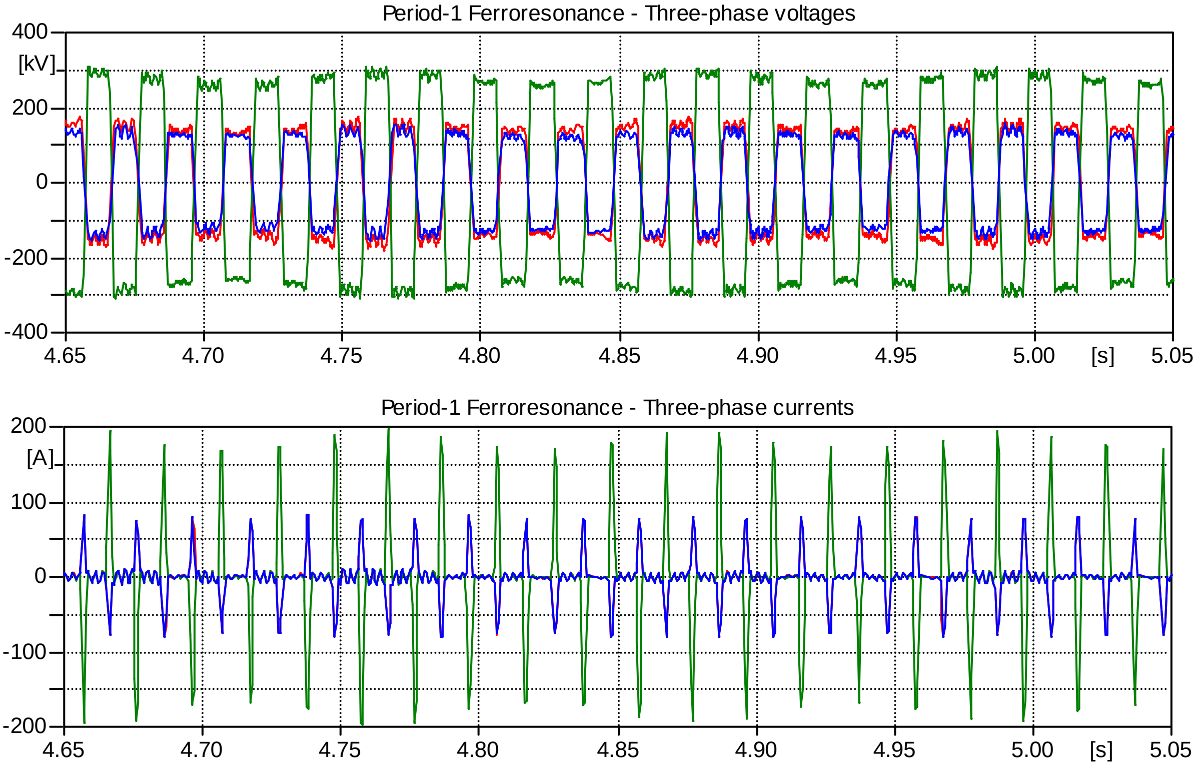

Figure 5.100: Period-1 ferroresonance - Top: Three-phase voltages, Bottom: Three-phase Currents

The results suggest that the developed lumped model can be used for further analysis to determine the key capacitance that causes the ferroresonance to occur. With the lumped representation, the analysis of the key parameter is then carried out by removing the shunt/ground capacitances, the line-to-line capacitances and the circuit1-to-circuit2 capacitances in a step by step fashion.

The results of simulation after removing the ground capacitance and the line-to-ground capacitance from the line are depicted in Figure 5.101 and Figure 5.102, respectively.

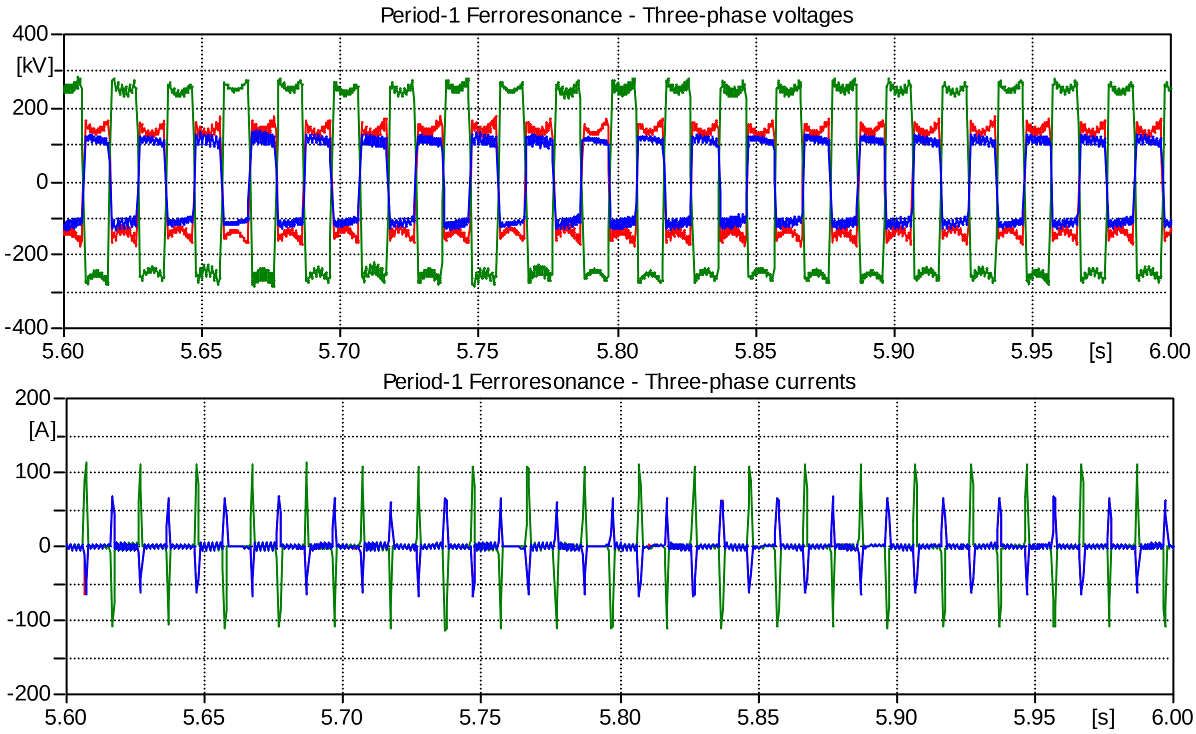

Figure 5.101: Predicted three-phase voltages and currents after ground capacitance removed from the line

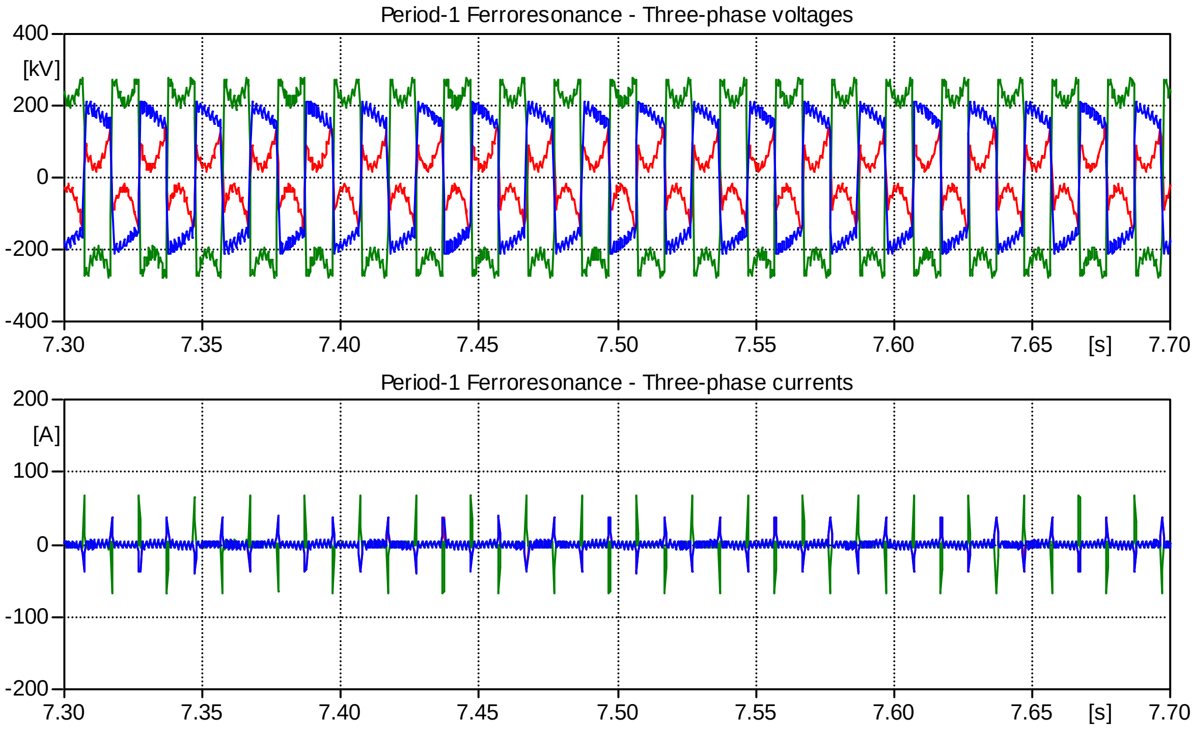

Figure 5.102: Line-to-line capacitances removed from the line

The results without the ground capacitances show that Period-1 ferroresonance still exists but there are some changes happened in both the voltage and current waveforms. For the voltage waveforms, it can be seen that the shapes around the voltage peak were affected when more capacitances were removed from the line. However, in the current perspective, it can be seen that the reduction of capacitance from the line has a significant effect of reducing the magnitude of the Period-1 ferroresonance current. In addition, the effect also introduces more harmonic contents into the system. This outcome is analysed by using FFT plots as shown in Figure 5.103.

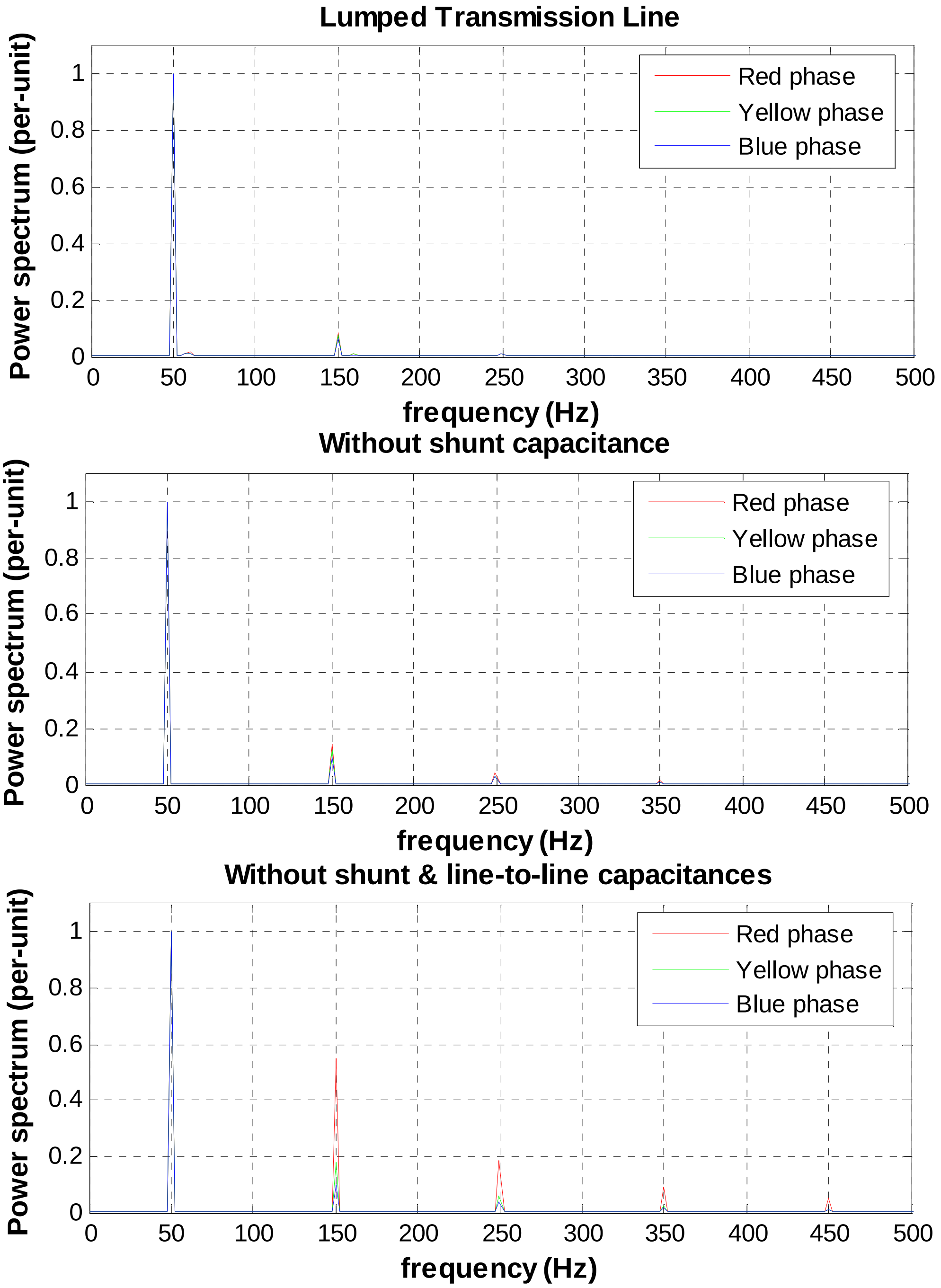

Figure 5.103: FFT plots for the three cases

Figure 5.103 shows that the line without the presence of the shunt and line-to-line capacitances has the influence of introducing harmonics into the system.

From the investigation, it has been found that each of the coupling capacitances of the line play an important role as a key parameter for the occurrence of Period-1 ferroresonance. Without the shunt and the line-to-line capacitances taking part in the line, the arrangement of the circuit-to-circuit capacitances are actually connected in series with the transformer. This study showed that the series arrangement of the capacitances and the transformer serve as a purpose of sustaining the amplitude of the three-phase voltages and currents. On the other hand, the studies without the shunt and the line-to-line capacitances has shown that there is a dramatic effect of reducing the amplitude of the ferroresonance currents, and this suggests that both of them are actually contributing to the current boosting of the phenomenon.

5.8 Summary

The simulations involved in all the six case studies using both the BCTRAN+ and HYBRID transformer models combined with either PI, Bergeron or Marti transmission line model have been carried out. Out of all the six combinations of the simulation models have been developed, and the comparisons between the simulations and the field recording results draw the following observations;

(1) A great deal of simulation attempts are required in order to reproduce the types of ferroresonance responses (Period-1 and Period-3) by the simulation models. The reason is because of the initial condition of the three-voltage waves after the current interruption are not repeatable from one cycle to another cycle.

(2) Degree of saturation for the transformer core was chosen as $n = 27$ because the simulation results are comparable with the field recording waveforms.

(3) There is not single simulation model, out of the six models developed, can be regarded as the best. All of them are comparable and are equally capable to replicate both the Period-1 and Period-3 ferroresonance waveforms. However, the limitations of these models are that they are not able to match the current magnitudes of the red and blue phases of the Period-1 ferroresonance and also the three-phase currents of the Period-3

ferroresonance. In addition, there is no high frequency ripples appearing on both the 3-phase voltages and currents.

(4) All the six simulation models can be employed for the study of ferroresonance but one particular model i.e. modeling the transformer using HYBRID and the transmission line in PI has been preferred.

(5) The preferred model is then further improved by modifying the core characteristic and the improved model is able to provide the high frequency ripples on the three-phase voltage and current waveforms for only the Period-3 ferroresonance. In addition to that, the magnitude of the yellow phase current has been drastically manifested.

(6) Discrepancy between recorded and predicted current still exists for Red and Blue phases. One of the possible reasons could be due to the core characteristic used to model the transformer is not fully representative to account for the flux distribution into airgap and its fringing effect, particularly, in the case of deep saturation. However, the shapes (see waveform figures) match quite well between the simulation and the field recording waveforms.

The observations on the key parameters that would influence the occurrence of the Period-1 ferroresonance are explained as follows:

(1) Both the transformer's coupling capacitances and the cable capacitance do not provide any significant influence on the occurrence of the Period-1 ferroresonance.

(2) From the investigation, all the coupling capacitances of the line have contributed individually to the occurrence of the phenomenon. The role of the circuit-to-circuit capacitances is to provide the sustainable amplitude of the ferroresonance while the rest provides the additional energy transfers from the line to the saturable core inductance.

CHAPTER 6

6. MODELING OF 400 KV IRON-ACTON/MELKSHAM SYSTEM

6.1 Introduction

In the preceding chapter, modeling of power system components to represent a 400 kV transmission system was carried out. The simulation model which has been developed is able to reproduce both the Period-1 and Period-3 ferroresonance waveforms in good agreement with the field test recording waveforms.

The aim of this chapter is to carry out a case study on a particular circuit configuration, regarding the likelihood of occurrence of sustained fundamental frequency (Period-1) ferroresonance. The study considered a complex arrangement including a mesh corner substation connected by overhead lines to a transformer feeder. The assessment upon the circuit is carried out by simulation studies using the ATPDraw. Since there are no field recording waveforms available for comparative verification, modeling of the individual components to represent the system are based of the criteria that have been obtained previously.

In addition to evaluating the system, this chapter also investigates the effectiveness of mitigation measure to quench the intended ferroresonance by switching-in a 60 MVAR shunt reactor which is connected at the 13 kV tertiary winding.

Furthermore, a sensitivity study on transmission line length is also carried out with an aim to find out the likelihood of occurrence of ferroresonance.

6.2 Description of the Transmission System

Figure 6.1 shows the single-line arrangement of one of the circuits on the National Grid transmission systems. The circuit arrangement which is believed to have a potential risk of inducing the Period-1 ferroresonance consists of a 33 km long double-circuit transmission line connecting with two power transformers: a 750 MVA, 400/275/13 kV (SGT5) and a 180 MVA, 275/132 kV (SGT4). One unit is a transformer feeder and the other on the mesh corner.

This study is based on National Grid enquiry to re-evaluate the existing Period-1 ferroresonance mitigating methods on the Iron Acton/Melksham system. It is noted that the current standard practice in the case of ferroresonance occurrence, is to quench ferroresonance current through the opening of the line disconnectors labeled as L13 and H43, as identified diagrammatically in Figure 6.1.

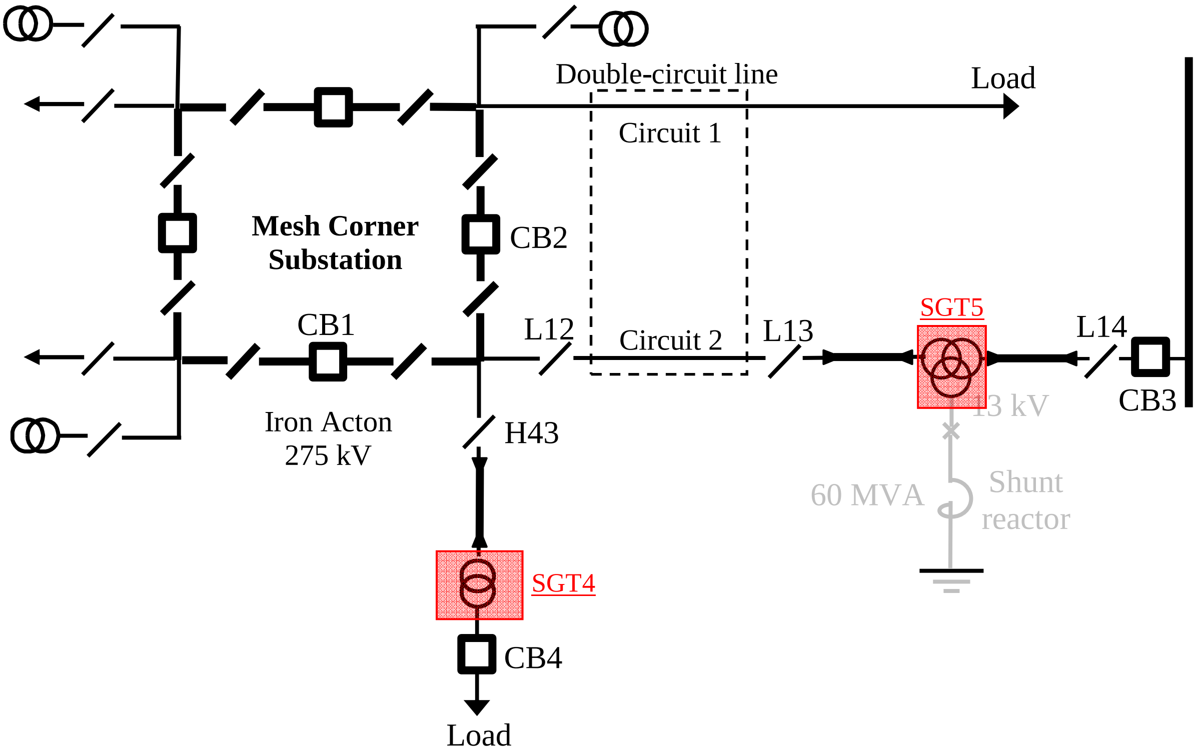

Figure 6.1: Single-line diagram of Iron Acton/Melksham system

Table 6.1 summarises the initial circuit conditions (normal operation), i.e. prior to ferroresonance occurrence. The circuit arrangement of the Iron Acton/Melksham system is likely to experience ferroresonance; the conditions needed to initiate this scenario are tabulated in Table 6.2.

Table 6.1: Status of circuit-breakers and disconnectors for normal operation

Iron Acton substation					**Melksham substation**		
Circuit-breaker			***Switch***		***Circuit-breaker***	***Switch***	
CB1	**CB2**	**CB4**	**L12**	**H43**	**CB3**	**L13**	**L14**
close	**open**	close	close	close	close	Close	close

Table 6.2: Status of circuit-breakers and disconnectors triggering ferroresonance

Iron-Acton substation					**Melksham substation**			**Remark**
Circuit-breaker			***Switch***		***Circuit-breaker***	***Switch***		
CB1	**CB2**	**CB4**	**L12**	**H43**	**CB3**	**L13**	**L14**	
open	**open**	open	close	close	open	close	close	SGT4 and SGT5 experience ferroresonance

The assessment of ferroresonance was carried out with the assumption that all the circuit breakers (i.e. CB1, CB3 and CB4) are simultaneously opened, CB2 has either already been opened or is tripped under the same protection scheme. The point to note is that although the circuit is tripped both transformers remain electrically connected to the overhead line and are therefore candidates for ferroresonance.

6.3 Identify the Origin of Ferroresonance

Conditioning the circuit of Figure 6.1 into ferroresonance state following the switching events of the three circuit breakers is identified, as a result, a ferroresonance path as indicated by the red line *is* shown in Figure 6.2 will involve the interaction between the double-circuit transmission line and the two power transformers, SGT4 and SGT5. From this event, there are two transient events that have been impinged upon the system; the first one is the opening of the three circuit breakers i.e. CB1, CB3 and CB4, and the second one is the energisation of Circuit 2 by adjacent live line (Circuit 1) via the transmission line's coupling capacitances.

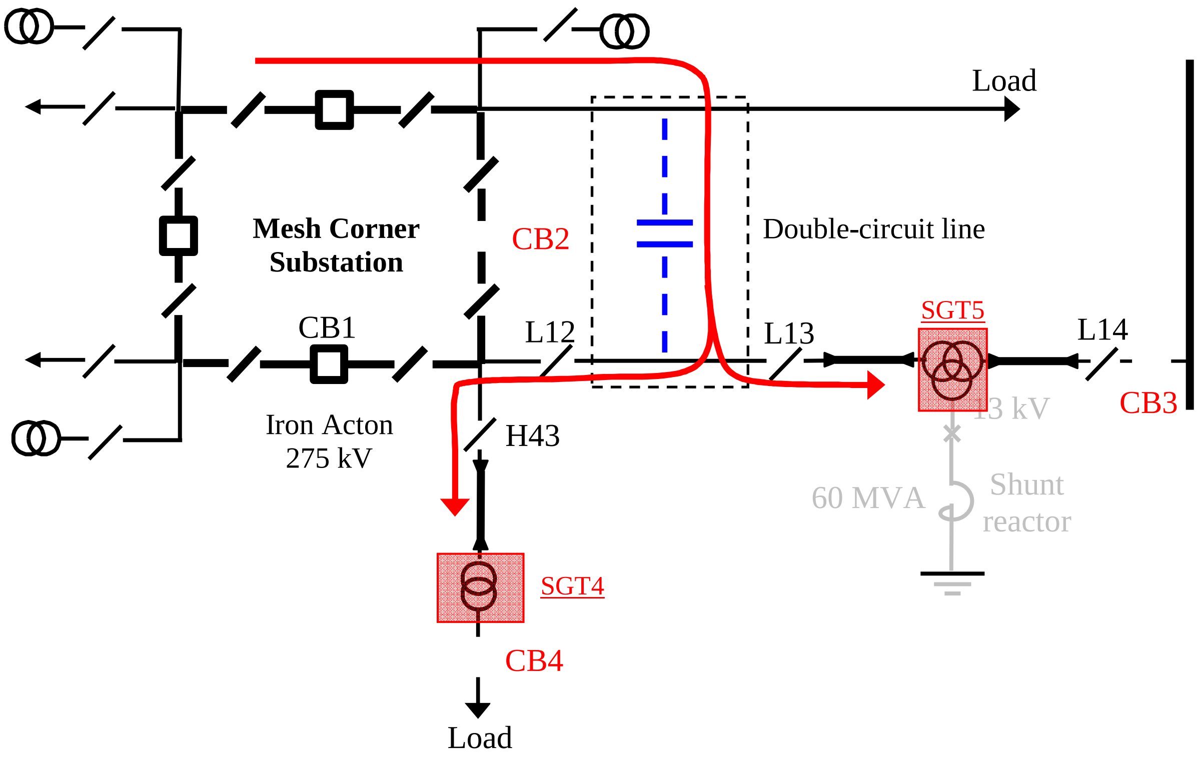

Figure 6.2: Single-line diagram of Iron Acton/Melksham system

It is expected that a similar type of Period-1 ferroresonance to the one that has been induced in the previous system network will occur upon this system arrangement. The reason is that the two circuits have been similarly energised via the transmission line's coupling capacitances. In addition, the methods that both the circuits have been reconfigured into ferroresonance condition are also identical with each other.

6.4 Modeling the Iron-Acton/Melksham System

The main task in this section is to model the whole system such that the model can be used for the study of ferroresonance. In order to do that, each of the components that are involved in the circuit is firstly modeled and they are presented in the following sections.

6.4.1 Modeling the Source Impedance and the Load

Figure 6.3 shows the simplified single-line diagram of the Iron-Acton/Melksham system and the ways the source impedances and the load are determined.

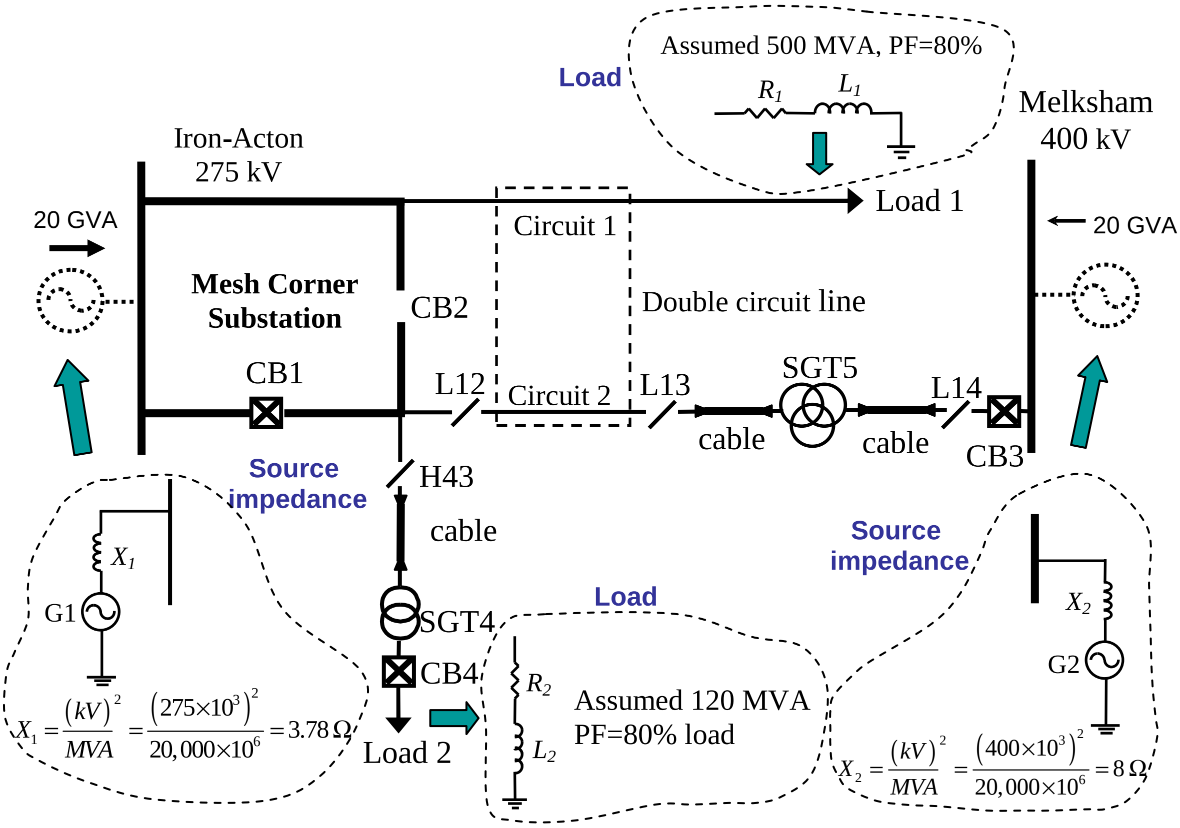

Figure 6.3: Modeling of the source impedance and the load

The rest of the system connected at the mesh corners 3 and 4 of Figure 6.3 are then simplified by assuming that the substation has an infinite bus with a fault level of 20 GVA. Furthermore, this assumption is also applied to the Melksham 400 kV substation. The inductive reactance is calculated based on the voltage level at the bus-bar. Detailed calculations of the reactances at the two substations are shown in Figure 6.3. For the load impedances which are identified as Load 1 and Load 2, each of them is assumed to have a load of 500 MVA and 120 MVA with a power factor of 80%, respectively.

6.4.2 Modeling the Circuit Breaker

It has been mentioned that the evaluation of ferroresonance was carried out with the assumption that all the circuit breakers (i.e. CB1, CB3 and CB4) are simultaneously opened, CB2 is assumed to be open. In this case study the three circuit breakers are modeled by using the 3-phase time-controlled switches with no current margin, the same criterion applied to the circuit breaker of the Marsh Thorpe/Brinsworth system.

6.4.3 Modeling the Cable

The cables which are connected at the primary side of SGT4 and at both sides (i.e. primary and secondary) of SGT5 are assumed to have a cable length of 500 m each. All of them are modeled as capacitor and the respective values are determined by referring to the technical cable data as [70]:

SGT4: 275 kV cable, C = 0.128 μF
400 kV cable, C = 0.1075 μF

SGT5: 275 kV cable, C = 0.128 μF

6.4.4 Modeling the 33 km Double-Circuit Transmission Line

The double-circuit line connected between the Iron Acton and Melksham substations is 33 km in length on L3/1 tower design. It can well be described as a short line; therefore the line can be represented by un-transposed configuration. The physical dimensions for the L3/1 tower are shown in Figure 6.4. Other relavant conductor parameters can be found in Appendix A [47].

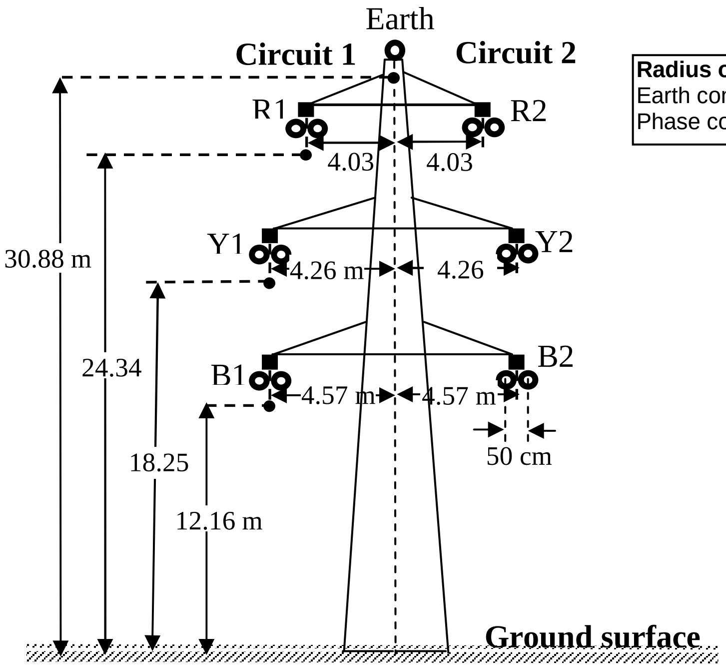

Radius of conductors:
Earth conductor = 9.765 mm
Phase conductor = 18.63 mm

Figure 6.4: Double-circuit transmission line physical dimensions

Based on the transmission line's physical dimensions and parameters which are available, it was modeled in ATPDraw using the integrated LCC objects and the mathematical approach to model the line is based on the travelling wave theory by using the Bergeron model. To verify the line is accurately modeled, line parameters check, line parameters frequency check, transmission line model rules check and transmission line model length check are shown in Appendix D.

6.4.5 Modeling of Power Transformers SGT4 and SGT5

Two transformer models, BCTRAN and HYBRID have been discussed earlier. Since the HYBRID model required core dimensions of the transformer which is not available, the BCTRAN+ model is therefore employed. Both transformers SGT4 and SGT5 are modeled using BCTRAN+ [44] transformer model based on the open- and short-circuit test data. The open-circuit test (No-load test) was carried out at the 13 kV winding consisting of measured per-unit voltage, no-load current and power loss. The short-circuit test performed at the respective winding consists of measured impedances and power loss. The electrical specifications of both the transformers are described in Table 6.3 and Table 6.4.

Table 6.3: Open and short circuit test data for the 180 MVA rating transformer

NO-LOAD LOSS on TERT. (30 MVA)				
VOLTS			**AMPS**	**kWatts**
%	**MEAN**	**R.M.S**		
			4.15	68.05
90	11700	11620	5.20	
			7.25	
			7.15	87.25
100	13000	12960	8.10	
			11.50	
			14.60	113
110	14300	14316	15.75	
			22.15	

LOAD-LOSS on HV				
VOLTS	**IMP**	**AMPS**	**kWATTS**	
			At 20^{o}C	**Corrected to 75^{o}C**
HV/LV @180 MVA				
39730	14.40%	378	-	533.40
HV/TERT @ 30 MVA				
32480	11.81%	63	-	57.00
LV/TERT @ 30 MVA				
12750	9.66%	131.20	-	57.60

(1) No-load calculation:

90%:

$$I_{ex} = \frac{(4.15+5.20+7.25)}{3} = 5.53\,\text{A (line current)}$$

$$I_{ex}(pu) = 5.53\times\frac{\sqrt{3}\times 11.62\times 10^{3}}{180\times 10^{6}}\times 100 = 0.06\%\ \text{@180 MVA}$$

100%:

$$I_{ex} = \frac{(7.15+8.1+11.5)}{3} = 8.92\,\text{A (line current)}$$

$$I_{ex}(pu) = 8.92\times\frac{\sqrt{3}\times 12.96\times 10^{3}}{180\times 10^{6}}\times 100 = 0.11\%\ \text{@ 180 MVA}$$

110%:

$$I_{ex} = \frac{(14.6+15.75+22.15)}{3} = 17.50\,\text{A (line current)}$$

$$IEXPOS = 17.50\times\frac{\sqrt{3}\times 14.32\times 10^{3}}{180\times 10^{6}}\times 100 = 0.24\%\ \text{@ 180 MVA}$$

(2) Load loss calculation:

$$Z_{HV-LV} = \frac{39730}{\sqrt{3}\times 378}\frac{180\times 10^{6}}{\left(275\times 10^{3}\right)^{2}}\times 100 = 14.44\ \%\ \text{@ 180 MVA}$$

$$Z_{HV-TV} = \frac{32480}{\sqrt{3}\times 63}\frac{30\times 10^{6}}{\left(275\times 10^{3}\right)^{2}}\times 100 = 11.81\ \%\ \text{@ 30 MVA}$$

$$Z_{LV-TV} = \frac{12750}{\sqrt{3}\times 131.20}\frac{30\times 10^{6}}{\left(132\times 10^{3}\right)^{2}}\times 100 = 9.66\ \%\ \text{@ 30 MVA}$$

Table 6.4: Open and short circuit test data for the 750 MVA rating transformer

NO-LOAD LOSS on TERT. (30 MVA)				
VOLTS			AMPS	kWatts
%	MEAN	R.M.S		
			5.89	55.97
90	11700	11716	5.22	
			6.68	
			6.04	72.27
100	13000	13021	5.09	
			6.96	
			8.01	102.34
110	14300	14392	5.79	
			7.83	

LOAD-LOSS on HV				
VOLTS	IMP	AMPS	kWATTS	
			At 20°C	Corrected to 75°C
HV/LV @750 MVA				
47499	11.87%	1083	-	988.80
HV/TERT @ 60 MVA				
27900	7.01%	86.18	-	104.30
LV/TERT @ 60 MVA				
15070	5.46%	126.42	-	108.70

The required per-unit open-circuit test currents for each of the 90%, 100% and 110% are calculated as follows:

(1) No-load calculation:

90%:

$$I_{ex} = \frac{(5.89+5.22+6.68)}{3} = 5.93\,\text{A (line current)}$$

$$I_{ex}(pu) = 5.93\times\frac{\sqrt{3}\times 11.72\times 10^{3}}{750\times 10^{6}}\times 100 = 0.016\,\%\ \text{@ 750 MVA}$$

100%:

$$I_{ex} = \frac{(6.04+5.09+6.96)}{3} = 6.03\,\text{A (line current)}$$

$$I_{ex}(pu) = 6.03\times\frac{\sqrt{3}\times 13.02\times 10^{3}}{750\times 10^{6}}\times 100 = 0.018\,\%\ \text{@ 750 MVA}$$

110%:

$$I_{ex} = \frac{(8.01+5.79+7.83)}{3} = 7.21\,\text{A (line current)}$$

$$IEXPOS = 7.21\times\frac{\sqrt{3}\times14.392\times10^{3}}{750\times10^{6}}\times100 = 0.024\,\%\ \text{@ 750 MVA}$$

(2) Load loss calculation:

$$Z_{HV-LV} = \frac{47499}{\sqrt{3}\times1083}\frac{750\times10^{6}}{\left(400\times10^{3}\right)^{2}}\times100 = 11.87\ \%\ \text{@ 750 MVA}$$

$$Z_{HV-TV} = \frac{27900}{\sqrt{3}\times86.18}\frac{60\times10^{6}}{\left(400\times10^{3}\right)^{2}}\times100 = 7.01\ \%\ \text{@ 60 MVA}$$

$$Z_{LV-TV} = \frac{15070}{\sqrt{3}\times126.42}\frac{60\times10^{6}}{\left(275\times10^{3}\right)^{2}}\times100 = 5.46\ \%\ \text{@ 60 MVA}$$

Once the transformer model has been developed, it is then verified with the real test data and the results of comparison are presented as shown in Table 6.5 and Table 6.8. The results suggest that the simulation values are comparable with the real measurement results in general, only the simulated power loss at 110% open-circuit test is lower than the measured one, indicating that core resistance is not well represented in BCTRAN+ for saturation or near to saturation region. .

SGT4: 180 MVA

Table 6.5: Comparison of open-circuit test between measured and BCTRAN

Vrms [kV]	Measured		BCTRAN	
	Irms [A]	P [kW]	Irms [A]	P [kW]
11.7 (90%)	5.53	68.05	5.22	69.66
13 (100%)	8.92	87.25	8.36	86.63
14.3 (110%)	17.50	113	17.08	105.61

Table 6.6: Comparison of short-circuit test between measured and BCTRAN

Vrms [V]	Measured		BCTRAN	
	Irms [A]	P [kW]	Irms [A]	P [kW]
HV/LV @180 MVA				
39730	378	533.40	379.14	536.91
HV/TERT @ 30 MVA				
32480	63	57	63.02	57.80
LV/TERT @ 30 MVA				
12750	131.2	57.6	131.28	58.417

SGT5: 750 MVA

Table 6.7: Comparison of open-circuit test between measured and BCTRAN

Vrms [kV]	**Measured**		**BCTRAN**	
	Irms [A]	**P [kW]**	**Irms [A]**	**P [kW]**
11.7 (90%)	5.93	55.97	5.55	58.70
13 (100%)	6.03	72.27	6.06	72.50
14.3 (110%)	7.21	102.34	7.56	88.57

Table 6.8: Comparison of short-circuit test between measured and BCTRAN

Vrms [V]	**Measured**		**BCTRAN**	
	Irms [A]	**P [kW]**	**Irms [A]**	**P [kW]**
HV/LV @180 MVA				
47499	1083	988.8	1083	989.6
HV/TERT @ 30 MVA				
27900	86.18	104.3	86.17	103.52
LV/TERT @ 30 MVA				
15070	126.42	108.7	126.43	109.74

The magnetic core of the transformer which accounts for saturation effect has been modeled externally connected via the tertiary winding. The saturation curves for SGT4 and SGT5 are derived according to the previous modeling technique and it is depicted in Figure 6.5 and Figure 6.6.

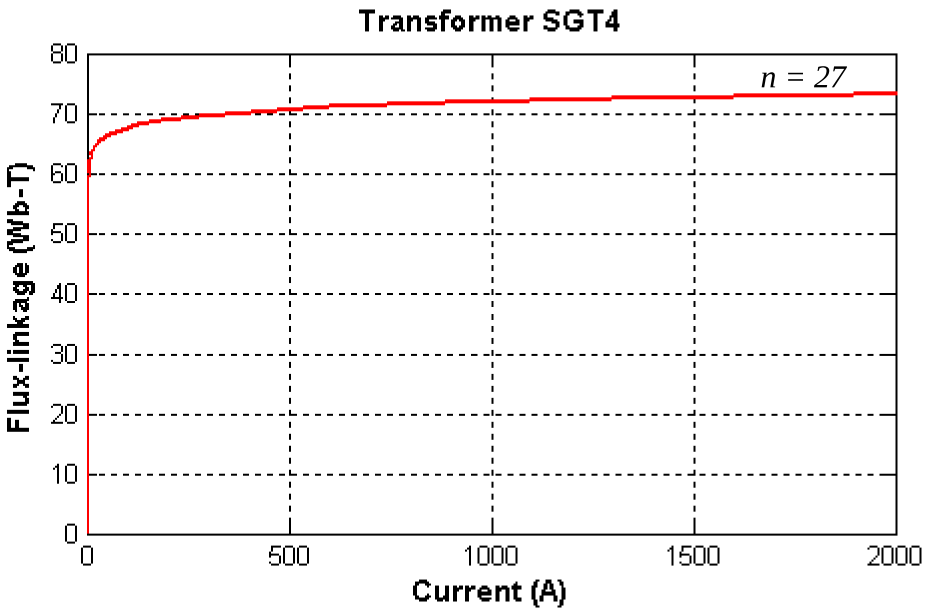

Figure 6.5: Saturation curve for SGT4

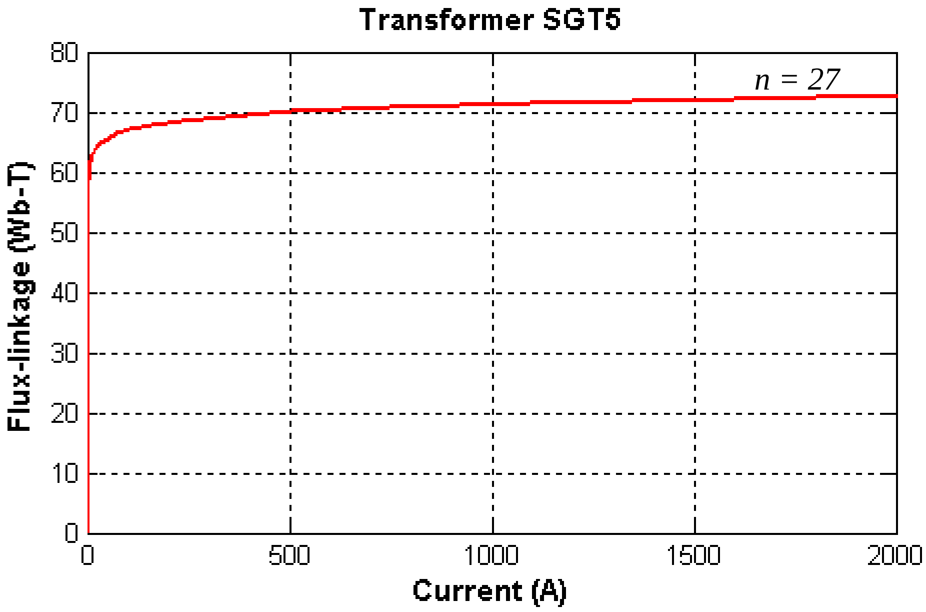

Figure 6.6: Saturation curve for SGT5

The degree of saturation of the core characteristics for both the 180 MVA and the 750 MVA transformers is chosen as *n* = 27. This level of saturation was used because the similar core saturation characteristic has been validated through ferroresonance study in Chapter 5.

6.5 Simulation Results of Iron-Acton/Melksham System

All the components in the system are modeled in detail, Figure 6.7 represents the complete simulation model.

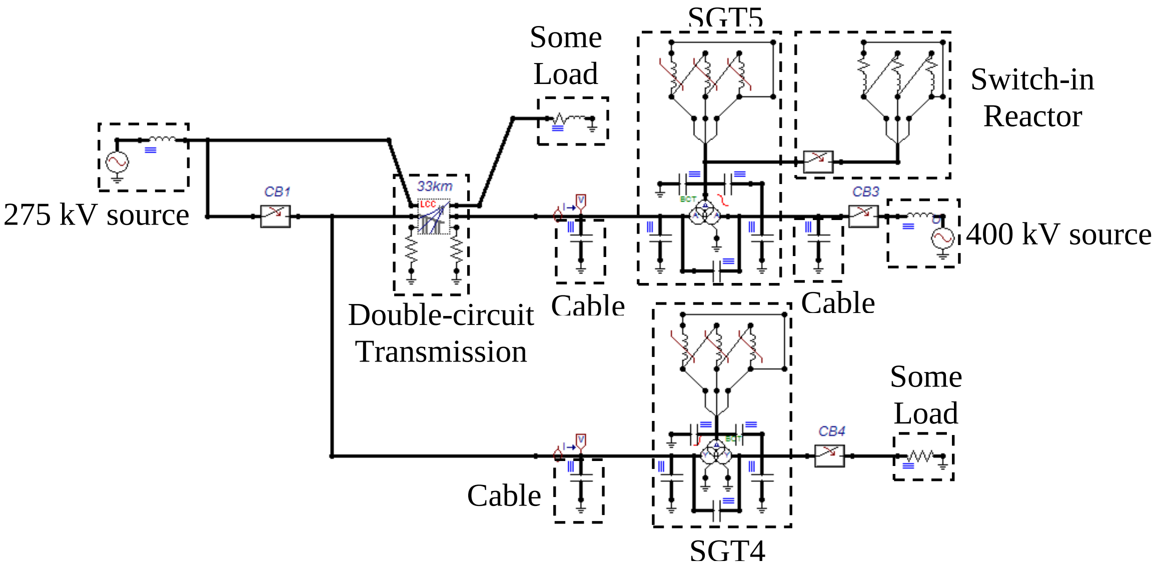

Figure 6.7: Single-line diagram of transmission system

The model included a 33 km double-circuit transmission line, two 3-phase transformers with different ratings, circuit breakers, a shunt reactor and cables. The models are based on manufactures' data sheets, test reports and other related information supplied by National Grid, UK.

A total of 100 simulations were performed without the presence of switching-in of a 60 MVA shunt reactor. Figure 6.8 shows the simulation result at the 275 kV side of transformers SGT4 and SGT5 when the circuit breakers CB1, CB3 and CB4 are simultaneously opened by protection at t = 0.546 seconds.

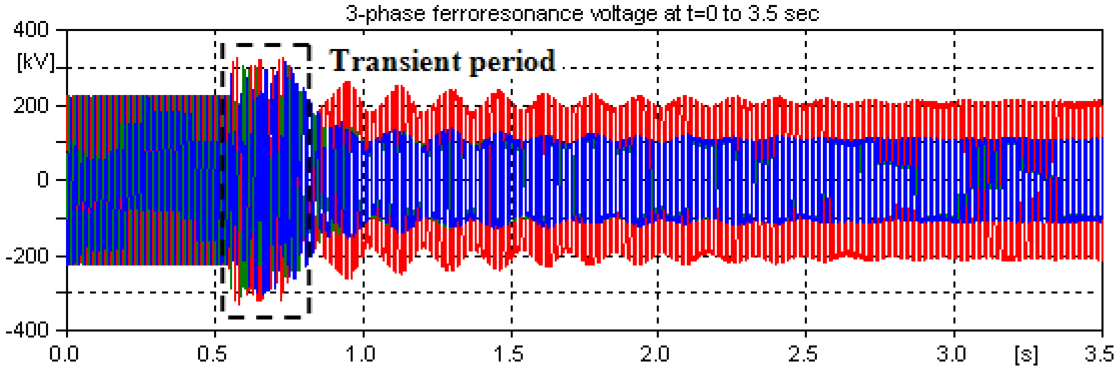

Figure 6.8: 3-phase sustained voltage fundamental frequency ferroresonance

At the instant when all the three circuit breakers are simultaneously opened, there is evidence of transient overvoltage occurring in the period between 0.546 seconds to 0.8 seconds before locking into sustained steady-state fundamental frequency ferroresonance.

Figure 6.9 shows the steady-state ferroresonance 3-phase voltages. The 3-phase voltage waveforms are rectangular in shape with the magnitude of the A-phase being twice of the magnitude of the B- and C- phases.

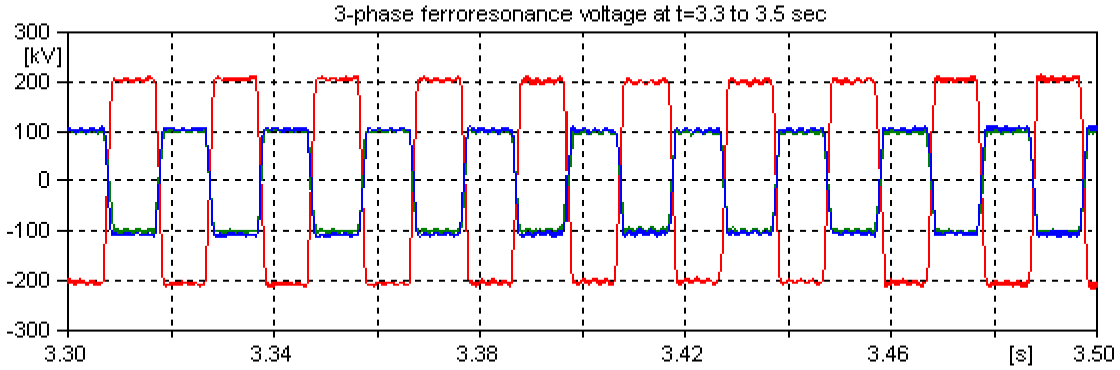

Figure 6.9: Sustained fundamental frequency ferroresonance (t=3.3 to 3.5 sec)

Figure 6.10 shows the corresponding 3-phase currents. At the instant of t = 0.546 seconds when all the three circuit breakers are simultaneously opened, there is a transient overcurrents occurring in the period between 0.546 seconds and 0.8 seconds.

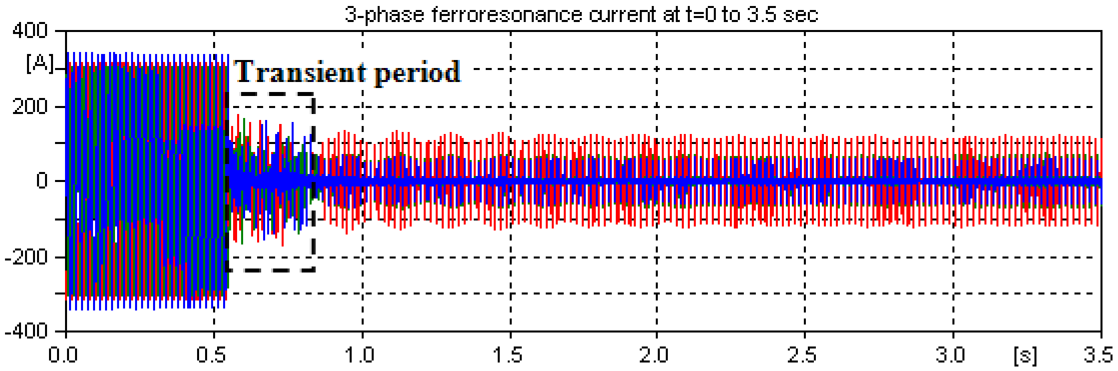

Figure 6.10: 3-phase sustained current fundamental frequency ferroresonance

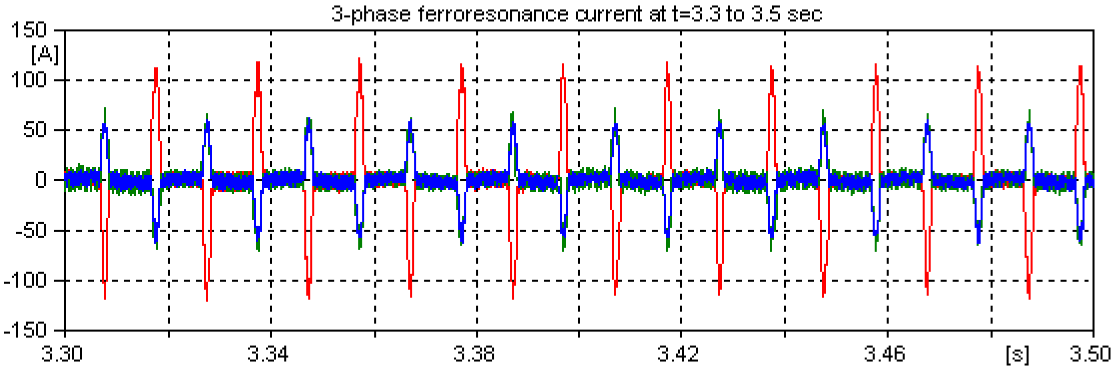

Figure 6.11: Sustained fundamental frequency ferroresonance (t=3.3 to 3.5 sec)

Figure 6.11 shows the steady-state ferroresonance circuit waveforms. The magnitude of the current waveform in Red-phase is much higher than Yellow-phase and Blue-phase of transformer SGT5. The waveshapes of the 3-phase currents are peaky in shape which signified that transformer SGT5 is operating in the saturation region.

Circuit breaker pole scatter has not been considered in detail, but would be difficult to control in practice.

A power spectrum of the voltage waveforms and phase-plane diagrams was created to assist classification of the observed ferroresonant mode. Figure 6.12 shows the frequency contents of the 3-phase voltages between 3 to 3.5 seconds, which mainly reveal the presence of fundamental frequency (50 Hz). Note that the power spectrum has been normalized.

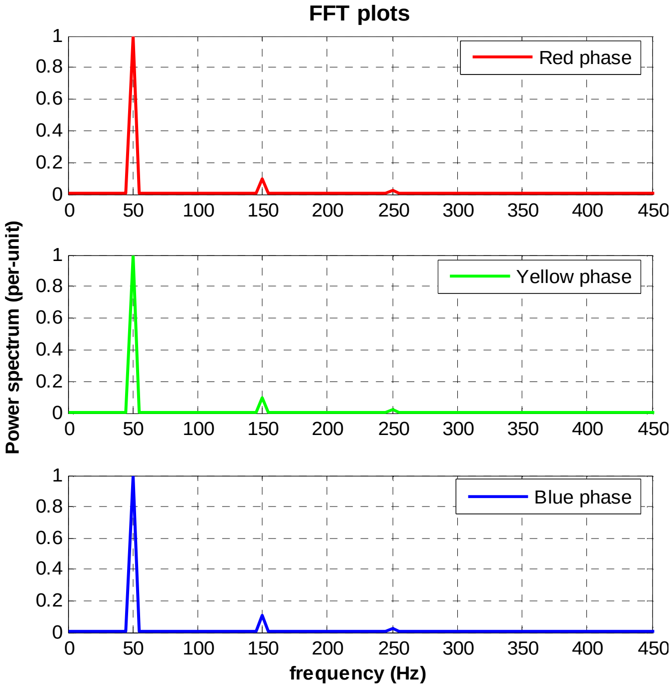

Figure 6.12: FFT plots

A good and brief explanation about phase-plane diagram is presented in [14]. A phase-plane diagram provides an indication of the waveform periodicity since periodic signals follow a closed-loop trajectory. One closed-loop means that a fundamental frequency periodic signal; two closed-loops for a signal period twice the source period, and so on.

The phase-plane diagram (i.e. flux-linkage versus voltage) of this response is shown in Figure 6.13. The orbits shown encompass a time interval of only one period of excitation. The structure of the phase-plane diagram consists of only one major repeated loop for each phase which provides an indication of a fundamental frequency signal. Note that the phase-plot has been normalized.

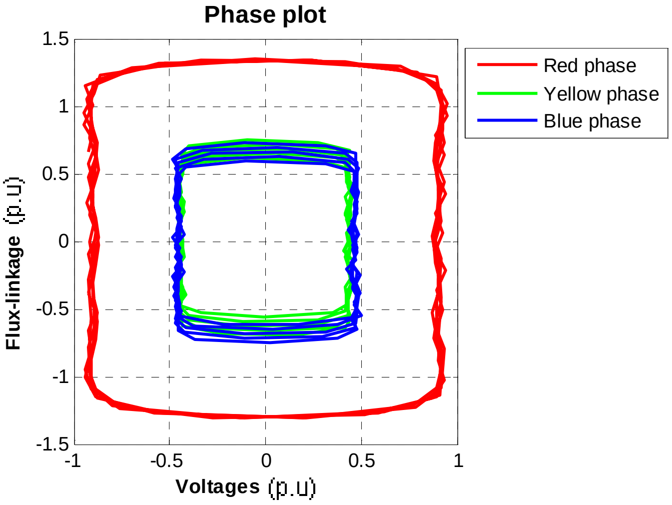

Figure 6.13: Phase plot of Period-1 ferroresonance

FFT and phase-plane diagrams are useful tools in recognising sustained fundamental frequency ferroresonance. However, if the response is random such as chaotic mode ferroresonance, then the construction of the Poincaré map [73] would be suitable for identification of the type of ferroresonant mode.

If the ferroresonance is allowed to persist without any preventive measures, a catastrophic failure of transformer might occur.

6.6 Mitigation of Ferroresonance by Switch-in Shunt Reactor

Several mitigation measures have been proposed to prevent ferroresonance in the literatures.

A good explanation about the employment of temporary insertion of damping resistors for voltage transformers is presented in [40]. The resistor connected in the secondary of a VT (voltage transformer) has been considered as a practical means to damp out ferroresonance. However, this requires ferroresonance to be determined at the design stage such that a device to detect the presence of ferroresonance is added and hence provide an automatic connection of the damping resistor as soon as the circuit breaker is opened. Besides, the selection of the most efficient damping resistor for optimum damping and the necessary connection time of the resistor need to be pre-determined.

In terms of power transformers, a practical example presented in [13, 16] was the employment of a damping resistor connected across the secondary of the transformers. Alternative methods include the use of air-core reactor connected across the HV winding [13] and connected permanently at the bus [16]. The proper design of the switching operation to avoid power systems configuring into a ferroresonant condition [4] also provides the other mean of preventing ferroresonance from occurring.

This study considers suppression of the sustained fundamental frequency ferroresonance by switching-in the shunt reactor connected across the 13 kV winding of SGT5. The reason that shunt reactor switching is considered in this study as a ferroresonance mitigation measure is the cost effectiveness, which is to use the existing installed reactor in the substation rather than purchasing new damping resistor. A sensitivity study has been carried out to identify the critical value of the shunt reactor in terms of reactor rating

(MVA value). Five values of shunt reactor ratings were analysed and the results of simulations are presented in Figure 6.14.

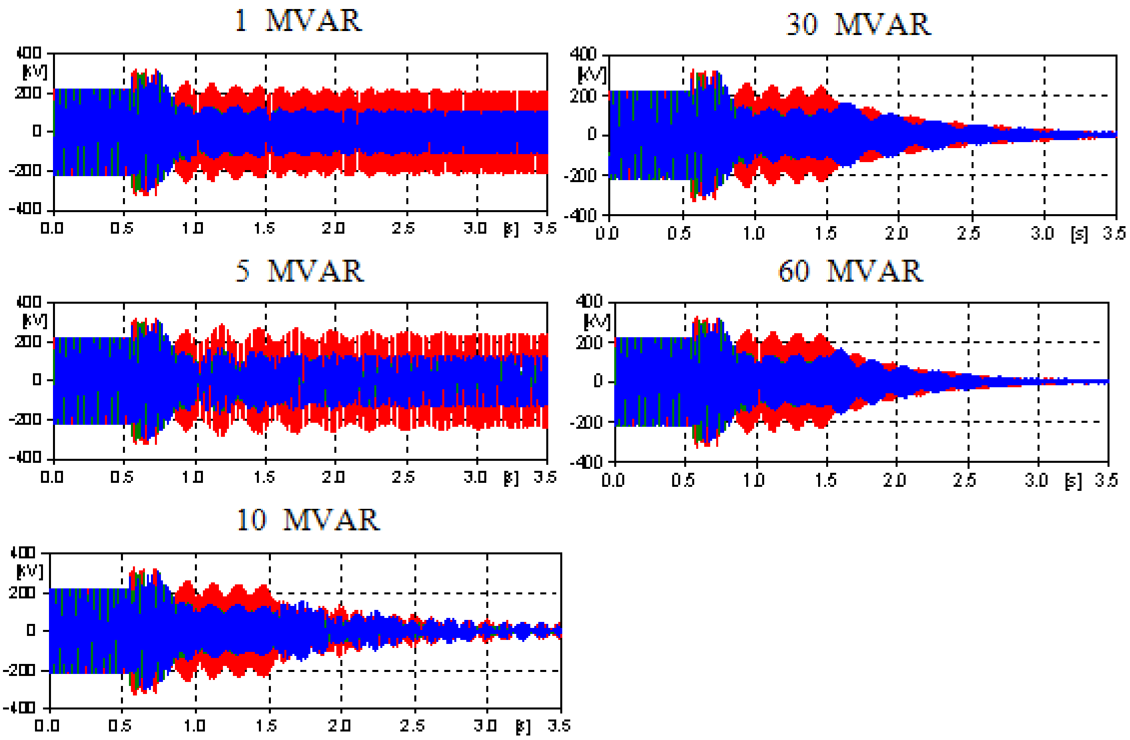
1 MVAR

30 MVAR

5 MVAR

60 MVAR

10 MVAR

Figure 6.14: Suppression of ferroresonance using switch-in shunt reactors at t=1.5 sec

Figure 6.14 shows the effects of suppressing the sustained ferroresonance using shunt reactor ratings of 1 MVAR, 5 MVAR, 10 MVAR, 30 MVAR and 60 MVAR. Values up to 5 MVAR do not succeed in suppressing the ferroresonance as the ferroresonance is disturbed slightly when the reactor is switched-in and then tends to build up again. On the other hand, the 10 MVAR manages to damp out the ferroresonance but not effective, it generates repetitive oscillation. The only shunt reactor ratings which effectively suppress the ferroresonance are the 30 and 60 MVAR reactors and the later one has shown to be most effective in terms of a faster damping rate. It should be noted that the purpose of the shunt reactor is to control system voltage during periods of light system loading, so this technique would not be routinely available for ferroresonance alone.

The five voltage waveforms of Figure 6.14 are the outcomes of damping out ferroresonance with switching-in of five different ratings of shunt reactors. The main reason that the 60 MVAR can provide highly effective damping is due to the fact that the presence of this shunt reactor provides the smallest linear inductance connected in parallel with the non-linear transformer core inductance (Figure 6.15).

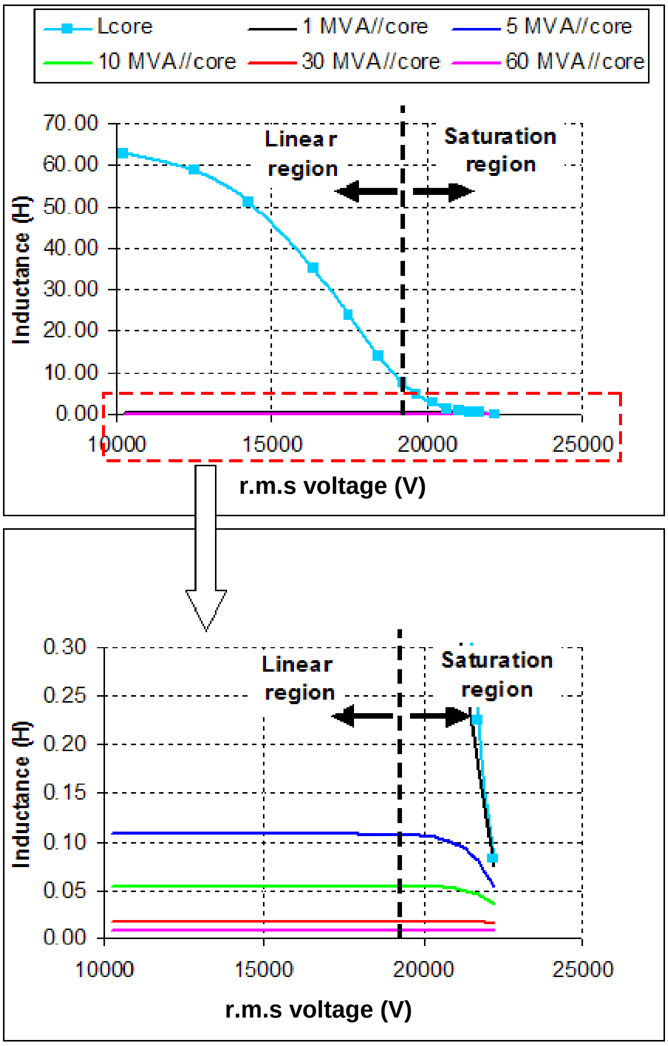

Figure 6.15: Core connected in parallel with shunt reactor characteristics

As a result of that, the resonance condition of matching the equivalent coupling capacitive reactance and the core inductive reactance would be destroyed, and this change of inductive characteristic discontinues the maximum energy transferred between the network coupling capacitance and the transformer core inductance and eventually dissipates the energy into the resistive part of the system. The magnitude of the ferroresonance voltage could not be sustained and eventually dies out.

6.7 Sensitivity Study of Double-Circuit Transmission Line

The main aim of this section is to investigate the level of influence on ferroresonance by varying to the line length. With this knowledge, it is useful for system engineers to plan ahead the type of protection schemes with the known line length which is able to cause the onset of ferroresonance.

When the line length is varied from 5 km to 35 km in step of 5 km, a number of ferroresonant waveforms as shown in Figure 6.16 to Figure 6.17 have been observed. Both the 10 Hz and $16^{2/3}$ Hz were observed when the line length is varied to 15, 20, 25, 30 and 35 km. These responses consist of frequency components of f/5 and f/3 respectively. The chaotic response of Figure 6.18 was observed when the line length is at 30 km, it is a non-periodic which appears to have an aspect of randomness in terms of its magnitude and frequency. The FFT plot revealed that the signal consists of continuous spectrum of frequency.

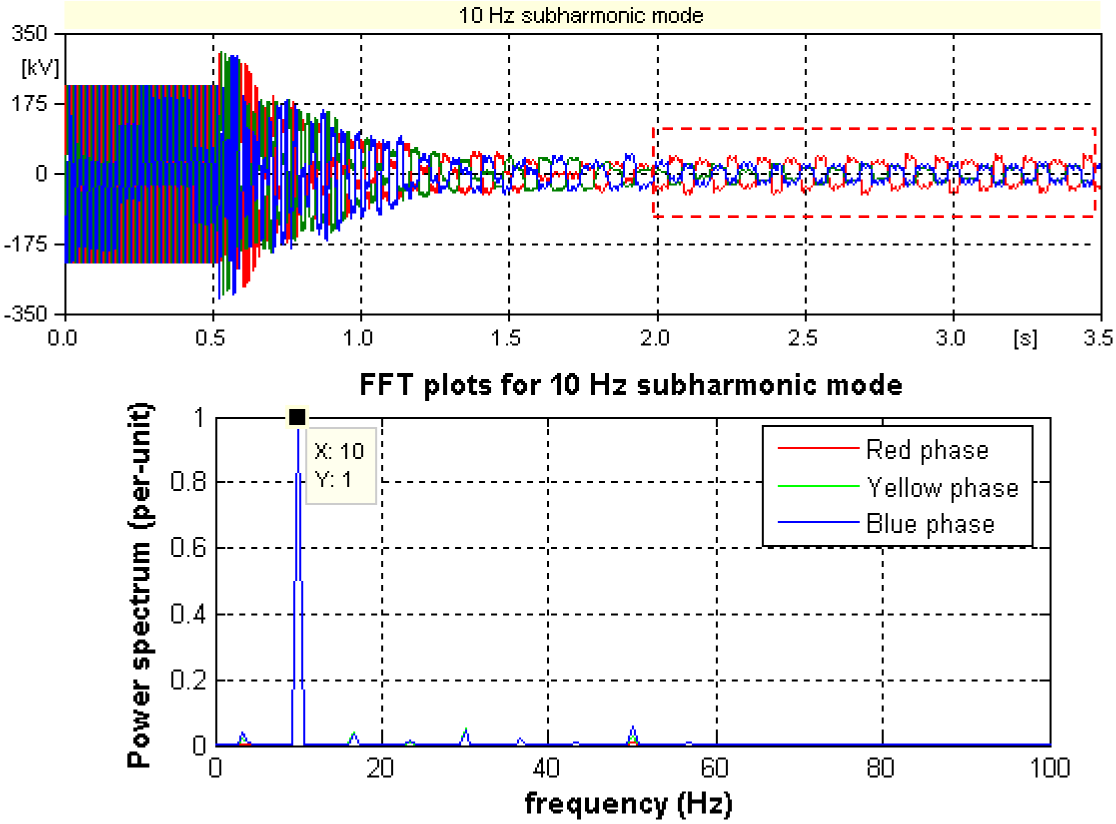

Figure 6.16: Top: 10 Hz subharmonic ferroresonant mode, **Bottom:** FFT plot

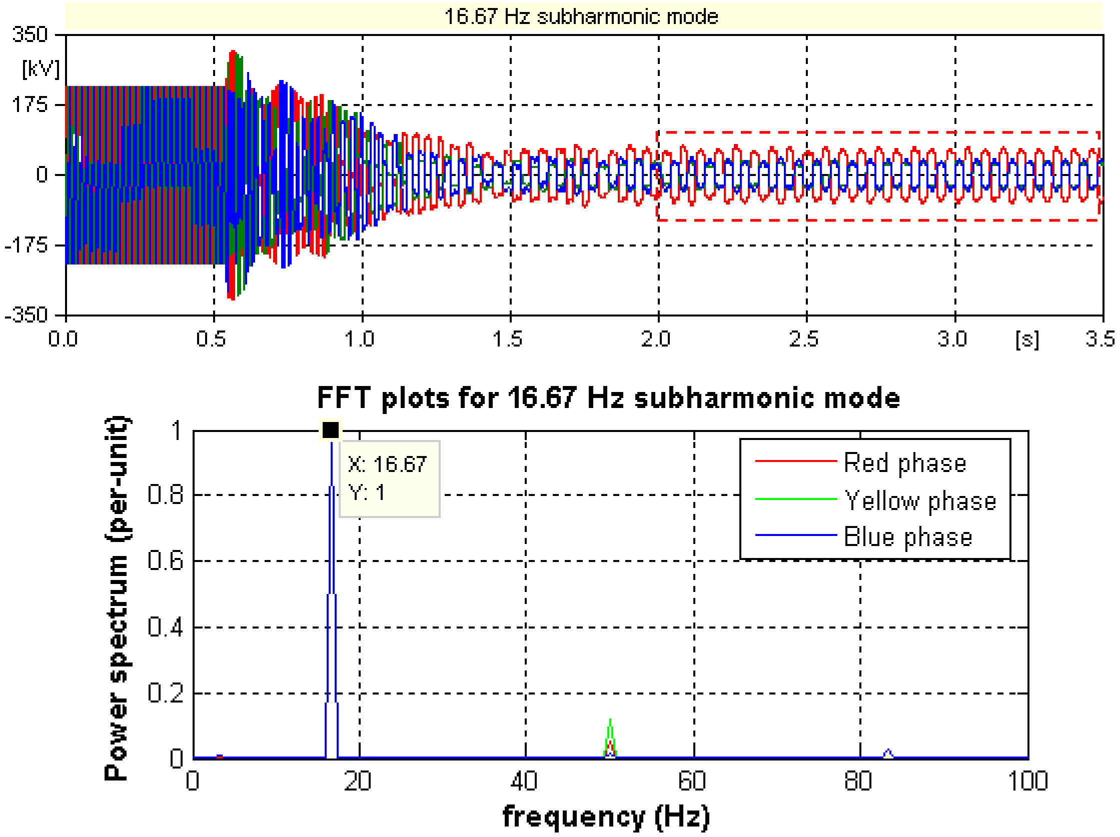

Figure 6.17: Top: $16^{2/3}$ Hz subharmonic ferroresonant mode, **Bottom:** FFT plot

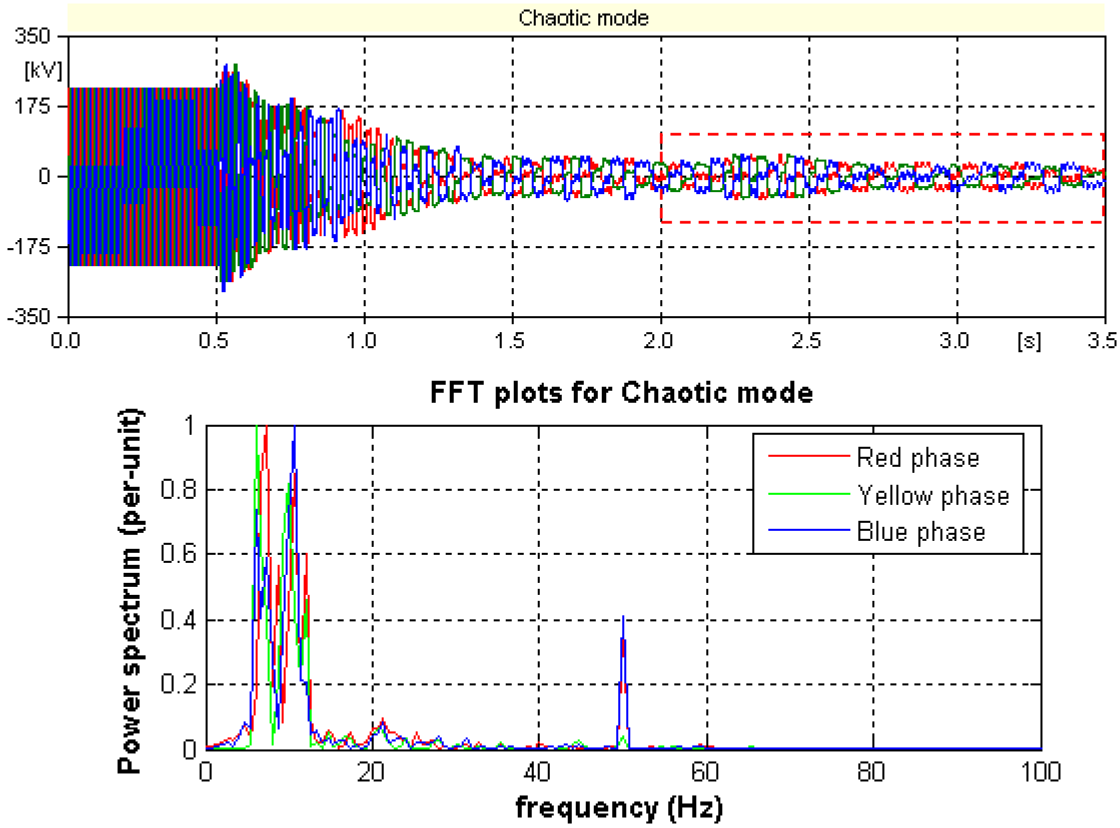

Figure 6.18: Top: Chaotic ferroresonant mode, **Bottom:** FFT plot

The fundamental mode of Figure 6.8 is considered to be the most severe one as its sustained amplitude is the highest as compared to the other types of ferroresonant modes. This is due to that the maximum energy has been transferred between the transmission line's coupling capacitance and the nonlinear inductance of the core. The transfer of energy without any damping can repeatedly drive the core into saturation for every cycle of the system frequency. Then excessive peaky current will be drawn from the system as a result of excessive flux migrates out of the core.

A total of 700 simulations were carried out with the line length varied from 5 km to 35 km, in step of 5 km. For each incremental step, the circuit breakers (CB1, CB3 and CB4) are assumed open simultaneously, starting from 0.5 seconds up to 0.6 seconds, in step of 1 ms. The probability of occurrence for each of the ferroresonant mode was determined and the results are presented in Figure 6.19.

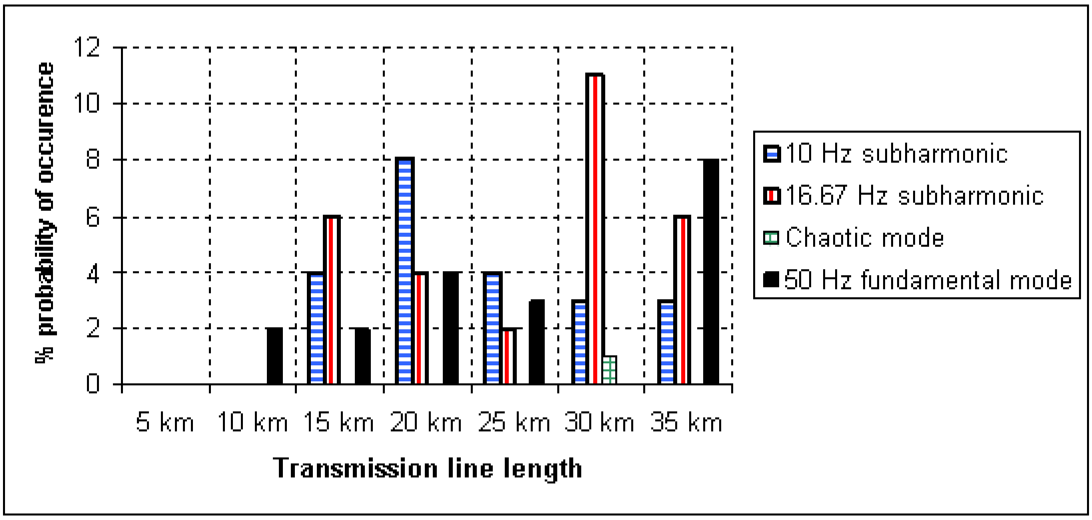

Figure 6.19: Probability of occurrence for different ferroresonant modes

Figure 6.19 shows that several ferroresonant modes have been induced into the transmission system; there are the 10 Hz subharmonic mode, the 16.67 Hz subharmonic mode, the 50 Hz fundamental mode and the chaotic mode. The chart shows that none had happened for the line length of 5 km. However, the trend reveals that both types of subharmonic and fundamental modes are more pronounced when the line length is increased to 35 km but the trend is in stochastic fashion. The probabilities of ferroresonance occurrences are not directly proportional to the increased in the line length.

6.8 Summary

Ferroresonance is a complex low-frequency transient phenomenon which may occur due to the interaction between network coupling capacitance and the nonlinear inductance of a transformer. In this case, the UK transmission network has provided an ideal configuration for ferroresonance to occur, when one circuit of the double-circuit transmission line is switched out but it continues to be energised through coupling capacitance between the double-circuit transmission lines.

The ATP software has been employed to assess any likelihood of sustained fundamental frequency ferroresonance. The graphical simulation results presented in this chapter clearly show that ferroresonance can occur. However, the intended ferroresonance has been successfully and effectively damped by a switched-in shunt reactor.

The onset of ferroresonance phenomenon in this case study is caused by the energisation of both transformers SGT4 and SGT5 which were capacitively coupled via adjacent live line when one of the double-circuit lines has been switched out. A number of ferroresonant modes have been induced; there are the 10 Hz subharmonic mode, the $16^{2/3}$ Hz subharmonic mode, the chaotic mode and the 50 Hz fundamental mode. However, the statistically analysis shows that the probability of occurrence of a particular ferroresonant mode is random in nature as the line length is increased. Interestingly, ferroresonance is not likely to occur for the transmission line length of below 5 km. The reason is due to the fact that the circuit-to-circuit capacitances of the double-circuit line are not sufficiently large enough to cause the core working in the saturation region.

CHAPTER 7

7. CONCLUSION AND FUTURE WORK

7.1 Conclusion

The study begins by briefly outlining the main function of power system network and the status of the network due to the development of technological equipment, population growth and industrial globalisation. Along with network expansion and integration, serious concern has been raised on the occurrence of transient related events. The consequences of such event may be system breakdown and catastrophic failure of power system components such as arrestors, transformers etc.

One of the transients which are likely to be caused by switching events is a low frequency transient, for example ferroresonance. Prior to the introduction of such a phenomenon, a linear resonance in a linear *R*, *L* and *C* circuit is firstly discussed, particularly the mechanism on how resonance can occur in a linear circuit. Then the differences between the linear resonance and ferroresonance are identified in terms of the system parameters, the condition for the occurrence of ferroresonance and the types of responses. Several ferroresonant modes can be identified and they are namely the fundamental mode, subharmonic mode, quasi-periodic mode and chaotic mode. In addition, the tools to identify these modes employing frequency spectrum (FFT), Poincaré map and phase-plane diagram have been presented. This is followed by looking into the implications of ferroresonance on a power system network, ranging from the mal-operation of protective device to insulation breakdown. Two general methods of mitigating ferroresonance have been discussed to avoid the system being put into stress.

Survey into different approaches on modeling of ferroresonance in terms of practical and simulation aspects has been carried out. There are five categories of ferroresonance studies which have been presented in the literatures; the analytical approach, the analog simulation approach, the real field test approach, the laboratory measurement approach and the digital computer program approach. The drawback of analytical approach is the complexity of the mathematical model to represent an over simplified circuit. The analog simulation and the small scale laboratory approaches on the other hand do not truly represent all the characteristics of the real power network. In contrary, the real field test being carried out upon the power network will put the test components under stress and even in a dangerous position. Despite of the major advantages of computer simulation approach, the major drawback of employing computer simulation for modeling the power system network is the lack of definite explanation on modeling requirements in terms of selecting the suitable predefined models and validating the developed models. The only way to find out the validities of the developed models is to compare the simulation results with the field recording waveforms.

Prior to the identification of the individual component model and hence the development of the simulation model for a real case scenario, one of the main aims of this study is to look into the influence of system parameters on a single-phase ferroresonant circuit. This includes (1) the study of the influence of magnetising resistance, R_m (2) the study of influence of degree of core saturations with each case in relation to the change of grading capacitor of circuit breaker and the ground capacitance. The studies from part (1) turned out to be that high core-loss has an ability to suppress the sustained Period-1 ferroresonance as compared to low-loss iron core which is employed in modern transformers. On the other hand, the study from part (2) revealed the followings: (a) high degree of core saturation – sustained fundamental mode is more likely to occur, however, subharmonic mode is more likely to happen at high value of shunt capacitor and low value of grading capacitor (b) low degree of core saturation - fundamental mode occurs at high value of grading capacitor but limited at higher range of shunt capacitor, however, subharmonic mode is more likely to occur at high value of shunt capacitor and low value of grading capacitor. Chaotic mode starts to occur with low degree of core saturation.

The fundamental understanding upon the influence of system parameters on ferroresonance in a single-phase circuit has been described. Prior to the development of the simulation model for the real case three-phase power system network, the identification of the models of the circuit breakers, the transformers and the transmission lines in ATPDraw which are suitable for ferroresonance study is firstly carried out. The appropriateness of each of the predefined model is assessed by applying the criteria supported by CIGRE WG 3.02. In regards to the circuit breaker, a simplistic model based on current zero interruption has been found to be appropriate as the current study of ferroresonance is only focused on the sustained responses, not the transient part. Next is the transformer model, as this device has a great influence on low frequency transients therefore the mathematical derivation of the saturation were carried out in order to understand the theoretical background. In addition, the influence of harmonic contents when the core operates in deep saturation is also studied. It is found that transformer representation for ferroresonance study required the following effect to be modeled: the saturation effect, the iron-losses, the eddy current and the hysteresis. Saturation effect is for the transformer to include the nonlinearity of core characteristic. Iron-loss is actually consists of hysteresis and eddy current losses, these losses are used to represent the ohmic loss in the iron core. On the other hand, the hysteresis loss is depending on the type of core material. Modern transformers usually employed low loss material aimed at improving the efficiency of the transformer. Two predefined transformer models in ATPDraw have been identified to provide these features: they are the BCTRAN+ and the HYBRID models. The main difference between the two is the way the core has been represented. On the other hand, for the transmission line, three predefined models in ATPDraw haven been considered: the PI model, the Bergeron model and Marti model. As the main aim is to determine the best possible model for ferroresonance study, the following combinations as shown in the table have been drawn up as case studies.

	Power Transformer model	**Transmission line model**
Case Study 1	BCTRAN	PI
Case Study 2	BCTRAN	Bergeron
Case Study 3	BCTRAN	Marti
Case Study 4	HYBRID	PI
Case Study 5	HYBRID	Bergeron
Case Study 6	HYBRID	Marti

With each of the case as shown in the table, a simulation model was developed in ATPDraw to represent a real test scenario (Thorpe-Marsh/Brinsworth) with an aim to reproduce the 3-phase Period-1 and Period-3 ferroresonance matched with the field recording ones. The overall outcomes produced from the simulations for all the cases suggest that they are all able to match quite well. However, the magnitudes of the Period-1 red-phase and the blue-phase currents were found to be 50% lower than the real test case. On the other hand for the Period-3 ferroresonance, the magnitudes of all the 3-phase currents are considerably smaller and in addition to that there is no ripple being introduced in both the voltage and current waveforms in the simulation results. Slight improvements have been made to the simulation model, and the results suggest that only the Period-3 ferroresonance has a slight improvement in terms of their current magnitude and the ripple. From the study, it is suggested that transmission line using PI model and transformer employed HYBRID model are the most suitable for ferroresonance study. The investigations into the key parameter that influence the occurrence of ferroresonance have been carried out. The study began by looking into the removal of the transformer coupling capacitance, and then followed by removing cable capacitance, the simulation results revealed that Period-1 ferroresonance still occurred. Further study is then carried out by representing the line in lumped parameter in PI representation and each of the coupling capacitances are then evaluated. The studies showed that the sustainable resonance is supported by the interaction between the series capacitance (i.e. the circuit-to-circuit capacitance) and the saturable core inductance. They in fact provide the resonance condition of matching the saturable core inductive reactances thus providing sustainable energy transfer. On the other hand, both the ground and line-to-line capacitors supply additional discharging currents to the core.

Once the types of transmission line and the transformer model have been identified which are suitable for ferroresonance study, they are then employed to develop another case study on a National Grid transmission network with an aim to evaluate the likelihood of occurrence of Period-1 ferroresonance. From the simulation, it has been found that the Period-1 ferroresonance can be induced into the system. An effort was then carried out to suppress the phenomena by switching-in the shunt reactor which is connected at the 13 kV winding side. A series of different shunt reactor ratings have been evaluated and it was found that a 60 MVAR reactor is able to quench the phenomena in an effective way. In addition, sensitivity study on transmission line length was also carried out and the simulation results suggests that sustained fundamental frequency ferroresonance will occur for the line length of 15, 20, 25, 30 and 35 km.

7.2 Future Work

The major achievement in this project is the identification of the circuit breaker, transformer and transmission line models which can be used for ferroresonance study.

A simplistic time-controlled switch to represent a circuit breaker can be employed without considering the circuit breaker’s complex interruption characteristic if a sustained steady-state phenomenon is of interest. The predefined transformer models namely the BCTRAN+ and the HYBRID are equally capable of representing their saturation effect for the transformer magnetic core characteristic to account for ferroresonance events. The transmission line models employing both the lumped-parameter (i.e. the PI representation) and the distributed-parameter (i.e. the Bergeron and the Marti) models are able to represent the double-circuit line.

However the predefined models may not be sufficiently accurate when they are used to represent the power system components, especially when differences are noticed as we compare the simulation results with the field test recordings. Further work can be done at the following aspects:

I) The method for modeling the core of the transformer in the predefined model is based on the open-circuit test report using the 90%, 100% and 110% data. This type of core representation to account for saturation effect does not characterise the joint effect of the core when being driven into deep saturation. In fact, transformer driven into deep saturation may cause more flux distributed into air-gap which in effect will create different type of core characteristic which is different from the one extrapolated from the open-circuit test result. Future work on self built transformer core models should be conducted based on real saturation test results. In the case that the deep saturation test results are not available, sensitivity studies should be done on the characteristics of the core with various degrees of deep saturation.

II) For the transmission line model, either the PI, the Bergeron or the Marti models represents the reactance part of the line well, however the resistive losses are differently represented and their representation accuracy is hard to assess. For example, there is no loss in the PI representation, and some spurious oscillation can be seen in the transient simulation results. In view of this, future work should be focusing on how to accurately represent the resistive loss in the system and how the loss could affect the initiation of the ferroresonance phenomena.

III) For the modeling of circuit breaker, the time-controlled switch may be suitable for the sustained steady-state ferroresonance, however, the detailed interruption characteristics such as the high frequency transient currents, the time lags of pole operations and etc may not be fully represented at this stage and can be vital important for the detail studies of ferroresonance. Such detailed modeling of normal operations of circuit breakers may require further studies.

Besides, the investigation of the initiation of different modes of ferroresonance is an area for the future work. The study can be to look into the stochastic manner of the ferroresonant circuit following the opening of the circuit breaker at different initial conditions, and to look into the onset conditions of different modes which are sensitive to system parameters.

REFERENCES

[1] A. Greenwood, *Electrical Transents in Power Systems*, Second Edition ed.: John Willey & Sons, Inc, 1991.

[2] J. A. Martinez-Velasco, "Computer Analysis of Electric Power System Transients," *The Institute of Electrical and Electronics Engineers, Inc*, p. 121, 1997.

[3] *Cadick Corporation, "Ferroresonance" TECHNICAL BULLETIN-004a, May 29, 2002.*

[4] *P. Ferracci, "Ferroresonance, Cashier Technique no 190", Groupe Schneider. March 1998.*

[5] C. Charalambous, Z. D. Wang, M. Osborne, and P. Jarman, "Sensitivity studies on power transformer ferroresonance of a 400 kV double circuit," *Generation, Transmission & Distribution, IET*, vol. 2, pp. 159-166, 2008.

[6] S. K. Chakravarthy and C. V. Nayar, "Series ferroresonance in power systems," *International Journal of Electrical Power & Energy Systems*, vol. 17, pp. 267-274, 1995.

[7] C. B. K.Pattanapakdee, "Failure of Riser Pole Arrester due to Station Service Transformer Ferroresonance," in *Internatioinal Conference on Power Systems Transients (IPST'07)* Lyon, France, 2007.

[8] S. C. Preecha Sakarung, "Application of PSCAD/EMTDC and Chaos Theory to Power System Ferroresonance Analysis," in *International Conference on Power Systems Transients (IPST'05)* Montreal, Canada, 2005.

[9] Y. Yuhong and Z. Hao, "Study on Simulation of Ferroresonance Elimination in 10kV Power System," in *Transmission and Distribution Conference and Exhibition: Asia and Pacific, 2005 IEEE/PES*, 2005, pp. 1-7.

[10] B. A. T. Al Zahawi, Z. Emin, and Y. K. Tong, "Chaos in ferroresonant wound voltage transformers: effect of core losses and universal circuit behaviour," *Science, Measurement and Technology, IEE Proceedings* -, vol. 145, pp. 39-43, 1998.

[11] Z. Emin, B. A. T. Al Zahawi, D. W. Auckland, and Y. K. Tong, "Ferroresonance in electromagnetic voltage transformers: a study based on nonlinear dynamics," *Generation, Transmission and Distribution, IEE Proceedings-*, vol. 144, pp. 383-387, 1997.

[12] K. Milicevic and Z. Emin, "Impact of initial conditions on the initiation of ferroresonance," *International Journal of Electrical Power & Energy Systems*, vol. 31, pp. 146-152, 2009.

[13] M. Val Escudero, I. Dudurych, and M. Redfem, "Understanding ferroresonance," in *Universities Power Engineering Conference, 2004. UPEC 2004. 39th International*, 2004, pp. 1262-1266 vol. 2.

[14] M. Val Escudero, I. Dudurych, and M. A. Redfern, "Characterization of ferroresonant modes in HV substation with CB grading capacitors," *Electric Power Systems Research*, vol. 77, pp. 1506-1513, 2007.

[15] E. J. Dolan, D. A. Gillies, and E. W. Kimbark, "Ferroresonance in a Transformer Switched with an EHV Line," *IEEE Transactions on Power Apparatus and Systems*, vol. PAS-91, pp. 1273-1280, 1972.

[16] D. A. N. Jacobson, D. R. Swatek, and R. W. Mazur, "Mitigating potential transformer ferroresonance in a 230 kV converter station," in *Transmission and Distribution Conference, 1996. Proceedings., 1996 IEEE*, 1996, pp. 269-275.

[17] J. B. Wareing and F. Perrot, "Ferroresonance overvoltages in distribution networks," in *Warning! Ferroresonance Can Damage Your Plant (Digest No: 1997/349), IEE Colloquium on*, 1997, pp. 5/1-5/7.

[18] M. Osborne, P. Jarman, C. Charalambous, and Z. D. Wang, "The Impact of Ferroresonance and Low frequency Phenomena on Power Transformers and Transmission Systems," *CIGRE,* 2007.

[19] J. P. Bickford, *Computation of Power System Transients, IEE Monograph Series 18,* 1976.

[20] J. A. Martinez, J. Mahseredjian, and R. A. Walling, "Parameter determination: procedures for modeling system transients," *Power and Energy Magazine, IEEE,* vol. 3, pp. 16-28, 2005.

[21] Z. Emin, B. A. T. Al Zahawi, and Y. K. Tong, "Voltage transformer ferroresonance in 275 kV substation," in *High Voltage Engineering, 1999. Eleventh International Symposium on (Conf. Publ. No. 467),* 1999, pp. 283-286 vol.1.

[22] Z. Emin, B. A. T. Al Zahawi, T. Yu Kwong, and M. Ugur, "Quantification of the chaotic behavior of ferroresonant voltage transformer circuits," *Circuits and Systems I: Fundamental Theory and Applications, IEEE Transactions on,* vol. 48, pp. 757-760, 2001.

[23] S. Mozaffari, S. Henschel, and A. C. Soudack, "Chaotic Feroresonance in Power Transformers," *IEE Proceeding Generation, Transmission and Distribution,* vol. 142, pp. 247-250, May 1995.

[24] Ta-Peng Tsao and Chia-Ching Ning, "Analysis of Ferroresonance Overvoltages at Maanshan Nuclear Power Station in Taiwan," *IEEE Transactions on Power Delivery,* vol. 21, pp. 1006-1012, April 2006.

[25] S. Mozaffari, M. Sameti, and A. C. Soudack, "Effect of Initial Conditions on Chaotic Ferroresonance in Power Transformers," *IEE Proceeding Generation, Transmission and Distribution,* vol. 144, pp. 456 - 460, September 1997.

[26] R. F. Karlicek and E. R. Taylor JR., "Ferroresonance of Grounded Potential Transformers on Ungrounded Power Systems," *AIEE Transactions,* pp. 607-618, August 1959.

[27] R. H. Hopkinson, "Ferroresonance During Single-Phase Switching of 3-Phase Distribution Transformer Banks," *power apparatus and systems, ieee transactions on,* vol. 84, pp. 289-293, 1965.

[28] R. H. Hopkinson, "Ferroresonant Overvoltage Control Based on TNA Tests on Three-Phase Wye-Delta Transformer Banks," *power apparatus and systems, ieee transactions on,* vol. PAS-87, pp. 352-361, 1968.

[29] "Ferroresonance Tests on Brinsworth-Thorpe Marsh 400 kV Circuit," *Technical Report TR(E) 389 Issue 1,* July 2001.

[30] F. S. Young, R. L. Schmid, and P. I. Fergestad, "A Laboratory Investigation of Ferroresonance in Cable-Connected Transformers," *power apparatus and systems, ieee transactions on,* vol. PAS-87, pp. 1240-1249, 1968.

[31] M. Roy and C. K. Roy, "Experiments on Ferroresonance at Various Line Conditions and Its Damping," in *Power System Technology and IEEE Power India Conference, 2008. POWERCON 2008. Joint International Conference on,* 2008, pp. 1-8.

[32] T. Fugel and D. Koeing, "Influence of Grading Capacitors on Breaking Performance of a 24-kV Vacuum Breaker Series Design," *IEEE Transactions on Dielectrics and Electrical Insulation,* vol. 10, pp. 569-575, August 2003.

[33] T. Tran-Quoc and L. Pierrat, "An efficient non linear transformer model and its application to ferroresonance study," *Magnetics, IEEE Transactions on,* vol. 31, pp. 2060-2063, 1995.

[34] T. Tran-Quoc and L. Pierrat, "Correction of the measured Core Losses under Distorted Flux," *IEEE Transactions on Magnetics,* vol. 33, pp. 2045-2048, March 1997.

[35] T. T. Quoc, S. L. Du, D. P. Van, N. N. Khac, and L. T. Dinh, "Temporary overvoltages in the Vietnam 500 kV transmission line," in *Transmission & Distribution Construction, Operation & Live-Line Maintenance Proceedings, 1998. ESMO '98. 1998 IEEE 8th International Conference on*, 1998, pp. 225-230.

[36] J. R. Marti and A. C. Soudack, "Ferroresonance in power systems: fundamental solutions," *Generation, Transmission and Distribution [see also IEE Proceedings-Generation, Transmission and Distribution], IEE Proceedings C,* vol. 138, pp. 321-329, 1991.

[37] C. C. Ning and T. P. Tsao, "Using lattice approach to scan nonlinear resonance region," in *Transmission and Distribution Conference and Exposition, 2003 IEEE PES*, 2003, pp. 13-18 Vol.1.

[38] M. Roy and C. K. Roy, "A study on ferroresonance and its depedence on instant of switching angle of the source voltage," in *Power Systems, 2009. ICPS '09. International Conference on*, 2009, pp. 1-6.

[39] J. Horak, "A review of ferroresonance," in *Protective Relay Engineers, 2004 57th Annual Conference for*, 2004, pp. 1-29.

[40] P. Shein, S. Zissu, and W. Schapiro, "Voltage Transformer Ferroresonance in One 400 Kv Gis Substation," in *Electrical and Electronics Engineers in Israel, 1989. The Sixteenth Conference of*, 1989, pp. 1-5.

[41] A. Belan, Z. Eleschova, and M. Smola, "Resonance overvoltages in electric power networks," in *Power Tech, 2005 IEEE Russia*, 2005, pp. 1-4.

[42] S. Rahimi, W. Wiechowski, J. Ostergaard, and A. H. Nielsen, "Identification of problems when using long high voltage AC cable in transmission system II: Resonance & harmonic resonance," in *Transmission and Distribution Conference and Exposition, 2008. T&D. IEEE/PES*, 2008, pp. 1-8.

[43] R. Rudenberg, *Transient Performance of Electric Power Systems*: McGraw-Hill Book Company, Inc, 1950.

[44] *ATP Rule Book and Theory Book, European EMTP-ATP Users Group e.V. (EEUG),* 2007.

[45] J. A. Martinez, J. Mahseredjian, and B. Khodabakhchian, "Parameter determination for modeling system transients-Part VI: Circuit breakers," *Power Delivery, IEEE Transactions on,* vol. 20, pp. 2079-2085, 2005.

[46] J. A. Martinez-Velasco, "Digital Computation of Electromagnetic Transients in Power Systems. Current Status," in *EEUG News Feb-May*, 1998, pp. 48-70.

[47] "National Grid, UK data sheet, TGN(E)166," February 2002.

[48] T. Tran-Quoc, L. Pierrat, A. Montmeat, and A. Giard, "Harmonic overvoltages in industrial power system with capacitors and saturated transformers," in *Industry Applications Conference, 1995. Thirtieth IAS Annual Meeting, IAS '95., Conference Record of the 1995 IEEE,* 1995, pp. 2206-2210 vol.3.

[49] T. Tran-Quoc and L. Pierrat, "Influence of Random Variables on Protective Current Transformer Transient Performance," in *First International Conference on Digital Power System Simulators (ICDS 95')* College Station, Texas, USA, April 5-7,1995.

[50] Bromwich, "Bromwich Formula," http://mathworld.wolfram.com/Multiple-AngleFormulas.html, 1991.

[51] J. A. Martinez, R. Walling, B. A. Mork, J. Martin-Arnedo, and D. Durbak, "Parameter determination for modeling system transients-Part III: Transformers," *Power Delivery, IEEE Transactions on*, vol. 20, pp. 2051-2062, 2005.

[52] J. A. Martinez and B. A. Mork, "Transformer modeling for low- and mid-frequency transients - a review," *Power Delivery, IEEE Transactions on*, vol. 20, pp. 1625-1632, 2005.

[53] Juan A. Martinez and B. A. Mork, "Transformer Modeling for Low Frequency Transients - The State of the Art," in *International Conference on Power System Transients (IPST 2003)* New Orleans, USA, 2003.

[54] J. A. Martinez-Velasco, "ATP Modeling of Power Transformers," *Technical Notes - EEUG News*, pp. 63 - 76, Aug - Nov 1998.

[55] V. Brandwajn, H. W. Donnel, and I. I. Dommel, "Matrix Representation of Three-Phase N-Winding Transformers for Steady-State and Transient Studies," *Power Apparatus and Systems, IEEE Transactions on*, vol. PAS-101, pp. 1369-1378, 1982.

[56] H. K. Hoidalen, "New Features in ATPDraw ver. 4.0 for advanced simulation of electromagnetic transients in power systems," October 2004, pp. 1-58.

[57] B. A. Mork, F. Gonzalez, D. Ishchenko, D. L. Stuehm, and J. Mitra, "Hybrid Transformer Model for Transient Simulation - Part I: Development and Parmeters," *IEEE Trans. Power Deliv.*, pp. 248-255, 2007.

[58] E. Collin Cherry, "The Duality between Interlinked Electric and Magnetic Circuits and the Formation of Transformer Equivalent Circuits," *Proceedings of the Physical Society, Part B*, vol. 62, pp. 101-111, 1949.

[59] Sung Don Cho, "Parameter Estimation for Transformer Modeling." vol. Ph.D Thesis: Michigan Technological University, USA, 2002.

[60] Hans K. Hoidalen, Bruce A. Mork, Laszlo Prinkler, and James L. Hall, "Implementation of New Features in ATPDraw Version 3," in *International Conference on Power Systems Transients - IPST 2003* New Orleans, USA, 2003.

[61] A. I. Ibrahim, S. Henschel, A. C. Lima, and H. W. Dommel, "Applications of a new EMTP line model for short overhead lines and cables," *International Journal of Electrical Power & Energy Systems*, vol. 24, pp. 639-645, 2002.

[62] *Tutorial on Electromagnetic Transient Program Applications to Power System Protection, IEEE Power Engineering Society (PES)*, 2000.

[63] D. W. Durbak, A. M. Gole, E. H. Camm, M. Marz, R. C. Degeneff, R. P. O'Leary, R. Natarajan, J. A. Martinez-Velasco, K.-C. Lee, A. Morched, R. Shanahan, E. R. Pratico, G. C. Thomann, B. Shperling, A. J. F. Keri, D. A. Woodford, L. Rugeles, V. Rashkes, and A. Sarshar, "Modeling Guidelines for Switching Transients " *Report prepared by Switching Tranient Task Force of IEEE Modeling and Analysis of System Transients Working Group 15.08*.

[64] A. I. Ibrahim, "An Intelligent Support System For The Analysis of Power System Transients." vol. Ph.D Thesis: University of British Columbia, 2000.

[65] J. R. Marti, "Accurate Modeling of Frequency Dependent Transmission Lines in Electromagnetic Transient Simulations," *IEEE Transactions on Power Apparatus and Systems*, vol. PAS-101, pp. 147 - 157, January 1982.

[66] J. R. Marti, L. Marti, and H. W. Dommel, "Transmission Line Models for Steady-State and Transients Analysis," *IEEE/NTUA Athens Power Tech Conference: "Planning Operation and Control of Today's Electric Power Systems"* pp. 744 - 750, Sept 5-8, 1993.

[67] Neville Watson and Jos Arrillaga, *Power Systems Electromagnetic Transients Simulation, IET Power and Energy Seried 39*, 2007.

[68] D. A. N. Jacobson, L. Marti, and R. W. Menzies, "Modeling Ferroresonance in a 230 kV Transformer-Terminated Double-Circuit Transmission Line," *IPST'99 International Conference on Power Systems Transients*, pp. 451-456, June 20-24, 1999.

[69] M. R. Iravani, A. K. S. Chaudhary, W. J. Giesbrecht, I. E. Hassan, A. J. F. Keri, K. C. Lee, J. A. Martinez, A. S. Morched, B. A. Mork, M. Parniani, A. Sharshar, D. Shirmohammadi, R. A. Walling, and D. A. Woodford, "Modeling and analysis guidelines for slow transients. III. The study of ferroresonance," *Power Delivery, IEEE Transactions on*, vol. 15, pp. 255-265, 2000.

[70] G. F. Moore, *Electric Cable Handbook* 3rd Edition ed.: Blackwell Publishing, 1997.

[71] "Transformers Test Report - National Grid."

[72] Y. K. Tong, "NGC experience on ferroresonance in power transformers and voltage transformers on HV transmission systems," *IEE Seminar Digests*, vol. 1997, pp. 4-4, 1997.

[73] T. D. Burton, *Introduction to Dynamic System Analysis*, International Edition ed.: McGraw-Hill.

APPENDIX A

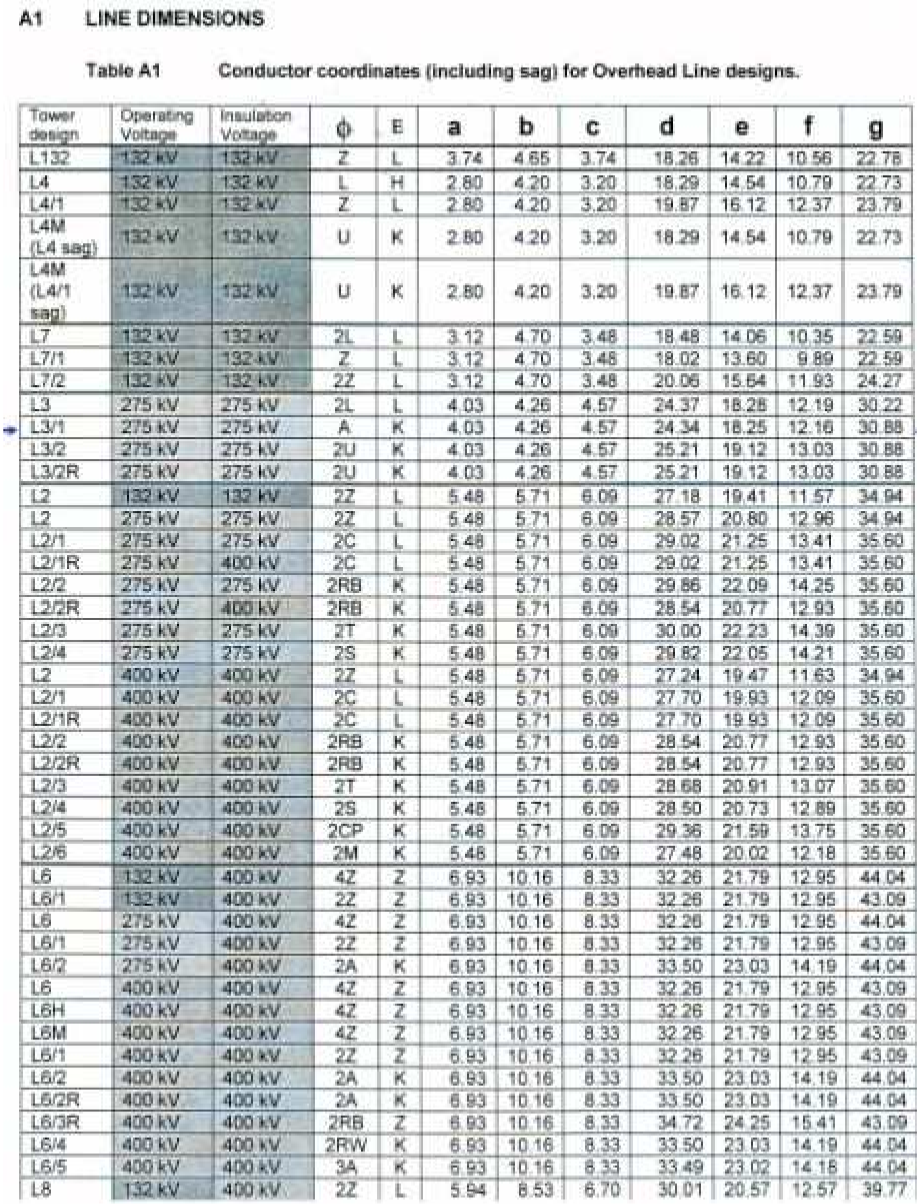

A1 LINE DIMENSIONS

Table A1 Conductor coordinates (including sag) for Overhead Line designs.

Tower design	Operating Voltage	Insulation Voltage	ϕ	E	a	b	c	d	e	f	g
L132	132 kV	132 kV	Z	L	3.74	4.65	3.74	18.26	14.22	10.56	22.78
L4	132 kV	132 kV	L	H	2.80	4.20	3.20	18.29	14.54	10.79	22.73
L4/1	132 kV	132 kV	Z	L	2.80	4.20	3.20	19.87	16.12	12.37	23.79
L4M (L4 sag)	132 kV	132 kV	U	K	2.80	4.20	3.20	18.29	14.54	10.79	22.73
L4M (L4/1 sag)	132 kV	132 kV	U	K	2.80	4.20	3.20	19.87	16.12	12.37	23.79
L7	132 kV	132 kV	2L	L	3.12	4.70	3.48	18.48	14.06	10.35	22.59
L7/1	132 kV	132 kV	Z	L	3.12	4.70	3.48	18.02	13.60	9.89	22.59
L7/2	132 kV	132 kV	2Z	L	3.12	4.70	3.48	20.06	15.64	11.93	24.27
L3	275 kV	275 kV	2L	L	4.03	4.26	4.57	24.37	18.28	12.19	30.22
L3/1	275 kV	275 kV	A	K	4.03	4.26	4.57	24.34	18.25	12.16	30.88
L3/2	275 kV	275 kV	2U	K	4.03	4.26	4.57	25.21	19.12	13.03	30.88
L3/2R	275 kV	275 kV	2U	K	4.03	4.26	4.57	25.21	19.12	13.03	30.88
L2	132 kV	132 kV	2Z	L	5.48	5.71	6.09	27.18	19.41	11.57	34.94
L2	275 kV	275 kV	2Z	L	5.48	5.71	6.09	28.57	20.80	12.96	34.94
L2/1	275 kV	275 kV	2C	L	5.48	5.71	6.09	29.02	21.25	13.41	35.60
L2/1R	275 kV	400 kV	2C	L	5.48	5.71	6.09	29.02	21.25	13.41	35.60
L2/2	275 kV	275 kV	2RB	K	5.48	5.71	6.09	29.86	22.09	14.25	35.60
L2/2R	275 kV	400 kV	2RB	K	5.48	5.71	6.09	28.54	20.77	12.93	35.60
L2/3	275 kV	275 kV	2T	K	5.48	5.71	6.09	30.00	22.23	14.39	35.60
L2/4	275 kV	275 kV	2S	K	5.48	5.71	6.09	29.82	22.05	14.21	35.60
L2	400 kV	400 kV	2Z	L	5.48	5.71	6.09	27.24	19.47	11.63	34.94
L2/1	400 kV	400 kV	2C	L	5.48	5.71	6.09	27.70	19.93	12.09	35.60
L2/1R	400 kV	400 kV	2C	L	5.48	5.71	6.09	27.70	19.93	12.09	35.60
L2/2	400 kV	400 kV	2RB	K	5.48	5.71	6.09	28.54	20.77	12.93	35.60
L2/2R	400 kV	400 kV	2RB	K	5.48	5.71	6.09	28.54	20.77	12.93	35.60
L2/3	400 kV	400 kV	2T	K	5.48	5.71	6.09	28.68	20.91	13.07	35.60
L2/4	400 kV	400 kV	2S	K	5.48	5.71	6.09	28.50	20.73	12.89	35.60
L2/5	400 kV	400 kV	2CP	K	5.48	5.71	6.09	29.36	21.59	13.75	35.60
L2/6	400 kV	400 kV	2M	K	5.46	5.71	6.09	27.48	20.02	12.18	35.60
L6	132 kV	400 kV	4Z	Z	6.93	10.16	8.33	32.26	21.79	12.95	44.04
L6/1	132 kV	400 kV	2Z	Z	6.93	10.16	8.33	32.26	21.79	12.95	43.09
L6	275 kV	400 kV	4Z	Z	6.93	10.16	8.33	32.26	21.79	12.95	44.04
L6/1	275 kV	400 kV	2Z	Z	6.93	10.16	8.33	32.26	21.79	12.95	43.09
L6/2	275 kV	400 kV	2A	K	6.93	10.16	8.33	33.50	23.03	14.19	44.04
L6	400 kV	400 kV	4Z	Z	6.93	10.16	8.33	32.26	21.79	12.95	43.09
L6H	400 kV	400 kV	4Z	Z	6.93	10.16	8.33	32.26	21.79	12.95	43.09
L6M	400 kV	400 kV	4Z	Z	6.93	10.16	8.33	32.26	21.79	12.95	43.09
L6/1	400 kV	400 kV	2Z	Z	6.93	10.16	8.33	32.26	21.79	12.95	43.09
L6/2	400 kV	400 kV	2A	K	6.93	10.16	8.33	33.50	23.03	14.19	44.04
L6/2R	400 kV	400 kV	2A	K	6.93	10.16	8.33	33.50	23.03	14.19	44.04
L6/3R	400 kV	400 kV	2RB	Z	6.93	10.16	8.33	34.72	24.25	15.41	43.09
L6/4	400 kV	400 kV	2RW	K	6.93	10.16	8.33	33.50	23.03	14.19	44.04
L6/5	400 kV	400 kV	3A	K	6.93	10.16	8.33	33.49	23.02	14.18	44.04
L8	132 kV	400 kV	2Z	L	5.94	8.53	6.70	30.01	20.57	12.57	39.77

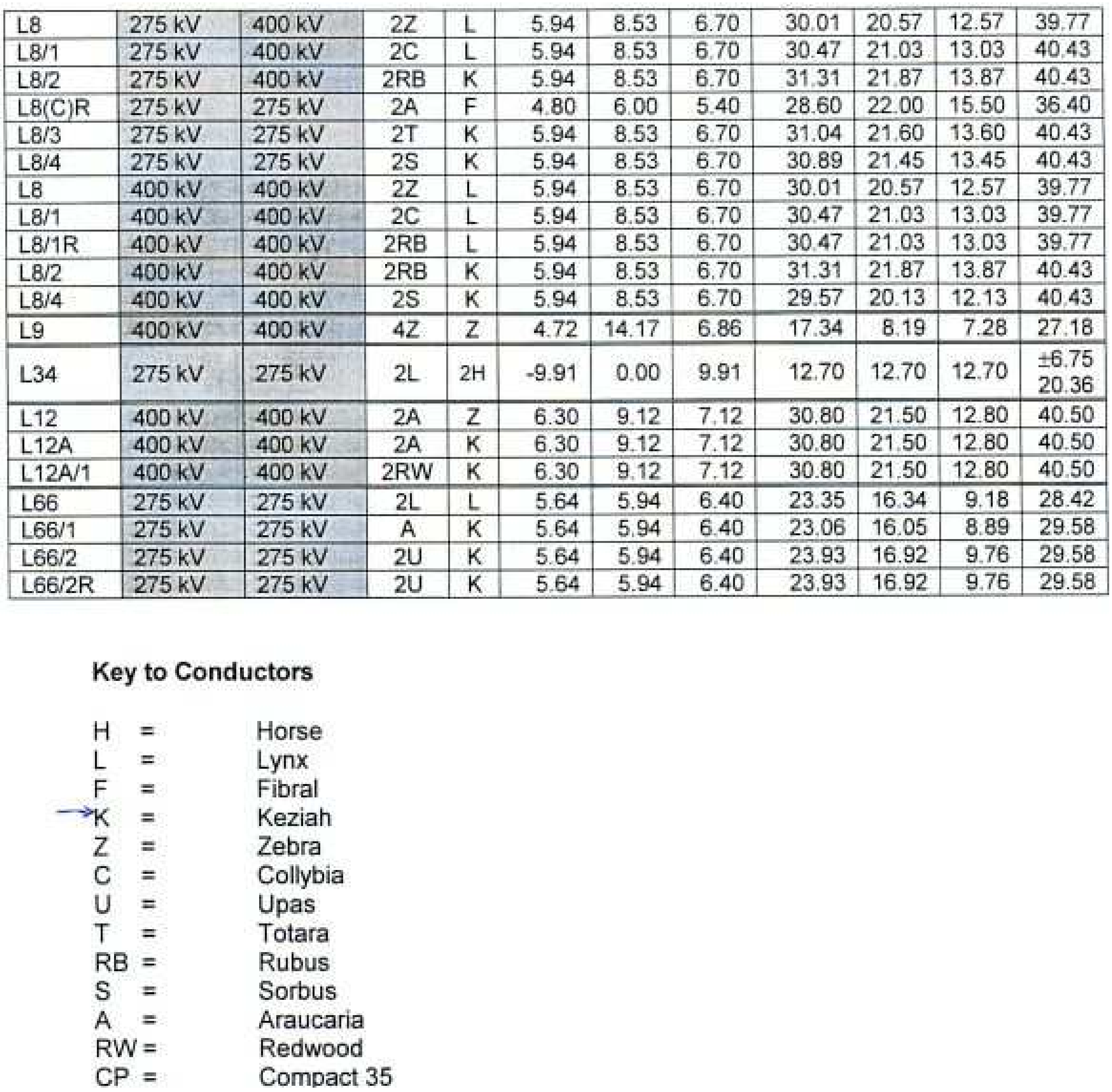

L8	275 kV	400 kV	2Z	L	5.94	8.53	6.70	30.01	20.57	12.57	39.77
L8/1	275 kV	400 kV	2C	L	5.94	8.53	6.70	30.47	21.03	13.03	40.43
L8/2	275 kV	400 kV	2RB	K	5.94	8.53	6.70	31.31	21.87	13.87	40.43
L8(C)R	275 kV	275 kV	2A	F	4.80	6.00	5.40	28.60	22.00	15.50	36.40
L8/3	275 kV	275 kV	2T	K	5.94	8.53	6.70	31.04	21.60	13.60	40.43
L8/4	275 kV	275 kV	2S	K	5.94	8.53	6.70	30.89	21.45	13.45	40.43
L8	400 kV	400 kV	2Z	L	5.94	8.53	6.70	30.01	20.57	12.57	39.77
L8/1	400 kV	400 kV	2C	L	5.94	8.53	6.70	30.47	21.03	13.03	39.77
L8/1R	400 kV	400 kV	2RB	L	5.94	8.53	6.70	30.47	21.03	13.03	39.77
L8/2	400 kV	400 kV	2RB	K	5.94	8.53	6.70	31.31	21.87	13.87	40.43
L8/4	400 kV	400 kV	2S	K	5.94	8.53	6.70	29.57	20.13	12.13	40.43
L9	400 kV	400 kV	4Z	Z	4.72	14.17	6.86	17.34	8.19	7.28	27.18
L34	275 kV	275 kV	2L	2H	-9.91	0.00	9.91	12.70	12.70	12.70	±6.75 20.36
L12	400 kV	400 kV	2A	Z	6.30	9.12	7.12	30.80	21.50	12.80	40.50
L12A	400 kV	400 kV	2A	K	6.30	9.12	7.12	30.80	21.50	12.80	40.50
L12A/1	400 kV	400 kV	2RW	K	6.30	9.12	7.12	30.80	21.50	12.80	40.50
L66	275 kV	275 kV	2L	L	5.64	5.94	6.40	23.35	16.34	9.18	28.42
L66/1	275 kV	275 kV	A	K	5.64	5.94	6.40	23.06	16.05	8.89	29.58
L66/2	275 kV	275 kV	2U	K	5.64	5.94	6.40	23.93	16.92	9.76	29.58
L66/2R	275 kV	275 kV	2U	K	5.64	5.94	6.40	23.93	16.92	9.76	29.58

Key to Conductors

H = Horse
L = Lynx
F = Fibral
→K = Keziah
Z = Zebra
C = Collybia
U = Upas
T = Totara
RB = Rubus
S = Sorbus
A = Araucaria
RW = Redwood
CP = Compact 35

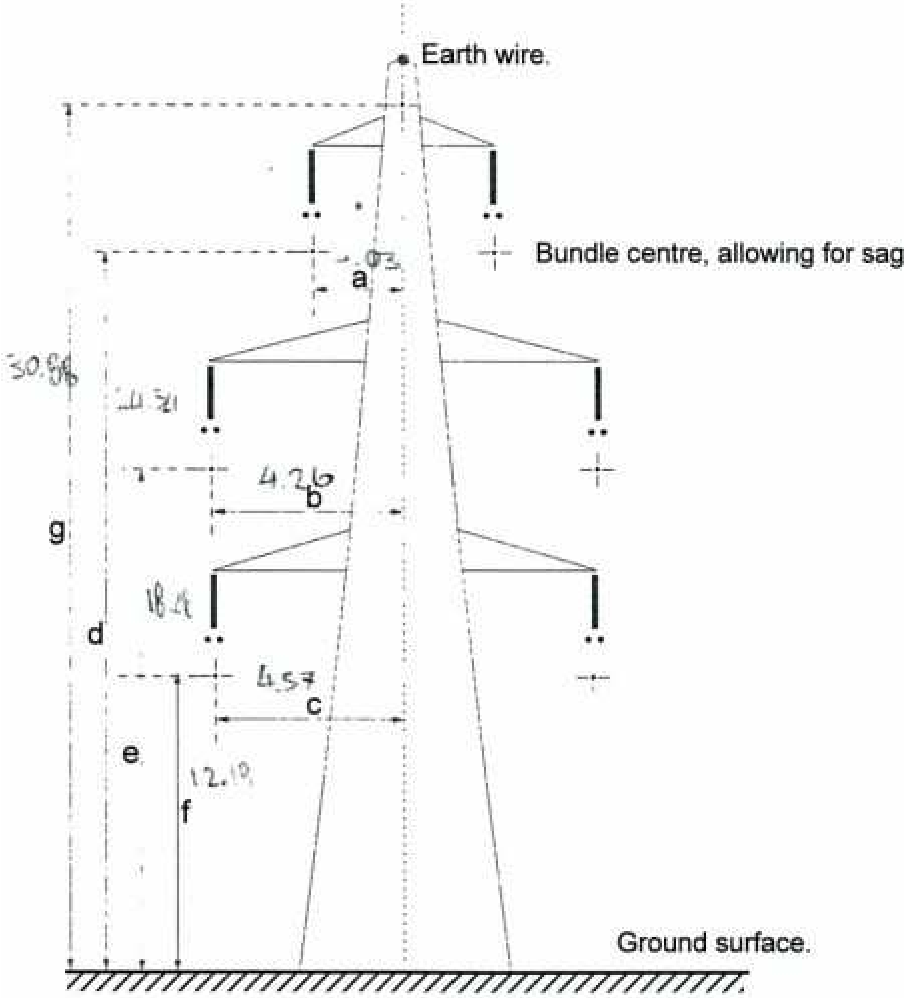

Figure A1. Conductor coordinates of overhead lines – refer to Table A1.

A2 CONDUCTOR PARAMETERS

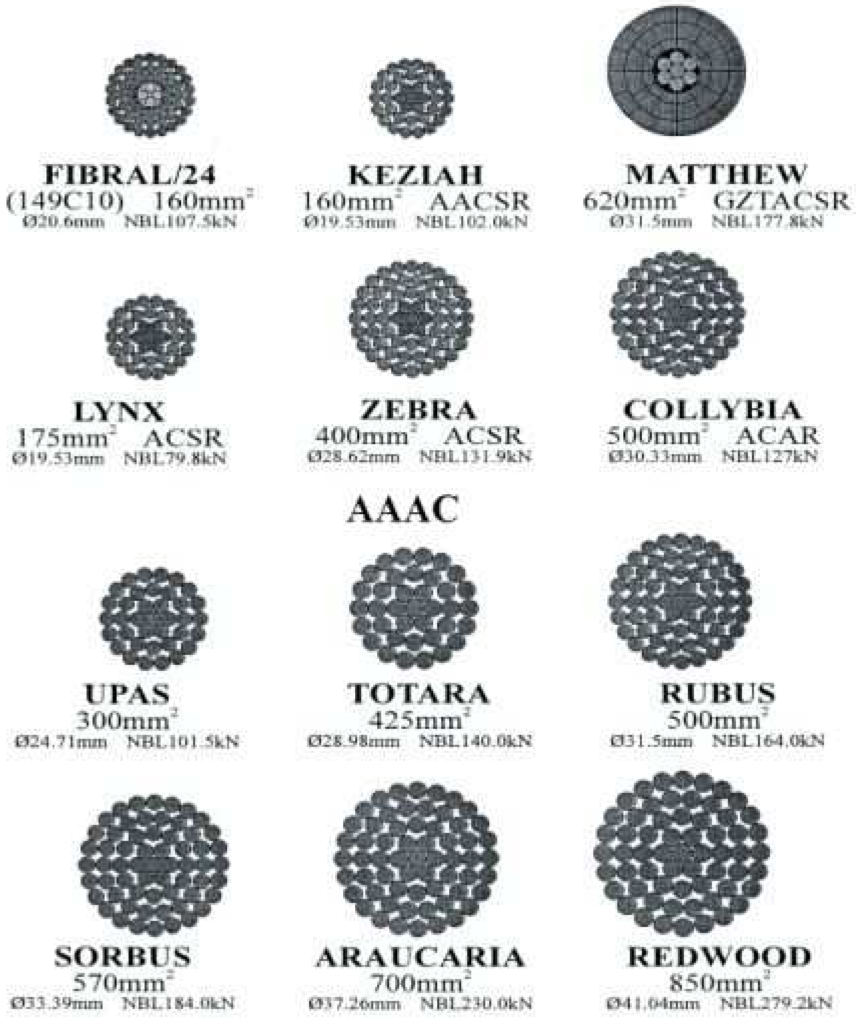

Figure A2 The Common Conductor Types

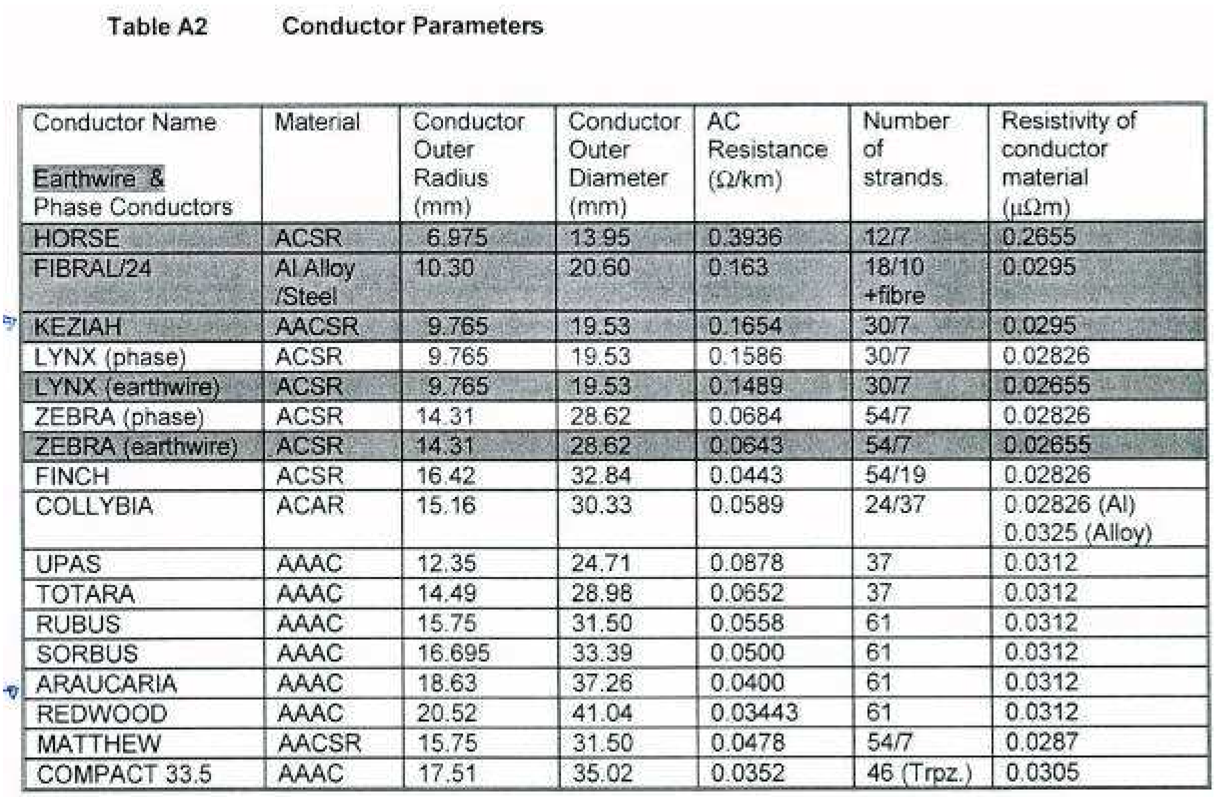

Table A2 Conductor Parameters

Conductor Name Earthwire & Phase Conductors	Material	Conductor Outer Radius (mm)	Conductor Outer Diameter (mm)	AC Resistance (Ω/km)	Number of strands.	Resistivity of conductor material (μΩm)
HORSE	ACSR	6.975	13.95	0.3936	12/7	0.2655
FIBRAL/24	Al Alloy /Steel	10.30	20.60	0.163	18/10 +fibre	0.0295
KEZIAH	AACSR	9.765	19.53	0.1654	30/7	0.0295
LYNX (phase)	ACSR	9.765	19.53	0.1586	30/7	0.02826
LYNX (earthwire)	ACSR	9.765	19.53	0.1489	30/7	0.02655
ZEBRA (phase)	ACSR	14.31	28.62	0.0684	54/7	0.02826
ZEBRA (earthwire)	ACSR	14.31	28.62	0.0643	54/7	0.02655
FINCH	ACSR	16.42	32.84	0.0443	54/19	0.02826
COLLYBIA	ACAR	15.16	30.33	0.0589	24/37	0.02826 (Al) 0.0325 (Alloy)
UPAS	AAAC	12.35	24.71	0.0878	37	0.0312
TOTARA	AAAC	14.49	28.98	0.0652	37	0.0312
RUBUS	AAAC	15.75	31.50	0.0558	61	0.0312
SORBUS	AAAC	16.695	33.39	0.0500	61	0.0312
ARAUCARIA	AAAC	18.63	37.26	0.0400	61	0.0312
REDWOOD	AAAC	20.52	41.04	0.03443	61	0.0312
MATTHEW	AACSR	15.75	31.50	0.0478	54/7	0.0287
COMPACT 33.5	AAAC	17.51	35.02	0.0352	46 (Trpz.)	0.0305

APPENDIX B

Appendix B1 – Lumped Parameter

(1) Line parameters check

Firstly, the elements of the modeled line in ATPDraw such as the resistance, inductance and the capacitance are compared with the ones determined from MATLAB. The comparison between them is shown in Table B1 and Table B2 and the results suggest that both of them agreed well with each other.

The equivalent of the lumped parameters of the 37 km un-transposed double-circuit transmission are derived by using the ‘LINE PARAMETERS’ supporting routine in ATP-EMTP and validated by using MATLAB.

Table B1: Equivalent capacitance matrix in farads/km derived from ATP-EMTP

1	1.0137E-08					
2	-1.9887E-09	1.0469E-08				
3	-6.3986E-10	-1.9168E-09	1.0783E-08			
4	-1.4912E-09	-7.2185E-10	-3.8463E-10	1.0137E-08		
5	-7.2185E-10	-6.2432E-10	-5.3740E-10	-1.9887E-09	1.0469E-08	
6	-3.8463E-10	-5.3740E-10	-8.5257E-10	-6.3986E-10	-1.9168E-09	1.0783E-08

(a) capacitance matrix in farads/km for the system of equivalent phase conductors

1	5.8718E-02 4.6352E-01					
2	3.6893E-02 1.7754E-01	5.7761E-02 4.8452E-01				
3	3.6721E-02 1.4427E-01	3.7009E-02 1.9684E-01	5.8483E-02 4.9292E-01			
4	3.7695E-02 1.4982E-01	3.6837E-02 1.3887E-01	3.6674E-02 1.3049E-01	5.8718E-02 4.6352E-01		
5	3.6837E-02 1.3887E-01	3.6683E-02 1.4759E-01	3.6932E-02 1.5142E-01	3.6893E-02 1.7754E-01	5.7761E-02 4.8452E-01	
6	3.6674E-02 1.3049E-01	3.6932E-02 1.5142E-01	3.7427E-02 1.7153E-01	3.6721E-02 1.4427E-01	3.7009E-02 1.9684E-01	5.8483E-02 4.9292E-01

(b) Impedance matrix in ohms/km for the system of equivalent phase conductors

Equivalent Impedance and capacitance derive from MATLAB is shown in Table B2.

Table B2: Equivalent Impedance and capacitance derived from MATLAB

1.0137E-08	-1.9889E-09	-6.4026E-10	-1.4913E-09	-7.2196E-10	-3.8303E-10
-1.9889E-09	1.0468E-08	-1.9175E-09	-7.2207E-10	-6.2477E-10	-5.3351E-10
-6.4026E-10	-1.9175E-09	1.0782E-08	-3.8507E-10	-5.3840E-10	-8.4472E-10
-1.4913E-09	-7.2207E-10	-3.8507E-10	1.0137E-08	-1.9883E-09	-6.4010E-10
-7.2196E-10	-6.2477E-10	-5.3840E-10	-1.9883E-09	1.0471E-08	-1.9216E-09
-3.8303E-10	-5.3351E-10	-8.4472E-10	-6.4010E-10	-1.9216E-09	1.0782E-08

(a) capacitance matrix in farads/km

5.8700E-02	3.6800E-02	3.6700E-02	3.7700E-02	3.6800E-02	3.6600E-02
3.6800E-02	5.7700E-02	3.7000E-02	3.6800E-02	3.6600E-02	3.6900E-02
3.6700E-02	3.7000E-02	5.8500E-02	3.6700E-02	3.6900E-02	3.7400E-02
3.7700E-02	3.6800E-02	3.6700E-02	5.8700E-02	3.6800E-02	3.6700E-02
3.6800E-02	3.6600E-02	3.6900E-02	3.6800E-02	5.7700E-02	3.7000E-02
3.6600E-02	3.6900E-02	3.7400E-02	3.6700E-02	3.7000E-02	5.8500E-02

(b) Resistance matrix in ohms/km

1.4754E-03	5.6609E-04	4.5958E-04	4.7685E-04	4.4292E-04	4.1527E-04
5.6609E-04	1.5430E-03	6.2672E-04	4.4292E-04	4.7037E-04	4.8131E-04
4.5958E-04	6.2672E-04	1.5688E-03	4.1565E-04	4.8203E-04	5.4456E-04
4.7685E-04	4.4292E-04	4.1565E-04	1.4754E-03	5.6609E-04	4.5959E-04
4.4292E-04	4.7037E-04	4.8203E-04	5.6609E-04	1.5430E-03	6.2715E-04
4.1527E-04	4.8131E-04	5.4456E-04	4.5959E-04	6.2715E-04	1.5688E-03

(c) Inductance matrix in ohms/km

As can be seen from both Tables B1 and B2, the self and mutual impedances, and capacitances derived from both methods have shown a good agreement between each other.

(2) Line parameters frequency scan check

Here, the overview performance of the developed line model that is developed in the PI model is verified with the line model with an exact PI equivalent (baseline) as a function of frequency. The aim here is to check the parameters of the modeled line operating at a required specific frequency range are being modeled correctly. As ferroresonance is a low frequency phenomenon which has a frequency range from 0.1 Hz to 1 kHz, then the developed line is put into test by sweeping over a range of frequency from 1 Hz up to 10 kHz to see whether it is able to represent its parameters correctly for ferroresonance study. The outcomes of the frequency scans are shown in Figure B1 to Figure B6, displaying the positive-sequence impedance, the zero-sequence impedance and the mutual-sequence impedances with all the three phases, labelled as Red, Yellow and Blue phases.

PI model

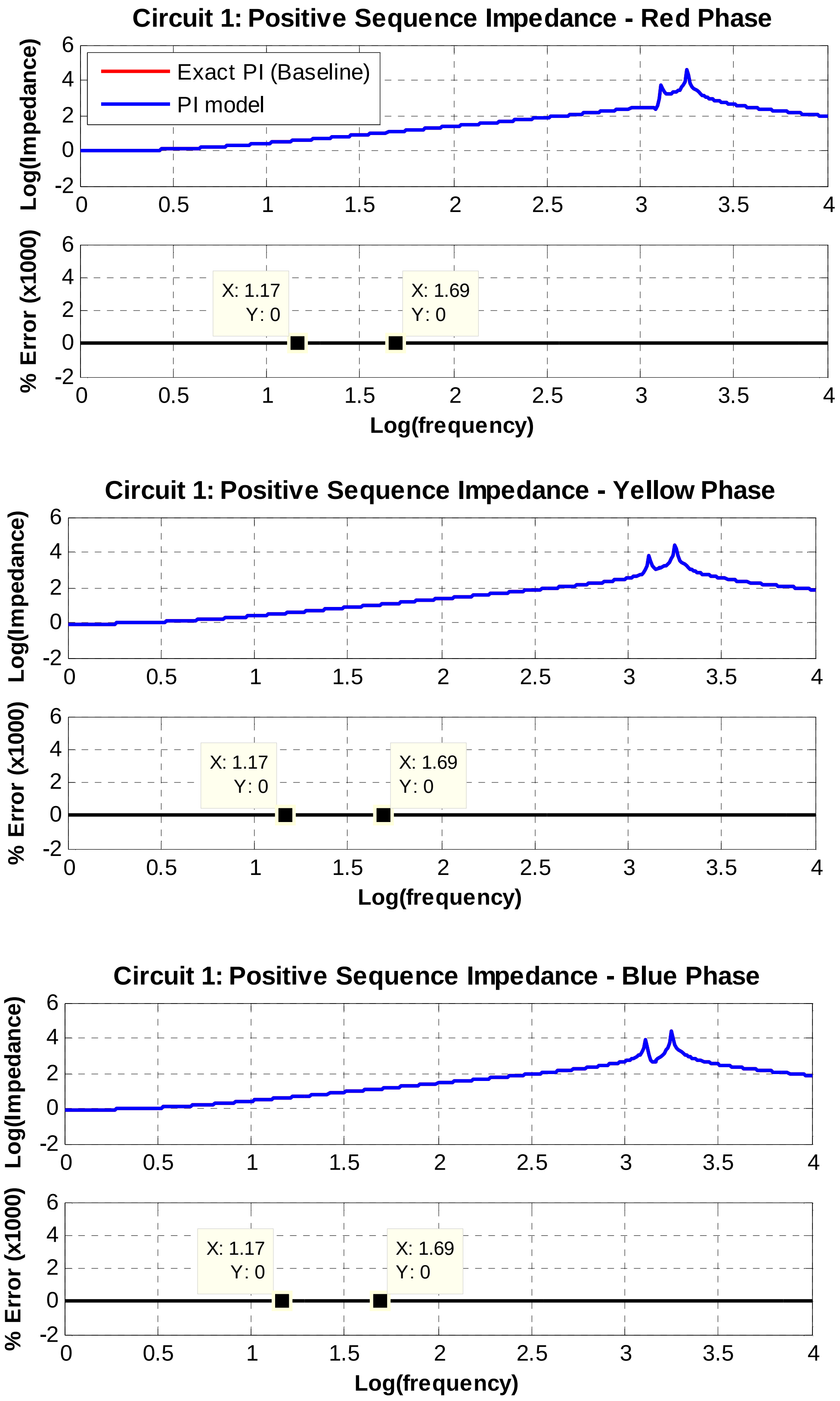

Figure B1: Circuit 1: Positive sequence impedance for phase red, yellow and blue

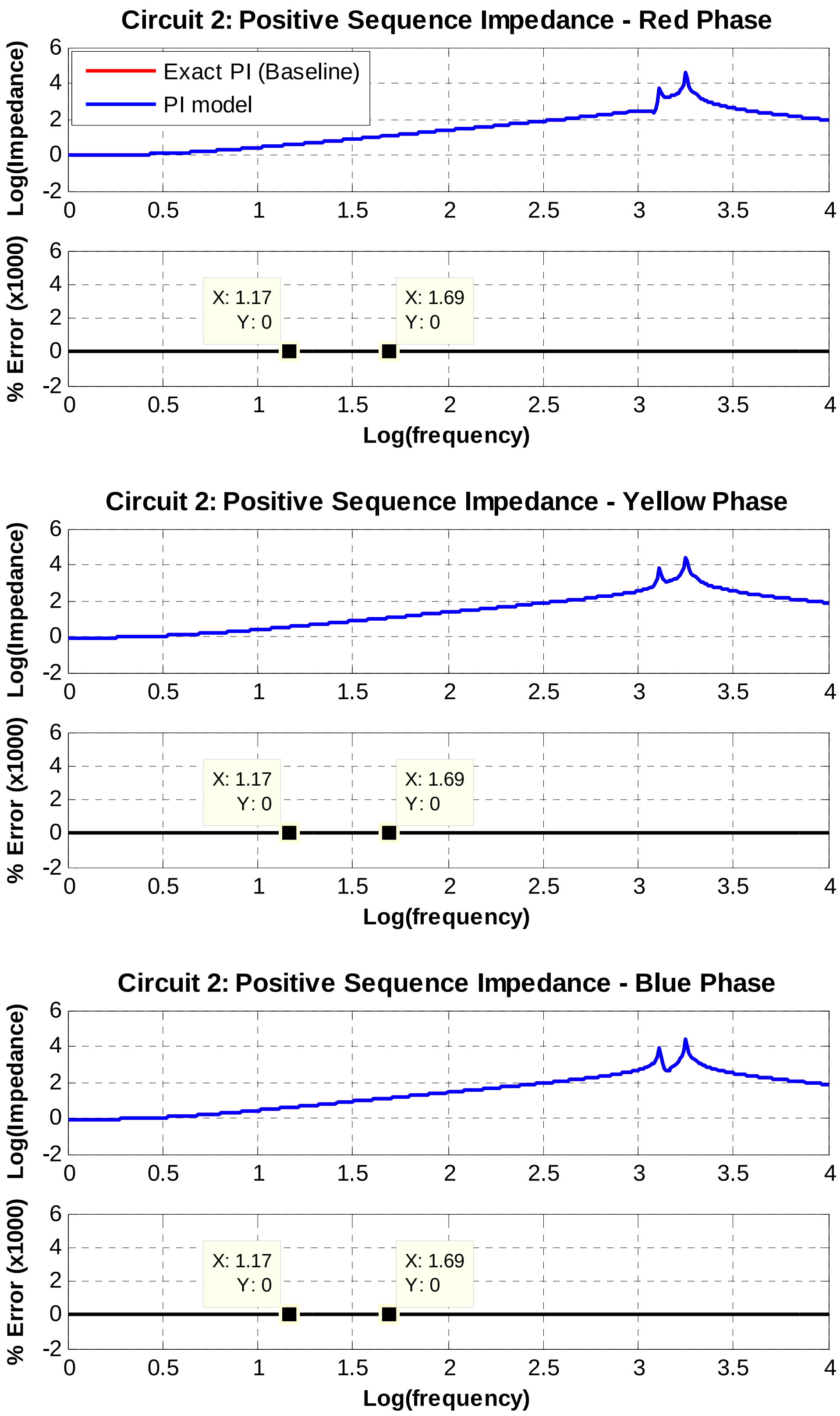

Figure B2: Circuit 2: Positive sequence impedance for phase red, yellow and blue

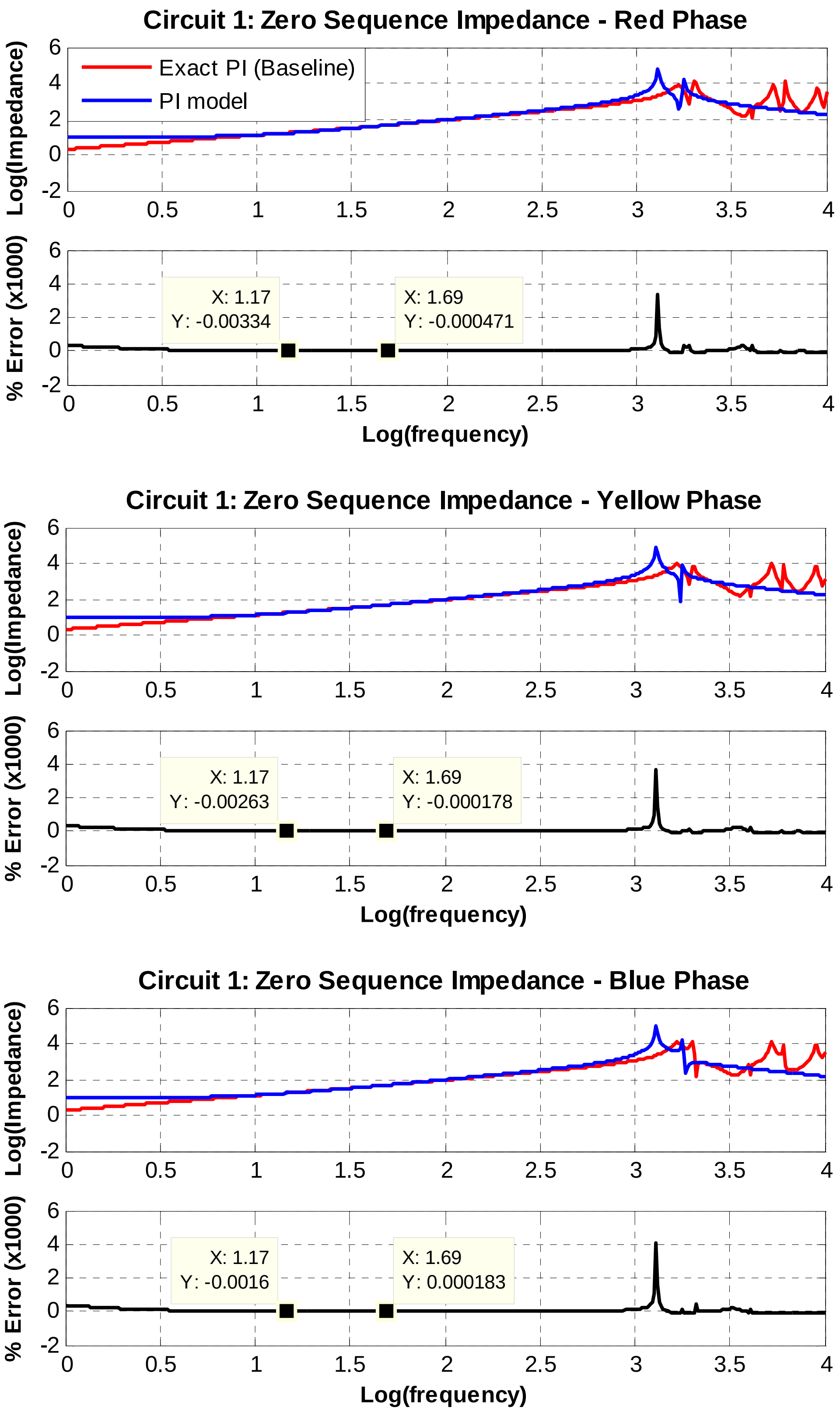

Figure B3: Circuit 1: Zero sequence impedance for phase red, yellow and blue

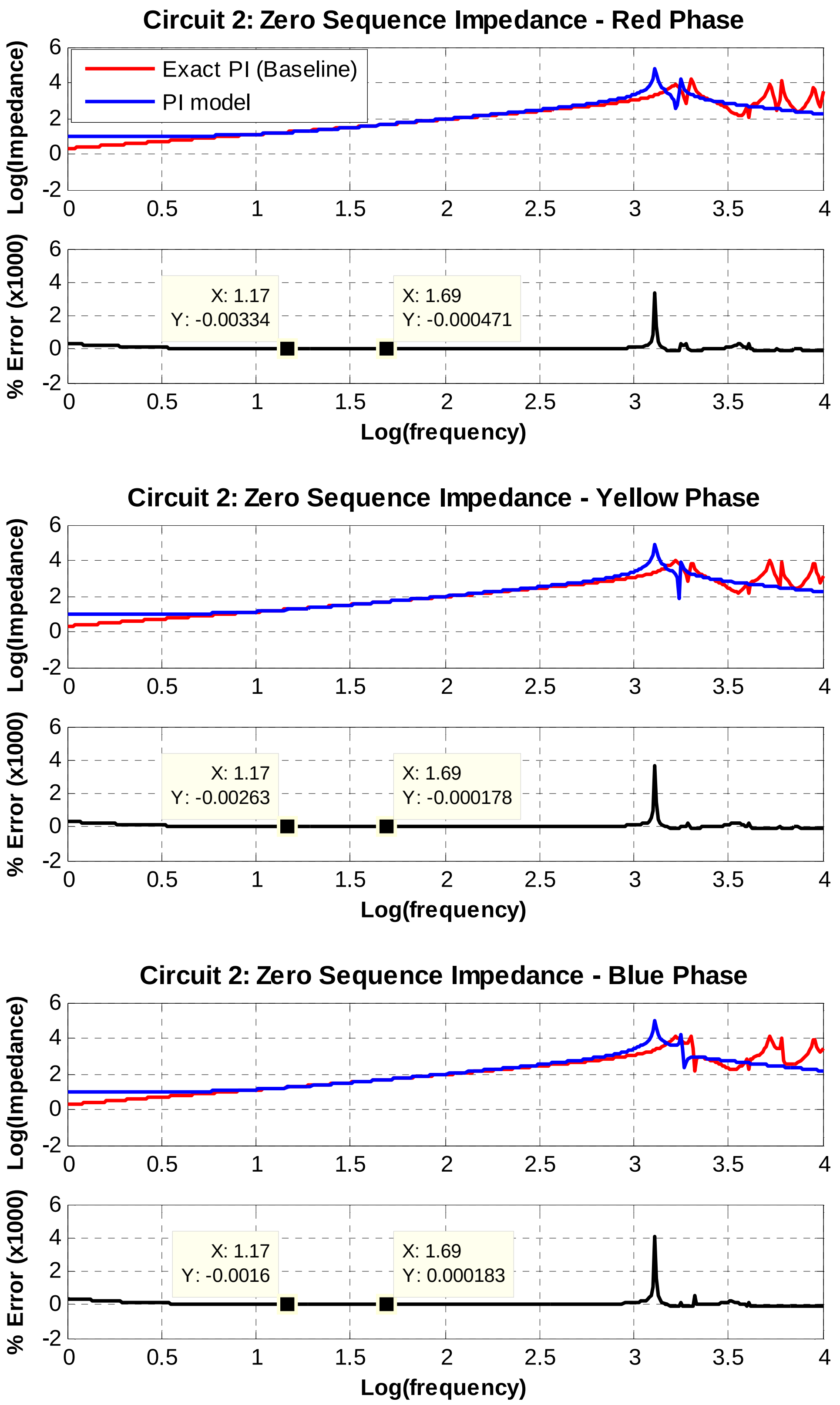

Figure B4: Circuit 2: Zero sequence impedance for phase red, yellow and blue

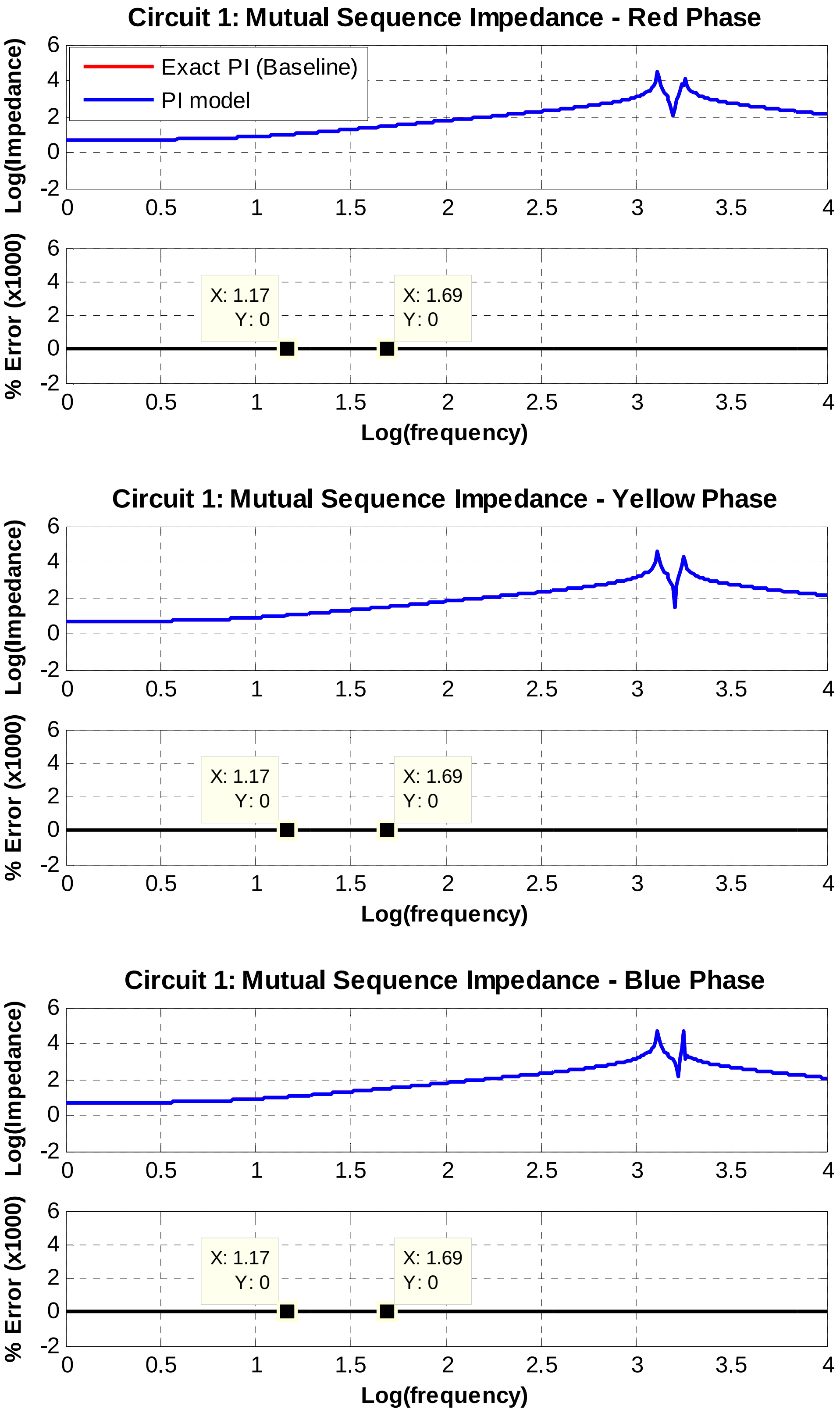

Figure B5: Circuit 1: Mutual sequence impedance for phase red, yellow and blue

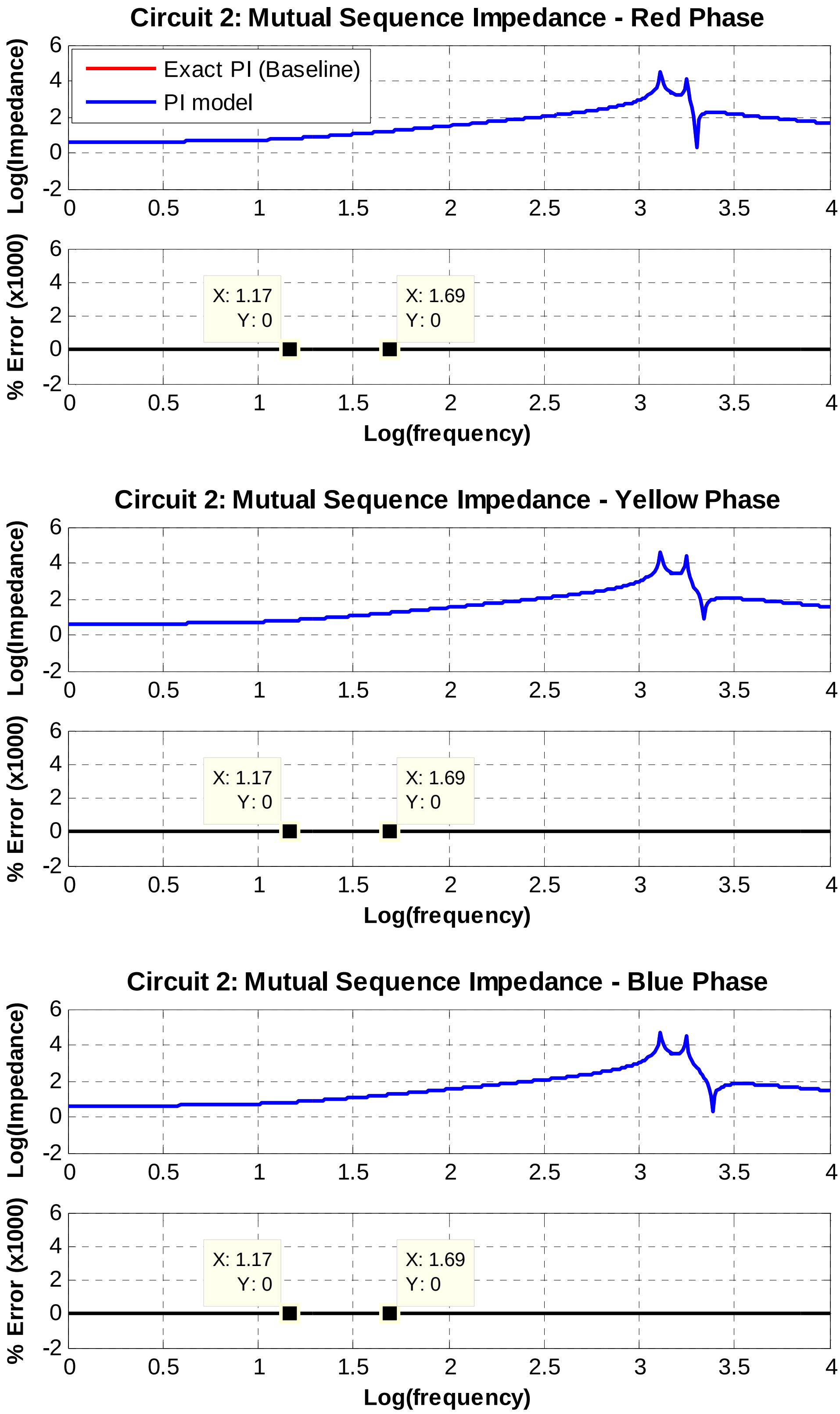

Figure B6: Circuit 2: Mutual sequence impedance for phase red, yellow and blue

As it is expected that the line is able to model correctly for Period-1 and Periofd-3 therefore the percentage errors of the impedance reproduced by the modeled line at frequencies of 15 Hz and 50 Hz are compared with the ones generated from the baseline model. The results are presented in Table B3 suggest that the errors reproduced by the modeled line are relatively low and in good accuracy.

Table B3: Percentage errors of modeled line in PI

	Circuit 1						**Circuit 2**					
Baseline Exact PI	**Line Red**		**Line Yellow**		**Line Blue**		**Line Red**		**Line Yellow**		**Line Blue**	
Frequency (Hz)	**15**	**50**	**15**	**50**	**15**	**50**	**15**	**50**	**15**	**50**	**15**	**50**
Modeled line in PI	**Positive sequence (% Error)**											
	0	0	0	0	0	0	0	0	0	0	0	0
	Zero sequence (%Error)											
	-3.3	0.5	-2.6	-0.2	-1.6	0.2	-3.3	-0.5	-2.6	-0.2	-1.6	0.2
	Mutual sequence (% Error)											
	0	0	0	0	0	0	0	0	0	0	0	0

Appendix B2 – Distributed Parameter

Once the line has been setup accordingly in the predefined model, the next step is to verify the line such that it is accurately be represented for modeling of ferroresonance. Since experimental results are not available for comparing purposes, the way to deal with this is to carry out the line checks as follows;

(1) Line parameters frequency scan check

Similar to PI model, the performance of the developed line in Bergeron and J. Marti models are verified with the baseline as a function of frequency. Similar to the previous way, the results from the scans are presented as shown in Figure B7 to Figure B12 for Bergeron model and Figure B13 to Figure B18 for J. Marti model.

Bergeron model

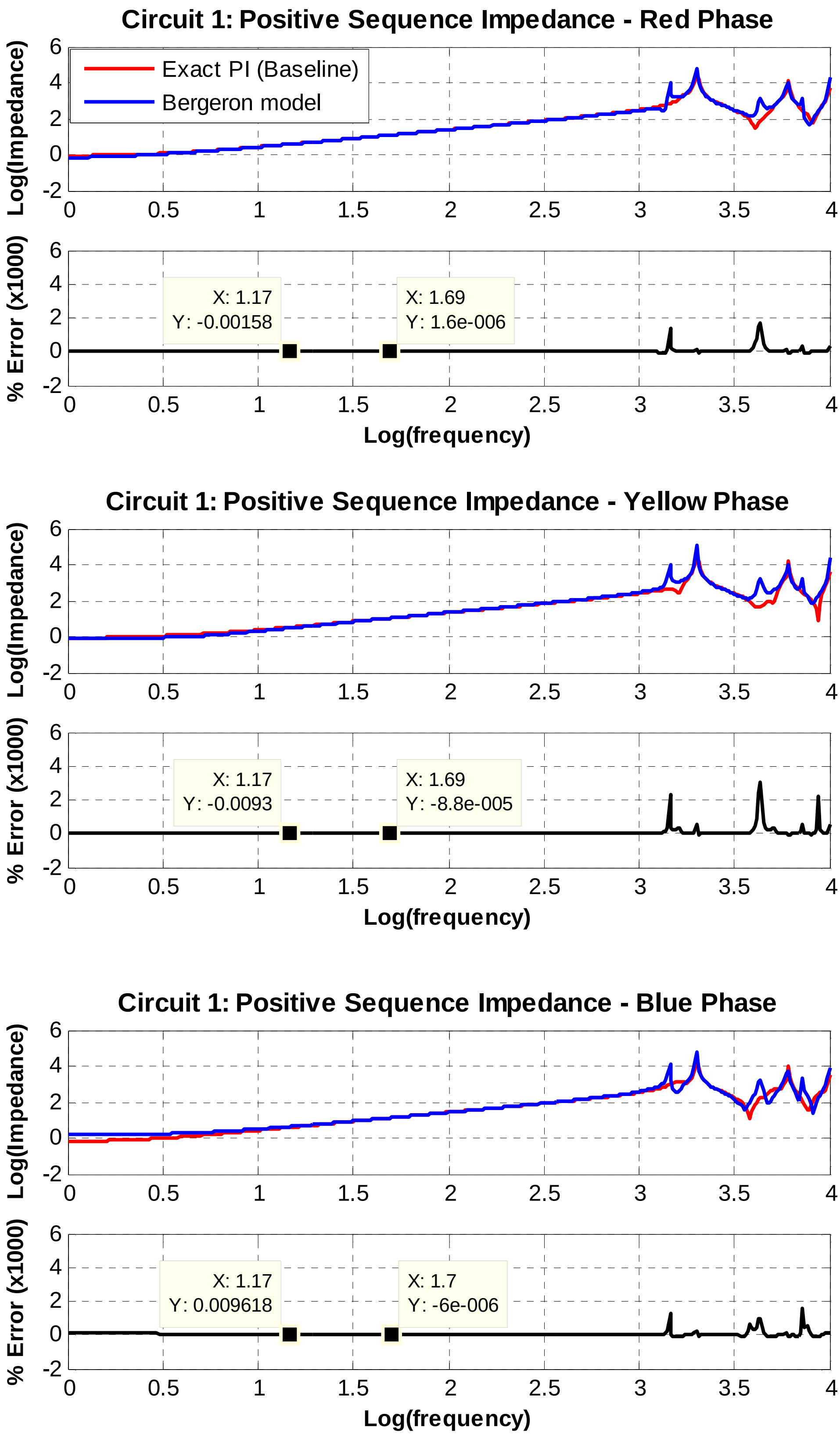

Figure B7: Circuit 1: Positive sequence impedance for phase red, yellow and blue

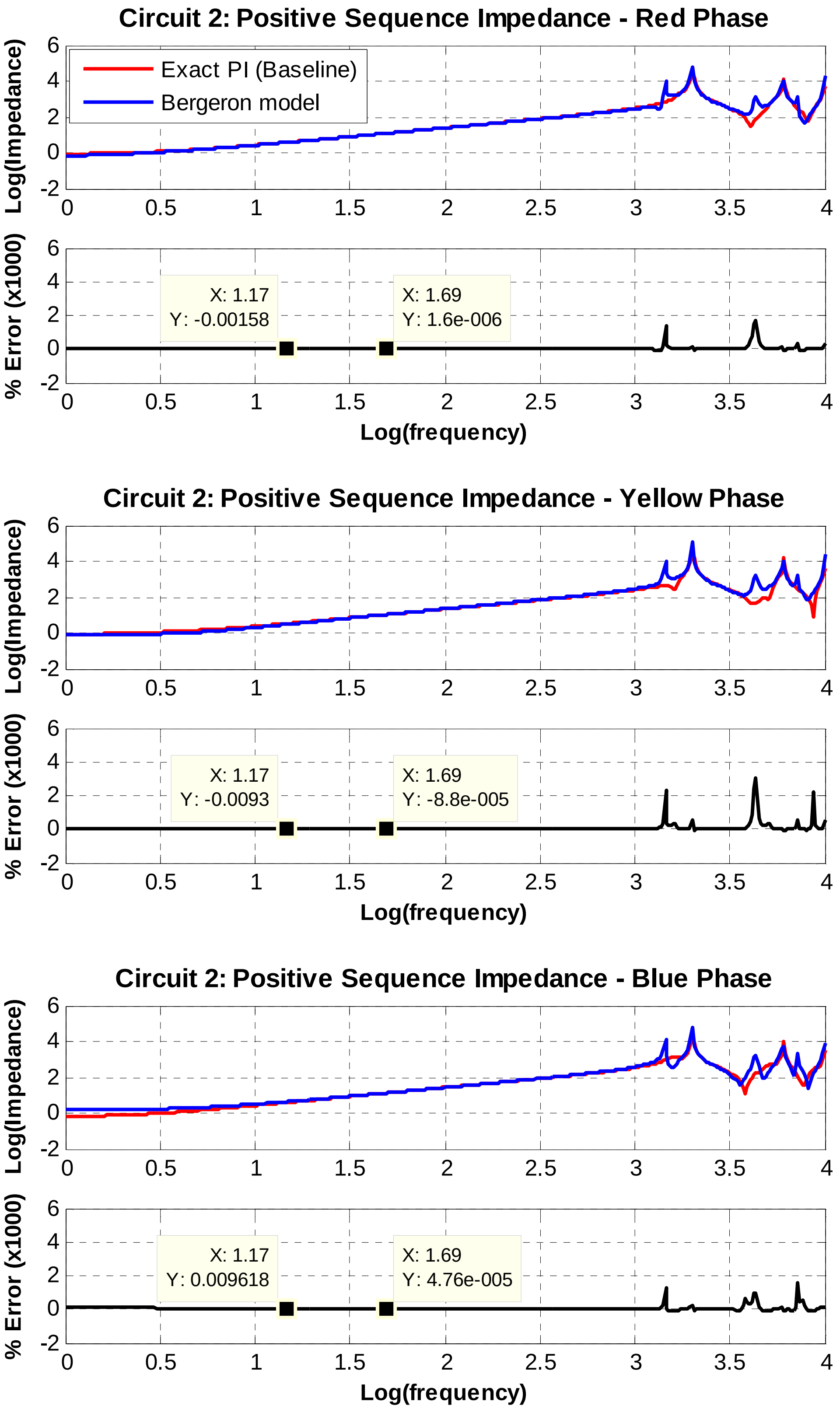

Figure B8: Circuit 2: Positive sequence impedance for phase red, yellow and blue

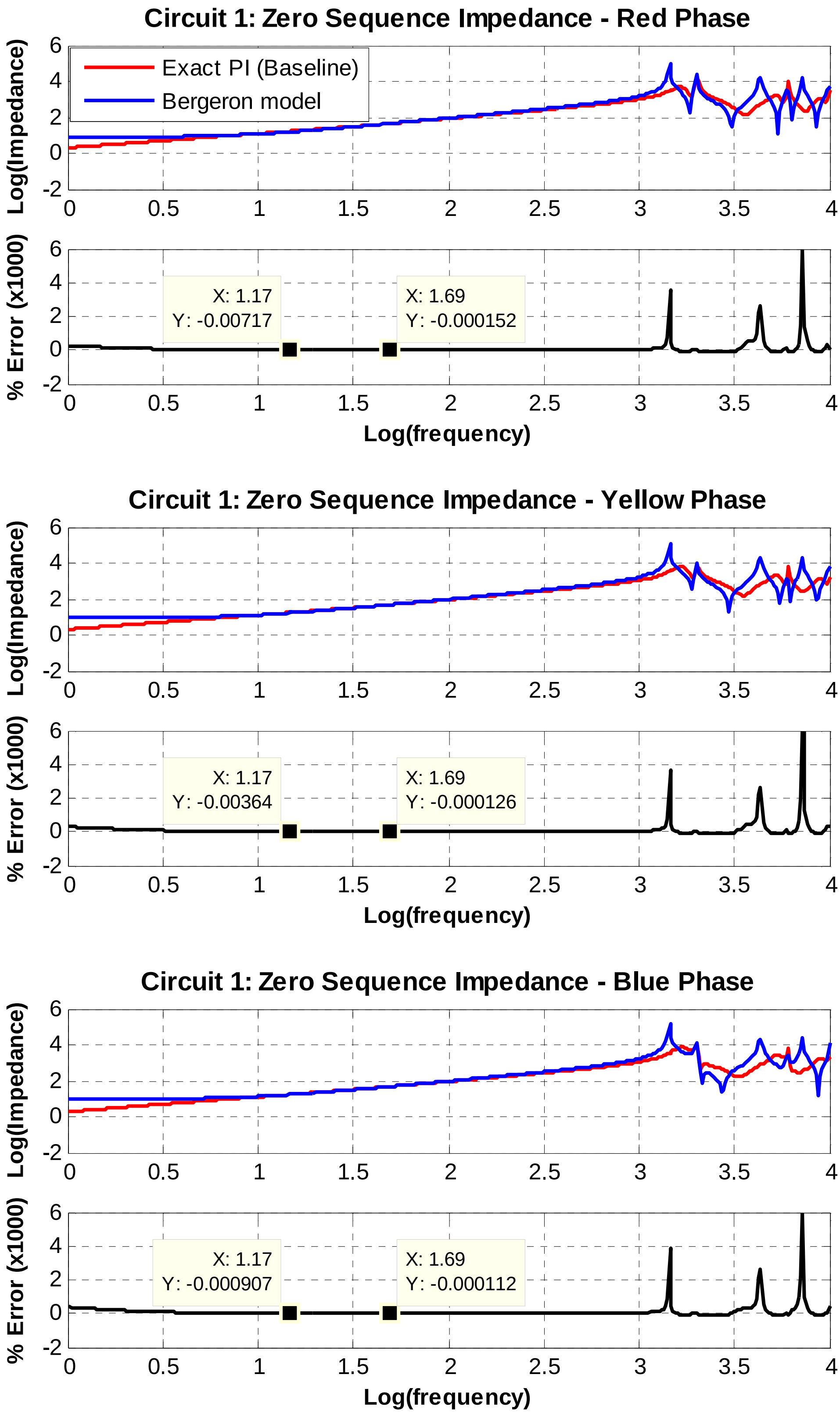

Figure B9: Circuit 1: Zero sequence impedance for phase red, yellow and blue

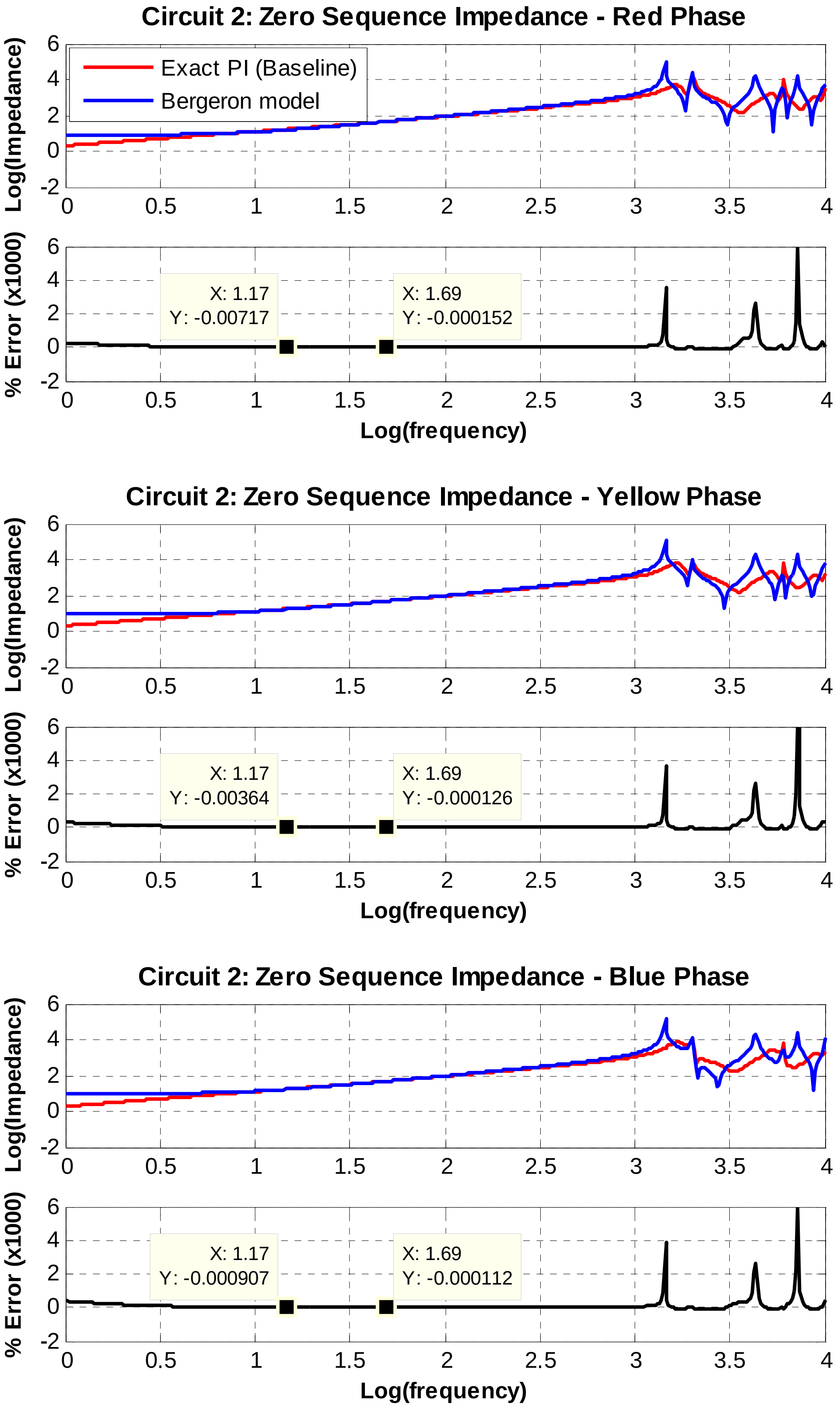

Figure B10: Circuit 2: Zero sequence impedance for phase red, yellow and blue

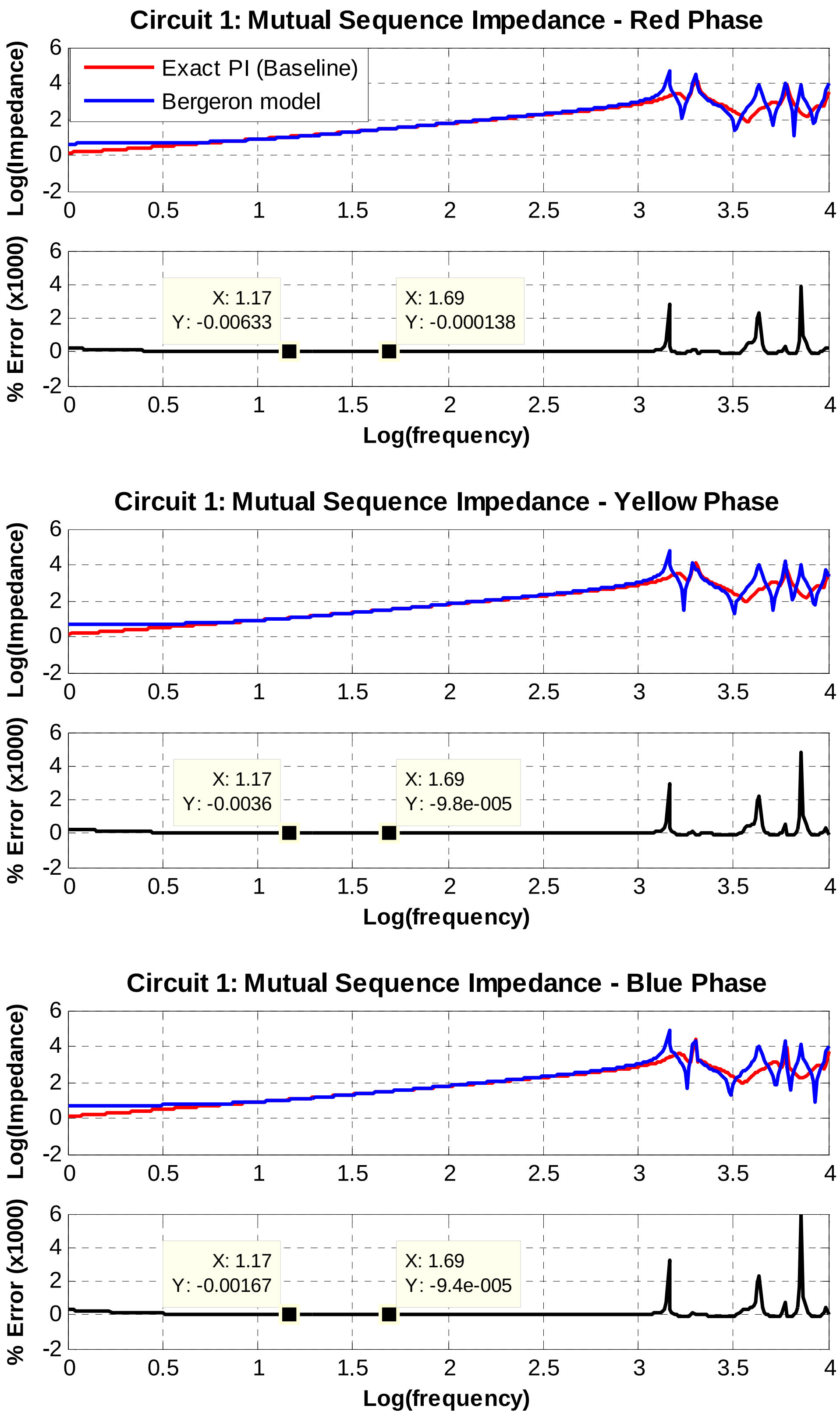

Figure B11: Circuit 1: Mutual sequence impedance for phase red, yellow and blue

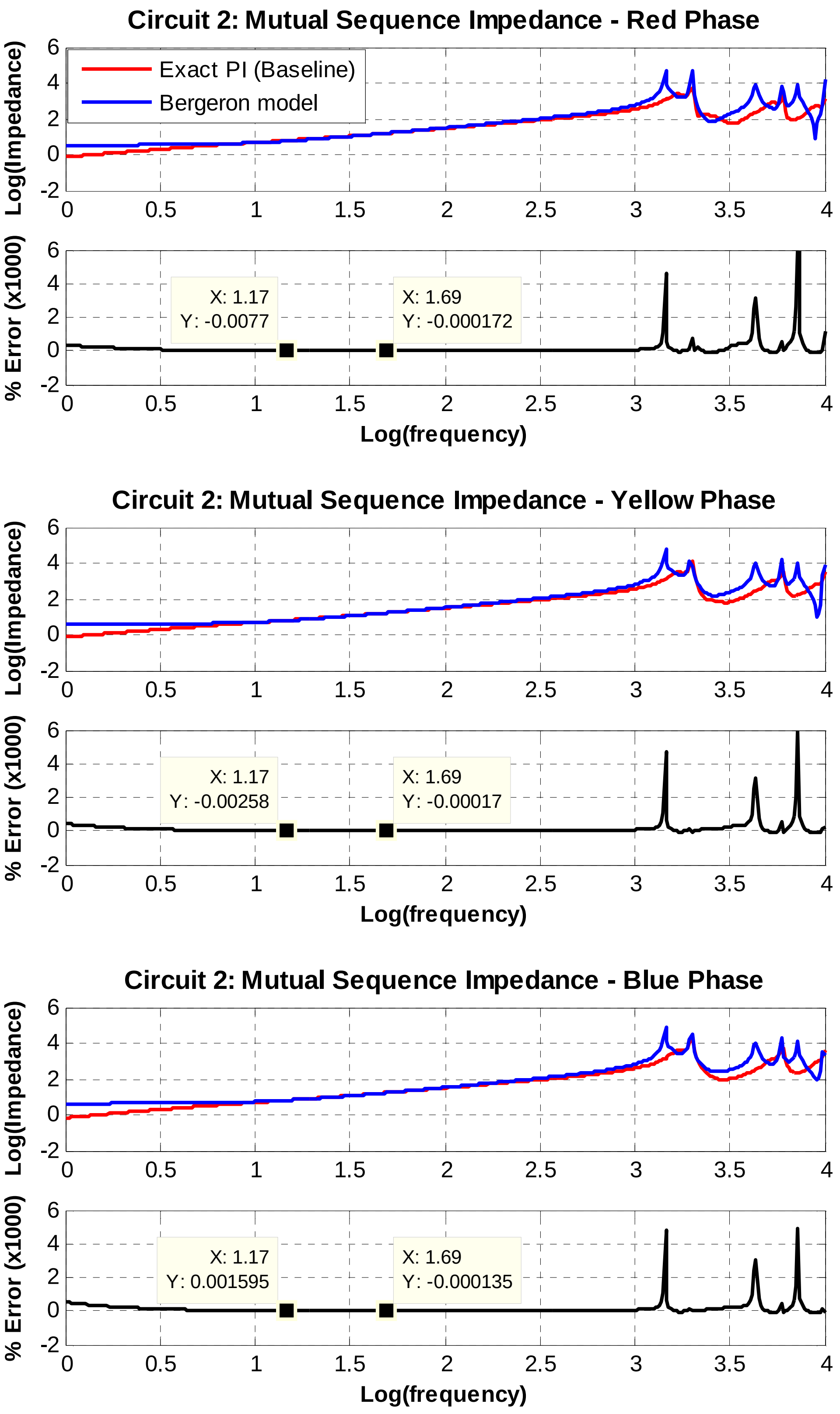

Figure B12: Circuit 2: Mutual sequence impedance for phase red, yellow and blue

Table B4 shows the percentage errors reproduced by the modeled line as compared with the baseline one.

Table B4: Percentage errors of modeled line in Bergeron

	Circuit 1						**Circuit 2**					
Baseline Exact PI	**Line Red**		**Line Yellow**		**Line Blue**		**Line Red**		**Line Yellow**		**Line Blue**	
Frequency (Hz)	**15**	**50**	**15**	**50**	**15**	**50**	**15**	**50**	**15**	**50**	**15**	**50**
Modeled line in Bergeron	**Positive sequence (% Error)**											
	-1.6	1.6e-3	-9.3	0.09	9.6	0.006	-1.6	1.6e-3	-9.3	0.09	9.6	0.006
	Zero sequence (%Error)											
	-7.2	-0.2	-3.6	-0.1	-0.9	-0.1	-7.2	-0.2	-3.6	-0.1	-0.9	-0.1
	Mutual sequence (% Error)											
	-6.3	-0.1	-3.6	-0.1	-1.7	-0.09	-7.7	-0.2	-2.6	-0.2	1.6	-0.1

J. Marti model

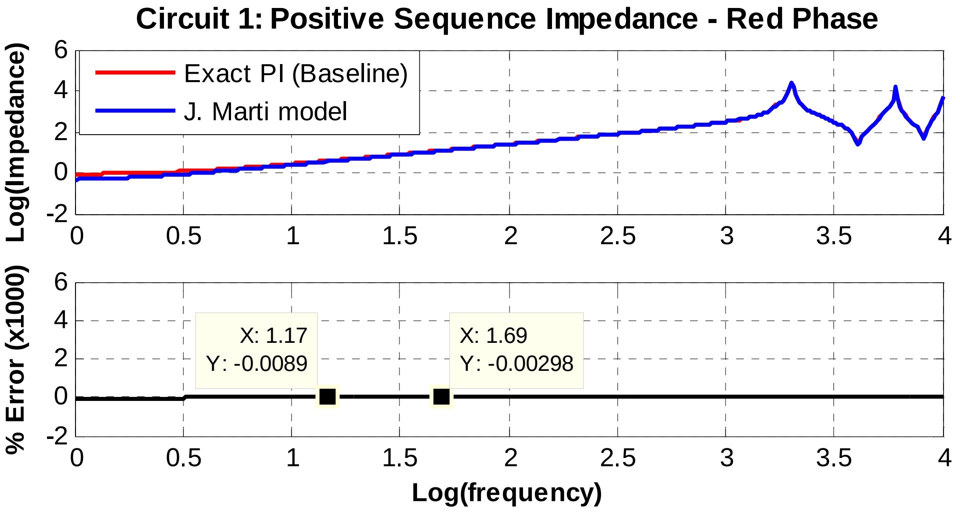

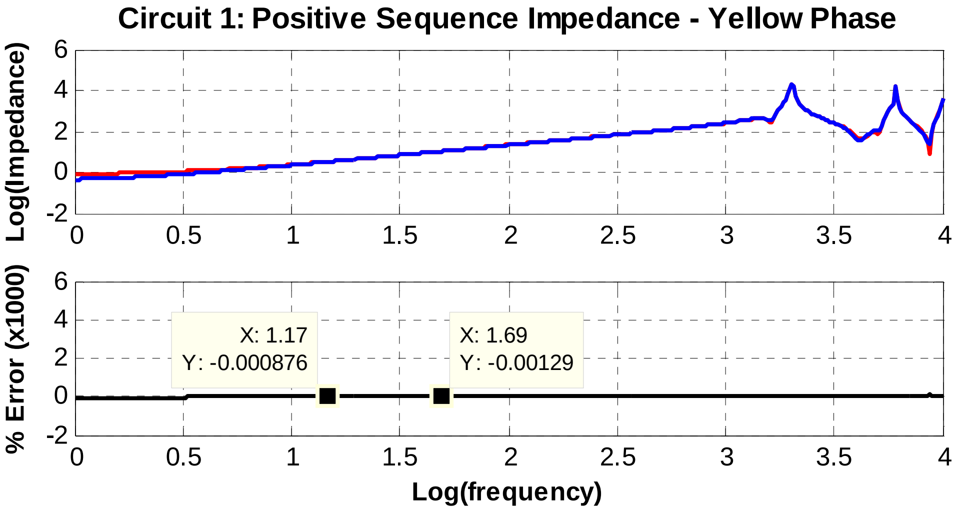

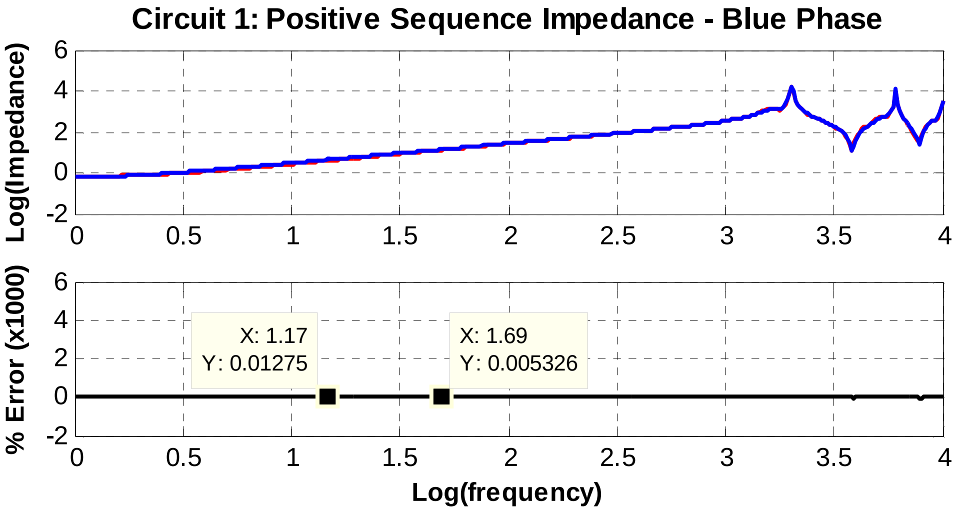

Figure B13: Circuit 1: Positive sequence impedance for phase red, yellow and blue

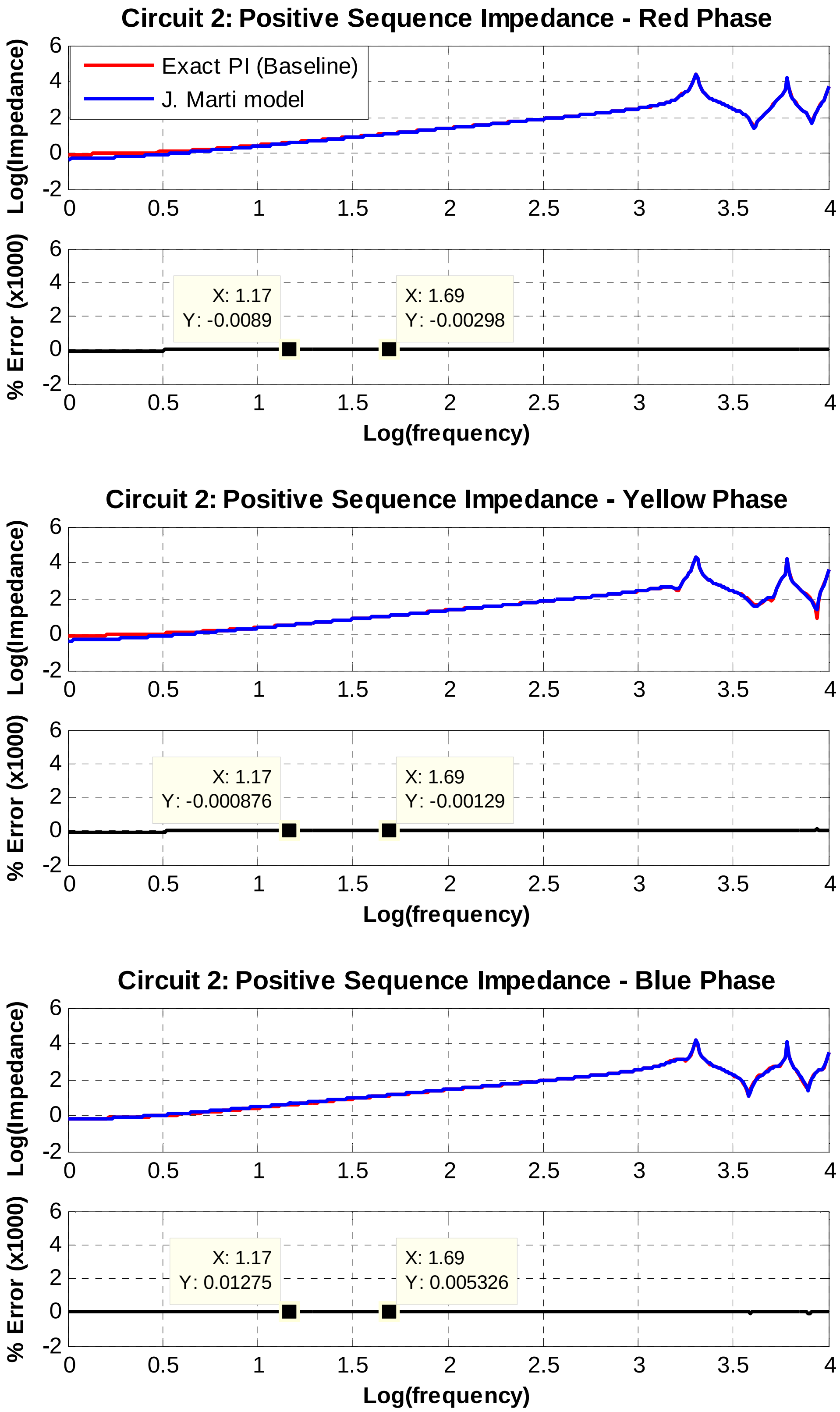

Figure B14: Circuit 2: Positive sequence impedance for phase red, yellow and blue

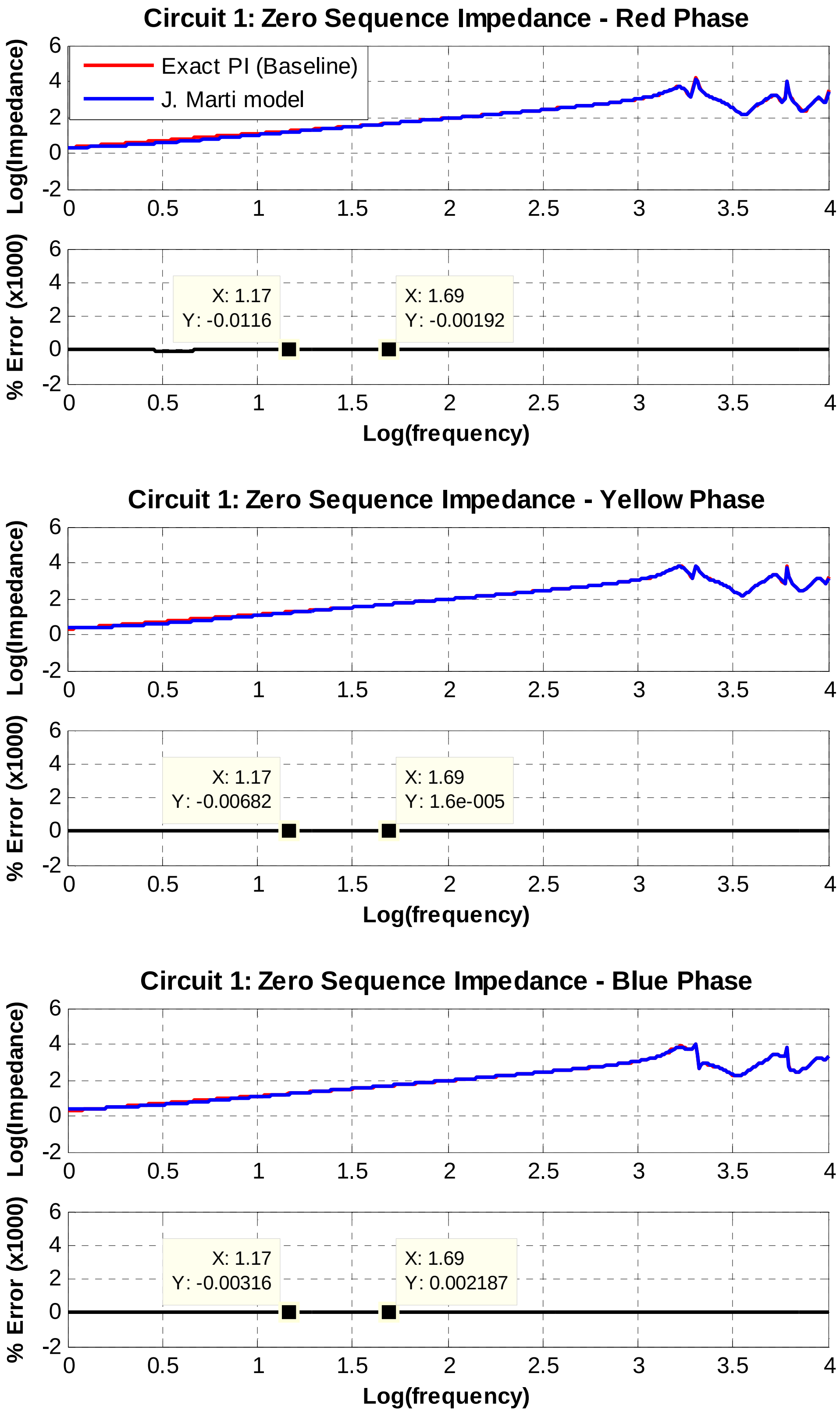

Figure B15: Circuit 1: Zero sequence impedance for phase red, yellow and blue

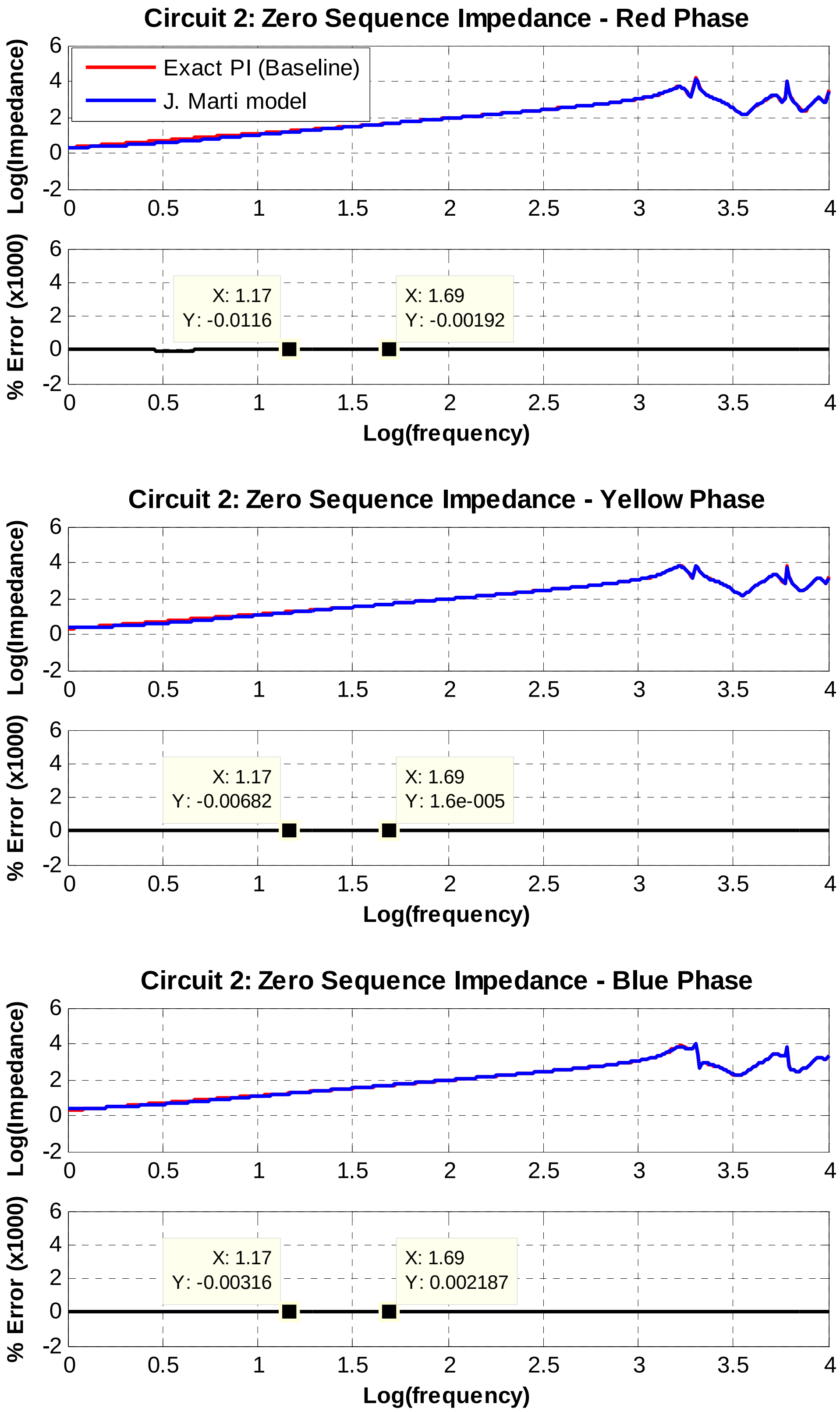

Figure B16: Circuit 2: Zero sequence impedance for phase red, yellow and blue

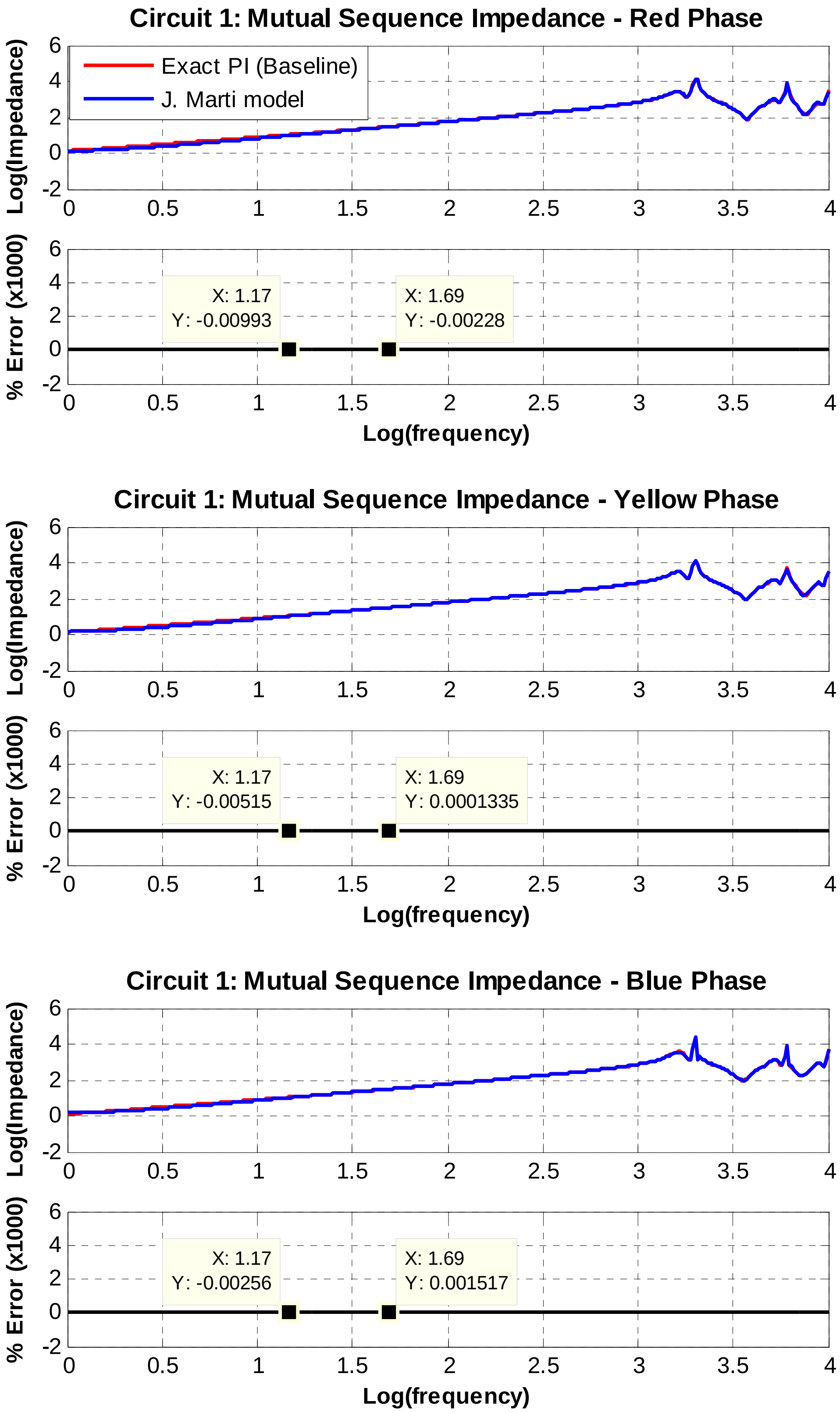

Figure B17: Circuit 1: Mutual sequence impedance for phase red, yellow and blue

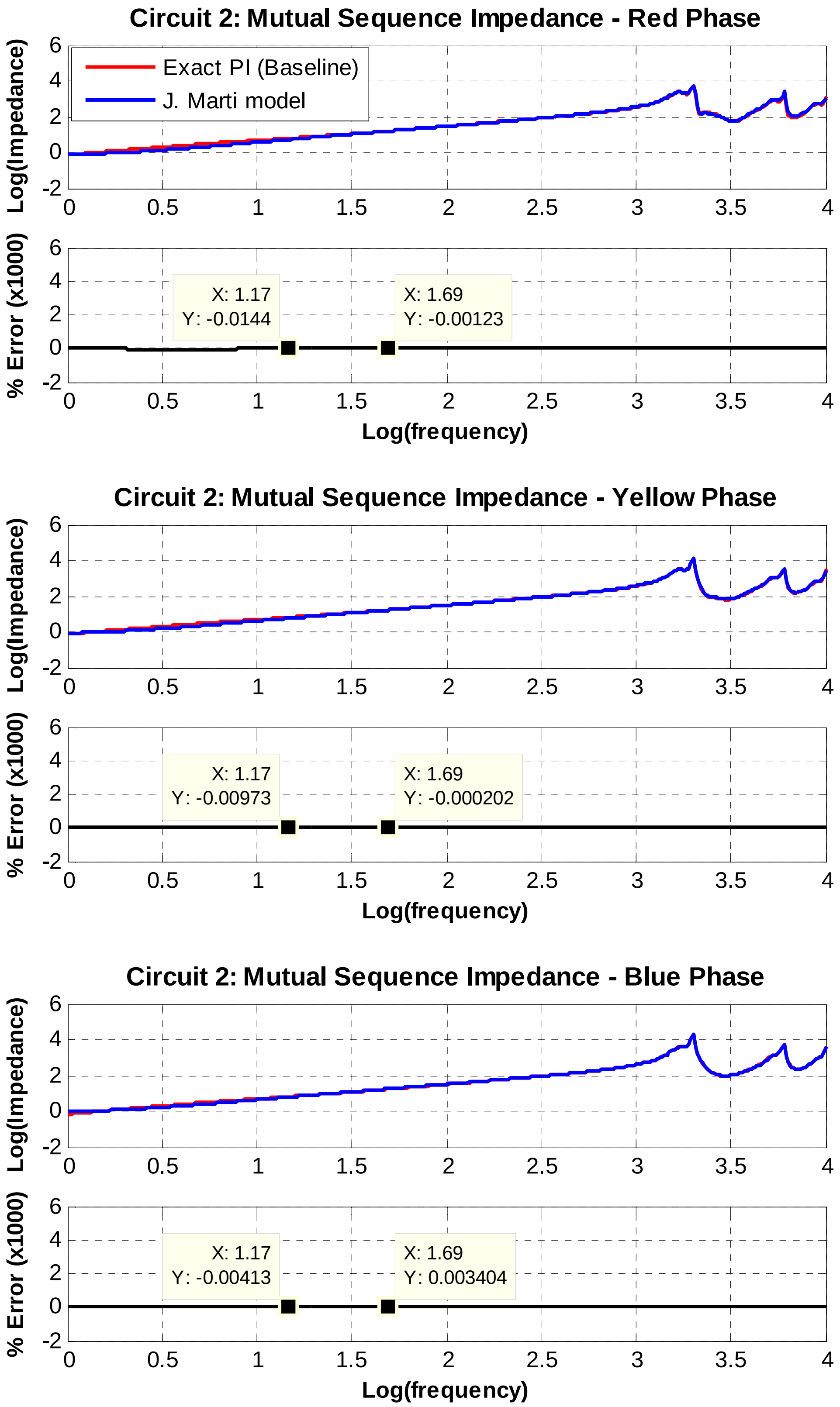

Figure B18: Circuit 2: Mutual sequence impedance for phase red, yellow and blue

Table B5 shows the percentage errors reproduced by the modeled line as compared with the baseline one.

Table B5: Percentage errors of modeled line in J. Marti

	Circuit 1						Circuit 2					
Baseline Exact PI	**Line Red**		**Line Yellow**		**Line Blue**		**Line Red**		**Line Yellow**		**Line Blue**	
Frequency (Hz)	**15**	**50**	**15**	**50**	**15**	**50**	**15**	**50**	**15**	**50**	**15**	**50**
Modeled line in PI	**Positive sequence (% Error)**											
	-8.9	-3	-0.9	-1.3	12.8	5.3	-8.9	-3	-0.9	-1.3	12.8	5.3
	Zero sequence (%Error)											
	-11.6	-1.9	-7	0.016	-3.2	2.2	-11.6	-1.9	-7	0.016	-3.2	2.2
	Mutual sequence (% Error)											
	-9.9	-2.3	-5.2	-0.13	-2.6	1.5	-14.4	-1.2	-9.7	-0.2	-4.1	3.4

(2) Transmission line model rules check [64]

There are three criteria that the users must make sure to check when a predefined model based on Bergeron is employed to model a transmission line and they are listed as follows:

i) ***Rule 1*** - *"If the parameters of the line such as the inductance and the capacitance are equal to zero, then it is not a line model".*

ii) ***Rule 2*** - *"The characteristic impedance of the transmission line,* $Z_c = \sqrt{L/C}$ *(Ω) must lie within 200 Ω* $\leq Z_c \leq$ *1000 Ω, otherwise the surge impedance of the line is not correct".*

iii) ***Rule 3*** - *"The propagation speed of the transmission line,* $v = 1/\sqrt{LC}$ *(m/s) must be within 250,000 km/s* $\leq v \leq$ *300,000 km/s, or else the speed of the line is not correct".*

Now, let us see whether the developed line model can be classified as a valid line by assessing its characteristics to the three rules which have been described above. Rule 1 has been met because the parameters of the line are not zero and this can be seen in Table B1 and Table B2. The surge impedances and the velocities for the developed lines that are generated from the ATPDraw is shown in Table B6.

Table B6: Surge impedance and velocity from Bergeron model

Modal Mode	**Surge impedance**			**Velocity (km/s)**
	Real (Ω)	**Imaginary (Ω)**	Calculated $\lvert Z_c \rvert$ **(Ω)**	
1	8.0164E+02	-7.3601E+01	8.0501E+02	2.1241E+05
2	3.5059E+02	-9.8551E+00	3.5073E+02	2.9107E+05
3	3.4015E+02	-1.1975E+01	3.4036E+02	2.9370E+05
4	2.9266E+02	-9.8378E+00	2.9282E+02	2.9555E+05
5	2.6990E+02	-1.0037E+01	2.7008E+02	2.9542E+05
6	2.5996E+02	-9.8378E+00	2.6014E+02	2.9531E+05

From Table B6, Mode 1 is the ground mode which is normally less than the speed of light because of the wave propagates back through the ground conductor. On the other hand, the rest are the line-to-line modes which are normally have a travelling speed close to the speed of light.

Therefore the modes which are required to take into consideration to meet Rule 2 and Rule 3 are Mode 2 to Mode 6 of the modeled line. The results to meet Rule 2 and Rule 3 are presented in Table B7 and these suggest that the line characteristic impedances and the speed of the travelling wave has been modeled correctly.

Table B7: 37 km modeled line applied to Rule 1, 2 and 3 – Bergeron model

	Rule 1
	***L* and *C* = 0?**
37 km modeled line	The line consists of all the parameters which can be referred to Table B1 and Table B2

33 km modeled line	***Rule 2***	***Rule 3***
	200 Ω ≤ Z_c ≤ 1000 Ω	**250,000 km/s ≤ v ≤ 300,000 km/s**
Mode 2	3.5073E+02	2.9107E+05
Mode 3	3.4036E+02	2.9370E+05
Mode 4	2.9282E+02	2.9555E+05
Mode 5	2.7008E+02	2.9542E+05
Mode 6	2.6014E+02	2.9107E+05

Since there is no surge impedance and velocity of wave generated from the J. Marti model therefore an alternative way to check the line is to carry out the transmission line check as presented in the following section.

(3) Transmission line model length check

Lastly, the validation of the line is further checked by determining its line length via traveling wave approach. This is carried out by determining the time delay, t_d that is the time of the wave propagates from sending-end from point A to receiving-end at point C at the instant when the switch SW is closed, which is shown in Figure B55.

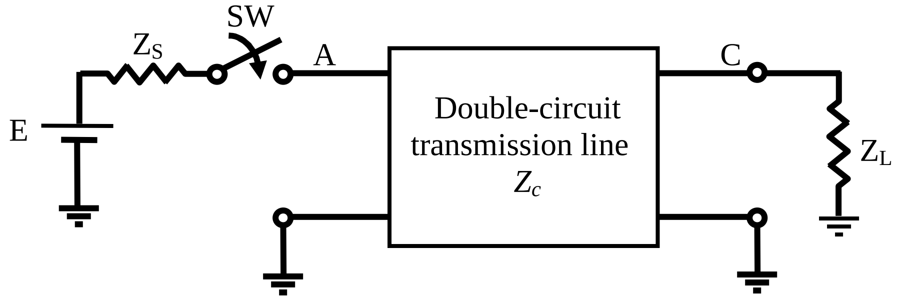

Figure B55: Wave propagation along the line

The time delay, t_d is determined by using ATPDraw and it is shown in Table B8. The distance of the transmission line is obtained as 36.6 km, with the speed of light being 3×10^5 km/s. Therefore the line can be considered modeled correctly.

Table B8: Line distant obtained from travelling wave

Modeled line	**Time delay (μs)**	**Distance (km)**
Bergeron	122	36.6
J. Marti	122	36.6

APPENDIX C

Determination of current-flux characteristic using supporting routine SATURA

The input data-deck for the supporting routine SATURA has been developed which has the following Data Case.

(a) SATURA Supporting Routine

```
BEGIN NEW DATA CASE
################################################################################
                         Supporting Routine SATURA
################################################################################
SATURATION
$ERASE
################################################################################
                         Per-unit base specification
################################################################################
         1         2         3         4         5         6         7         8
12345678901234567890123456789012345678901234567890123456789012345678901234567890
< FREQ ><VBASE ><SBASE ><IPUNCH><KTHIRD>

################################################################################
                         IR.M.S and VR.M.S Data
################################################################################
         1         2         3         4         5         6         7         8
12345678901234567890123456789012345678901234567890123456789012345678901234567890
< IR.M.S (P.U) >< VR.M.S (P.U) >

################################################################################
                         Termination
################################################################################
         1         2         3         4         5         6         7         8
12345678901234567890123456789012345678901234567890123456789012345678901234567890
            <  >
            9999
$PUNCH
BLANK LINE ending saturation data
BEGIN NEW DATA CASE
BLANK LINE ENDING ALL CASES
```

(i) **Per-unit base specification**

- **FREQ:** frequency (in Hz) of the impressed sinusoidal voltage source.

  $\therefore$FREQ = 50

- **VBASE:** single-phase base voltage (in kV) on which the input break points are based.

  $\therefore$**VBASE** = 13

- **SBASE:** single-phase base power (in MVA) on which the input break points are based.

  $\therefore$**SBASE** = 60/3 = 20

- **IPUNCH:** parameters controlling the punched card output of the derived (flux-current) characteristic.

  IPUNCH = 0: no curve will be punched;
  = 1: curve will be punched, provided the $PUNCH card is being specified

  ∴**IPUNCH** = 1

- **KTHIRD:** parameters controlling the type of output.

  KTHIRD = 0: only first quadrant;
  = 1: full curve (first- and third-quadrant output)

  ∴ **KTHIRD = 0**

(ii) **IR.M.S and VR.M.S data**

Values are in per-unit, based on the previously-specified single-phase based.

$$I_{base} = \frac{S_{base}}{V_{base}},\ I_{RMS}\left(pu\right) = \frac{I_{RMS}\left(A\right)}{I_{base}\left(A\right)},\ V_{RMS}\left(pu\right) = \frac{V_{RMS}\left(kV\right)}{I_{base}\left(kV\right)}$$

(b) Transformer SGT1: 1000 MVA, 400/275/13 kV, Vector: YNa0d11 (5 legs)

Table 1: No-load loss data

NO-LOAD LOSS on TERT. (60 MVA)				
VOLTS			**AMPS**	**kWatts**
%	**MEAN**	**R.M.S**		
			5.25	96.3
90	11700	11810	6.00	
			7.28	
			12.30	127.9
100	13000	13217	12.40	
			14.75	
			55.2	175.3
110	14300	14903	54.3	
			56.8	

Where R.M.S Volts = excitation voltage (line-line value), AMPS = excitation current (RMS, three-phase values), kWatts = excitation loss (three-phase value)

At a first approximation, the RMS excitation current $I_{ex,w}$ in DELTA winding equals

$$I_{ex,w} = \frac{I_{ex}}{\sqrt{3}} \text{ (harmonic neglected)}$$

Further, the RMS magnetizing current, $I_{m,w}$ in the DELTA is approximated by

$$I_{m,w} \approx \sqrt{I_{ex,w}^2 - \left(\frac{P_{ex}}{3U_{ex}}\right)^2}$$

Where U_{ex} = excitation voltage (RMS, line-line value)
I_{ex} = excitation current (RMS, three-phase values)
P_{ex} = excitation loss (three-phase value)

Hence, the above measured Table reduces to following saturation characteristic:

Irms(pu)	Vrms(pu)
1.5006E-03	9.0846E-01
4.4674E-03	1.0167E+00
2.0646E-02	1.1464E+00

Current (A)	Flux-linkage (Wb-T)
3.2649E+00	5.3164E+01
1.5849E+01	5.9498E+01
7.3791E+01	6.7088E+01

The corresponding output from the punch file looks as follows:

```
C  <++++++>  Cards punched by support routine on  16-Mar-10  15:53:38  <++++++>
C SATURATION
C $ERASE
C C ############################################################################
C C                      Per-unit base specification
C C ############################################################################
C C        1         2         3         4         5         6         7
C C 3456789012345678901234567890123456789012345678901234567890123456789012345678
C C FREQ ><VBASE ><SBASE ><IPUNCH><KTHIRD>
C 50           13.    20.      1       0
C C ############################################################################
C C                      IR.M.S and VR.M.S Data
C C ############################################################################
C C        1         2         3         4         5         6         7
C C 3456789012345678901234567890123456789012345678901234567890123456789012345678
C C IR.M.S (P.U) >< VR.M.S (P.U) >
C       1.5006E-03      9.0846E-01
C       4.4674E-03      1.0167E+00
C       2.0646E-02      1.1464E+00
C C ############################################################################
C C                      Termination
C C ############################################################################
C C        1         2         3         4         5         6         7
C C 3456789012345678901234567890123456789012345678901234567890123456789012345678
C C           <  >
C             9999
  3.26487519E+00  5.31635884E+01
  1.58486260E+01  5.94978539E+01
  7.37913599E+01  6.70879706E+01
            9999
```

APPENDIX D

(1) Line parameters check

The equivalent of the lumped parameters of the 33 km un-transposed double-circuit transmission are derived by using the ‘LINE PARAMETERS’ supporting routine in ATP-EMTP and validated by using MATLAB. The results of the capacitance and impedance matrices are presented as shown in Table D1 and Table D2.

Table D1: Equivalent capacitance matrix in farads/km derived from ATP-EMTP

1	1.1068E-08					
2	-2.3598E-09	1.1563E-08				
3	-7.3718E-10	-2.2536E-09	1.1355E-08			
4	-1.7211E-09	-9.5576E-10	-4.0548E-10	1.1068E-08		
5	-9.5576E-10	-1.2594E-09	-8.1546E-10	-2.3598E-09	1.1563E-08	
6	-4.0548E-10	-8.1546E-10	-1.2339E-09	-7.3718E-10	-2.2536E-09	1.1355E-08

(b) capacitance matrix in farads/km for the system of equivalent phase conductors

1	6.1130E-02 4.4535E-01					
2	3.8924E-02 1.8902E-01	5.9265E-02 4.6750E-01				
3	3.8235E-02 1.5333E-01	3.7991E-02 2.0592E-01	5.8980E-02 4.8011E-01			
4	4.0118E-02 1.5977E-01	3.8898E-02 1.5630E-01	3.8209E-02 1.4075E-01	6.1130E-02 4.4535E-01		
5	3.8898E-02 1.5630E-01	3.8247E-02 1.7844E-01	3.7959E-02 1.7060E-01	3.8924E-02 1.8902E-01	5.9265E-02 4.6750E-01	
6	3.8209E-02 1.4075E-01	3.7959E-02 1.7060E-01	3.7956E-02 1.8662E-01	3.8235E-02 1.5333E-01	3.7991E-02 2.0592E-01	5.8980E-02 4.8011E-01

(c) Impedance matrix in ohms/km for the system of equivalent phase conductors

Equivalent Impedance and capacitance derive from MATLAB is shown in Table D2.

Table D2: Equivalent Impedance and capacitance derived from MATLAB

1.1068E-08	-2.3598E-09	-7.3718E-10	-1.7211E-09	-9.5575E-10	-4.0548E-10
-2.3598E-09	1.1563E-08	-2.2536E-09	-9.5575E-10	-1.2594E-09	-8.1546E-10
-7.3718E-10	-2.2536E-09	1.1355E-08	-4.0548E-10	-8.1546E-10	-1.2339E-09
-1.7211E-09	-9.5575E-10	-4.0548E-10	1.1068E-08	-2.3598E-09	-7.3718E-10
-9.5575E-10	-1.2594E-09	-8.1546E-10	-2.3598E-09	1.1563E-08	-2.2536E-09
-4.0548E-10	-8.1546E-10	-1.2339E-09	-7.3718E-10	-2.2536E-09	1.1355E-08

(d) capacitance matrix in farads/km

6.1200E-02	3.8900E-02	3.8300E-02	4.0200E-02	3.8900E-02	3.8200E-02
3.8900E-02	5.9300E-02	3.8000E-02	3.8900E-02	3.8300E-02	3.8000E-02
3.8300E-02	3.8000E-02	5.9000E-02	3.8200E-02	3.8000E-02	3.8000E-02
4.0200E-02	3.8900E-02	3.8200E-02	6.1200E-02	3.8900E-02	3.8300E-02
3.8900E-02	3.8300E-02	3.8000E-02	3.8900E-02	5.9300E-02	3.8000E-02
3.8200E-02	3.8000E-02	3.8000E-02	3.8300E-02	3.8000E-02	5.9000E-02

(e) Resistance matrix in ohms/km

1.4177E-03	6.0169E-04	4.8801E-04	5.0864E-04	4.9751E-04	4.4793E-04
6.0169E-04	1.4880E-03	6.5534E-04	4.9751E-04	5.6791E-04	5.4291E-04
4.8801E-04	6.5534E-04	1.5281E-03	4.4793E-04	5.4291E-04	5.9384E-04
5.0864E-04	4.9751E-04	4.4793E-04	1.4177E-03	6.0169E-04	4.8801E-04
4.9751E-04	5.6791E-04	5.4291E-04	6.0169E-04	1.4880E-03	6.5534E-04
4.4793E-04	5.4291E-04	5.9384E-04	4.8801E-04	6.5534E-04	1.5281E-03

(f) Inductance matrix in ohms/km

As can be seen from both Tables D1 and D2, the self and mutual impedances, and capacitances derived from both methods have shown a good agreement between each other.

(2) Line parameters frequency scan check

The outcomes of the frequency scans are depicted in Figure D1 to Figure D6, showing the positive-sequence impedance, the zero-sequence impedance and the mutual-sequence impedances with all the three phases. Those results suggest that the model is suitable for the study of the expected Period-1 ferroresonance because the parameters of developed model are able to fit well with the baseline exact PI equivalent at 50 Hz frequency, with very small percentage error.

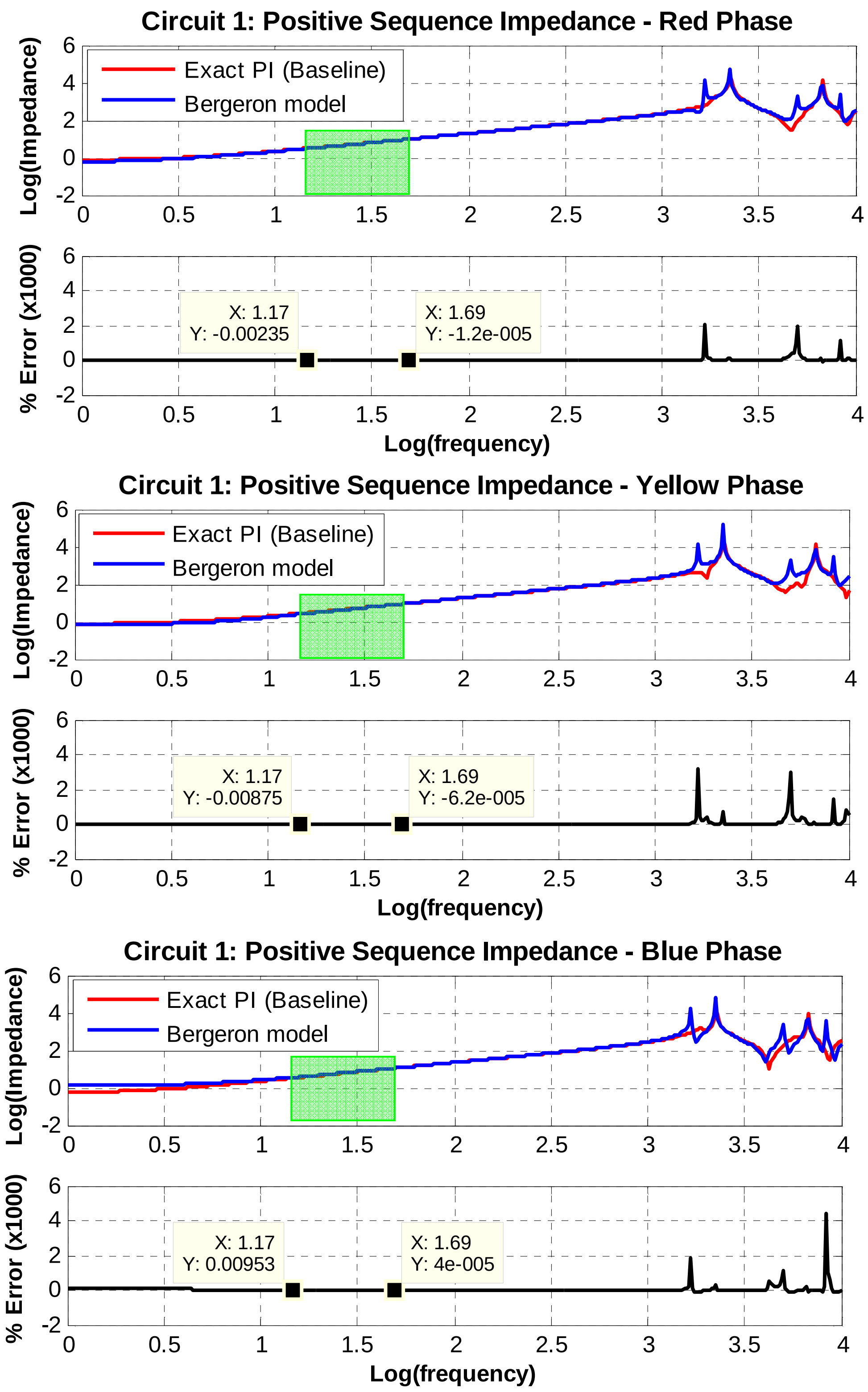

Figure D1: Circuit 1: Positive sequence impedance for phase red, yellow and blue

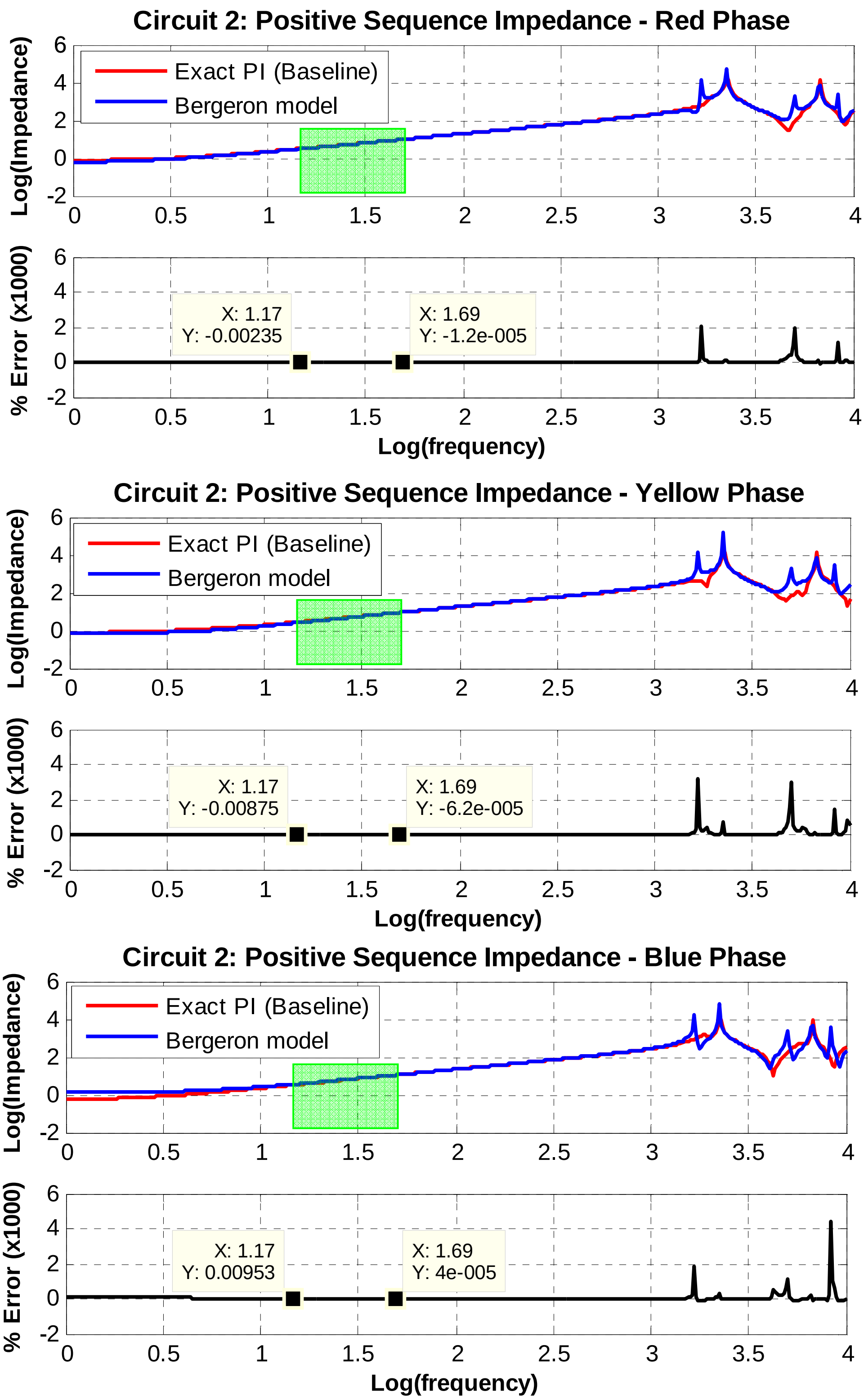

Figure D2: Circuit 2: Positive sequence impedance for phase red, yellow and blue

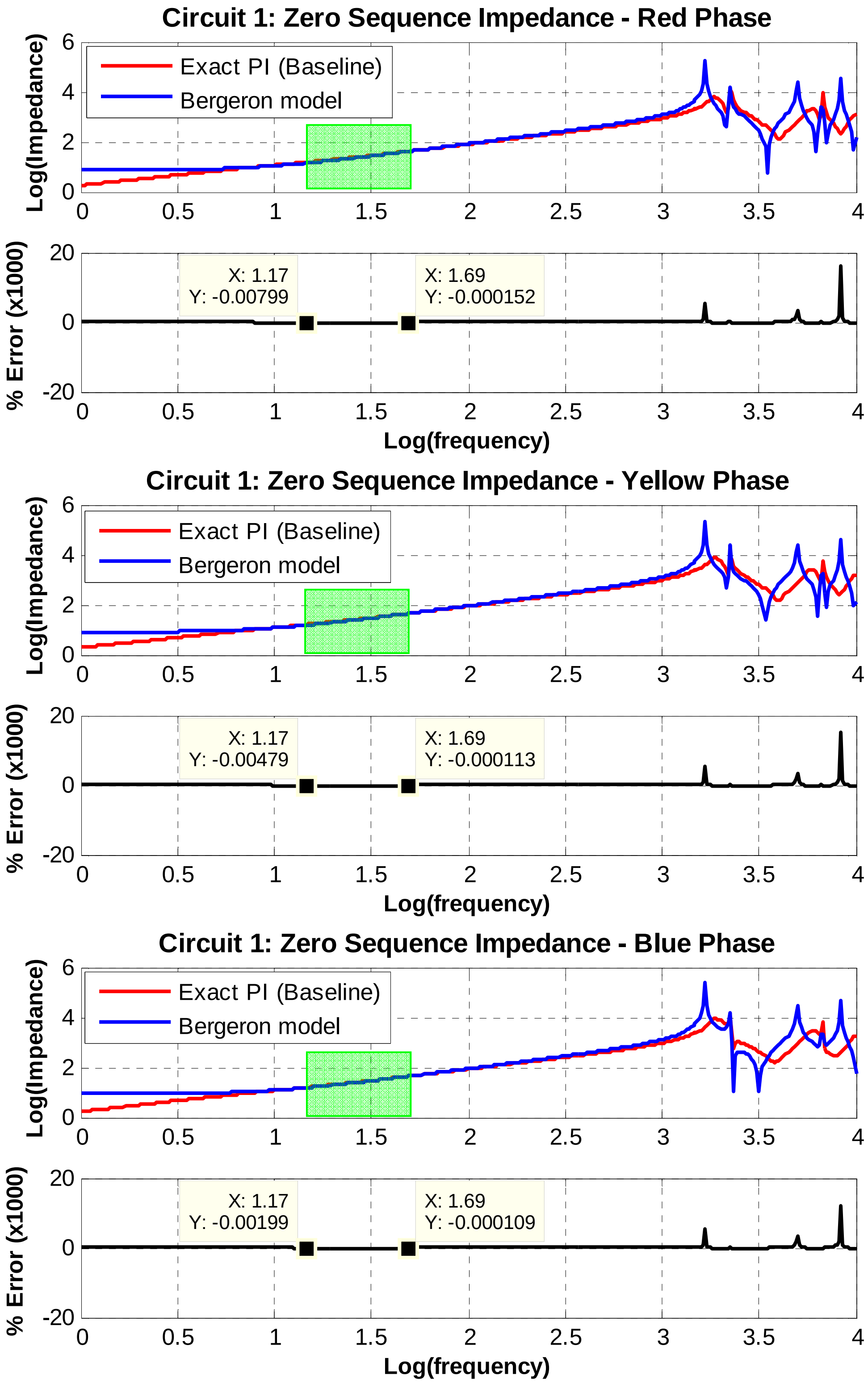

Figure D3: Circuit 1: Zero sequence impedance for phase red, yellow and blue

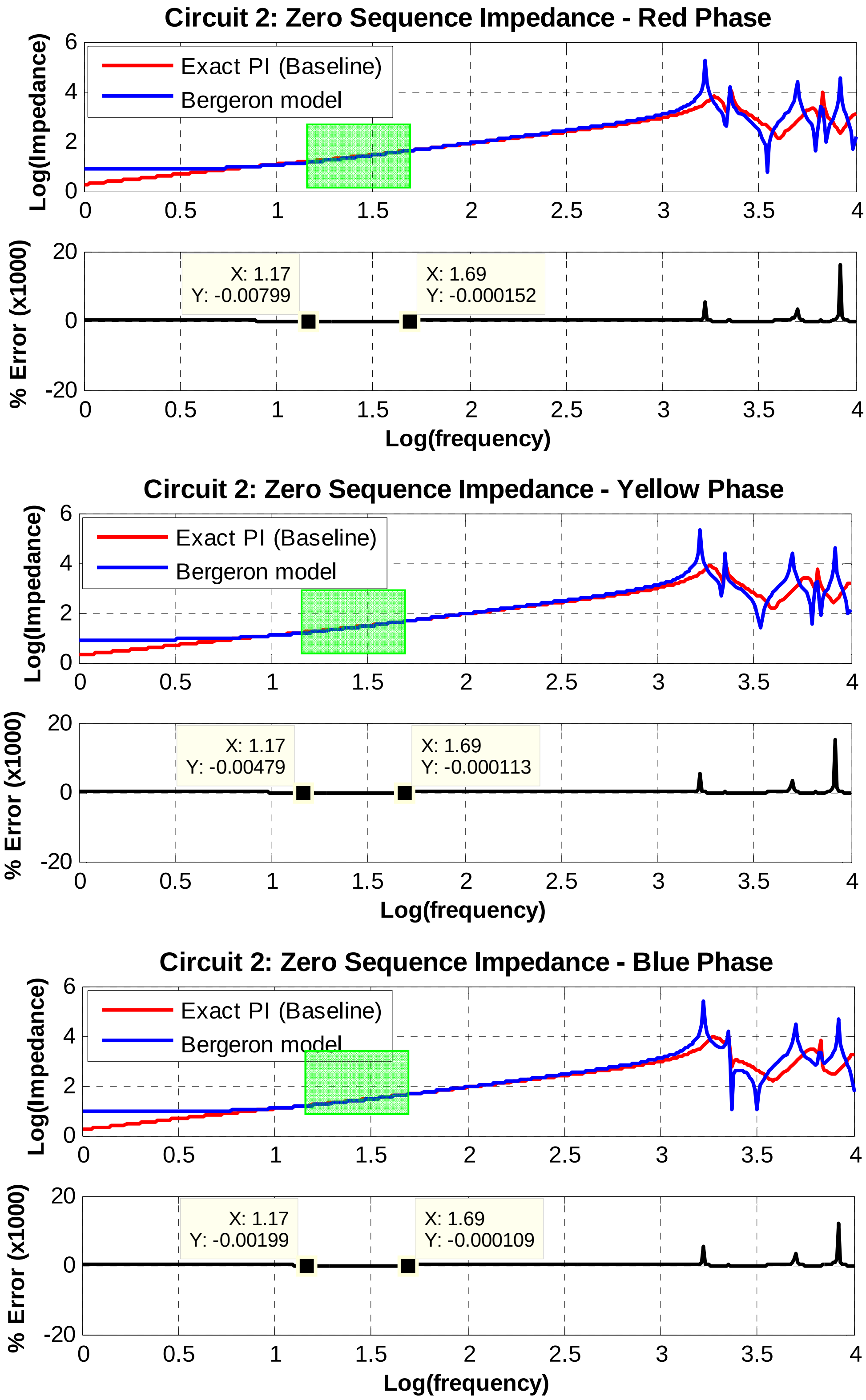

Figure D4: Circuit 2: Zero sequence impedance for phase red, yellow and blue

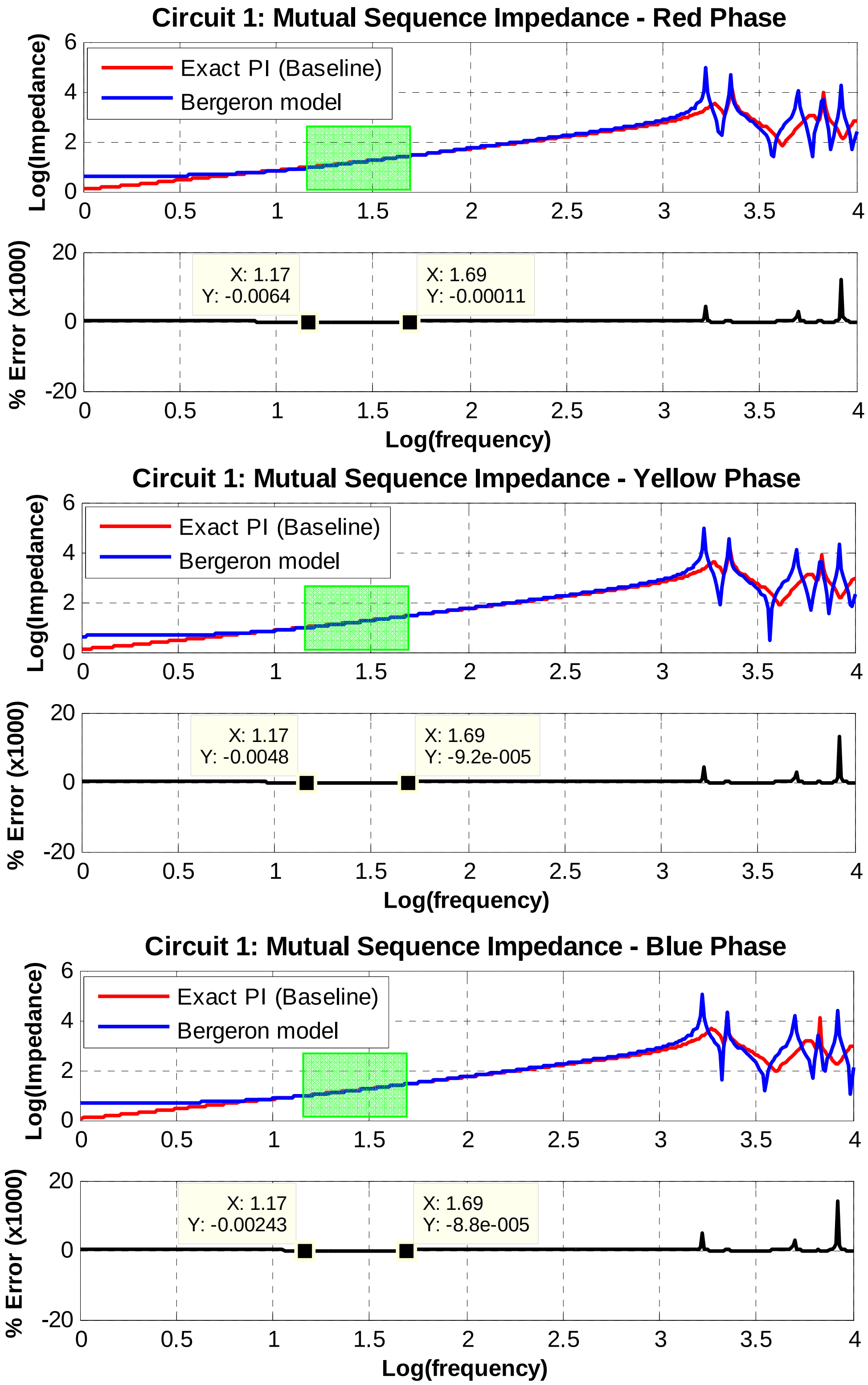

Figure D5: Circuit 1: Mutual sequence impedance for phase red, yellow and blue

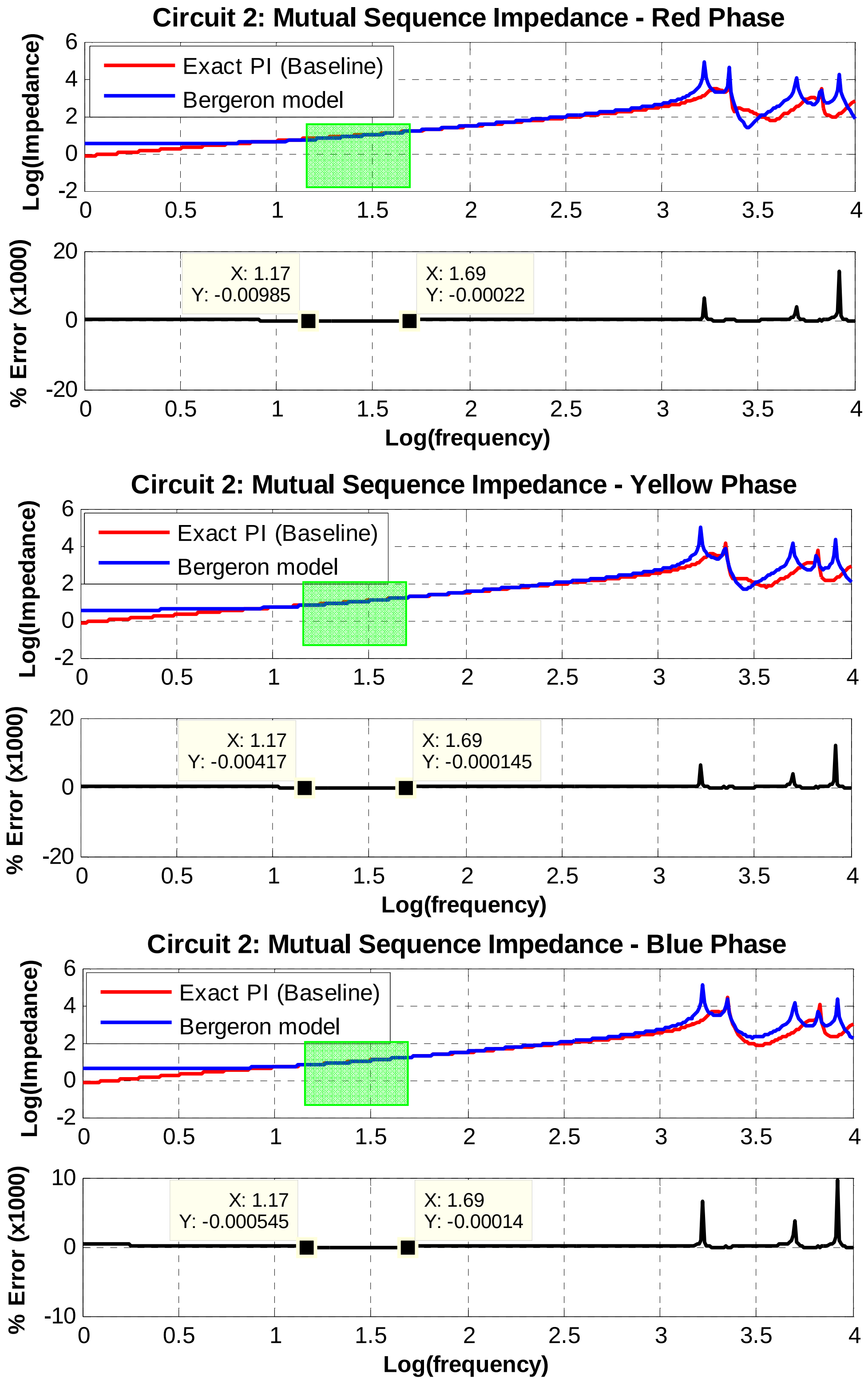

Figure D6: Circuit 2: Mutual sequence impedance for phase red, yellow and blue

(3) Transmission line model rules check

Rule 1 has been met because the parameters of the line are not zero and this can be seen in Table D1 and Table D2. The surge impedances and the velocities for the developed line model are determined as shown in Table D3.

Table D3: Data generated from the ATPDraw

Modal Mode	Surge impedance Real (Ω)	Imaginary (Ω)	Calculated $\|Z_c\|$ (Ω)	Velocity (km/s)
1	8.5350E+02	-7.8235E+01	8.5708E+02	2.1806E+05
2	3.1775E+02	-1.0009E+01	3.1791E+02	2.9354E+05
3	3.2310E+02	-1.2062E+01	3.2333E+02	2.9394E+05
4	2.6212E+02	-9.7396E+00	2.6230E+02	2.9519E+05
5	2.3210E+02	-9.7934E+00	2.3231E+02	2.9478E+05
6	2.4466E+02	-9.9108E+00	2.4486E+02	2.9502E+05

The results to meet Rule 2 and Rule 3 are presented in Table D4 and these suggest that the line characteristic impedances and the speeds of the travelling wave have been modeled correctly.

Table D4: 33 km modeled line applied to Rule 1, 2 and 3

	Rule 1 ***L* and *C* = 0?**
33 km modeled line	The line consists of all the parameters which can be referred to Table D1 and Table D2

33 km modeled line	***Rule 2*** **200 Ω ≤ Z_c ≤ 1000 Ω**	***Rule 3*** **250,000 km/s ≤ *v* ≤ 300,000 km/s**
Mode 2	3.1791E+02	2.9354E+05
Mode 3	3.2333E+02	2.9394E+05
Mode 4	2.6230E+02	2.9519E+05
Mode 5	2.3231E+02	2.9478E+05
Mode 6	2.4486E+02	2.9502E+05

(4) Transmission line model length check

Lastly, the validation of the line is further checked by determining its line length via traveling wave approach. The simulation result of sending and receiving wave are shown in Figure D5. The time delay, t_d is determined by using ATPDraw as 111 μs and the line distance is obtained as 33.3 km. Therefore the line can be considered modeled correctly.

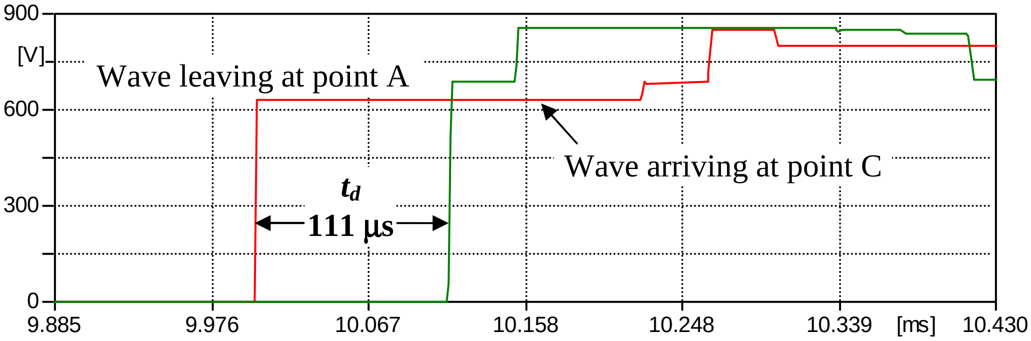

Figure D5: Time delay of the two propagate waves